University of Alberta

Diffusion Weighted Magnetic Resonance Spectroscopy of Human Brain

by

Jacob Ellegood

A thesis submitted to the Faculty of Graduate Studies and Research in partial fulfillment of the requirements for the degree of **Doctor of Philosophy**.

in

Medical Sciences - Biomedical Engineering

Edmonton, Alberta
Spring 2008

Your file Votre référence
ISBN: 978-0-494-45421-3
Our file Notre référence
ISBN: 978-0-494-45421-3

Abstract

Diffusion measurements of water have been shown to be useful in a variety of different neurological disorders. Prior to the work presented in this thesis, Diffusion Weighted Magnetic Resonance Spectroscopy (DW-MRS) had only been performed twice in the human brain and was only measured in a single direction. This thesis builds on that preliminary research.

First, the diffusion of the metabolites N-acetyl aspartate (NAA), creatine and phosphocreatine (tCr), and choline (Cho) were measured in three orthogonal directions, in three regions, in human brain to calculate the rotationally invariant mean diffusivity (MD). The MD of NAA was determined to be significantly less than tCr and Cho in brain. Next, Diffusion Tensor Spectroscopy (DTS) was performed for the first time in healthy human brain, which required diffusion measurements in six non-collinear directions, and was performed on six different regions. Directional information previously seen with water diffusion was confirmed using a purely intracellular metabolite, NAA. This study also reported the first measurements of Fractional Anisotropy (FA) of the metabolites NAA, tCr, and Cho. High FA values of tCr and Cho when compared to NAA were unexpected and led to the examination of a simpler model system, an excised frog peripheral nerve, which confirmed the FA measurements in human brain. DTS was performed again in human brain to examine a new metabolite myo-inositol (mI). This study helped to answer some unsettling questions about high metabolite FA values in gray matter reported in the original DTS study. Furthermore, this work helped to improve the methods used for calculating MD and FA in human brain. The results from these experiments indicate that the metabolites examined may be located in different intracellular compartments, which may help in the examination of different neurological disorders.

Preliminary work on adapting a diffusion weighted spectroscopy sequence to measure the MD of metabolites in human brain in a single shot is also discussed. The main focus of that study was on shortening the scan time, which may be required for the transition to clinical experimentation.

ACKNOWLEDGEMENTS

First and Foremost I would like to acknowledge my supervisor, Dr. Christian Beaulieu. Not only for his effort and input throughout the work presented in this thesis, but for always being available, no matter how busy, to answer my questions or look over my work. Second I would like to thank my unofficial co-supervisor Dr. Chris Hanstock. For all his help and advice, whether it be scaring the 3T into giving me a good shim or answering my many spectroscopy/metabolite questions. I am very thankful to Dr. Ryan McKay for all his help with the 18.8 T NMR system at NANUC, especially due to the time crunch for that project. Furthermore, I would like to thank my supervisory committee, Dr. Peter Allen, Dr. Alan Wilman, and Dr. Wayne Martin for their effort and time spent discussing and evaluating my work. I would like to thank Dr. Richard Thompson and Dr. Brian Sykes for being members of my candidacy exam committee, and Dr. Leo Spyracopoulos for reading my thesis and being a examiner at my thesis defense. A special thanks to Dr. Alex MacKay for flying out from UBC for my thesis defense. I appreciated his thoughtful questions and careful examination of my thesis.

I am indebted to Dr. David Naylor for introducing me to scientific research and convincing me to finish my physics degree rather than pursue an education degree, as well as Dr. David Siminovitch for introducing me to NMR and helping me get a head start in the field prior to coming to the U of A.

I am grateful to Dr. Changho Choi and Dr. Hanstock for their help with pulse sequence implementation on the 3T. Also, Dan Gheorghiu, Karim Damji, and Peter Seres for keeping the 3T system up and running, and for not complaining when I used huge blocks of time, Beau Sapach for all his help with my computer issues, both in my office and in the lab, and special thanks to Dr. Richard Snyder and Isidro "Chilo" Bonilla for their help with the froggies.

I am extremely grateful to Maisie Goh for always having a smile on her face, her assistance with all my complicated financial issues over the years, and for always fighting on behalf of the students. Thanks to Carol Hartle, for all her help with Pete, as well as providing goodies in the NMR centre. Also, Gritchi Castro and Brenda Carrier for their help with organizing meetings, seminars, and handling alot of the paper work.

It is essential that I acknowledge my fellow graduate students who have made coming to work rather enjoyable over the years. My old and new office mates for putting up with me: Hyeonjin Kim, Lindsay Snook, M. Shazam Hussain (the once or twice he was around), and Adrian Tsang. Yusuf Bhagat for always being willing to answer my questions, Marc Lebel for picking me up for "Coffee" in the mornings, Catherine Lebel for always being willing to chat when I dropped by her office, Dr. Luis Concha for not only providing me with DTI colormaps/tractography pictures whenever I asked but for rooming with me during conferences and helping me with my LaTeX issues, Jeff Snyder who hopefully will still find me at ISMRM to smoke cigars, Rob Stobbe for being available to talk hockey. And the many other students in the department past and present Amir Eissa, Kelvin Chow, June Cheng, Robert Gaunt, Farnaz Khosrow-Khavar, Gaolong Gong, Steve Thomas, Jason Mendes, Sasha Holden, and Allison Campbell. I cannot tell you how much I appreciate the countless volunteers for the long spectroscopy scans I ran. They were a little reluctant at first but were always available when I needed them.

I greatly appreciated the funding provided to me by the faculties of Graduate Studies and Medicine and Dentistry, the Province of Alberta, and the Natural Sciences and Engineering Research Council (NSERC) of Canada.

I appreciate very much the love and support I've gotten from my two sets of parents. My parents Paul and Margo. My Dad who has always been there for me, whether it was wrecking his car or chatting about the Oilers, the man he is I strive to be. My Mom for always been my confidant, I could tell her anything and still do, she worries about me a little too much but it's appreciated. And Tom and Cynthia, the best in-laws I could ask for. Cynthia for always calling to check up on me, whether it be a question of my eating habits or to check in to see how I was doing. Tom for teasing me about the Oilers, and for fixing anything and everything I needed and didn't have the time to do, I can only hope to be that handy. I can't forget to thank my brother, Nick, it is the sibling rivalry that we share and thrive on that I appreciate. Although, a Doctor is better than a Lawyer right?

Lastly I must express my shear admiration of my wife, Jennifer. The love of my life. I couldn't have done this, the last five years, without her. I appreciate every last thing she's done for me, especially in the final push, it would have been impossible without her. She has my heart.

Table of Contents

I Introduction 1

1 Preliminary Remarks 2
- 1.1 Introduction to the Thesis . . . 2
  - 1.1.1 Spectroscopy . . . 2
  - 1.1.2 Diffusion . . . 3
  - 1.1.3 Diffusion Weighted Magnetic Resonance Spectroscopy (DW-MRS) . 3
  - 1.1.4 Overview . . . 4

2 Spectroscopy 6
- 2.1 Spin and Magnetic Moment . . . 6
- 2.2 Preparation . . . 7
- 2.3 Excitation . . . 10
- 2.4 Signal . . . 11
  - 2.4.1 Relaxation . . . 12
    - 2.4.1.1 Longitudinal Relaxation . . . 13
    - 2.4.1.2 Transverse Relaxation . . . 13
- 2.5 Spatial Localization . . . 14
  - 2.5.1 Gradients . . . 14
  - 2.5.2 Slice Selection and Single Voxel Localization . . . 16
- 2.6 Chemical Shift . . . 17
- 2.7 Indirect Scalar Coupling (J-Coupling) . . . 19
- 2.8 Water Suppression . . . 19
  - 2.8.1 Selective Excitation . . . 20
  - 2.8.2 Inversion Recovery . . . 21
  - 2.8.3 Pre-Saturation . . . 22
  - 2.8.4 Pre-Saturation vs. Inversion Recovery . . . 23
- 2.9 Cell Biology . . . 24
- 2.10 Metabolites . . . 26
  - 2.10.1 N-Acetyl Aspartate . . . 28
  - 2.10.2 Creatine . . . 29
  - 2.10.3 Choline . . . 30
  - 2.10.4 Myo-Inositol . . . 30
  - 2.10.5 Glutamate and Glutamine . . . 32
  - 2.10.6 Taurine . . . 33
  - 2.10.7 Metabolite Summary . . . 33

3 Diffusion 36
- 3.1 The Diffusion Process . . . 36
  - 3.1.1 History . . . 36
  - 3.1.2 How Diffusion is Measured . . . 40
- 3.2 Types of Diffusion . . . 42
  - 3.2.1 Isotropic . . . 42
  - 3.2.2 Anisotropic . . . 43
- 3.3 Measuring Anisotropy . . . 43
  - 3.3.1 The Diffusion Tensor . . . 44
    - 3.3.1.1 Eigenvalues . . . 44
    - 3.3.1.2 Mean Diffusivity . . . 45
    - 3.3.1.3 Fractional Anisotropy . . . 45

3.3.1.4 Diffusion Tensor Imaging . . . 46
3.4 Diffusion Spectroscopy . . . 47
3.4.1 History of Diffusion Spectroscopy . . . 47
3.4.2 Diffusion Tensor Spectroscopy . . . 48
3.4.3 Diffusion Spectroscopy Sequences . . . 49
3.4.4 PRESS vs. STEAM . . . 51

4 Methods **52**
4.1 Introduction . . . 52
4.2 Acquisition . . . 52
4.3 Postprocessing Methods . . . 55
4.3.1 Single Average Phase Correction . . . 56
4.3.1.1 NAA vs. Water Phase Correction . . . 57
4.4 Analysis . . . 60
4.4.1 Calculating Peak Intensity . . . 60
4.4.2 Calibration using a Phantom . . . 64

II Experiments **66**

5 Trace Apparent Diffusion Coefficient of Metabolites in Human Brain **67**
5.1 Introduction . . . 67
5.2 Methods . . . 68
5.3 Results . . . 74
5.4 Discussion . . . 76

6 Diffusion Tensor Spectroscopy (DTS) of Human Brain **82**
6.1 Introduction . . . 82
6.2 Methods . . . 83
6.3 Results . . . 87
6.4 Discussion . . . 90
6.5 Summary . . . 96

7 Anisotropic Diffusion of Metabolites in Peripheral Nerve using Diffusion Weighted Magnetic Resonance Spectroscopy at Ultra-High Field **97**
7.1 Introduction . . . 97
7.2 Methods . . . 99
7.2.1 Nerve Sample Preparation . . . 99
7.2.2 NMR Experiments . . . 100
7.3 Results . . . 103
7.4 Discussion . . . 105
7.5 Conclusions . . . 111
7.6 Addendum to Published Paper . . . 111
7.6.1 Methods . . . 111
7.6.2 Results . . . 111

8 Diffusion Tensor Spectroscopy of Myo-Inositol: Implications for the Measurement of FA **117**
8.1 Introduction . . . 117
8.2 Methods . . . 119
8.2.1 Phantom Work . . . 120
8.2.2 In-Vivo Work . . . 121
8.2.3 Alcohol Work . . . 124
8.3 Results . . . 128
8.3.1 In-Vivo Work . . . 128
8.3.2 Alcohol Work . . . 129
8.4 Discussion . . . 131
8.4.1 In-Vivo Work . . . 131
8.4.2 Alcohol Work . . . 134
8.5 Addendum . . . 136

9 Single Shot Diffusion Trace Spectroscopy 137
9.1 Introduction . . . 137
9.2 SS-PRESS sequence . . . 140
9.2.1 Phantom Work . . . 140
9.2.1.1 Isotropic Phantom . . . 142
9.2.1.2 Anisotropic Phantom . . . 142
9.2.2 In Vivo Work . . . 144
9.3 STEAM sequences . . . 146
9.3.1 The Sequences . . . 146
9.3.2 Results and Discussion . . . 148
9.3.2.1 Isotropic Phantom . . . 148
9.3.2.2 Anisotropic Phantom . . . 150
9.4 Summary . . . 152

III Conclusions and Future Directions 153

10 Concluding Remarks 154
10.1 Summary . . . 154
10.1.1 Trace ADC in Human Brain . . . 154
10.1.2 DTS of Human Brain . . . 155
10.1.3 DW-MRS of Frog Sciatic Nerve . . . 155
10.1.4 DTS of Myo-Inositol: Implications for the Measurement of FA . . . 156
10.1.5 Single-Shot Diffusion Trace Spectroscopy . . . 156
10.2 Limitations . . . 156
10.2.1 Trace ADC in Human Brain . . . 156
10.2.2 DTS of Human Brain . . . 157
10.2.3 DW-MRS of Frog Sciatic Nerve . . . 158
10.2.4 DTS of Myo-Inositol: Implications for the Measurement of FA . . . 159
10.2.5 Single-Shot Diffusion Trace Spectroscopy . . . 159
10.3 Future Directions . . . 160
10.3.1 Single Shot Diffusion Trace Spectroscopy . . . 160
10.3.1.1 Acute Cerebral Ischemia . . . 161
10.3.1.2 Cancer . . . 161
10.3.1.3 Parkinson's Disease . . . 161
10.3.2 The Future of DW-MRS in Brain . . . 162

Bibliography 162

List of Tables

2.1 T_1 and T_2 values in human brain at 3 T 14
2.2 Metabolite concentration changes in a variety of diseases 35

4.1 Preliminary DW-MRS measurements in the human brain 54
4.2 Previous Data and Our Corrected Results in Human Brain 55
4.3 Testing of three separate phase correction methods on two regions in human brain. 59
4.4 Diffusion measurements using two different quantification methods 62

5.1 Phantom measurements of NAA, Cr, and Cho 69
5.2 Trace/3 ADC measurements of NAA, tCr, and CHo in three different brain regions using two different phase correction methods 73
5.3 An intra- and intersubject comparison for the SWM region 76
5.4 In-vivo SNR values for each region 79
5.5 ADC values calculated with the proposed NAA phasing routine on single average spectra which were simulated with random phase errors and various SNR 79

6.1 Phantom measurements of NAA, Cr, and Cho 88
6.2 Diffusion measurements from all six regions in human brain 91

7.1 In-vitro diffusion measurements of NAA, Cr, Cho, Pcr, Tau, Glu, and Gln . 104
7.2 ADC values perpendicular (X and Y) and parallel (Z) to the long axis of the frog sciatic nerve as well as derived diffusion parameters, Trace/3 ADC and fractional anisotropy. 107
7.3 ADC values measured at 18.8T along the X, Y, and Z directions as well as the Trace/3 ADC for 19 different chemicals in aqueous solution (~25 mmol/L) 112

8.1 Trace/3 ADC and FA calculations for different ADC variabilities in the eigenvalues 119
8.2 Diffusion measurements in phantom 121
8.3 Diffusion measurements for the OGM region for both the low and high b-value studies 128
8.4 Diffusion measurements in the SWM and OGM regions for the high b-value study 129
8.5 1-octanol diffusion measurements for the 4 peak in the octanol spectrum each with a different SNR 130
8.6 Alcohol diffusion measurements for both the low and high b-value studies 130

9.1 Diffusion measurements from isotropic and anisotropic phantom 143
9.2 Diffusion measurements using three different single-shot sequences in isotropic phantom 149
9.3 Diffusion measurements using LDT-STEAM of water in an anisotropic phantom 151
9.4 Diffusion measurements of water in the X, Y, Z direction, and the single shot LDT-STEAM, from the body of the corpus callosum in human volunteers . 151

List of Figures

2.1 Body of randomly orientated nuclear magnets . . . 7
2.2 Nuclear magnets in the presence of a magnetic field . . . 8
2.3 The net magnetization in a static magnetic field . . . 8
2.4 Precession of a nuclear magnetic moment within an external magnetic field 10
2.5 The effect of B_1 on the net magnetization . . . 11
2.6 Ideal FID . . . 12
2.7 Real FID . . . 12
2.8 Linear field gradients, and their affect on the main magnetic field B_o. . . . 15
2.9 Single voxel localization . . . 16
2.10 Water spectrum in human brain . . . 18
2.11 Selective excitation . . . 20
2.12 Selective Inversion . . . 21
2.13 Water magnetization over time following inversion . . . 22
2.14 Water, gray matter, and white matter magnetization over time in a dual inversion sequence . . . 23
2.15 The effect of pre-saturation on the water magnetization in the transverse plane . . . 23
2.16 Complete Neuron Cell Diagram . . . 25
2.17 Cells of Central Nervous System . . . 26
2.18 Typical metabolite spectrum from human brain at 3 T . . . 27
2.19 Typical metabolite spectrum from frog sciatic nerve at 18.8 T . . . 27
2.20 N-acetyl aspartate . . . 28
2.21 Creatine . . . 30
2.22 Choline . . . 31
2.23 Myo-inositol . . . 31
2.24 Glutamate and Glutamine . . . 32
2.25 Taurine . . . 33
2.26 Metabolite Spectra at 18.8 T . . . 34

3.1 The spin echo pulse sequence . . . 37
3.2 A diffusion weighted spin echo pulse sequence . . . 38
3.3 The effect of diffusion on the transverse magnetization during a spin-echo pulse sequence . . . 39
3.4 Water spectra at increasing diffusion sensitization . . . 40
3.5 Metabolite spectra at increasing diffusion sensitization . . . 40
3.6 Diffusion attenuation curves . . . 42
3.7 Isotropy and Anisotropy Diagrams . . . 43
3.8 The visualization of the diffusion tensor with an ellipsoid . . . 45
3.9 A diffusion tensor imaging colormap . . . 46
3.10 An example of fiber tractography . . . 47
3.11 Diffusion weighted PRESS sequence . . . 49
3.12 Diffusion weighted STEAM sequence . . . 50

4.1 STEAM pulse sequence used for the majority of studies . . . 53
4.2 PRESS pulse sequence used for some of studies . . . 54
4.3 An overplot of 64 single average diffusion-weighted spectra and the spectrum produced by the sum of those 64 single averages . . . 56

4.4 An overplot of 64 single average diffusion-weighted spectra and the spectrum produced by the sum of those 64 single averages before and after phase correction . . . 57
4.5 Example spectra from three different phase correction methods . . . 60
4.6 Peak height calculation example diagram . . . 61
4.7 Diffusion measurements using two different quantification methods . . . 63
4.8 Metabolite spectra in phantom . . . 64
4.9 Diffusion attenuation curves for creatine and water in phantom . . . 65

5.1 Diffusion weighted STEAM sequence used . . . 69
5.2 Phase corrections which were required for both phantom and in-vivo . . . 71
5.3 Example spectra at low and high b-values for each of the 3 regions . . . 72
5.4 An overplot of 64 single average diffusion-weighted spectra and the spectrum produced by the sum of those 64 single averages before and after phase correction . . . 75
5.5 The effect of SNR on the calculation of the metabolite ADCs . . . 81

6.1 The six brain regions that were examined . . . 85
6.2 Example spectra taken from two of the regions used in human brain . . . 88
6.3 Trace/3 ADC values of NAA, tCr, and Cho from the six different brain regions 89
6.4 FA values of NAA, tCr, and Cho from the six different brain regions . . . 89
6.5 Diffusion directional information obtained for NAA . . . 92

7.1 Diagram of the setup for the 5 mm NMR tube . . . 99
7.2 Over-plotted Phantom spectra of NAA, Creatine and Phosphocreatine, Choline, Glutamate, Glutamine, Taurine, and Lactate . . . 102
7.3 Changes in Creatine and Phosphocreatine over time in dying nervous tissue 103
7.4 Example spectra from excised frog sciatic nerve at 18.8 T . . . 105
7.5 Diffusion attenuation curves for Phantom, NAA, tCr, Cho, Tau, and Glx . . 106
7.6 ADC vesrsus molecular weight in aqueous solutions of 19 different metabolites . . . 113
7.7 Metabolite Spectra for NAA, Glu, Cr, Gln, Cho, Tau, and mI . . . 114
7.8 Metabolite Spectra for Glutathione, Phosphocreatine, Glycerophosphocholine, N-Acetyl Aspartate Glutamate, Phosphorylcholine, and Scyllo-Inositol . . . 115
7.9 Metabolite Spectra for Phosphoethanolamine, Glucose, Lactate, Alanine, Aspartate, and GABA . . . 116

8.1 Diffusion-weighted PRESS sequence . . . 120
8.2 Example spectra from phantom for NAA, Cr, Cho, and mI . . . 121
8.3 Voxel localization for the two regions used . . . 122
8.4 Example spectra from the low and high b-value study in the OGM region . 123
8.5 Example spectra from two different directions in the SWM region . . . 123
8.6 Sixty-four single average and summed spectra of NAA using either the water phase correction method or the NAA phase correction method . . . 125
8.7 Sixty-four water phase corrected single average spectra of NAA for the OGM region at the two max b-values used . . . 125
8.8 Example Spectra from 1-Octanol at the 4 different b-values used in this study 126
8.9 Example Spectra from 1-propanol, 1-butanol, 1-pentanol, 1-hexanol, 1-octanol, and 1-nonanol. . . . 127
8.10 Fractional anisotropy versus Trace/3 ADC for both the low and high b-value study . . . 131
8.11 Directional preference of NAA in the SWM for the 5 volunteers . . . 134

9.1 Different bipolar gradient schemes used for calculating the Trace/3 ADC in a single shot . . . 138
9.2 Pulse sequence with a long diffusion time for single-shot diffusion trace spectroscopy . . . 139
9.3 A single shot diffusion trace spectroscopy sequence . . . 140
9.4 DW-PRESS sequences used for the measure of diffusion in the X, Y, and Z Direction. . . . 141

9.5 Example spectra taken from low to high b in the human brain at 3T using the SS-PRESS method 144
9.6 Summed spectra indicating a much greater diffusion attenuation than expected 145
9.7 Overplot of 64 single average spectra from NAA 146
9.8 The single shot STEAM sequence (SS-STEAM) 147
9.9 The bipolar STEAM sequence (BP-STEAM) 148
9.10 The long diffusion time STEAM sequence (LDT-STEAM) 148

List of Symbols and Abbreviations

$\Delta - \delta/3$ Diffusion Time, page 42

ΔE Energy difference, page 10

Δ Diffusion gradient separation, page 42

δ Diffusion gradient length, page 42

ϵ_1, ϵ_2, ϵ_3 eigenvectors of the diffusion tensor, page 45

γ Gyromagnetic Ratio, page 8

$\hbar$ Planck's constant divided by 2π, page 7

ν Frequency in Hz, page 10

$\omega_\circ$ Larmor Frequency, page 10

ω Frequency in rads, page 10

σ Shielding Constant, page 18

$\vec{\mu}$ Magnetic Moment, page 7

$\vec{B}$ Static Magnetic Field, page 9

$\vec{D}$ The diffusion tensor, page 45

$\vec{M}$ Net magnetization, page 8

^{1}H Hydrogen, page 3

h Planck's constant, page 7

I Spin operator, page 7

λ_1, λ_2, λ_3 eigenvalues of the diffusion tensor, page 45

ADC Apparent Diffusion Coefficient, page 43

b the b-value, diffusion sensitization factor, page 42

B_1 Radio frequency magnetic field, page 11

CHESS CHEmical Shift Selective imaging, page 24

Cho Choline, page 5

CNS Central Nervous System, page 25

Cr Creatine, page 5

CSF Cerebral Spinal Fluid, page 22

D Diffusion Coefficient, page 41

D_{xx}, D_{yy}, D_{zz} Diagonal elements of the diffusion tensor, page 45

D_{xy}, D_{xz}, D_{yz} Off-diagonal elements of the diffusion tensor, page 45

DTI Diffusion Tensor Imaging, page 5

DTS Diffusion Tensor Spectroscopy, page 5

DW-MRS Diffusion Weighted Magnetic Resonance Spectroscopy, page 4

DWI Diffusion Weighted Imaging, page 4

FA Fractional Anisotropy, page 46

FID Free Induction Decay, page 11

G Gradient strength, page 16

Gln Glutamine, page 27

Glu Glutamate, page 27

Glx Glutamate and Glutamine, page 27

Hz Hertz, page 10

J Joules, page 8

k Boltzmann constant, page 8

M_z Longitudinal magnetization, page 11

M_{xy} Transverse magnetization, page 11

MD Mean Diffusivity, page 46

mI Myo-Inositol, page 4

MR Magnetic Resonance, page 3

MRI Magnetic Resonance Imaging, page 3

MRS Magnetic Resonance Spectroscopy, page 3

NAA N-Acetyl Aspartate, page 4

NMR Nuclear Magnetic Resonance, page 3

PNS Peripheral Nervous System, page 25

ppm Parts per million, page 18

PRESS Point REsolved SpectroScopy sequence, page 17

RF Radio Frequency, page 11

S Signal Intensity, page 41

SNR Signal to Noise Ratio, page 3

STEAM STimulater Echo Acquisition Mode sequence, page 17

T Tesla, page 8

T_1 Longitudinal relaxation, page 14

T_2 Transverse relaxation, page 14

Tau Taurine, page 27

tCr Creatine and Phosphocreatine, page 5

TE Echo Time, page 52

TI Inversion Time, page 22

TM Mixing Time, page 52

TMS Tetra-Methyl Silane, page 18

TR Repetition Time, page 52

Trace/3 ADC Mean Diffusivity, page 46

$X\rho$,$Y\rho$,$Z\rho$ Rotating Frame, page 11

X,Y,Z Cartesian coordinate system - Lab Frame, page 11

Part I

Introduction

CHAPTER 1

PRELIMINARY REMARKS

1.1 INTRODUCTION TO THE THESIS

The work in this thesis merges two areas of research in the field of Nuclear Magnetic Resonance (NMR), namely the combination of Magnetic Resonance Spectroscopy (MRS) with the measurement of diffusion in-vivo. While these topics will be discussed in depth in the upcoming chapters, a brief overview of some the previous research in this subject area will be discussed first.

1.1.1 SPECTROSCOPY

NMR is a non-invasive method for examining human tissues in-vivo. The "N" in NMR refers to the nucleus of the atom, which is what gives rise to the magnetic resonance (MR) phenomenon. NMR has been used by chemists and physicists for years for examining a wide range of liquids and solids. In 1973, image formation using NMR was introduced and was the birth of Magnetic Resonance Imaging (MRI) [1]. MRI has become indispensable in the clinical realm because of its non-invasive nature (i.e. no ionizing radiation is used, unlike X-rays) as well as its ability to provide a variety of different tissue contrast that can be used to highlight different pathologies.

MRS allows us to examine the metabolites (i.e. chemicals other than water) in living tissue non-invasively. The most common nucleus examined using MRS is the hydrogen atom (^{1}H). ^{1}H has been the nucleus of choice because of its high sensitivity to the MR phenomenon as well as its high natural abundance in the human body. ^{1}H-MRS therefore, has played an important role in the study of a variety of different diseases, such as Parkinson's [2–4], Multiple Sclerosis [5, 6], Stroke [7], and Cancer [8]. MRS also has the ability to branch out and not only perform studies using the ^{1}H, but also ^{31}P [9, 10], ^{13}C [11], and ^{19}F [12] to name a few. Despite the variety of different techniques and

molecules we can examine using MRS, MRS is still not employed routinely in the clinical realm. The main limitation of MRS is the low signal to noise ratio (SNR), which is due to the molecular concentration of the metabolites being on the order of mmol/L, whereas the water concentration is $\sim$55 mol/L. The SNR can, of course, be improved by averaging; however with patients, this may not be possible due to time constraints. Despite these challenges MRS can provide greater insight, when compared to MRI of water, into the diseases mentioned above, because of the simultaneous information available from a variety of metabolites.

1.1.2 Diffusion

Diffusion is the random thermally driven motion of molecules in a given environment. Water molecules in human brain, in the time period of an NMR experiment, will diffuse around and sample their local environment, which allows inferences to be made about the microstructural characteristics about that environment.

Measuring diffusion in NMR was first introduced in 1954 [13]. Presently, measuring the diffusion of water using NMR, called Diffusion Weighted Magnetic Resonance Imaging (DW-MRI) or Diffusion Weighted Imaging (DWI) for short, has been used to examine a variety of different diseases such as acute stroke [14, 15], cancer [16, 17], Parkinson's [18], and multiple sclerosis [17, 19–21]. It was shown in 1990, that diffusion in a cat brain was anisotropic (i.e. has a directional preference) [22], which led to the invention of Diffusion Tensor Imaging (DTI) in 1994 [23, 24]. Measuring the diffusion tensor of water allows one to examine a variety of diffusion characteristics all at once, such as the directional preference, the mean diffusivity, and the degree of anisotropy from a given area or voxel. DTI has allowed the extensive examination of fiber tracts [25] in both diseased [26] and normal [27] brain. If we take this investigation one step further and examine the metabolites in the human brain, what additional information will we be able to get?

1.1.3 Diffusion Weighted Magnetic Resonance Spectroscopy (DW-MRS)

DWI of tissue water is known to include contributions from rapidly exchanging intra- and extracellular water, which makes compartment specific interpretation of diffusion characteristics rather complex. Metabolites such as N-acetyl aspartate (NAA) and myo-inositol (mI) are thought to be localized in specific intracellular compartments in the human brain; mI is primarily located in glial structures, whereas NAA is primarily located in the neurons and axons. Therefore, examination of the metabolites, instead of water, will provide a greater insight into the underlying intracellular environment and possibly different com-

partments within the intracellular environment.

Prior to the work presented in this thesis only a few groups had performed DW-MRS on human brain [28, 29]. In both of those studies the examination was rather limited, with single direction measurements in a single area of the human brain. The second paper [29], expanded the single direction measurements to different pathologies, acute stroke and brain tumors.

The purpose of the work presented here was to examine the diffusion characteristics of the primary visible metabolites NAA, creatine and phosphocreatine (tCr), and choline (Cho) in the human brain at 3T, using a variety of different sequences, and to establish a baseline for comparison between research groups as well as different pathologies.

1.1.4 Overview

The introduction of this thesis has been divided into three chapters: Chapter 2 is an in depth look at spectroscopy, from the phenomenon of magnetic resonance to the production of a spectrum resulting from various metabolites. Chapter 3 is an in depth look at diffusion in NMR, from the history of diffusion in NMR to the sequences used to measure diffusion. Chapter 4 is a detailed description of the methods used in the acquisition and analysis of the diffusion MRS data, which are consistent throughout the experiments unless otherwise mentioned.

The experimental section is divided into 5 chapters: Chapter 5 is concerned with the determination of the mean diffusivity of three metabolites in the human brain. The mean diffusivity requires three diffusion measurements in three orthogonal directions. This study was used to test a diffusion weighted sequence that was created as well as the reproducibility of that sequence. The mean diffusivity was measured in three distinct areas, two gray matter and one white matter. Chapter 6 is concerned with the determination of the diffusion tensor of three metabolites in the human brain. This is the first reported measurement of the diffusion tensor of metabolites, and has been termed Diffusion Tensor Spectroscopy (DTS). DTS was performed in six different regions in the brain, two gray matter and four white matter. Chapter 7 is concerned with measurements of the degree of anisotropy and mean diffusivity of five different metabolites in the frog sciatic nerve at 18.8 T. This study allowed investigation of the diffusion of metabolites in a much easier model environment. Chapter 8 is concerned with the diffusion measurement of the metabolite myo-inositol in human brain, which is complicated due to the relatively low signal. A specific sequence was required for this measurement, as well as improvements were made for accurate measurement of the degree of anisotropy. Chapter 9 is concerned with acquisition of the mean diffusivity of the metabolites in a single shot, which will

allow for clinical experimentation. A shorter diffusion spectroscopy sequence is required because the time for the previous human experiments was approximately 75 minutes, which is too long for most clinical work.

Chapter 10 will conclude with a brief summary of the work and some remarks on the limitations of the experiments performed, as well as some future directions.

CHAPTER 2

SPECTROSCOPY

2.1 SPIN AND MAGNETIC MOMENT

A given nucleus, in order to be useable in NMR, must be magnetic (i.e. must have a magnetic moment ($\vec{\mu}$)). The nucleus of an atom is composed of protons and neutrons (called nucleons). Protons give a nucleus its static positive charge, and both the protons and neutrons contribute to the nuclear mass; furthermore, the protons and neutrons contribute to the magnetic moment as well. The neutron has no net static charge; however, it still has a magnetic moment, and from this fact, one can deduce that the overall static charge is not responsible for the magnetization, but rather that the circulating currents internal to the nucleus are relevant. Whether or not a given atom has a nuclear magnetic moment, as it turns out, depends on the number of protons and neutrons in the given nucleus of that atom. If the number of protons and neutrons are both even (called an EVEN-EVEN nucleus) then they pair off with their like nucleons and no nuclear magnetic moment results. However, if the number of one or both of the nucleons is odd (called an EVEN-ODD, ODD-EVEN, or ODD-ODD nucleus) a nuclear magnetic moment will result. The hydrogen nucleus is composed of one proton and no neutrons and would be considered an (ODD-EVEN) nucleus, and therefore, it has a nuclear magnetic moment. Hydrogen (^{1}H) as it turns out is the main focus of this thesis.

Not all nuclei are the same, a given nucleus, which has a magnetic moment, will have a "spin angular momentum" or "spin", (I), which is measured in units of $\hbar$ ($\hbar = h/2\pi = 1.055 \times 10^{-34}$ J s rad^{-1}), where h is the Planck's constant ($h = 6.63 \times 10^{-34}$ J s). The magnitude, therefore, of the spin angular momentum of a given nuclei is $I\hbar$. For all nuclei we find that I takes on one of the integral or half integral values from $1/2$ to $9/2$. The spin (I) for the hydrogen nucleus is $1/2$. Quantum mechanics describes that a nucleus of spin I will have $2I + 1$ possible orientations. Therefore, for the hydrogen nucleus with a

spin of 1/2, we will have two possible energy levels ($\pm 1/2$).

The nucleus of the hydrogen atom has a positive charge and is spinning, which generates a small magnetic field. Therefore, the nucleus possesses a magnetic moment, $\vec{\mu}$, which is proportional to the overall spin of the hydrogen nucleus (Equation 2.1).

$$\vec{\mu} = \gamma I \hbar \tag{2.1}$$

where $\hbar$ is the Planck constant divided by 2π and γ, the gyromagnetic ratio, is a nucleus specific constant. In the case of hydrogen γ is 2.6752×10^8 rad $s^{-1}T^{-1}$.

2.2 Preparation

Since, in the majority of the spectroscopy studies, the hydrogen atom is the species of interest, the spin quantum number will be $I = 1/2$. Hydrogen, as it turns out, is the simplest case. Now if you imagine that a body (a person or sample) as being a bag of little nuclear magnets, then at thermal equilibrium the net magnetization $\vec{M}$ of that body is zero because of the random orientation of these nuclear magnets (Fig. 2.1).

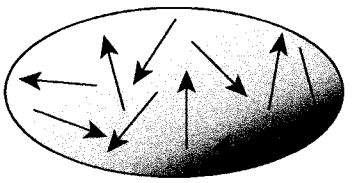

FIGURE 2.1: A body of randomly orientated nuclear magnets. At thermal equilibrium net magnetization $\vec{M} = 0$

If we place this body of nuclear magnets inside a uniform, static, magnetic field (B_o), this random orientation of the nuclear magnets will change (Fig. 2.2). The magnetic moments of the nuclear magnets will either align parallel or anti-parallel to the main magnetic field B_o.

A slim majority of the magnetic moments will align parallel to the magnetic field, which will cause a net magnetic moment (M_o,) within the body, to align with the external magnetic field B_o.

$$M_o = n_\downarrow / n_\uparrow = \exp\{-E_z/kT\} \tag{2.2}$$

Equation 2.2 arises from classical Boltzmann statistics (k = Boltzmann constant = 1.38 x 10^{-23} J K^{-1} and T is the temperature in Kelvins). In this equation E_z is the energy difference between the parallel ($n_\uparrow$) and anti-parallel ($n_\downarrow$) orientation of the magnets in

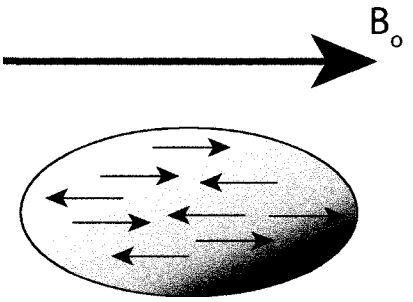

FIGURE 2.2: The same body of magnets from Figure 2.1 in the presence of the magnetic field B_o causes the net magnetization to no longer be zero

Figure 2.2. Equation 2.2 can also be represented as a net magnetization M_o, which is the sum of all the magnetic moments or spins ($\vec{\mu}$) in the body (Equation 2.3), aligned along the z-axis (i.e. the axis of the bore of the magnet) in a cartesian coordinate system or lab frame as it is sometimes called (Fig. 2.3).

$$\vec{M} = \sum \vec{\mu} \tag{2.3}$$

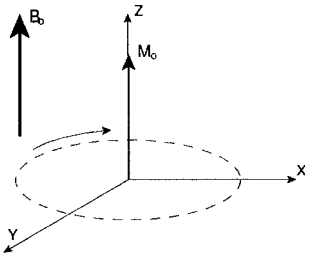

FIGURE 2.3: The net magnetization M_o aligned with the main magnetic field in the MRI scanner (B_o)

Equation 2.3 is the net magnetization for all the magnetic moments within the body. However, what about one of those magnetic moments, how does $\vec{\mu}$ interact with the main magnetic field? The interaction energy of a single nuclear magnetic moment $\vec{\mu}$, with an external magnetic field $\vec{B}$, is given by equation 2.4.

$$E = -\vec{\mu} \bullet \vec{B} \tag{2.4}$$

Furthermore, if we include the definition of $\vec{\mu}$ from equation 2.1 we find the interaction energy in equation 2.5.

$$E = -\gamma I \hbar B \tag{2.5}$$

As mentioned above, the spin (I) of the nucleus we are examining (^{1}H) is $\pm 1/2$, and therefore the interaction energy for the spin is either $E_{|\beta>} = \gamma\hbar B_\circ/2$ or $E_{|\alpha>} = -\gamma\hbar B_\circ/2$, Where I=-1/2 would be the anti-parallel state (β) and I=1/2 would be the parallel state (α). The energy difference between the α and the β state therefore would be given by equation 2.6.

$$\Delta E = E_{|\beta>} - E_{|\alpha>} = \gamma\hbar B_\circ \tag{2.6}$$

At $B_\circ$ = 1.5 T, a typical clinical magnetic field strength, the ΔE for protons ($\gamma = 2.6752 \times 10^8$ rad $s^{-1}T^{-1}$) in the human brain (i.e. T = 310 K = 37°C) is 4.23×10^{-26} J. Which yields an $n_\downarrow/n_\uparrow$ (Equation 2.2) of 0.99999011. The inverse ratio is 1.0000098. Therefore for every 10,000,000 spins in the anti parallel state there are 10,000,098 in the parallel state. This is a small excess of parallel spins; however, if we consider the number of water protons in a given mL ($\sim 7 \times 10^{22}$), then the number of excess protons aligned with $B_\circ$ is $\sim 7 \times 10^{17}$. For the same situation at $B_\circ$ = 3 T, the field strength used in the majority of this thesis, that values jumps to 1.4×10^{18}, and hence the benefit of going to a higher field; it increases the available signal. You can also change this population difference by using a nuclear species (i.e. different γ) or by decreasing the temperature, which may or may not be practical in a given situation.

The magnetic moments that give rise to $M_\circ$, which is aligned along the Z-axis, are actually not stationary they precesses around the main magnetic field, $B_\circ$. This precession happens because the magnetic field induces a torque on any given magnetic moment. This torque is given by equation 2.7, where $\times$ is the vector cross product.

$$\vec{\tau} = \vec{\mu} \times \vec{B} \tag{2.7}$$

The ^{1}H nucleus' angular momentum causes this torque and allows the magnetic moment to precess around the main magnetic field $B_\circ$, as shown in Fig. 2.4. Because the spin angular momentum can either be positive or negative the nuclear magnetic moment will either precess around the positive or negative z-axis.

If we look back at equation 2.6, we have a relationship between the energy difference between the spin states (ΔE), the gyromagnetic ratio (γ), and the external magnetic field ($B_\circ$), and from that, the frequency of precession can be determined. Energy is related to frequency by the equation $E = h\nu$; therefore, $\gamma\hbar B_\circ/2\pi = h\nu$. If we keep in mind that the units of ν are Hz and that $\nu = \omega/2\pi$ we can determine the frequency of precession in rad/s (Equation 2.8).

$$\omega_\circ = -\gamma B_\circ \tag{2.8}$$

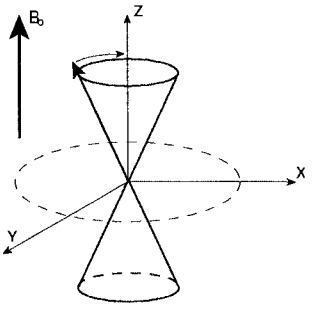

FIGURE 2.4: A given nuclear magnetic moment when placed within a external magnetic field (B_o) will start to precess around the external magnetic field due to a torque induced because of the nucleus' angular momentum.

The frequency of nuclear precession in NMR is known as the Larmor frequency (ω_o).

2.3 EXCITATION

Now that the magnetization has been prepared, and is precessing at the Larmor frequency; it must be excited so that data can be acquired. Excitation in NMR means that the net equilibrium magnetization ($M_z = M_o$) has been tipped from the positive z-axis, such that it has a transverse XY component (M_{xy}), it is the transverse magnetization alone that we detect in NMR. If a Radio Frequency (RF) coil that has been tuned to the Larmor frequency of ^1H is placed around the body/sample of tiny ^1H magnets in Figure 2.2, and if those nuclear magnetic moments have been tipped into the transverse plane rotating at the Larmor frequency, then they will induce an oscillating electromotive force (EMF) in the RF coil. This induction is caused by the change in magnetic flux over time (i.e. Faraday's law of electromagnetic induction). The signal that is detected is in the time domain and known as the Free Induction Decay (FID). This FID consists of a sinusoid oscillating at ω_o. In the frequency domain, which we obtain by performing a Fourier transform on the FID, this signal is represented by a delta function at ω_o. This frequency space representation is called a spectrum. In the ideal case the spectrum would be a delta function (i.e. a single vertical line at the Larmor frequency); however, in a real spectrum those delta functions change into Lorentzian lineshapes because of the decay of the sinusoidal oscillation over time. This decay over time will be discussed in section 2.4.

Tipping the equilibrium magnetization into the transverse plane is quite involved. A second magnetic field, B_1, is added, and will be required to rotate around the Z-axis at the same speed as the precession frequency, ω_o. In the presence of B_o the B_1 field perturbs M_o from its equilibrium orientation. This B_1 field is created in the RF coil surrounding the

bag of nuclear magnets by producing a time varying RF pulse that is perpendicular to B_o and rotates at the same frequency as the precession of the hydrogen nucleus; when these conditions are satisfied the B_1 field will apply a torque on M_o causing its angle with the static magnetic field to change. If this B_1 field is switched off right when the magnetization is fully in the transverse plane (i.e. $M_z \rightarrow 0$ and $M_{xy} \rightarrow M_o$), it is called a 90° or $\pi/2$ pulse. Instead of a regular coordinate X, Y, Z axis with a precessing magnetization, it is easier to visualize by using a rotating coordinate axis that is spinning around the Z axis at the Larmor frequency and in that case the on-resonant magnetization will be stationary. The new coordinates $X\rho$, $Y\rho$, and $Z\rho$, are used to indicate this change in coordinate systems, which is known as the Rotating Frame (Fig. 2.5).

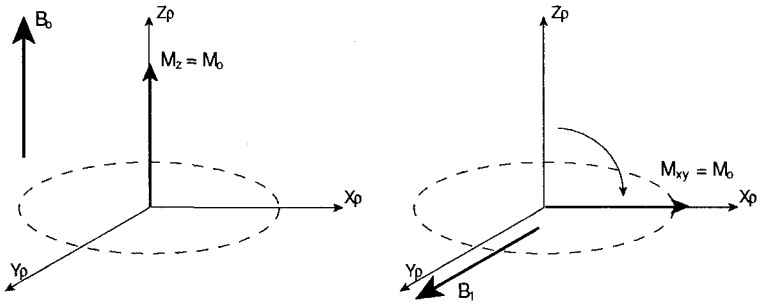

FIGURE 2.5: The effect of a B_1 field on the equilibrium magnetization. Shown in the rotating frame.

2.4 SIGNAL

In an ideal world, after the magnetization has been excited into the transverse plane, it would stay there forever rotating at the Larmor frequency at the magnitude M_o. This would be represented as a sinusoid oscillating at ω_o, Figure 2.6. However, in the real world, this FID would be represented more accurately by Figure 2.7.

In both Figures 2.6 and 2.7 the corresponding frequency spectra are also shown. The frequency spectra is the fourier transform of the FID. This decay in the FID comes from two sources, one of which will be discussed in detail in section 2.4.1. The other source comes from imperfections in the magnet design and construction, which can give rise to static inhomogeneities which lead to variations in the magnetic field. Since these decays are static they can be rephased throughout the experiment by the use of a spin echo. However, this only refocuses the static inhomogeneities.

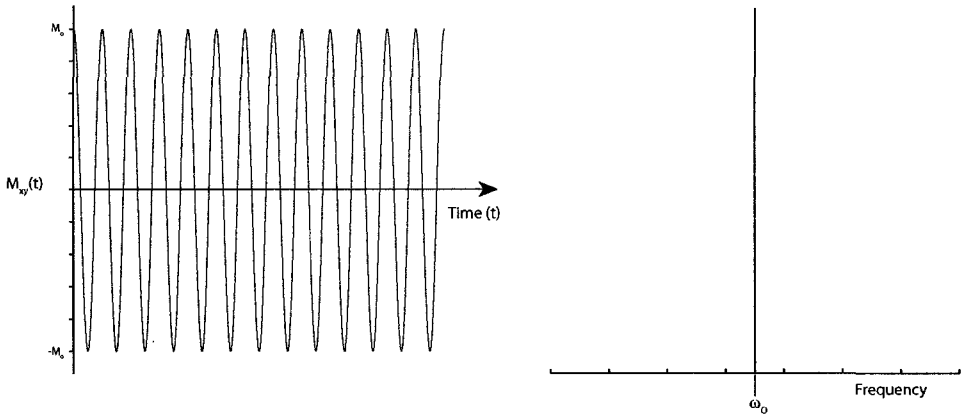

FIGURE 2.6: An ideal Free Induction Decay (FID) and corresponding frequency spectrum

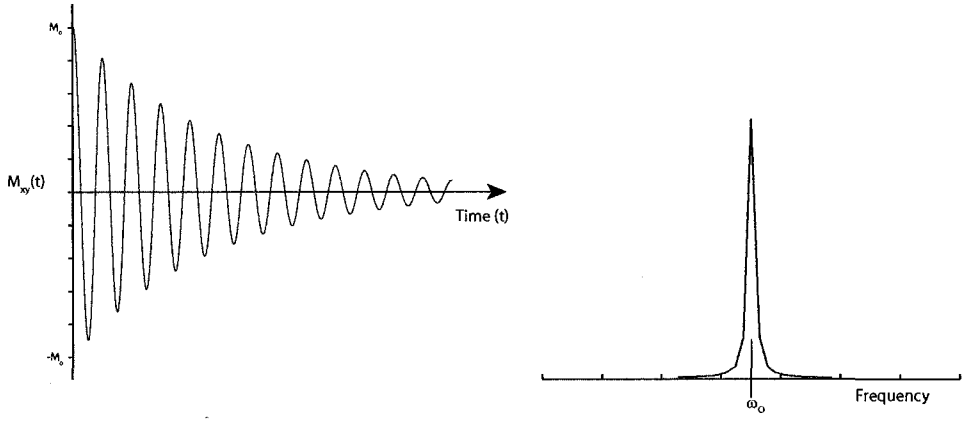

FIGURE 2.7: A real Free Induction Decay (FID) and corresponding frequency spectrum

Aside from refocussing the static inhomogeneities using a spin echo, the inhomogeneity of the field can be limited by the use of shim coils, which are designed to make the area of interest more homogeneous, since not every magnet automatically generates a uniform field. Shim coils are wrapped around the bore of the magnet, and magnetic fields produced by these coils are controlled by the operator which allows adjustments to be made to improve the overall field homogeneity.

The other source mentioned above is an irreversible decay, which is due to the relaxation of the transverse magnetization.

2.4.1 RELAXATION

Initially right after the $\pi/2$ pulse, $M_z = 0$ and $M_{xy} = M_o$. Both the M_z and the M_{xy} are in excited states and want to relax back to thermal equilibrium (i.e. $M_z = M_o$ and $M_{xy} = 0$).

M_z returning to its equilibrium state is called longitudinal relaxation, and M_{xy} decaying to 0 is called transverse relaxation.

2.4.1.1 Longitudinal Relaxation

Longitudinal relaxation as mentioned above refers to the magnetization in the Z direction returning to its thermal equilibrium state ($M_z = M_o$). This is governed by the following rate equation.

$$\frac{dM_z}{dt} = -\frac{(M_o - M_z(t))}{T_1} \tag{2.9}$$

T_1, in equation 2.9, is the called the longitudinal relaxation time. Solutions of the differential equation (Eq. 2.9) lead to an exponential dependence on the recovery of the magnetization. The following two equations show the recovery of M_z in two different scenarios: After a $\pi/2$ pulse (Eq. 2.10) and after a π pulse (Eq. 2.11).

$$M_z(t) = M_o\left(1 - \exp(-\frac{t}{T_1})\right) \tag{2.10}$$

$$M_z(t) = M_o\left(1 - 2\exp(-\frac{t}{T_1})\right) \tag{2.11}$$

Water protons in different brain tissues have slightly different T_1 values, and therefore, sequence timing can be altered to exhibit different contrast on images, which is a staple of NMR imaging. The T_1 is also important for water suppression which will be discussed in section 2.8.

2.4.1.2 Transverse Relaxation

Transverse relaxation as mentioned above is the decay of the magnetization in the transverse plane ($M_{xy} = M_o$, directly after a $\pi/2$ pulse). M_{xy} wants to return to its thermal equilibrium state of $M_{xy} = 0$. This is governed by the following rate equation.

$$\frac{dM_{xy}}{dt} = -\frac{M_{xy}(t)}{T_2} \tag{2.12}$$

T_2, in equation 2.12, is the called the transverse relaxation time. Solutions of the differential equation (Eq. 2.12) lead to an exponential dependence on the decay of the transverse magnetization. Since, the transverse magnetization is rotating in the transverse plane at the Larmor frequency and varying from M_{xy} to -M_{xy}, the equation governing the envelope (env) of that decay is Equation 2.13.

$$M_{xy}[env] = M_o \exp\left(-\frac{t}{T_2}\right) \tag{2.13}$$

Again, just like above with the T_1 relaxation time, water protons in different tissues also have different T_2 values, which also allow the sequence timings to be altered to take advantage of these timings.

T_1 values in biological tissue are of the order of seconds, whereas T_2 values are somewhat smaller, for water and metabolites at 3T T_2 values are $\leq$300 ms. Therefore, the transverse magnetization usually decays to zero before the longitudinal magnetization has fully recovered. Table 2.1 shows the approximate values for T_1 and T_2 for the metabolites and water in human brain at 3T [30, 31].

	Water	NAA	Cr	Cho
Gray Matter				
T_1 (ms)	1330	1470	1460	1300
T_2 (ms)	109	247	152	207
White Matter				
T_1 (ms)	832	1350	1240	1080
T_2 (ms)	79	295	156	187

TABLE 2.1: Approximate T_1 and T_2 values for Water, NAA, Cr, and Cho in the Human Brain at 3 T

2.5 SPATIAL LOCALIZATION

Since the magnetization has now been tipped successfully into the transverse plane, and is precessing about the z-axis at a rate of ω_o, information must be encoded into that precession that relates to position. A linear spatially varying magnetic field along the direction of the main magnetic field B_o is applied in order to encode spatial position. This linear spatially varying magnetic field has been termed a linear field gradient or gradient for short.

2.5.1 GRADIENTS

Gradients can be applied in all 3 axes, X, Y, or Z or a combination thereof. Linear field gradients are formed by adding or subtracting to the main magnetic field. In the isocenter of the magnetic field there is no magnetization added or subtracted by the addition of the gradient; however, for an X gradient, as you travel further and further from the isocenter, along the X-axis, the bigger the addition or subtraction from the main magnetic field, B_o (Figure 2.8A). The Y, and Z gradient have similar effect on B_o, Figures 2.8B, and 2.8C, respectively.

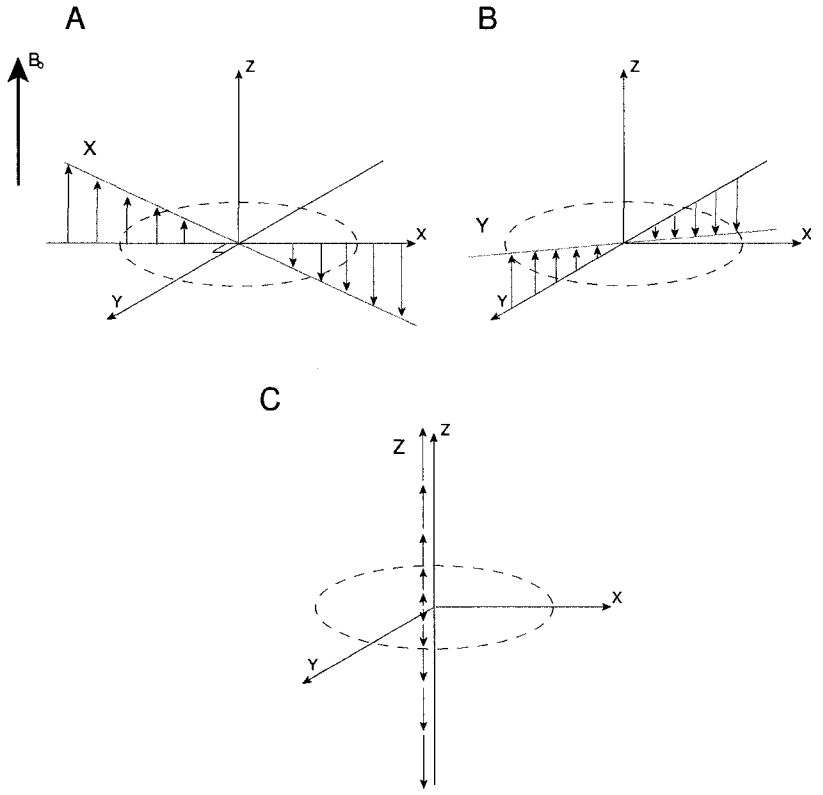

FIGURE 2.8: Linear field gradients, and their affect on the main magnetic field B_o.

If the addition or subtraction to the main magnetic field is termed B_z, and the gradient producing B_z is an X-gradient, then the equation for B_z is:

$$B_z = Gx \tag{2.14}$$

Where x is the position along the X-axis and G is the gradient strength usually reported in units of mT/m or G/cm. Then by applying the effect of B_z to the precession frequency by using equations 2.8 and 2.14, the new precession frequency can be calculated for all spins in position x (Equation 2.15), in which the total magnetic field applied at position x, therefore, would be $B_o + B_z$.

$$\omega = -\gamma (B_o + B_z) = \gamma (B_o + Gx) \tag{2.15}$$

By directly measuring the precessional frequencies, it can be determined what frequency is coming from which position along X because of the linear relationship between spatial position and precessional frequency.

2.5.2 Slice Selection and Single Voxel Localization

In an ideal case, when there is no linear field gradient on, then all spins would precess at the same frequency, ω_o, and the excitation would be non-selective. In order to excite a plane of the body a B_1 field must be applied in the presence of the B_o field; however, this time a linear magnetic field gradient is turned on during the B_1 RF pulse. This gradient, as mentioned in section 2.5.1, will cause the resonance frequencies of the spins to vary linearly depending on their position. A slice is then selected by first determining the center of the slice (x) and picking the appropriate carrier frequency for the RF pulse which corresponds to position x, then the bandwidth of the RF pulse is selected, which, together with the applied gradient strength, determines the thickness of the slice excited. These changes to the pulse sequence allow for the selective excitation of different slices in the brain.

For spectroscopy, the selection of three orthogonal slices is required, which will cause the excitation of a single voxel (i.e. a small cube). Figured 2.9 shows the voxel that gets excited at the intersection of three slices.

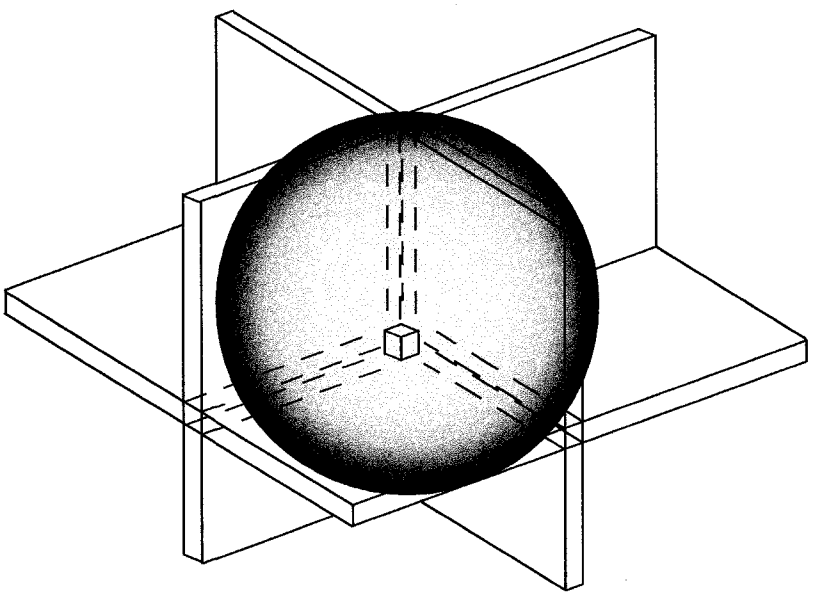

Figure 2.9: Single voxel localization, the voxel is excited by the three planes intersecting at the region specified in the body.

Two sequences are commonly used in single voxel excitation. One is the Point RESolved SpectroScopy (PRESS) sequence [32], and the other is the STimulated Echo Acquisition Mode (STEAM) sequence [33]. These sequences will be discussed in more detail and how they are used in diffusion spectroscopy in section 3.4.3; however, it should be

noted in this section that each of those sequences has 3 RF pulses which is a requirement for single voxel localization, since three intersecting slices must be excited. The intersection of the 3 slices, or voxel, is the only part of the body that gets refocussed by all three pulses.

2.6 Chemical Shift

In the Larmor frequency equation, Eq. 2.8, the gyromagnetic ratio is a species specific ratio, and different nuclei have unique Larmor frequencies. For example, the Larmor frequency at 3T of ^{13}C is 32.09 MHz where as ^{1}H is 127.67 MHz. These two frequencies are quite far apart and would require different RF coils tuned to their specific frequencies to collect data from either one. Protons (or ^{1}H atoms on molecules) are affected by their environment in such a way that the Larmor frequency is altered slightly. This slight change in frequency can be measured with the same RF coil, for Protons the chemical shift range at 3T is $\sim$10 ppm, but for the metabolites of interest in-vivo that ranges drops to $\sim$5 ppm. Since individual atoms are influenced by the distribution of the electrons in the chemical bonds of the molecule, a ^{1}H attached to the C-OH bond of an alcohol does not resonate at the same frequency as a ^{1}H on a C-CH_3 bond. This difference in frequency is known as the Chemical Shift.

The electron cloud surrounding a nucleus acts as a shield from B_o. This shield is formed because the B_o field induces circulations in the electron cloud, which generates a small magnetic field, B_i, that opposes B_o. This small field produced by the electron cloud is proportional to the main magnetic field, and therefore, can be calculated by equation 2.16, where σ is defined as the shielding constant.

$$B_i = \sigma B_o \tag{2.16}$$

The net magnetic field, B, acting on the nucleus is given by equation 2.17 and reflects the addition of the main magnetic field B_o and this new magnetic field formed from the induced circulations in the electron cloud, B_i.

$$B = B_o(1 - \sigma) \tag{2.17}$$

Therefore, the new precession frequency for this chemically shifted ^{1}H is determined by equation 2.18

$$\omega = -\gamma B_o(1 - \sigma) \tag{2.18}$$

The observed change in precession frequency, therefore, is dependent on B_o, which causes the chemical shift (i.e. change in frequency) to get larger with increasing field strength, which is actually quite beneficial for spectroscopy, since as B_o is increased the spread between the different molecules due to their intrinsic chemical shift increases, yielding a higher resolution. However, to allow accurate comparisons between different studies with differing B_o, the chemical shift is usually reported in units that are independent of B_o, namely ppm (parts per million). Ppm is determined by calculating the frequency of the molecules chemical shift minus a reference frequency divided by the spectrometer frequency (for 3T the frequency is 127.67 MHz). In ^1H the reference frequency is not actually a naked proton, but a molecule called TMS (Tetra-Methyl Silane) which was chosen because it does not overlap with other useful peaks. The ^1H protons on the water molecule have an approximate chemical shift of 4.75 ppm, and water is the most abundant molecule in the body, since people are approximately 55% water (50% adult females, 60% adult males [34]). Figure 2.10 is an example of a spectrum obtained from a person's brain in a single voxel.

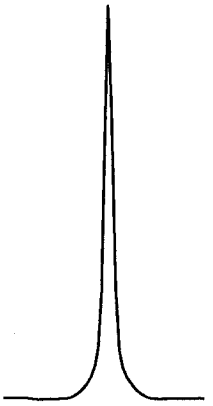

FIGURE 2.10: A spectrum from a single voxel in the human brain

The spectrum in Figure 2.10, while very high signal, and very high quality, is relatively boring. The exciting information is hidden in the baseline of the water peak, since the concentration of water in the brain is ~55 mol/L whereas metabolites (section 2.10) have concentrations on the order of mmol/L. This huge concentration difference makes it hard to measure the metabolites due to the dynamic range of the spectrometer, and therefore, the water peak needs to be suppressed without suppressing other valuable information from the metabolites.

2.7 Indirect Scalar Coupling (J-Coupling)

Scalar coupling is caused by the interaction of the electron bonds of neighboring nuclear spins. This phenomenon arises from the hyperfine contact interaction between a nucleus and an s-electron, which has a finite probability of existing at the nucleus [35]. Imagine two nuclei bonded together through an electronic covalent bond; if one of those two electrons is in the anti parallel alignment (to the nucleus), then, due to the Pauli exclusion principle, which states that two electrons in a covalent bond must have opposing states, and the second electron will align opposite the first (i.e. parallel to the original nucleus). Therefore, in a sense, the second nucleus can 'feel' the original nucleus, through this electronic interaction, and causes this indirect scalar coupling. This interaction, therefore, is sensitive to the various orientations of the nuclei, and causes the spectrum of an individual nuclei to split into a multiplet, and the amount of splitting is given by the scalar coupling constant, J, in unit of Hz.

The majority of metabolites in the brain exhibit this scalar coupling. There are many different subsets of scalar coupling, such as weak coupling, strong coupling, homonuclear coupling, and heteronuclear coupling. Weak coupling occurs when the chemical shift difference is much larger than the scalar coupling constant. If a spin $1/2$ nucleus is weakly coupled to n equivalent nuclei of spin $1/2$, then the resonance will split into $n+1$ lines, with intensities that follow a typical binomial distribution. A strong coupling system occurs when the chemical shift is of the same order of magnitude as the coupling constant. There is no general rule for the multiplicity structure of strongly coupled spins, but they can be calculated by using quantum mechanics. It should be noted that because the chemical shift increases as the B_o is increased, the degree at which two spins are strongly coupled together also decreases with B_o. Homonuclear coupling occurs when scalar coupling exists between two nuclei of the same species, whereas hetero nuclear coupling occurs when scalar coupling exists between two nuclei of different species. Glutamate/Glutamine, and Myo-Inositol exhibit strong homonuclear coupling, whereas the metabolites N-Acetyl Aspartate, Creatine, and Choline exhibit weak coupling. Heteronuclear coupling is always weak because the chemical shift difference is quite large.

2.8 Water Suppression

Water suppression is achieved by first selectively exciting the water peak, normally followed by one of two methods used to eliminate the water magnetization after it has been excited, inversion recovery, or pre-saturation. It has been shown that MRS can be per-

formed without water suppression [36–40], but these methods have intensive hardware demands and induced artifacts. A method using a two scan scheme proposed has eliminated some of those problems [41]. However this will add even more time to the current scan protocols, which are already long, and therefore typical water suppression is used in this thesis.

2.8.1 Selective Excitation

Before the water magnetization can be removed, thus allowing the metabolites hidden beneath to be seen; it must be selectively excited. Imagine two molecules, molecule A and molecule B, which resonate at different frequencies, ω_a and ω_b. In order to excite molecule A while leaving molecule B along the Z axis a soft pulse, which is usually a sinc pulse, is used. The Fourier transform of a sinc pulse is a rectangular profile, and therefore a sinc pulse in the time domain would transform into a rectangular profile in the frequency domain. By making the rectangular profile relatively small, only a small range of frequencies will be excited. Molecule A, therefore, can be selectively excited by choosing the appropriate carrier frequency (i.e ω_a) and an appropriate bandwidth, which determines the width of the rectangular profile in the frequency domain (Figure 2.11. Molecule B will not get excited, since its frequency was not within the range of excited frequencies.

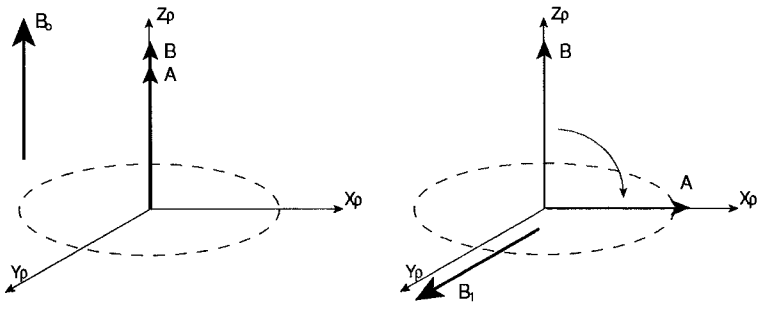

Figure 2.11: Selective excitation of molecule A

Allowing excitation of only a small range of frequencies allows the elimination of that molecule prior to the acquisition of the spectrum. Therefore, by exciting the water peak alone it facilitates the ability to remove the magnetization from the spectrum.

2.8.2 Inversion Recovery

One technique used to eliminate the water peak from a given spectrum is to selectively excite the water magnetization, which is completely analogous to the excitation of Molecule A in the above example. However, this time, instead of using a $\pi/2$ pulse for excitation, a π pulse is used, which causes the water magnetization to be completely inverted (i.e. aligned with the -Z axis, Figure 2.12). It is important to note that this is a selective inversion on the water peak, and therefore the metabolite signal will not be inverted, assuming that your metabolite of interest is not close, in chemical shift, to the water peak or it will also get inverted.

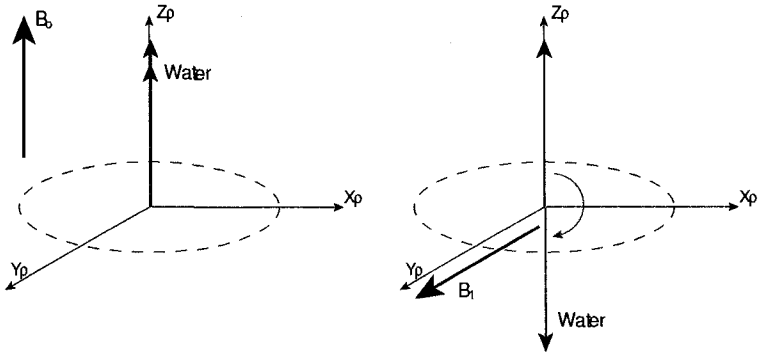

FIGURE 2.12: Selective inversion of Water to the -Z axis, While leaving the rest of the magnetization aligned along the +Z axis

Since the water magnetization has been excited, and is now aligned with the -Z axis, it will start to relax back to its thermal equilibrium state. If a time TI (Inversion Time) is defined to be when the magnetization is relaxed half way between M_0 and $-M_0$, then the net magnetization at time TI will be zero (Figure 2.13).

If the $\pi/2$ pulse is applied as soon as the TI time has elapsed then the magnetization from the water will not be excited into the transverse plane, and therefore, the metabolites will be visible and be able to be examined. In reality, the water magnetization has two or more different sets of T_1 values coming from the cerebral spinal fluid, white matter and gray matter. In practice it is useful to employ a dual inversion recovery in order to achieve adequate water suppression [42], the dual inversion needs to be optimized to get rid of the water signal from the cerebral spinal fluid (CSF), the gray matter, and the white matter.

For the sequences used in this thesis, we use the above technique. Figure 2.14 shows a plot of three T1 curves and the effect of the two inversion pulses. The approximate inversion times used for sequences in this thesis are approximately 1400 ms and 200

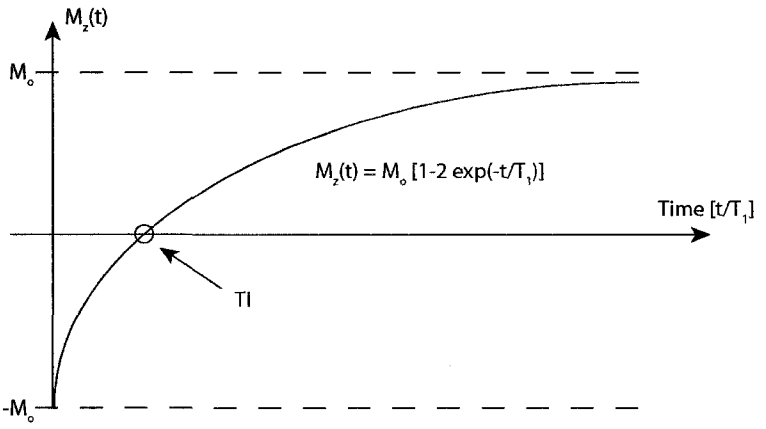

FIGURE 2.13: A plot of the water magnetization over time following an inversion pulse. Note the magnetization follows the pattern outline in Equation 2.11. This plot clearly identifies the TI, Inversion time.

ms, and in that case the first inversion pulse is applied at time 0, followed by a second pulse at ~1200 ms. At ~1400 ms the $\pi/2$ pulse will start the sequence. Just before the $\pi/2$ pulse the magnetization of the gray matter will be at approximately zero net-magnetization. However, the CSF will have a negative component and the white matter will have a positive component. The dual inversion recovery is designed to null one magnetization and set it up so that the second and third magnetization cancel each other out, which can be seen in Figure 2.14. In diffusion spectroscopy it is beneficial to leave some residual water signal as it is required for single average phase correction, which will be dealt with in section 4.3.1. It is important to note that the dual inversion timings will have to be optimized for each given region, since there will be different amounts of gray and white matter depending on the regions examined.

2.8.3 PRE-SATURATION

Another method used for water suppression is pre-saturation of the water magnetization. The first step is the selective excitation of the water molecule using a selective $\pi/2$ pulse, again completely analogous to the excitation of molecule A in figure 2.11. This will cause the water magnetization to rotate around the Z-axis in the transverse plane at the Larmor frequency. Once the magnetization has been excited a gradient pulse is applied (talked about in section 2.5.1) in order to dephase the water magnetization in the transverse plane. The gradient pulse adds and subtracts to the static magnetic field causing the frequencies of the spins to change (Figure 2.15). Figure 2.15 is an bird's eye view of the transverse XY-plane in the rotating frame, after the gradient has been applied the spins dephase, and

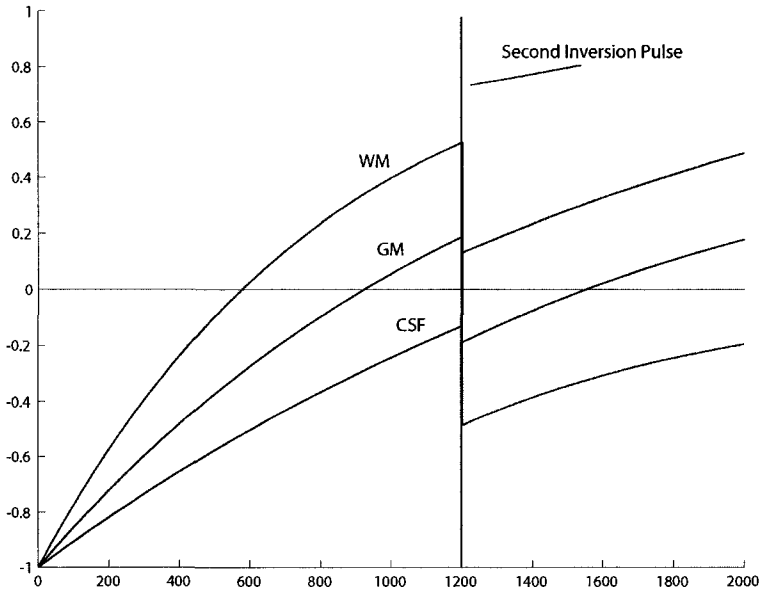

FIGURE 2.14: A plot of the water magnetization over time in the dual inversion recovery sequence. At ~1400 ms the PRESS and or STEAM sequence is started with a $\pi/2$ pulse.

if the gradient is then optimized, then a net-magnetization of ~ 0 can be achieved.

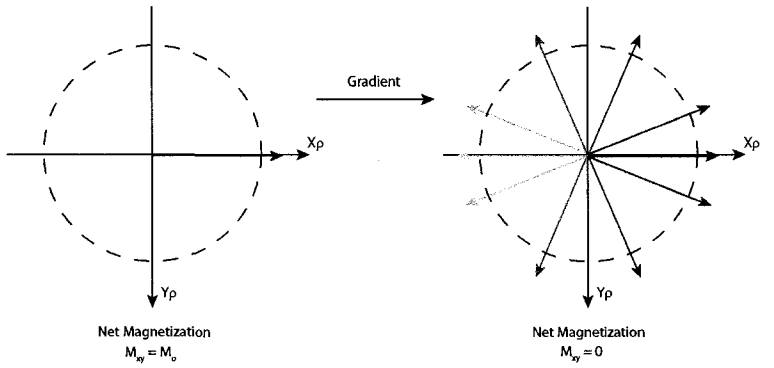

FIGURE 2.15: A bird's eye view of the transverse plane in the rotating frame after the magnetization has been excited. The first plot shows the magnetization immediately after the excitation, and the second plot shows the magnetization after the dephasing gradient is applied, spoiling the magnetization.

After which, the acquisition sequence can begin, since there will be no contribution from the water magnetization.

2.8.4 PRE-SATURATION VS. INVERSION RECOVERY

The two methods, pre-saturation and inversion recovery, work reasonably well. For the work in this thesis the water suppression was done using the dual inversion recovery

method. This was a benefit because the disruption to the phase of the water peak was minimal, which is required for DW-MRS, because the phase needs to be consistent between averages. A common pre-saturation method is call chemical shift selective imaging (CHESS) [43]. CHESS includes 3 or 4 pre saturation pulses and spoilers prior to the STEAM or PRESS acquisition. CHESS works extremely well and tends to eliminate the magnetization completely; therefore, it is more difficult to adjust in order to leave some residual water signal, something that is also required for DW-MRS. The dual inversion recovery method allowed a consistent phase between the water and metabolites, as well as an easy recovery of some residual water signal, which is why it was chosen for the majority of the studies presented here.

2.9 Cell Biology

Prior to talking about the metabolites in the human brain and describing their role in the central and peripheral nervous systems (CNS and PNS), it would be beneficial to understand the cellular structure of the neuron and glial cells.

Figure 2.16 shows the internal structure of the neuron as well as the relevant corresponding cellular structures.

Neurons occur in a variety of different sizes and shapes throughout the human nervous systems; however, one constant between all neurons is that they all communicate with other cells (neurons or glia) through their dendrites, axons, or axon terminals (Figure 2.16). The dendrites are a highly branched outgrowth of the cell body of the neuron; the cell body and the dendrites are the receptors of communication from other neurons. The axon, or nerve fiber as it is sometimes called, is a long process that extends from the cell body and carries output from the cell to target other cells. Axons can be up to a meter in length in some cases. Each axon ends by branching into the axon terminals which are responsible for releasing the neurotransmitters (Figure 2.16).

The individual axons are covered by myelin which consists of 20-200 layers of a highly modified plasma membrane wrapped around the axon by a nearby supporting cell [44]. In the CNS (the brain and spinal cord) the myelin forming cells are oligodendrocytes. Each oligodendrocyte may branch to form myelin on as many as 40 axons [44]. In the PNS the myelin producing cell is called the Schwann cell; the Schwann cell forms an individual myelin sheath around one axon.

Glial cells are support cells which surround the soma, axon, and dendrites of the neurons. Schwann cells and oligodendrocytes are glial cells. Another common glial cell is the astrocyte which helps to regulate the extracellular space in the CNS by removing

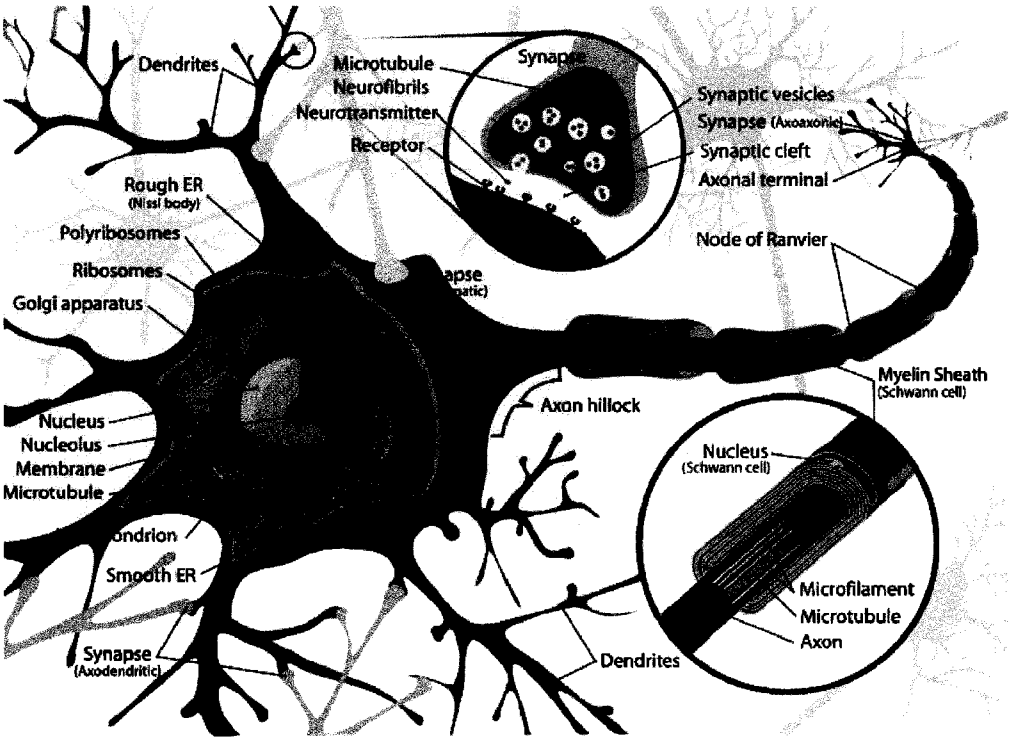

FIGURE 2.16: A complete neuron cell diagram for the peripheral nervous system. Wikipedia (public domain)

potassium and neurotransmitters from around the synapses, and sustaining the neurons metabolically. Other glial cells include microglia and meningeal cells. Glial cells tend to branch often and are relatively spread out (Figure 2.17).

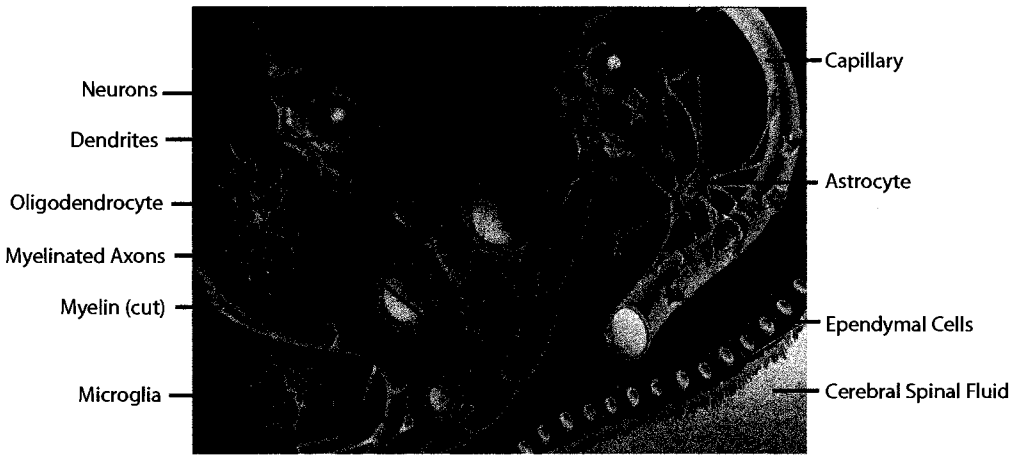

FIGURE 2.17: Cells of Central Nervous System. Adapted from Vander's Human Physiology 10th Edition [44].

The white matter in the human brain is primarily made up of the tightly packed axons relaying messages between different neurons in the gray matter; interspersed between the axons are the support cells such as astrocytes and oligodendrocytes. The gray matter is primarily made up of the neuron cell bodies and dendrites interspersed with small axons and the supporting glial cells (Figure 2.17).

2.10 METABOLITES

In the remainder of this thesis, there will be significant discussion about metabolites. A metabolite is a substance necessary for or taking part in a particular metabolic process. Metabolites, at least for the purpose of this thesis, are chemicals in the brain which aid in various processes throughout your body. The main metabolites examined were N-Acetyl Aspartate (NAA), Total Creatine (creatine and phosphocreatine, tCr), and Choline (Cho). The metabolite myo-inositol (mI) was also examined in one specific study because it is thought to be a glial specific marker, and therefore it is an interesting comparison to NAA (a neuron specific marker). Also, Glutamate/Glutamine (Glx) and Taurine (Tau) were examined in an in vitro tissue study where they were visible. Metabolite concentrations in vivo for NAA, Cr, Cho, and mI are approximately 8.89, 7.49, 1.32, and 6.56 mmol/kg, respectively, in adult brain [45].

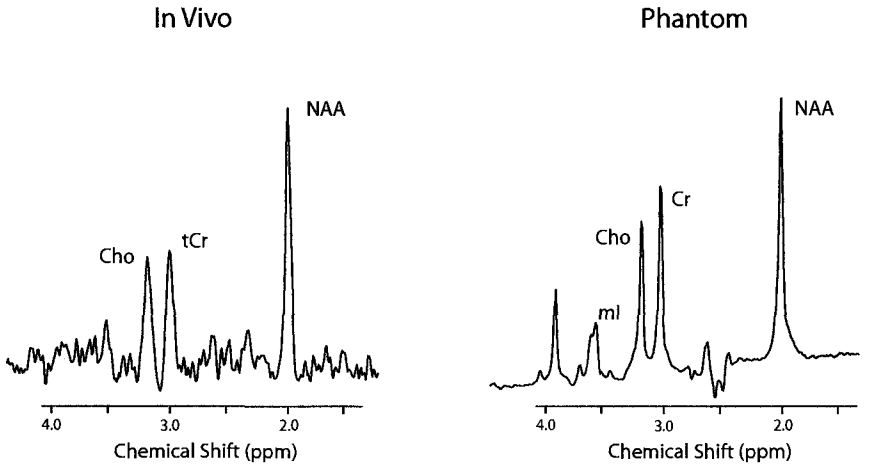

FIGURE 2.18: A water suppressed metabolite spectrum from human brain and a spherical phantom at 3T. Showing the metabolites peaks N-acetyl aspartate (NAA), creatine and phosphocreatine (tCr, only Cr in the phantom), and choline (Cho)

An example spectrum from the human brain and a 150 mL spherical phantom can be seen in Figure 2.18. The phantom consisted of physiological concentrations of NAA, Cr, Cho, and mI. Note the variety of peaks in the spectrum now, as opposed to the water spectrum in Figure 2.10. With a higher signal to noise ratio, a magnet with a larger magnetic field strength, and a more co-operative subject (such as an in vitro sample) the spectrum would be even more interesting (Fig. 2.19). Furthermore by decreasing the echo time there may be as many as 18 different chemicals visible in an NMR spectrum of brain [46].

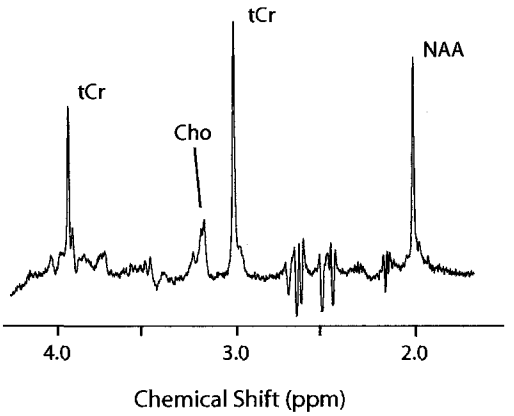

FIGURE 2.19: A water suppressed metabolite spectrum from frog sciatic nerve at 18.8T. Showing the metabolites peaks N-acetyl aspartate (NAA), creatine and phosphocreatine (tCr), and choline (Cho). Notice the higher signal to noise ratio and better resolutions when compared with figure 2.18. At 18.8T 1 ppm is a 600 Hz difference, whereas at 3T 1 ppm is a 128 Hz difference.

The main peaks of metabolites such as NAA, Cr, and Cho, are referred to as singlet peaks, this is because they experience no scalar coupling, section 2.7. Other metabolites that have considerably less SNR, due to their scalar coupling, are referred to as coupled metabolites. Coupled metabolite resonances usually have less SNR because of their concentration being spread out into a multiplet, as well as the fact that there is always some loss due to the scalar coupling evolution. Examples of coupled metabolites are myo-inositol, glutamate, glutamine, and taurine. The coupled metabolites, due to their lower SNR and multiplet spectrum, are much harder to measure, because the timings of the sequence used have a strong effect of the spectrum from these metabolites; however this effect can be calculated [47, 48].

2.10.1 N-Acetyl Aspartate

N-acetyl aspartate is an amino acid found in the human brain; it has a chemical formula of $HO_2CCH_2CH(NHCOCH_3)CO_2H$ (Figure 2.20). The main metabolite peak for NAA comes from the methyl CH_3 group and is located at 2.02 ppm in the NMR spectrum, figures 2.18, 2.19 and 2.26A. This peak was focused on because it is the strongest peak in the NMR spectrum for in-vivo MRS. Despite being the most abundant amino acid in the brain, NAA was only first discovered in 1956 [49].

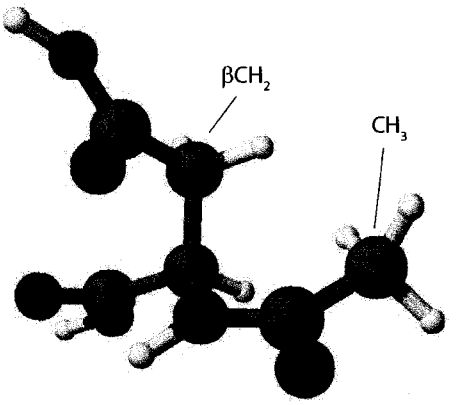

FIGURE 2.20: The N-Acetyl Aspartate (NAA) molecule. Hydrogen (white), Carbon (black/grey), Oxygen (red), and Nitrogen (blue).

NAA has been speculated to be a source of acetyl groups for lipid synthesis, a regulator of protein synthesis, a storage form of acetyl CoA or aspartate, a breakdown product of N-acetyl aspartate glutamate, or an osmolyte [50]. Using immunocytochemical techniques NAA has been shown to be predominately localized to neurons, axons, and

dendrites within the central nervous system ([51] and Figure 2.16). Studies of diseases known to involve some aspect of neuronal and or axonal loss (multiple sclerosis, infarcts, brain tumors) have shown to have decreases in NAA. Also, animal models have shown a correlation between NAA levels and measures of neuronal survivability [52]. Recently, NAA has been detected in cells other than neurons in in-vitro cell preparations [53, 54], and therefore, the possibility of NAA being a neuronal specific marker has come into question. However, the majority of NAA is still located within the neurons, axons, and dendrites.

Examining NAA with DW-MRS, should lead to a greater insight of the intracellular structure of neurons and axons as changes in NAA in MRS have been shown to be quite useful in disease. A case study involving the examination of a 3 year old child with neurodevelopmental retardation had a mildy abnormal MRI; however, upon examination using MRS it was determined that the child had a complete absence of NAA [55]. NAA concentration in the brain tends to increase during development [56], and also has been shown to decrease in a variety of diseases associated with neuronal loss, such as Alzheimer's disease [57], Parkinson's Disease [4], and Infarctions [58]. Investigation of the diffusion characteristics may yield further insight to the mechanism and/or structural abnormalities behind these changes.

2.10.2 Creatine

Creatine is another metabolite commonly found in NMR spectra; it has a chemical formula of $H_2NC(=NH)N(CH_3)CH_2CO_2H$ (Figure 2.21). The largest peak for creatine comes from the methyl CH_3 group and is located at 3.02 ppm in the NMR spectrum; it also has a smaller peak which is from the CH_2 and is located at 3.91 ppm, figures 2.18, 2.19 and 2.26C. Creatine and phosphocreatine are combined to make both of these peaks. In some cases at higher field strength (i.e greater resolution) you may be able to separate the two peaks at $\sim$3.91 ppm, but in this thesis the majority of experiments were performed at 3T where this resolution was not possible. Creatine was found in a variety of different structures in nervous tissue cell cultures [59, 60], such as neurons (dorsal root ganglion and cortical), schwann cells, perineural fibroblasts, astrocytes, and oligodendrocytes (Figures 2.16 and 2.17).

Creatine is thought to be a energy metabolite, and changes in creatine levels have been seen using ^{31}P NMR in exercising muscles [61]. Creatine and Phosphocreatine are constantly increasing and decreasing in concentration. Phosphocreatine is used to turn adenosine diphosphate (ADP) into adenosine triphosphate (ATP), and in turn phosphocreatine turns into creatine. ATP is often referred to as "free energy currency", because

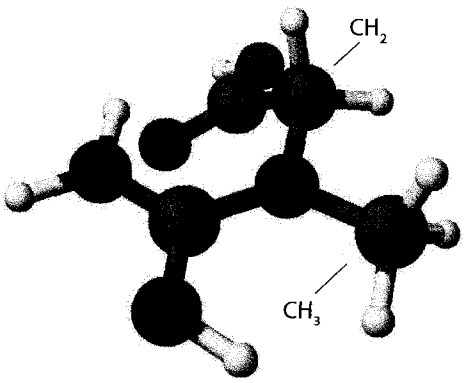

FIGURE 2.21: The Creatine molecule.

cells exchange the energy that is released from the breakdown of ATP, and use that energy to carry out essential functions, such as muscle contraction or conduction of nerve impulses [62]. Increases in creatine concentration are seen in diseases such as Temporal Lobe Epilepsy [63]. Further investigation of the diffusion of creatine in such diseases may yield insight into possible metabolic changes.

2.10.3 CHOLINE

Choline is a metabolite commonly found in NMR spectra; it has a chemical formula of $(CH_3)_3NCH_2CH_2OH$ (Figure 2.22). The largest peak for Cho comes from the methyl CH_3 group and is located at 3.22 ppm in the NMR spectrum, figures 2.18, 2.19 and 2.26E. Choline has been found in a variety of different structures, similar to creatine, in nervous tissue cell cultures [59, 60], such as neurons (dorsal root ganglion and cortical), schwann cells, perineural fibroblasts, astrocytes, and oligodendrocytes (Figures 2.16 and 2.17).

The choline signal in MRS may be better referred to as the signal coming from choline and choline containing compounds. Choline is required to make essential membrane phospholipids and therefore is thought to have a close association with membranes [64]. Choline is also the precursor for the biosynthesis of the neurotransmitter acetylcholine. Choline changes in MRS are commonly found in cancer studies [8, 65].

2.10.4 MYO-INOSITOL

Myo-inositol (mI) is a metabolite commonly found in NMR spectra; it has the chemical formula of $C_6H_6(OH)_6$ (Figure 2.23). The CH groups in mI are not magnetically equivalent, and therefore mI is a coupled metabolite. The [1,3]CH peak is at 3.53 ppm, the [2]CH peak is at 4.06 ppm, the [4,6]CH peak is at 3.62 ppm, and the [5]CH peak is at 3.28 ppm,

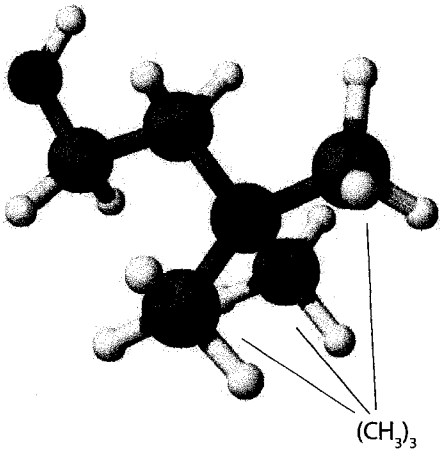

FIGURE 2.22: The Choline molecule.

Figure 2.26G. mI was initially found in astrocytes and not in neuronal cells of rat brain [66], which suggested that mI may in fact be a glial marker. mI is also thought to be a product of myelin degradation, which may be indicative of the changes seen in diseases such as Alzheimer's [57], and Multiple Sclerosis [67].

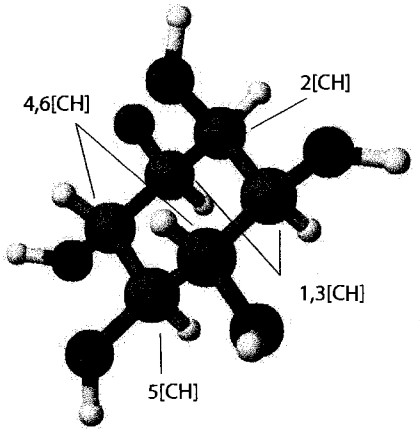

FIGURE 2.23: The myo-Inositol molecule.

Examination of the diffusion characteristic of mI in the human brain will provide an interesting comparison with NAA, because of their locations in the human brain. Since mI is thought to be a glial marker and located in astrocytes, then the diffusion of mI should be isotropic in the human brain due to the spread out nature of the glial cells (i.e. no distinct order, Figure 2.17), whereas NAA is thought to be an axonal marker, which

would cause the diffusion of NAA to be anisotropic in the white matter of human brain. Therefore, examination of the diffusion of NAA and mI should yield insights into two completely separate intracellular compartments in disease.

2.10.5 Glutamate and Glutamine

Glutamate (Glu), and glutamine (Gln) are two coupled metabolites in the human. The chemical formula for glutamate is $HO_2CCH_2CH_2CH(NH_2)CO_2H$, and glutamine, which is only slightly different, is $H_2NCOCH_2CH_2CH(NH_2)CO_2H$ (Figure 2.24). For glutamate the αCH peak is at 3.75 ppm, the βCH_2 peak is at 2.08ppm and the γCH_2 peak is at 2.35 ppm (Figure 2.26B), and, for glutamine the αCH peak is at 3.76 ppm, the βCH_2 peak is at 2.12ppm and the γCH_2 peak is at 2.45 ppm (Figure 2.26D).

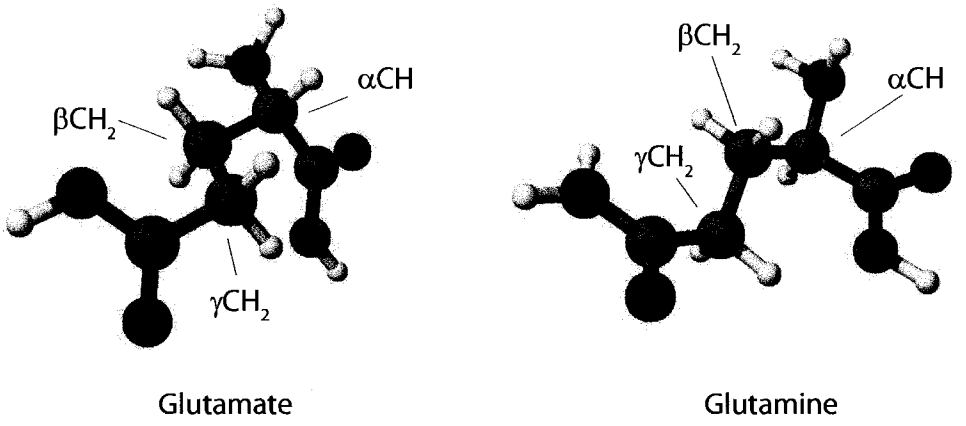

Figure 2.24: The Glutamate and Glutamine molecules.

Glutamate and Glutamine have been shown to be located in a variety of different structures in nervous tissue cell cultures [59, 60], such as neurons (dorsal root ganglion and cortical), schwann cells, perineural fibroblasts, astrocytes, and oligodendrocytes. In the white matter structures Glu tended to be higher in concentration than Gln. Whereas in the astrocytes and oligiodendrocytes (Figure 2.17) Gln is in a higher concentration [60].

Glutamate is the most abundant fast excitatory neurotransmitter in the mammalian nervous system. Glutamate/Glutamine (Glx) increases have been found in patients with ALS, which seems to indicate the occurrence of glutamate excitotoxicity in ALS [68, 69]. Excitotoxicity occurs when the glutamate receptors are overactivated. Glutamine is intricately linked to Glutamate through the glutamate-glutamine cycle; however it seems to be located in support cells such as schwann cells in the peripheral nervous system [70], and it is thought to have a role in both protein and DNA synthesis.

2.10.6 Taurine

Taurine (Tau) is a coupled metabolite found in the human brain. The chemical formula for Tau is $NH_2CH_2CH_2SO_3H$ (Figure 2.25). Taurine metabolite peaks are located at 3.25 and 3.42 ppm, which are from the NCH_2 and the SCH_2 groups respectively, Figure 2.26F.

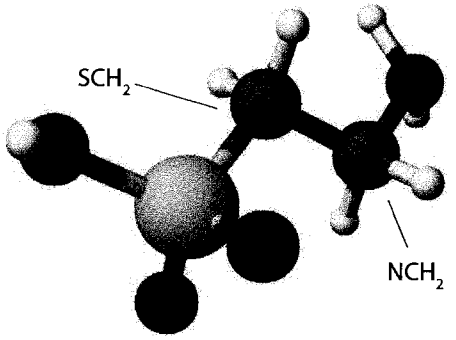

Figure 2.25: The Taurine molecule. Sulphur (yellow)

Taurine has been shown to be located in variety of different structures in nervous tissue cell cultures [59, 60], such as neurons (dorsal root ganglion and cortical), schwann cells, perineural fibroblasts, astrocytes, and oligodendrocytes. The concentration of Tau is however largest in the astrocytes [60]. Taurine has been shown to increase in specific types of tumors, in both in-vitro [71, 72] and in-vivo studies [73]. Taurine appears to have multiple functions in the brain participating both in volume regulation and neurotransmission [74].

2.10.7 Metabolite Summary

Table 2.2 show the metabolic changes associated with certain diseases when compared with control subjects [75]. These metabolic changes measured in MRS are interesting; however, they just correspond to changes in the concentration of the metabolites. Aside from concentration the T_1 and T_2 values have also been calculated in human brain [76–78] as well as magnetization transfer [79]. It would be interesting to examine the diffusion of these metabolites in different diseases, which may provide more information about the structure or function of the underlying tissue. Furthermore, this new metabolite information may help get a better understanding of the cause behind the concentration changes in different pathologies, and possibly diffusion changes in metabolites may occur in pathologies where no concentration changes were reported.

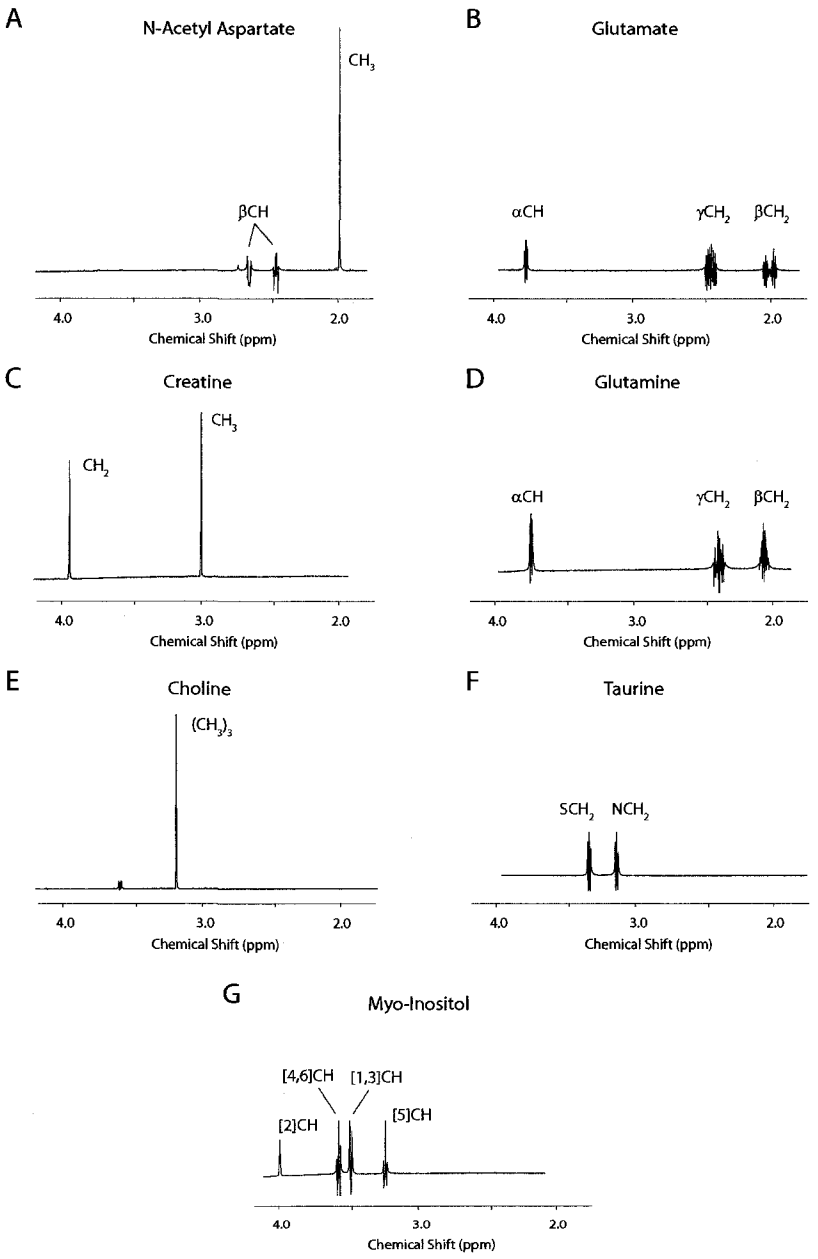

FIGURE 2.26: Metabolite Spectra for NAA (A), Glu (B), Cr (C), Gln (D), Cho (E), Tau (F), and mI (G). Spectra were acquired from phantoms (~25 mmol/L) at 18.8T. Spectra are not to scale. Refer to the individual ball and stick diagrams (Figures 2.20, 2.21, 2.22, 2.23, 2.24, and 2.25), for the location of the hydrogen atoms giving rise to the spectra here.

Pathology	Metabolite	Increase or Decrease	Brain Region
Alzheimer's Disease[80]	NAA	Decrease	Posterior of
	Cho	Increase	Cingulate Gyrus
	mI	Increase	
Parkinson's Disease[81, 82]	All	Typically Normal	Striatum
	NAA	Decrease	Temporoparietal
Parkinson's Symptoms[81]	NAA	Decrease	Striatum
Amyotrophic Lateral Sclerosis(ALS)[69]	NAA	Decrease	Precentral Gyrus
	Glu/Gln	Increase	Pons
			Medulla
Huntington's Disease[83]	mI	Increase	Putamen
	Glucose	Increase	
	Cr	Decrease	
Cancer [8, 65, 71–73]	Cho	Increase	Astrocytoma
	Cho	Increase	Glioma
	Alanine	Increase	Meningioma
	mI	Increase	Neurinoma
	Tau	Increase	Melanoma
	Cho	Increase	Melanoma
Infarction[22, 84, 85]			
Acute Infaction	Lactate	Increase	
	NAA	Decrease	
	Lipids	Increase	
Subacute/Chronic Infarction	Lactate	Normalizing	
	NAA	Decrease	
	Cr	Decrease	
	Cho	Decrease	
Penumbra	Lactate	Increase	
	NAA	Normal	
Temporal Lobe Epilepsy (TLE) [86]	NAA	Decrease	Hippocampus
	Cho	Increase	
	Cr	Increase	
	Lipids	Increase	
	Lactate	Increase	
	mI	Increase	
Multiple Sclerosis (MS) [87–89]			
Acute Plaques	Cho	Increase	
	Lipids	Increase	
	mI	Increase	
	Cr	Decrease	
	NAA	Decrease	
Chronic Plaques	Cho	Normalize	
	Lipids	Normalize	
	mI	Normalize	
	NAA	Decrease	

TABLE 2.2: Metabolite changes with respect to control subjects in a variety of different diseases

CHAPTER 3

DIFFUSION

3.1 THE DIFFUSION PROCESS

Diffusion involves the transfer of molecules from one part of a system to another via random thermally driven motion, and since its first application in NMR, has become an integral part of research and clinical application in the magnetic resonance field.

3.1.1 HISTORY

In 1950, Erwin Hahn discovered a technique for refocusing the magnetic moments in a spin system using an NMR spectrometer and produced a spin echo [90]. This discovery has become a fundamental technique used in pulse sequence development, and must be ranked among the most significant contributions to the field of magnetic resonance. After the spins have been excited with a $\pi/2$ pulse, the spins rotate 90° into the transverse plane (Fig. 3.1B) (see section 2.3 for an explanation on how this occurs). As soon as the spins are in the transverse plane they start to separate, with the fast spins pulling ahead, and the slower spins falling behind (Fig. 3.1C). This separation in the spins is due to inhomogeneity of the magnetic field, plus differences in the precessional frequencies due to subtle differences in the ^{1}H atoms. After a time τ a π_x pulse is applied which flips the spins over (Fig. 3.1D). Then at time 2τ the spins refocus to form a spin echo (Fig. 3.1E).

In 1954, Carr and Purcell measured the diffusion coefficient of water using the spin echo developed by Hahn [13]. The method used by Carr and Purcell required a magnetic field gradient to be present at all times during the experiment. However, this has some experimental limitations. The precise period of time in which diffusion is measured is ambiguous due to the incremented spin echo time, which causes problems in isolating the attenuation due to T_2 from that due to diffusion. As the gradient is increased to measure smaller values of the diffusion coefficient the linewidth also increases, with a

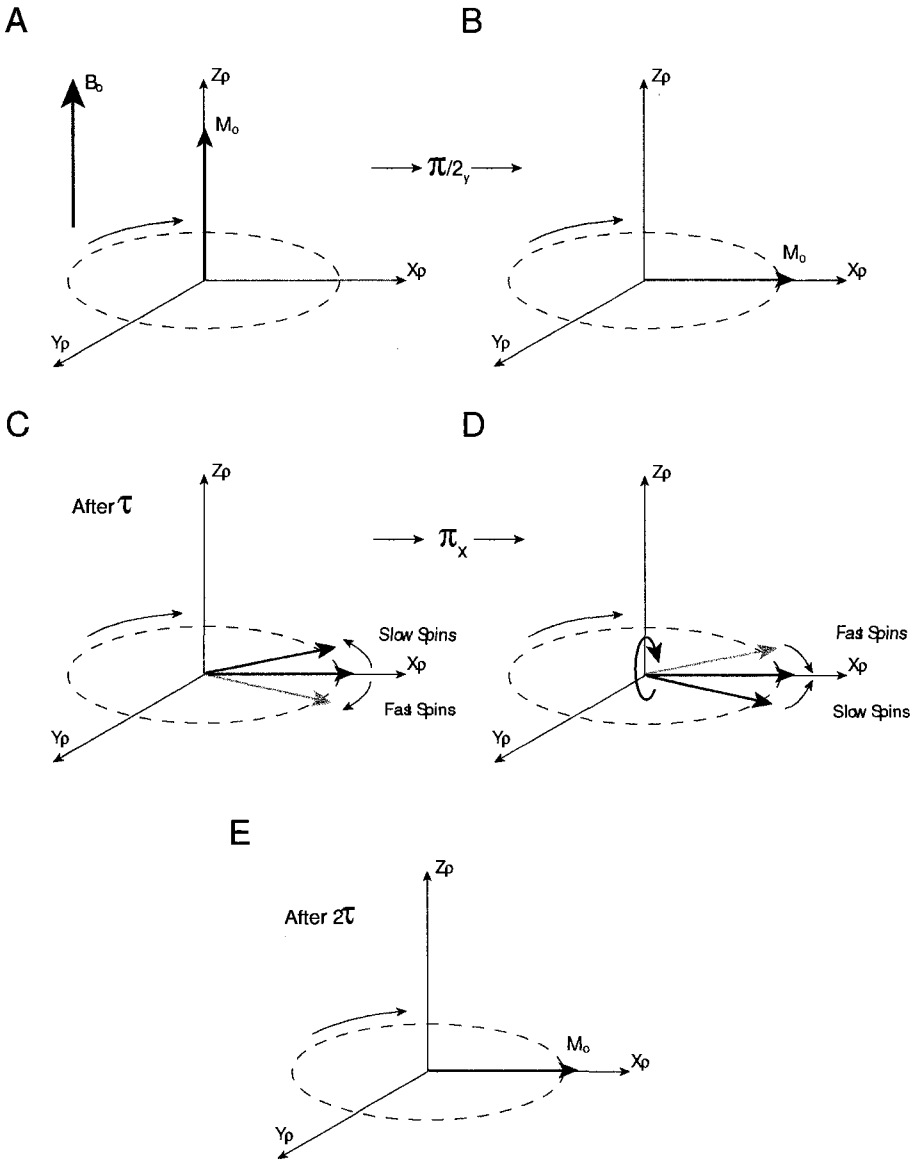

FIGURE 3.1: The magnetic moment of spins within a body, and the effect of a spin echo pulse sequence

corresponding decrease in the duration of the FID, which leads to a decrease in the information available from the echo, and the acquisition of that echo requires an increase in the bandwidth of the detection system, which causes an increase in the noise. In an attempt to eliminate some of these limitations, Stejskal and Tanner implemented a pulsed field gradient method that would avoid having linear field gradients on at times when the RF pulses were also on [91]. The Stejskal and Tanner sequence can be seen in Fig. 3.2.

These linear field gradients, placed before and after the π_x pulse, sensitize the spin

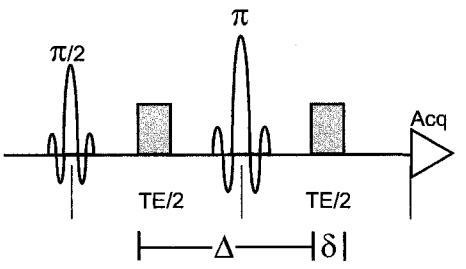

FIGURE 3.2: A spin echo pulse sequence, with pulsed field gradients implemented for the measurement of diffusion

echo pulse sequence to diffusion and are referred to as diffusion gradients. Figure 3.3 displays the effect of the diffusion gradients on the spins after they have been excited into the transverse plane.

The first diffusion gradient, prior to the π_x pulse, causes the spins to dephase by adding or subtracting a small amount of B field to the main B_o field because it is a linear magnetic field gradient (section 2.5.1). Therefore, this is analogous to speeding up or slowing down the spins in the above spin echo experiment (Fig. 3.3B). This addition or subtraction, since it is done in a linear fashion in the direction (X, Y, Z, or some combination) the gradient is applied, allows the sequence to "memorize" the position of the spins along the direction measured using equation 3.1 (assuming a X-gradient). Imagine one spin in position x_1, using equation 3.1 the new precession frequency (ω_1) can be calculated, which is just ω_o plus or minus a little bit of frequency.

$$\omega_1 = \gamma (B_o + G_x x_1) = \omega_o + \gamma G_x x_1 \tag{3.1}$$

After a certain time has passed, the spins are flipped 180° like a pancake by a π_x pulse and their directions are reversed (Fig. 3.3C). In the absence of diffusion (i.e. the spins in the system have not moved between the two diffusion gradients), and keeping in mind that the second diffusion gradient follows this π_x pulse, the second gradient will reverse exactly what was done with the first gradient. However, when the spins are moving around between the diffusion gradient pulses (i.e. diffusing) the refocusing of the spin magnetization will not be complete and will causes a decrease in the signal intensity acquired (Fig. 3.3D). The spins do not refocus completely because they are in a different position than when the diffusion gradient was originally applied. This incomplete refocussing of the spins in the system causes a loss of signal in the FID/Echo, which causes

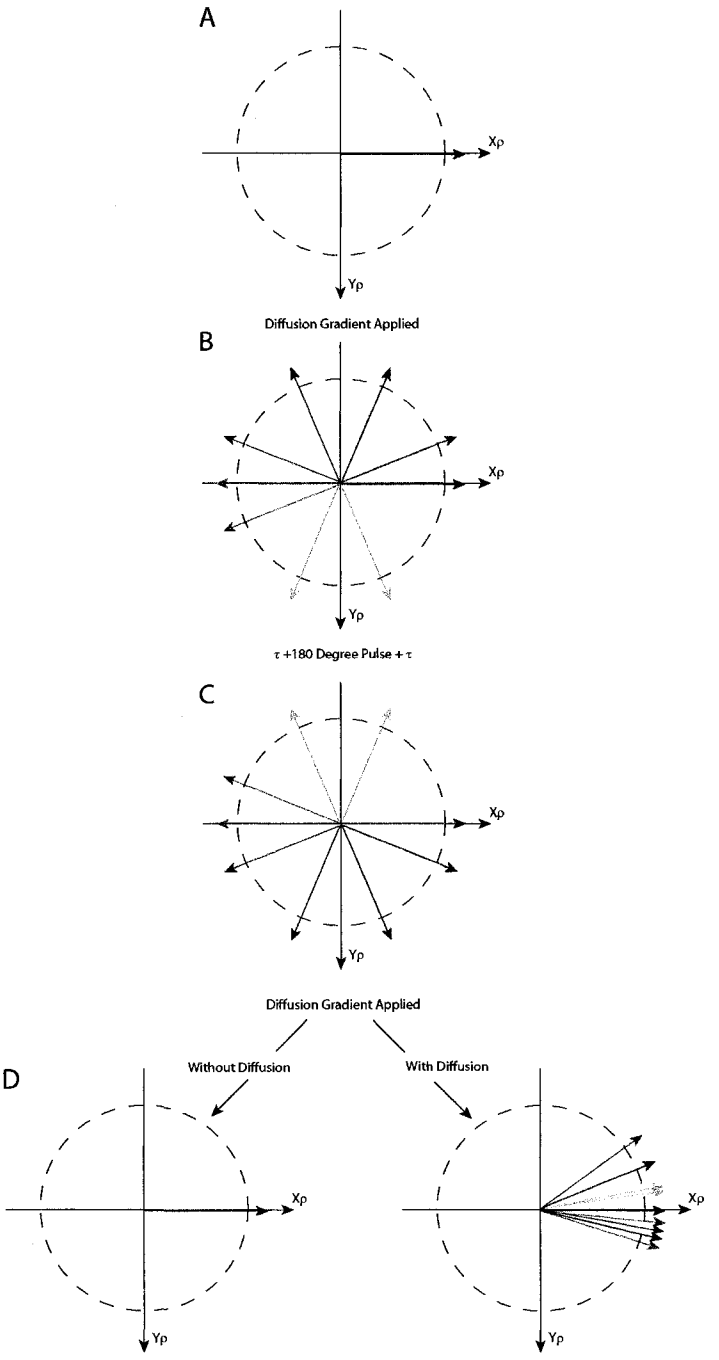

FIGURE 3.3: A bird's eye view of the rotating transverse plane after the spins have been excited. Shows the progression of the spins throughout a diffusion weighted spin echo pulse sequence A) prior to the first diffusion gradient, B) directly after the first diffusion gradient, C) after the 180 degree pulse, and D) after the second diffusion gradient with and without diffusion.

the peak intensity to decrease in the spectrum (Figures 3.4 and 3.5). Fortunately that decrease can be measured and related to the diffusion of the molecules in that system.

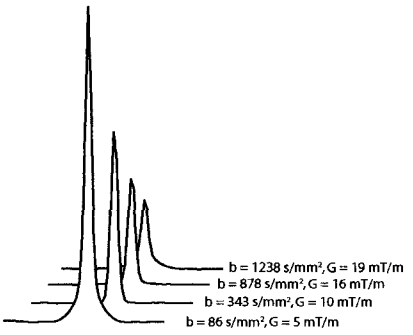

FIGURE 3.4: Four water spectra at increasing diffusion gradient strength highlighting the decay of signal as diffusion sensitization is increased. A diffusion-weighted PRESS sequence was used on a 125 mL spherical water phantom containing concentrations of NAA (9.0mM), Cr (6.4mM), Cho (1.7mM), and mI (6.8 mM) with diffusion parameters of: δ = 18 ms, Δ = 80 ms, which yielded a maximum b-value of 1238 s/mm^2.

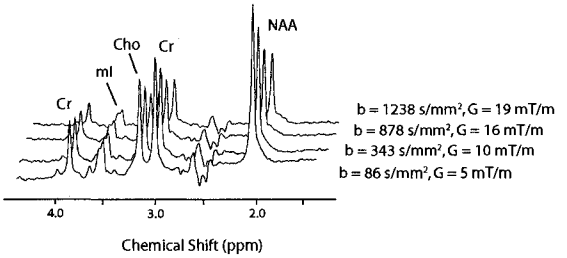

FIGURE 3.5: Four metabolite spectra at increasing diffusion gradient strength highlighting the decay of signal as diffusion sensitization is increased. A diffusion-weighted PRESS sequence was used on a 125 mL spherical water phantom containing concentrations of NAA (9.0mM), Cr (6.4mM), Cho (1.7mM), and mI (6.8 mM) with diffusion parameters of: δ = 18 ms, Δ = 80 ms, which yielded a maximum b-value of 1238 s/mm^2.

3.1.2 How Diffusion is Measured

Diffusion is measured by a drop in signal intensity due to an incomplete refocusing of the spin magnetization (Fig. 3.4). If we calculate the initial signal intensity (either by measuring the peak area or the peak height) when no diffusion gradients were applied (S_o) and the signal intensity when the diffusion gradients are on (S_i) we can calculate the diffusion coefficient 'D' by using equation 3.2, which assumes that the local gradients are minimal in comparison to the diffusion gradients.

$$\ln\left(\frac{S_i}{S_o}\right) = -bD \tag{3.2}$$

Equation 3.2 is the equation of a line with the natural log of the signal intensity on the y-axis, 'b' on the x-axis, and D is the slope of that line. The first step in calculating the slope is determining b, which is commonly referred to as 'the b-value' and can be thought of as the degree of diffusion sensitization. For rectangular gradients, the b-value is calculated from equation 3.3, where γ is the gyromagnetic ratio of the molecule (in our case hydrogen (2.674 x 10^8 rad $s^{-1}T^{-1}$)), G is the gradient strength (usually measured in mT/m or G/cm), δ is the gradient length, and Δ is the gradient separation (measured from the start of the first gradient to the start of the second).

$$b = \gamma^2 G^2 \delta^2 \left(\Delta - \frac{\delta}{3}\right) \tag{3.3}$$

The part of equation 3.3 in brackets, $\Delta - \delta/3$, is known as the diffusion time. The timings δ and Δ are also labeled in Figure 3.2. With a short diffusion time, a molecule will experience very few boundaries, and therefore it will diffuse similar to its intrinsic diffusion as long as this diffusion time is kept short enough. With increased diffusion times, more barriers are encountered, which hinder the diffusion and the diffusion attenuation curves drop off less rapidly. Typical diffusion times for DW-MRI are ~45 ms, whereas the in-vivo diffusion times in this thesis for DW-MRS range from ~75-200 ms. However, the one-dimensional root mean square displacement of water (ADC ~ 0.70 x 10^{-3} mm^2/s, diffusion time ~ 45 ms) and metabolites (ADC ~ 0.15 x 10^{-3} mm^2/s, diffusion time ~ 200 ms) are approximately the same (~8 μm).

Figure 3.6 is an example of a signal intensity vs. b-value plot for both the water diffusion coefficient and the Cr diffusion coefficient. You can clearly see the difference in the diffusion coefficient with the water diffusion coefficient at 1.92 x 10^{-3} mm^2/s and Cr at 0.80 x 10^{-3} mm^2/s. Also, notice the linearity of the lines as expected for a freely diffusing unrestricted sample.

A typical scan used for measuring diffusion would be composed of a measurement at b = 0 s/mm^2 (or a low b-value) and a measurement at high b-value (1000 - 2000 s/mm^2). These high and/or low b-values can also be measured in differing directions as required for determining the effects of the environment on the molecules being examined. Measuring diffusion in different directions is achieved by applying the diffusion gradients in the direction you wish to measure; for example applying a linear diffusion gradient in the X-direction will only measure changes in position along the X-direction, whereas a diffusion gradient in the Y-direction will only be sensitive to changes in position along the Y axis. The diffusion gradients can be applied in any direction X, Y, Z, or some combination. In order to increase the accuracy of the measurement more than two b-values can be used, which allows for a more accurate estimation of the slope.

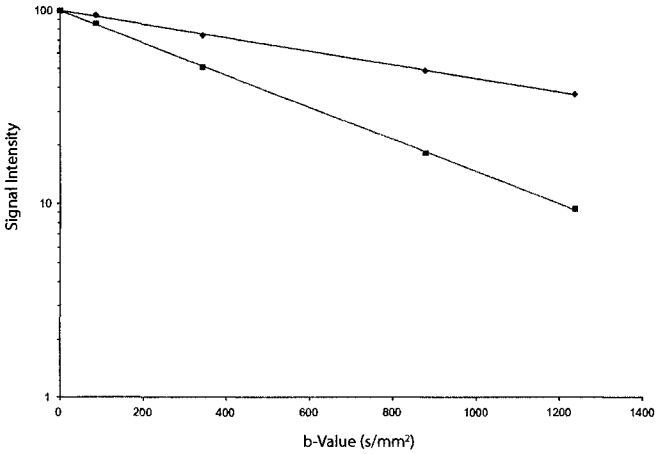

FIGURE 3.6: Diffusion attenuation curves for water (red) and creatine (black) in a 125 mL spherical phantom.

3.2 Types of Diffusion

Molecular diffusion is highly dependent on a variety of factors such as molecular weight, viscosity (i.e. intermolecular interactions), and temperature; aside from these factors, the underlying cellular microstructure can come into play by providing numerous barriers and/or various individual compartments restricting the diffusion in the system. A molecule with no barriers or hinderance to its diffusion would not act in the same way as the same molecule with many barriers or hindrances, and in some cases highly ordered barriers. For these reasons the diffusion coefficient we are measuring in tissue is known as the *Apparent* Diffusion Coefficient or ADC. Each molecule, will have its own intrinsic diffusion coefficient, which is not based on environmental factors; however, the environment in vivo will likely outweigh the importance of the individual molecules own intrinsic diffusion.

Diffusion in vivo can be generally described in one of two categories isotropic diffusion or anisotropic diffusion.

3.2.1 Isotropic

The definition of isotropic is: Identical in all directions; invariant with respect to direction. With that in mind, isotropic diffusion is diffusion in a system that is invariant with respect to direction (i.e. similar diffusion occurs in all directions). Isotropic diffusion is usually visible or seen in phantom studies where there are no barriers to diffusion in any given direction (Fig. 3.7A). In vivo near isotropic diffusion is usually found in the gray matter of the human brain where there tends to be less order or a symmetrical order (i.e. spheres)

in the structures and barriers to diffusion (Fig. 3.7B).

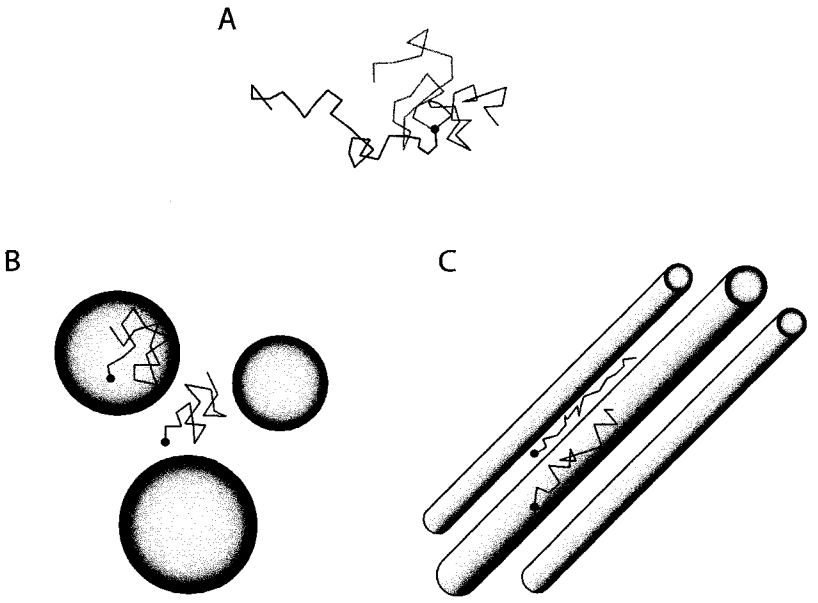

FIGURE 3.7: The random walk paths taken by molecules in given environments A) Isotropic Phantom, note the 3 different paths taken from the same starting point, B) Isotropic in vivo, the spherical nature of the environment yields comparable diffusion in all directions, and C) Anisotropic in vivo, the highly ordered nature of the diffusion environment cause a directional preference for the diffusion.

3.2.2 ANISOTROPIC

The definition of anisotropic is: Not isotropic. Therefore, anisotropic diffusion is not invariant with respect to direction (i.e. the diffusion in the system has a preferred direction). Anisotropic diffusion is often seen in the white matter of the human brain where the barriers to diffusion are highly ordered (Fig. 3.7C). The white matter of the corpus callosum is so densely packed that the diffusion of water and other chemicals in the brain is highly restricted in that region and tends to diffuse preferentially along those white matter tracts. In fact, different white matter tracts and different areas of the brain have differing degrees of anisotropy, which can be measured using the diffusion tensor.

3.3 MEASURING ANISOTROPY

Originally the degree of anisotropy was measured by calculating the diffusion ADC in the direction parallel to the fiber tract as well as in the direction perpendicular to that fiber tract. Then a simple ratio of the Parallel ADC / Perpendicular ADC was calculated.

While this is entirely valid in a system in which the orientation of the fiber tract can be controlled [92], it becomes questionable in an in-vivo system due to unknown and multiple orientations or fibers. Therefore, a more accurate measure of the diffusion in a system was developed using a diffusion tensor [23].

3.3.1 The Diffusion Tensor

The diffusion tensor ($\vec{D}$) is a 3 x 3 matrix (Equation 3.4). The diagonal elements D_{xx}, D_{yy}, and D_{zz} correspond to the diffusion coefficients in the direction of the 3 coordinate axes in the lab frame. The off diagonal elements are not diffusion coefficients, but reflect the correlation between the diffusion in the two directions (i.e. D_{yz} is the correlation of the diffusion along the y and z axes [23]). The off diagonal elements are also symmetric in the diffusion tensor.

$$\vec{D} = \begin{pmatrix} D_{xx} & D_{xy} & D_{xz} \\ D_{yx} & D_{yy} & D_{yz} \\ D_{zx} & D_{zy} & D_{zz} \end{pmatrix} \tag{3.4}$$

Diffusion tensor imaging and spectroscopy was first introduced in 1994 [23], and was used to show how the phenomenon of anisotropic diffusion of water can be exploited to determine fiber tract orientations and mean particle displacements. From $\vec{D}$ in equation 3.4 a variety of measures of the diffusion in the given system can be calculated, such as the eigenvalues, mean diffusivity, and fractional anisotropy.

3.3.1.1 Eigenvalues

For each estimated $\vec{D}$ three corresponding diffusion coefficients in three principal directions (i.e. principal diffusivities) can be calculated by diagonalizing the diffusion tensor, Λ (Equation 3.5).

$$\Lambda = \begin{pmatrix} \lambda_1 & 0 & 0 \\ 0 & \lambda_2 & 0 \\ 0 & 0 & \lambda_3 \end{pmatrix} \tag{3.5}$$

Since $\vec{D}$ is symmetric and positive definite, each of these eigenvalues calculated in equation 3.5 have corresponding eigenvectors, ϵ_1, ϵ_2, and ϵ_3.

The diffusion tensor, as it turns out, is best visualized as an ellipsoid (Figure 3.8), where the eigenvectors are the corresponding axes for that ellipsoid, and the eigenvalues provide the shape of the ellipsoid. For a white matter tract in the brain λ_1 is generally assumed to be parallel to the tract, and λ_2 and λ_3 are perpendicular to the tract.

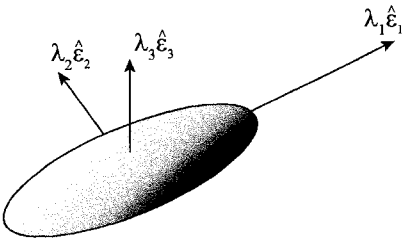

FIGURE 3.8: An ellipsoid, which is created by the eigenvectors and eigenvalues of the diffusion tensor. Notice how the ϵ_1 axis of the ellipsoid is much longer, this is due to the λ_1 eigenvalue being much larger than the λ_2 and λ_3

3.3.1.2 MEAN DIFFUSIVITY

Mean diffusivity (MD) is a rotationally invariant measure of the apparent diffusion coefficient in a specific region. MD can be measured by calculating the trace of the diffusion tensor and dividing it by 3, the average of the three eigenvalues (Equation 3.6).

$$MD = \frac{(\lambda_1 + \lambda_2 + \lambda_3)}{3} \tag{3.6}$$

It should be noted that MD is sometimes referred to as the Trace ADC, which is not entirely accurate as the trace of the diffusion tensor would not be the average of the three eigenvalues but $\lambda_1 + \lambda_2 + \lambda_3$. However, calling MD the Trace/3 ADC is entirely correct, and it will be called both throughout this text.

The mean diffusivity is used mainly to report a rotationally invariant measure of diffusion within a specific voxel or region. MD measurements are required for accurate comparisons between studies, as originally only single direction measurements were performed [28, 29]. While single direction measurement of ADC are valid, unless the studies were performed on the exact same region and the patient was in the exact same position relative to the diffusion gradients, the comparison is not accurate. If the region examined was 100% isotropic, it would not matter the direction measured.

Although the MD can be calculated from the average of the eigenvalues of the diffusion tensor, calculating the full diffusion tensor is not required for calculating MD. MD can be calculated by measuring the ADC values in any 3 directions, as long as those 3 directions are orthogonal to each other. The benefit of calculating the MD from the diffusion tensor is that the full tensor allows calculation of the fractional anisotropy as well as MD.

3.3.1.3 FRACTIONAL ANISOTROPY

Fractional Anisotropy (FA) is a measurement of the degree of anisotropy in a given system or voxel [93], and can be calculated once the eigenvalues and MD of the diffusion tensor

are known by using equation 3.7.

$$FA = \sqrt{\frac{3}{2}} \times \sqrt{\frac{\left((\lambda_1 - MD)^2 + (\lambda_2 - MD)^2 + (\lambda_3 - MD)^2\right)}{(\lambda_1^2 + \lambda_2^2 + \lambda_3^2)}} \tag{3.7}$$

FA values can vary anywhere from 0 to 1, with a value of 0 being a completely isotropic environment and 1 being a highly anisotropic environment. As was seen previously in Figure 3.7, different areas in the brain have differing degrees of anisotropy, a FA value of water in the gray matter of the human brain may be around 0.2, where as a FA value in the genu of the corpus callosum (a highly ordered white matter region) may be around $0.75 - 0.8$.

It should be noted that there are other measures of the anisotropy of a given system, such as relative anisotropy, RA [93]. However, the majority of the work using the diffusion tensor report values of FA and not RA.

3.3.1.4 Diffusion Tensor Imaging

Diffusion tensor imaging was first introduced in 1994 [23]. Using the phenomenon of anisotropic diffusion of water they were able to determine fiber tract orientation and mean particle displacements. From that information one is able to produce colormaps of the human brain [94], such as those presented in Fig. 3.9, where the color indicates a diffusion direction of left-right (red), superior-inferior (blue), and anterior-posterior (green).

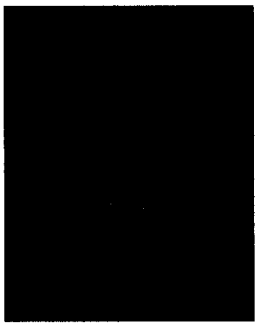

Figure 3.9: A colormap of the human brain, with the colors indicating the preferred direction of diffusion, left-right (red), superior-inferior (blue), and anterior-posterior (green). This color map can be obtained through Diffusion Tensor Imaging (DTI).

More recently this fundamental property of water in white matter has been used to perform 3D tractography of the fibers in the brain [25, 95–97]. Figure 3.10 is an example of fiber tractography of the genu of the corpus callosum in human brain.

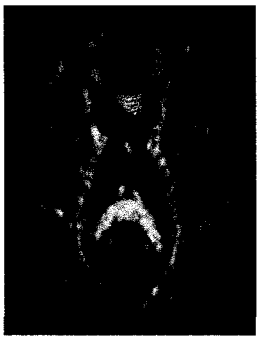

FIGURE 3.10: Fiber Tractography of the Genu of the Corpus Callosum in Human Brain emphasizing the utility of Diffusion Tensor Imaging of water.

3.4 DIFFUSION SPECTROSCOPY

The investigation of metabolite diffusion in vivo has lagged behind, when compared to the investigation of water diffusion, due to technical challenges such as limited signal-to-noise ratio, poor spatial resolution, pulse sequence availability, significant post-processing, lengthy acquisition times, and limited brain coverage. Despite these challenges, the pursuit of metabolite diffusion in diseased tissue is worthwhile since it may yield insights into changes in the underlying intra-cellular environment with disease [98–101].

It has long been shown that reductions in water diffusion are an extremely sensitive indicator of early cerebral ischemia [22], and that despite the theory that this decrease is due to a water shift from extra-cellular to intra-cellular space, purely intra-cellular metabolites also show a reduction of diffusion by a similar magnitude without any compartmental shifts in animal models of cerebral ischemia [100, 102–107]. Thus diffusion-weighted spectroscopy can add insight into the biophysical properties of diffusion in tissue, but it remains to be tested whether or not diffusion of intra-cellular metabolites will provide evidence of neuronal/axonal abnormalities in the absence of changes in either water diffusion or other MR properties in a variety of neurological disorders beyond ischemia.

3.4.1 HISTORY OF DIFFUSION SPECTROSCOPY

The main research focus of DW-MRS thus far has been on animal models of cerebral ischemia [100, 102–107] in which the ADCs of the singlet metabolites (NAA, tCr, and Cho) reduce significantly (12-19% for NAA, 16-44% for Cr, and 25-48% for Cho) in the acute phase of cerebral ischemia, similarly to the ADC reduction of water. These studies indicate that diffusion changes in metabolites may be useful in probing the effect of stroke and other pathologies on the intracellular environment. Aside from the studies on cerebral ischemia the diffusion of metabolites in animal models of skeletal muscle using ^{31}P MRS

[98, 108, 109], normal brain and nervous tissue [110–115], and cancer [99, 116] have also been examined.

DW-MRS was first performed in human brain in 1993 [28]. The diffusion coefficients of NAA, tCr, and Cho were determined from a region in the subcortical white matter. The diffusion was measured in a single arbitrary direction (i.e. all three gradients, X, Y, and Z, were on at the same time), which is not ideal. Diffusion, as mentioned previously in section 3.2, can vary greatly depending on the direction in which it is measured. Regardless, this study paved the way for accurate diffusion measurements and introduced the single average phase correction method, which will be discussed in section 4.3.1. More recently in 2002, Diffusion spectroscopy of the human brain was performed on normal, ischemic and cancerous human brain [29]. This was the first case in which the diffusion coefficients of metabolites were measured in abnormal human brain. The authors found that in the case of acute cerebral ischemia the diffusion coefficient decreased for the metabolites NAA, Cr, and Cho. In the case of the cancerous human brain the diffusion coefficient actually increased for the same three metabolites. However, again this study used a single arbitrary diffusion direction. Unless these two studies were performed using the exact same head and voxel placement, any differences between the studies can be attributed to a difference in direction alone. Accurate comparison between studies requires the calculation of the Trace/3 ADC or MD (section 3.3.1.2), also when comparing brain regions within an individual. These were the only two diffusion spectroscopy papers on human brain that existed when the work of this thesis began.

A recent study measured the diffusion in two directions and demonstrated a 2-3 fold greater ADC for NAA diffusion parallel to the axonal direction, relative to perpendicular in the splenium of the corpus callosum for two healthy volunteers [117]. Although this latter study demonstrated anisotropy of NAA diffusion, the full diffusion tensor, which requires the measurement of a minimum of 6 diffusion directions is the best way to characterize diffusion anisotropy in the brain.

3.4.2 Diffusion Tensor Spectroscopy

Since diffusion is known to be anisotropic in white matter, for either water or metabolites [22, 112, 117, 118], it can only be characterized properly by measuring the full diffusion tensor, with an unavoidable time penalty. In 1990, it was shown that water diffusion was anisotropic in the cat brain [22], which led to the invention of DTI [23]. It has been shown that diffusion anisotropy exists for the metabolites as well and has been measured in the bovine optic nerve [112], the rat brain [118], and the human corpus callosum [117]. While the anisotropy has been characterized by the measurement of the ADC in a direction

parallel to the known fiber tracts and perpendicular [112, 117] and has been measured in 3 directions in order to calculate the Trace/3 ADC of the rat brain [118], the diffusion tensor has never been measured in the human brain or any other tissue.

The mean diffusivity and the degree of anisotropy provide independent and unique inferences on the micro-structural integrity of the white matter tracts [93]. NAA is located primarily in the intracellular space of neurons and axons, while tCr, and Cho are located, not only in the neurons and axons, but also in the more presumably isotropic environments within astrocytes, oligodendrocytes, and meningeal cells [60]. It may be hypothesized that tCr and Cho might exhibit different degrees of anisotropy as compared to NAA within various human brain regions, depending on the cellular environment. Furthermore, the three primary singlet metabolites may have unique diffusion changes with neurological injury given their cellular distribution.

3.4.3 Diffusion Spectroscopy Sequences

There are a variety of sequences that can be used for diffusion spectroscopy. However, two main sequences have been used for single-voxel spectroscopy in the human brain. The first sequence is similar to the spin echo sequence mentioned in section 3.1.1 and is called the PRESS (Point REsolved SpectroScopy) sequence [32]. The PRESS sequence consists of two spin echoes (i.e. a $\pi/2$ pulse followed by two π pulses). An example of a diffusion-weighted PRESS sequence is shown in Figure 3.11.

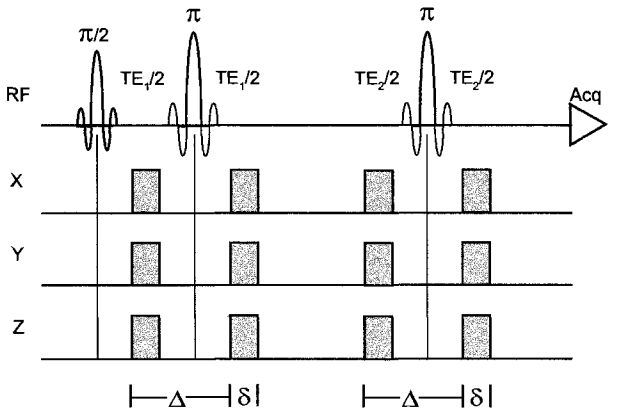

Figure 3.11: A diffusion-weighted PRESS (Point REsolved SpectroScopy) sequence, single voxel localization pulses and water supression not included in figure. Notice how the two echo times do not have to be consistent.

The diffusion gradients in figure 3.11 are placed around both π pulses. Normally, the gradients will only be applied in either a single direction (X, Y, or Z) at a time or in the the

case of DTS two directions at the same time, and therefore, having two sets of diffusion gradients around both π pulses makes it possible to go to a higher b-value (in fact, twice the b-value from one set of gradients) without increasing the echo time of the sequence due to longer diffusion gradients.

In some cases it may be useful to use a different sequence and minimize the echo time; this other sequence is called the diffusion-weighted STEAM (STimulated Echo Acquisition Mode) sequence [33]. In order to understand this sequence, we must first examine what exactly a "stimulated" echo is as opposed to a spin echo used in the PRESS sequence.

A stimulated echo can be created in a variety of ways, the STEAM sequence uses three $\pi/2$ pulses to achieve a stimulated echo. The first pulse causes the spins, initially aligned along the z-axis to rotate 90° and into the rotating transverse plane. The second pulse, that occurs at time τ, stores the memory of the phase angles, that were created throughout time τ, in the Z-direction, where they are unaffected by field gradients. The third $\pi/2$ pulse restores the phase angles to the transverse plane with their signs reversed, and therefore, and echo occurs at a time τ after the third $\pi/2$ pulse. Figure 3.12 is an example of a diffusion weighted STEAM sequence.

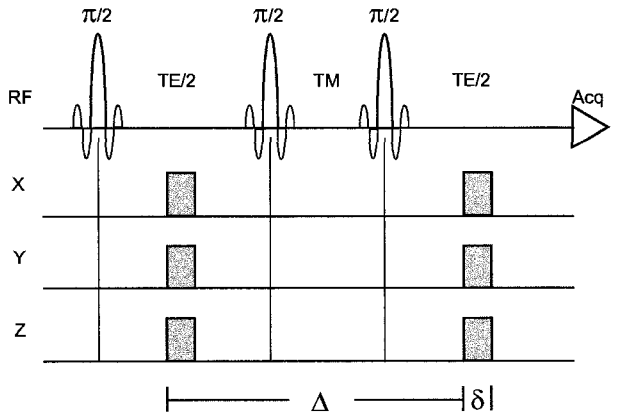

FIGURE 3.12: A diffusion-weighted STEAM (STimulated Echo Acquisition Mode) sequence, single voxel localization pulses and water suppression not included in figure. Notice in this sequence we only have one echo time (TE) unlike the PRESS sequence in Figure 3.11, and we have a "mixing time" (TM).

In Figure 3.12 there is only one echo time, and therefore, only allows for one diffusion gradient pair as opposed to the PRESS sequence. The mixing time (TM) is also different from the PRESS sequence; during the TM period the magnetization is aligned with the Z-axis, and therefore, no T_2 decay is occurring during that time.

3.4.4 PRESS vs. STEAM

Previous studies on the human brain using DW-MRS [28, 29] have used both the STEAM [28] and PRESS [29] sequences. The animal DW-MRS work has also used both sequences for single voxel localization where the STEAM sequence was used in 6 of the studies [100, 103, 104, 106, 115, 116], and the PRESS sequence was used 3 times [102, 105, 107].

The main disadvantage with using a PRESS sequence for diffusion weighted spectroscopy is the long echo time of the sequence, which is one of the benefits for the STEAM sequence when compared with the PRESS sequence. The TE can be kept short and still increase your b-value by increasing TM (i.e. increasing Δ in Figure 3.12). The disadvantage to the STEAM sequence, however, is that because of the nature of the stimulated echo only half of the signal is refocused, at least for the 3 main metabolites (NAA, tCr, and Cho), since the couple metabolites are also affected by the sequence timings.

For the majority of the work presented here the STEAM sequence was used. It was thought to be the best option because of its ability to keep the echo time short, while still being able to increase the b-value (required for diffusion spectroscopy). The PRESS sequence, was used for one specific study in Chapter 8 where the specific timing of the sequence and the sequence used was important for accurate quantification of mI. The methods used for the diffusion spectroscopy measurements used in this thesis will be discussed in detail in the next chapter.

CHAPTER 4

METHODS

4.1 INTRODUCTION

Diffusion weighted magnetic resonance spectroscopy (DW-MRS) in vivo is comprised of a variety of steps, each step is an integral part in receiving accurate information. In vitro DW-MRS is quite trivial, because, not only is the concentration higher of the metabolites, the shim is better due to the more homogenous region examined. In vivo measurements have a multitude of complications including low concentration, small ADCs, large voxel sizes (to make up for the low concentration), which include a variety of different neural structures, and since diffusion measurements are extremely sensitive to motion, macroscopic motion due to involuntary subject movements, respiration, and cerebrospinal fluid related brain pulsation all can be detrimental to in-vivo DW-MRS. These macroscopic changes due to motion need to be corrected for before any analysis of DW-MRS data is performed.

4.2 ACQUISITION

All experiments performed in this thesis were done on a SMIS 3T MRI scanner equipped with a bird cage head coil (Medical Advances, Milwaukee, WI powered by a AMT RF amplifier, 10-130 MHz, 8 kW)) and had a maximum gradient strength of 20 mT/m (Magnex Gradient Coil powered by a MTS Gradient Amplifier, min rise time 0.107 ms). The experiments were performed using either a PRESS or a STEAM sequence (discussed in 3.4.3), which had been modified to incorporate diffusion gradients.

The STEAM sequence, which was used for the majority of the studies, is pictured in Figure 4.1. It consists of two selective hyperbolic secant π pulses for the dual inversion recovery of the water signal, required for water suppression, followed by two spoiler

gradients used to disperse some of the remaining water signal. The other spoiler gradients are in the TM period and are used to spoil unwanted magnetization during that time period. The black gradients are the voxel selection gradients, and the Diffusion gradients are in gray. The spoilers and slice selection gradients effect on the overall b-value is minimal as the diffusion gradients are quite large in comparison. The TM spoilers between the second and third $\pi/2$ pulses do not effect the overall magnetization since during the TM the magnetization of interest is aligned along the z-axis. The parameters used in this sequence were dependent upon on the actual experiment, and therefore refer to Chapters 5 to Chapter 8 for the individual parameters.

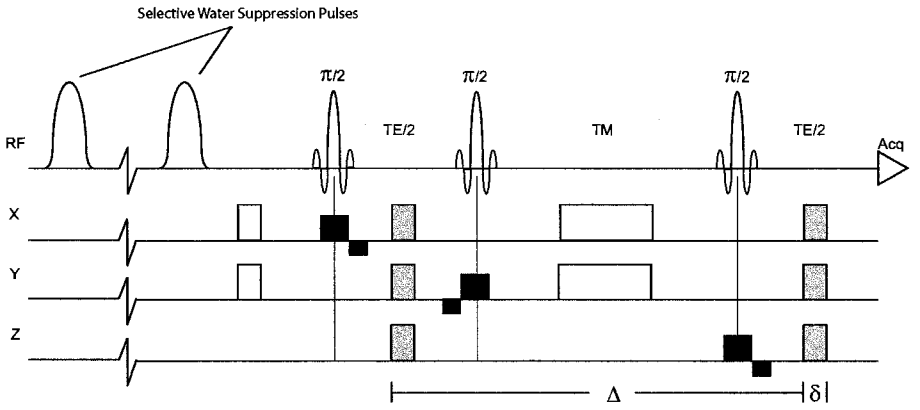

FIGURE 4.1: STEAM pulse sequence used for the majority of the studies in this thesis. All pulses are included. The two hyperbolic secant pulses were used for the Water Suppression π pulses, whereas sinc pulses were used for the three $\pi/2$ pulses. The spoiler gradients used are in white, the diffusion gradients are in gray, and the voxel selections gradients are in black. The gradients in this sequence are not to scale.

The PRESS sequence which was used for some experiments is pictured in Figure 4.2. The water suppression technique is consistent with the above STEAM sequence, and again the voxel selection gradients are in black, spoilers in white, and the diffusion gradients in gray. Again, the spoilers and slice selection gradients effect on the overall b-value is minimal as the diffusion gradients are quite large in comparison, even if that effect wasn't minimal it is corrected for in the calibration of the sequence, which will be discussed in section 4.4.2. One point to note about this specific PRESS sequence is that it is designed for optimization of signal from mI, which requires a first TE of 36 ms and a second TE of 180 ms, and therefore there was only room for diffusion gradients during the second TE.

The first DW-MRS experiments that were performed on the 3T consisted of a measurement of the ADCs of 3 metabolites N-acetyl aspartate (NAA), creatine and phosphocreatine (tCr), and choline (Cho) in vivo. A diffusion weighted STEAM sequence was used in this study, because of its ability to increase the b-value while not increasing the echo

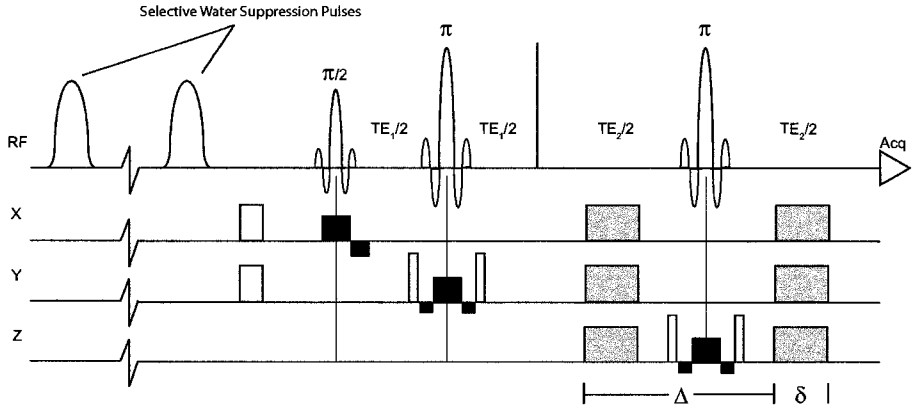

FIGURE 4.2: PRESS pulse sequence used for some of the studies in this thesis. All pulses are included. The two hyperbolic secant pulse were used for the Water Suppression π pulses, while sinc pulses were used for the two π pulses and one $\pi/2$ pulse. The spoiler gradients used are in white, the diffusion gradients are in gray, and the voxel selections gradients are in black. The gradients in this sequence are not to scale.

time of the sequence. The results of that first experiment are listed in Table 4.1. While the phantom data is in clear agreement with previous work [119], the in vivo ADC calculations are grossly inflated, in actuality the ADCs calculated in vivo in Table 4.1 are 2-3 times higher then what had been previously reported. This increased ADC in vivo is artefactual and is a direct result of the macroscopic motions mentioned below.

	ADC Values (x 10^{-3} mm^2/s)			
	X	Y	Z	Trace/3 ADC
Phantom (N=3) - Correct				
Water	2.04±0.03	2.00±0.01	2.01±0.01	2.02±0.01
Cr	0.79±0.02	0.76±0.01	0.78±0.01	0.78±0.01
Cho	0.96±0.02	0.91±0.03	0.92±0.01	0.93±0.02
In Vivo (N=3) (corona radiata / centrum semiovale) - Erroneous				
NAA	0.21±0.11	0.45±0.06	0.53±0.06	0.39±0.04
tCr	0.23±0.16	0.49±0.10	0.53±0.11	0.42±0.07
Cho	0.23±0.13	0.43±0.08	0.45±0.09	0.37±0.04

TABLE 4.1: Correct measurements (N = 3, Mean ± SD) of the X, Y, Z, and Trace/3 Apparent Diffusion Coefficients (ADC) in a 150-mL spherical phantom containing water, Cr (30 mM), and Cho (10 mM) at 20°C and erroneous measurements in a 2.5 x 2.5 x 2.5 cm^3 voxel in the periventricular white matter in three human volunteers. These in-vivo measurements were incorrect because of destructive interference between individual spectra that were not phase corrected before averaging.

Macroscopic motions in the subject can cause a phase shift in the output signal every single average during the sequence, these motions are caused by linear and nonlinear motion. The net phase of the total echo signal is dependent on the gradient strength, the pulse sequence timings, and the object's velocity. During signal averaging, the phase

shifts due to the object's velocity are usually incoherent from acquisition to acquisition and lead to signal loss. With an increased gradient strength, such as what is used in diffusion spectroscopy, the sequence becomes more sensitive to this motion. However, these macroscopic motions can be corrected for by incorporating a single average acquisition [28]. Table 4.2 shows a comparison of our phase corrected data with the previous two human studies. It can be clearly seen in this table the importance of the single average phase correction as our results are now consistent with the previous literature [28, 29].

	ADC Values (x 10^{-3} mm^2/s)		
	Posse et al. Single Direction (N=10)	Harada et al. Single Direction (N=6)	Our Results Mean Diffusivity (N=6)
NAA	0.18±0.03	0.17±0.02	0.14±0.02
tCr	0.15±0.03	0.19±0.01	0.19±0.04
Cho	0.13±0.03	0.20±0.02	0.18±0.06

TABLE 4.2: Reported values from two previous studies in human brain, and our results, which highlight the importance of single average phase correction when these values are compared with table 4.1

Instead of acquiring one 64 average spectra, we acquire 64 single average spectra. Figure 4.3 is an overplot of 64 single average spectra (Fig. 4.3A), as well as those same 64 single average spectra summed (Fig. 4.3B). It can clearly be seen that the phase of the 64 single average spectra is not consistent between averages and needs to be corrected for in post-processing. Aside from the single average phase correction, the previous human brain studies employed cardiac gating in order to eliminate some of the motion from cardiac induced brain pulsations. However, this was not readily available on our research scanner, and since our results were similar to the results shown in the two previous cardiac gated studies in the absence of cardiac gating, we felt it was not required for accurate assessment of the ADC of metabolites, and just employed the single average phase correction.

4.3 POSTPROCESSING METHODS

The post processing required for analysis of in-vivo DW-MRS is quite involved, and was designed to follow what had previously been used for analyzing human DW-MRS data [28].The first step was correcting for the eddy currents produced by the MRI. Eddy currents are caused by large gradients with short switching times or ramp times. The pulsed gradients induce these eddy currents, which in turn induce a time varying magnetic field within nearby conductors which affects the acquired signal. These eddy currents can

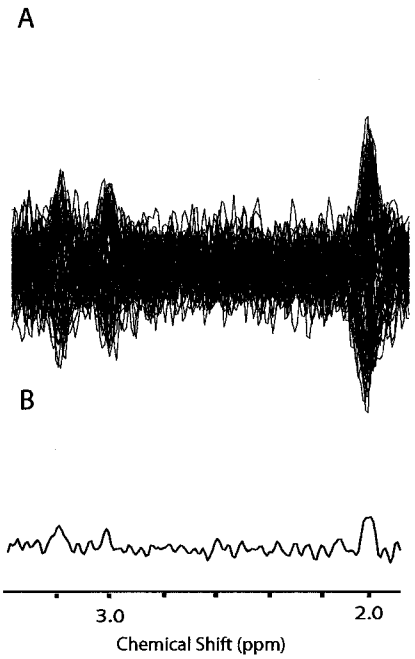

FIGURE 4.3: An overplot of 64 single average diffusion-weighted spectra obtained in the occipital gray matter region (A) and the spectrum produced by the sum of those 64 single average (B). This emphasizes the importance of phase correction required in post processing in order to avoid destructive interference and accurately quantify the peak heights used to calculate the apparent diffusion coefficients.

strongly distort the spectrum, and thus, need to be corrected for. An analytical approach is used to correct for these eddy current distortions [120]. The time dependence of the gradient, and the B_o shift is measured from the FID of the water peak, and then used to correct the FID of the water suppressed spectra using an automated program. Eddy currents can also be minimized by increasing the amount of time between gradients; however, if a short TE is required this may be detrimental to the desired outcome. After the eddy currents have been minimized and/or corrected for the 64 single average spectra need to be summed.

4.3.1 SINGLE AVERAGE PHASE CORRECTION

As was mentioned previously in section 4.2, if every single average is not in phase with one another, the final signal will not be a maximum due to the destructive interference of incoherent phases. Therefore, an automated program was written to correct the phase of each average independently prior to their summation. The program cycles through the zero and first order phase variations in an attempt to maximize the given signal intensity. The program also can be altered to only zero order phase correct, or a combination of a

zero ordered phase correction, and then a first order correction. The results of the phase correction are quite dramatic, as can be seen in Figure 4.4

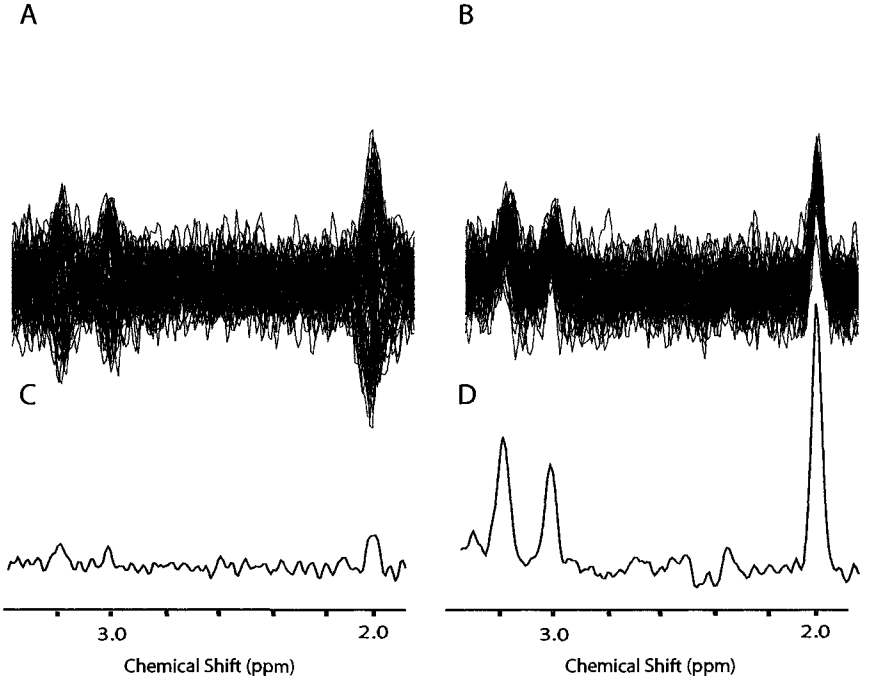

FIGURE 4.4: An overplot of all 64 single average diffusion-weighted spectra obtained in vivo (A) before phase correction and (B) after phase correction. (C) Summation of the unphased spectra displayed in (A) yielded a peak height that was artifactually less than expected. (D) Summation of the individual phased spectra in (B) emphasizes the importance of phase correction in order to accurately quantify the peak heights used to calculate the apparent diffusion coefficients.

4.3.1.1 NAA vs. WATER PHASE CORRECTION

Prior to the work presented in this thesis only zero order phase corrections were performed on the residual water peak [28, 29]. This was usually done because the water suppression can be altered so that a residual water peak, with reasonable intensity (i.e. decent SNR in a single spectrum), can be left. However, phase correction on the residual water peak, while entirely valid, may not be the most accurate measure. If NAA is the main metabolite of interest, perhaps phase correction on NAA would be more beneficial, assuming of course the SNR of NAA is large enough to perform a phase correction on.

Using three different phase correction methods in two different regions of the human

Some of section 4.3.1.1 was published in:
Ellegood, J., Hanstock, C.C., and Beaulieu, C. Phase Correction in Diffusion Tensor Spectroscopy. ISMRM Workshop on Methods for Quantitative Diffusion MRI of Human Brain, Lake Louise, AB, Canada (March 2005).

brain, the Trace/3 ADC and FA was calculated for NAA, tCr, and Cho, Table 4.3. The three phase correction methods used were a zero order phase correction on the NAA peak in order to maximize the given signal from NAA (Zero Order NAA), zero order phase correction on the H_2O peak in order to maximize the signal from H_2O (Zero Order H_2O), and zero order phase correction on the NAA peak in order to maximize the NAA peak with first order phase correction in order to minimize the H_2O peak (Zero Order NAA / First Order). While the two phase correction methods using the zero order correction on the NAA peak were similar, there were differences between zero order correction on water or NAA.

Phantom: The phantom data in Table 4.3 demonstrates the consistency of the Trace/3 ADC (SD < 5%), which would be expected since a phantom does not require the motion correction that an in-vivo study would. The Trace/3 ADC values are consistent with previous literature, regardless of phase correction method [119], and the low FA values (0.11 - 0.17) indicate little anisotropy, which is expected.

In-Vivo: Trace/3 ADC and FA values for two different regions (Fig. 4.5) in the human brain can be found in Table 4.3. Depending on the phase correction method used, different trends can be seen in the data. For example, if one were to use the Z-H2O phase correction method, the Trace/3 ADC trend between metabolites would be NAA $\sim$ Cr $\sim$ Cho; however, if one were to use the ZF-NAA or Z-NAA phase correction method, the trend would be NAA < Cr $\sim$ Cho, which could lead to differing conclusions of the relative Trace/3 ADC values.

Figure 4.5 shows example spectra from the human brain in the two regions in Table 4.3. It is clearly evident from both the Table and the Figure that the different phase correction methods yield different results.

The signal intensity of NAA tends to be higher in the ZF-NAA and Z-NAA phase correction methods, compared to the Z-H_2O method, whereas the signal intensity of Cr and Cho tend to be higher in the Z-H_2O method (Fig. 4.5). These changes in signal intensity with phase correction lead to the conclusion that the Z-H_2O method phase Cr and Cho more coherently, and the Z-NAA or ZF-NAA method phase NAA more coherently. Therefore, it may be beneficial to use different phasing methods for examining each specific metabolite.

From this information we concluded the best phase correction method for in-vivo DW-MRS or DTS was to zero order phase correct on the NAA peak, especially if NAA is your main metabolite of interest, for quantification of NAA. For quantification of Cr and Cho, on the other hand, it would appear that zero order phase correction on the water peak is the best method. It should be noted that the first order phase correction is not required

Phase Correction Method	Trace/3 ADC (x 10^{-3} mm^2/s)	Fractional Anisotropy
N-Acetyl Aspartate		
Phantom (n=8)		
Zero Order NAA	0.61±0.03	0.12±0.04
Zero Order H_2O	0.67±0.03*	0.17±0.02*
Zero (NAA) / First Order	0.62±0.02	0.11±0.04
Occipital Gray Matter (N=5)		
Zero Order NAA	0.13±0.02	0.49±0.08
Zero Order H_2O	0.14±0.02	0.45±0.14
Zero (NAA) / First Order	0.14±0.01	0.40±0.08
Splenium of the Corpus Callosum (N=5)		
Zero Order NAA	0.21±0.02	0.57±0.04
Zero Order H_2O	0.26±0.02*	0.54±0.06
Zero (NAA) / First Order	0.20±0.03	0.58±0.11
Creatine		
Phantom (n=8)		
Zero Order NAA	0.79±0.02*	0.11±0.03
Zero Order H_2O	0.84±0.03	0.14±0.03*
Zero (NAA) / First Order	0.81±0.02	0.11±0.03
Occipital Gray Matter (N=5)		
Zero Order NAA	0.16±0.04	0.65±0.09
Zero Order H_2O	0.14±0.03	0.56±0.04
Zero (NAA) / First Order	0.21±0.04	0.62±0.06
Splenium of the Corpus Callosum (N=5)		
Zero Order NAA	0.31±0.03	0.65±0.09
Zero Order H_2O	0.26±0.04	0.55±0.16
Zero (NAA) / First Order	0.32±0.06	0.60±0.08
Choline		
Phantom (n=8)		
Zero Order NAA	0.92±0.03*	0.12±0.03
Zero Order H_2O	0.97±0.03	0.15±0.04
Zero (NAA) / First Order	0.95±0.03	0.13±0.03
Occipital Gray Matter (N=5)		
Zero Order NAA	0.15±0.02	0.66±0.14
Zero Order H_2O	0.13±0.03*	0.66±0.14
Zero (NAA) / First Order	0.20±0.04	0.57±0.04
Splenium of the Corpus Callosum (N=5)		
Zero Order NAA	0.35±0.04*	0.63±0.12
Zero Order H_2O	0.27±0.07	0.57±0.12
Zero (NAA) / First Order	0.24±0.04	0.68±0.05

TABLE 4.3: Trace/3 ADC and FA values for NAA, Cr, and Cho in two separate regions in the human brain. Three different phase correction methods were used in this Table. Zero order phase correction on the NAA peak, Zero order phase correction on the H_2O peak, and Zero order phase correction on the NAA peak with First order phase correction on the H_2O peak. * indicates a significant difference ($p<0.05$) of the Z-NAA and Z-H2O phase correction methods compared with the ZF-NAA method using a paired t-test for each metabolite.

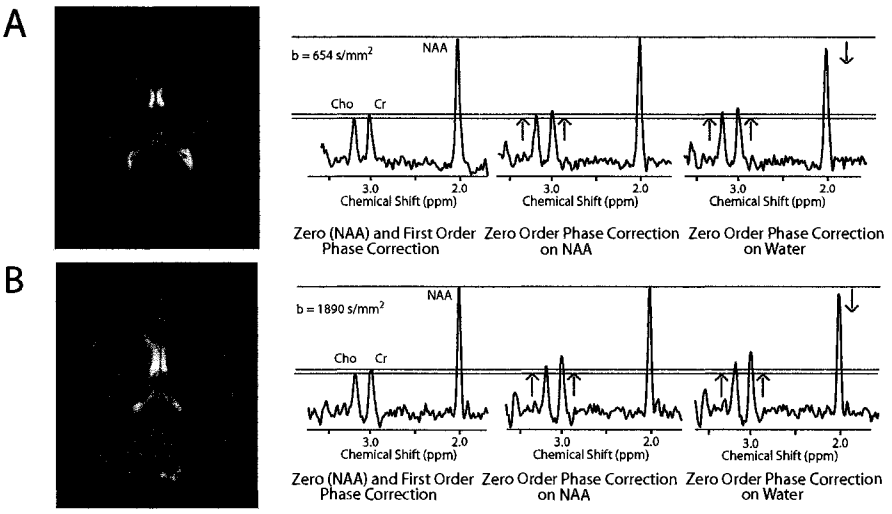

FIGURE 4.5: Example spectra for each phase correction method from both the corpus callosum region (A) and the occipital grey matter region (B). The changes in signal intensity illustrated above lead to the conclusion that the Z-H_2O method phases the Cr and Cho more coherently, and the Z-NAA or ZF-NAA method phase NAA more coherently.

for quantification of NAA or tCr and Cho, because the zero order phase correction is certainly adequate.

4.4 ANALYSIS

The analysis of DW-MRS data is relatively straight forward; however there is some debate about which is the best method. The signal intensity must be calculated in order to be used in equation 3.2; however, there are different ways to calculate it. The peak height can be measured by calculating the distance from the maximum of the peak to a spline fit of the baseline on the vertical of the maximum (Fig. 4.6), or you can calculate the area of the peak by using either a program such as LCModel [121], or by some other means similar to how peak height was measured except calculating the whole area under the peak. Each method has its own pros and cons.

4.4.1 CALCULATING PEAK INTENSITY

Determination of the peak height is extremely robust, and the variability in the measurement is rather low. The main problem with calculating the signal intensity of a given

Some of section 4.4.1 was published in:
Ellegood, J., Hanstock, C.C., and Beaulieu, C. Quantification Methods for Diffusion Tensor Spectroscopy of Human Brain. ISMRM Workshop on Data Processing for MR Spectroscopy and Imaging, Warrenton, Virginia, USA (November 2006).

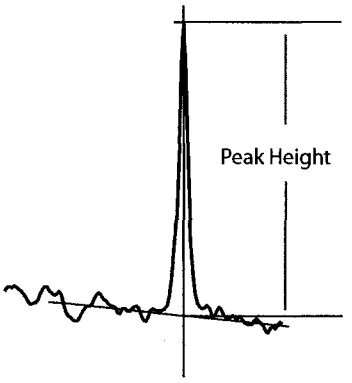

FIGURE 4.6: A diagram explaining the calculation of peak height for a given metabolite peak

metabolite, by any method, is the baseline placement. Variability in the baseline, however, does not have as strong an effect on the peak height calculation as it does on the peak area calculation. Imagine an isosceles triangle, the majority of the area is in the bottom 1/2 of the triangle; therefore, if the baseline is slightly off, it would have a larger effect on the calculation of the peak area. Peak height does have its disadvantages as well. An assumption one makes when measuring the peak height is that the shim is not changing considerably between measurements, which may or may not be the case. The shim in spectroscopy refers to the width of the peak at half its height. The area under the peaks in NMR spectra is conserved as long as the concentration of the metabolites in the voxel is not changing, and therefore a variation in the shim (i.e and increase in the width of the peak) would cause the peak height to increase or decrease, while the area remains consistent.

Because of subtle changes in the shim over time, peak area measurements are thought to be more accurate. Furthermore, LCmodel is a "hands off" approach to calculating the peak area of metabolites from in-vivo data [121]. However, the data is quite variable when compared with the spline fit methods, and is thought to be caused by the baseline placement not being as accurate in the LCModel program. While LCModel is extremely easy to use after the initial setup up, the "hands off" method may not be as desirable if a better job can be done manually.

Using an in-house diffusion-weighted STEAM (STimulated Echo Acquisition Mode) sequence (δ = 15ms,Δ = 208.3ms, TM = 170ms, TE = 76.6ms, TR = 3s, 2048 sample points, spectral width 2.5 kHz, and an acquisition time 800 ms) two signal intensity measurement methods were tested, namely measuring the peak height (Spline), or the peak area

(LCModel). The peak height was calculated in the Spline method, analogous to the above example, by measuring the distance from the maximum peak amplitude to a spline fit of the base of the peak after a 1 Hz linewidth filter was applied to the given data. The peak area was calculated using LCModel [121] using basis sets for metabolites generated by numerical simulation. The ADC values in six individual directions were then calculated by measuring the slope of the b-value versus ln(signal intensity), where signal intensity is either the peak area or peak height. The ADCs measured can then be used to calculate the mean diffusivity (MD) and fractional anisotropy (FA), which will allow us to determine the best method to use.

Both Spline and LCModel measurements yielded similar values for MD in the aqueous phantom (Table 4.4). In an ideal case the FA value would be zero, but due to the noise variations between the spectra, quantification is not ideal, and therefore, the FA is not zero for either method; however it would seem from Table 4.4 that the Spline method is less variable as indicated by the increased FA of the LCModel method, which was caused by a larger spread in the six directional ADC values.

	Spline		LCModel	
Metabolite	Mean Diffusivity (x 10^{-3} mm^2/s)	Fractional Anisotropy	Mean Diffusivity (x 10^{-3} mm^2/s)	Fractional Anisotropy
Phantom (n=3)				
NAA	0.65±0.01	0.15±0.04	0.62±0.02	0.20±0.01*
Cr	0.78±0.06	0.11±0.02	0.77±0.03	0.20±0.04*
Cho	0.92±0.04	0.08±0.02	0.93±0.03	0.16±0.03*
Gray Matter (N=10)				
NAA	0.14±0.03	0.52±0.10	0.22±0.05*	0.69±0.12*
tCr	0.15±0.03	0.69±0.09	0.20±0.07	0.72±0.14
Cho	0.16±0.03	0.73±0.12	0.19±0.08	0.62±0.15
White Matter (N=20)				
NAA	0.19±0.03	0.54±0.14	0.28±0.05*	0.60±0.17
tCr	0.24±0.04	0.64±0.14	0.28±0.08	0.68±0.13
Cho	0.25±0.06	0.64±0.15	0.22±0.07	0.74±0.09

TABLE 4.4: Aqueous phantom (N=3), in-vivo gray matter (N=10), and in-vivo white matter (N=20) measurements of Mean Diffusivity (MD) and Fractional Anisotropy (FA) of N-acetyl Aspartate (NAA), creatine (Cr, tCr in-vivo), and choline (Cho) using the two different quantification methods. * indicates significance ($p<0.05$, paired T-Test) when compared with the Spline method

The MD calculated for NAA using LCModel was significantly larger than calculated using the Spline method for all regions (paired t-test), this significance was not seen for tCr and Cho which are consistent with the phantom MD data which is similar in both

methods for all metabolites. While the FA tended to be larger for the LCModel method in the majority of comparisons it was not a significant difference most likely caused by the large variability in FA between subjects.

Simulated spectra with varying degrees of noise (ranging from zero noise to a signal to noise ratio (SNR) of $\sim$ 2.5 for NAA at b=654 s/mm^2) were created with appropriate amplitudes for NAA, Cr, and Cho. The amplitudes of the peaks were chosen to give FA and MD values consistent with the in-vivo data set. The simulated data consisted of spectra calculated to represent six different diffusion directions at three different b-values (0, 654, and 1890 s/mm^2) and were repeated for the six different levels of noise (SNR of , 12.8, 6.3, 4.2, 3.1, and 2.5 for NAA at 654 s/mm^2) with each level of noise including ten repetitions to determine the variability of the measurement. After the simulated spectra were created the peaks were quantified by using both the Spline and LCModel methods and the MD and FA were calculated for each metabolite at each SNR value.

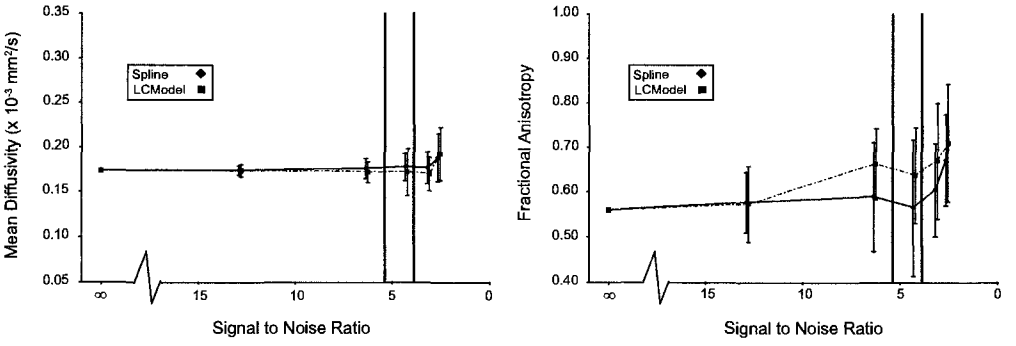

FIGURE 4.7: Mean Diffusivity (MD) and Fractional Anisotropy (FA) measured from simulated data by using two different quantification methods with increasing signal to noise ratio (SNR), Spline method (black line) and LCModel (red dashed line). The green lines indicate the range of SNR used in our in-vivo study (SNR of NAA peak at b=654 s/mm^2). At lower SNR (<7) we start to see a difference in reported FA values between the two methods.

Simulations show similar trends as to what was seen in phantom with MD showing little difference between the quantification methods, and at lower SNR the FA measured by using LCModel was elevated in comparison with the Spline method (Figure 4.7). Figure 4.7 also indicates the range of SNR values used in this study (between the green lines) which explains some of the differences seen in Table 4.4.

The LCModel approach was found to be more variable at lower SNR, which may be due to the complexity of the LCModel process and the propagation of errors. The Spline method may in fact be more robust and less variable because of its simplicity. Although LCModel may be favored due to its "hands off" approach, it appears that the low SNR associated with a DW-MRS data set can cause a greater variability in the ADC calculation,

when using LCModel to quantify the peaks, leading to an elevated FA in vivo. Therefore, in the majority of this thesis the Spline method was used for quantification of the signal intensity.

4.4.2 Calibration using a Phantom

An example of a metabolite spectra in phantom is shown in Figure 4.8. It can clearly been seen that as the b-value is increased the signal intensity drops as a result.

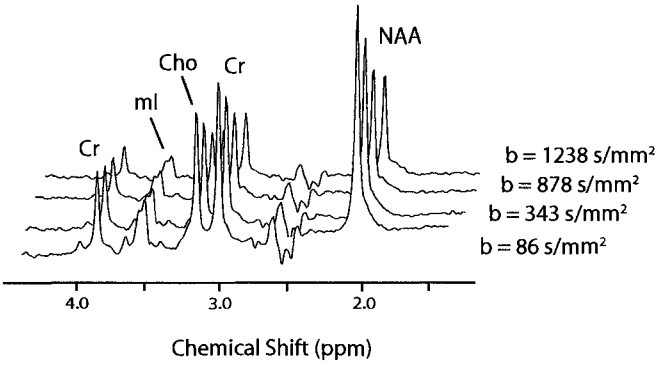

Figure 4.8: Metabolite spectra, which includes NAA, Cr, Cho, and mI at increasing b-value.

Figure 4.9 shows an example of the ADC curves for a properly calibrated phantom. While there is some separation in the slopes of the signal intensity vs. b-value graph, it is minimal, and actually yields a low FA value of 0.07 and an MD of 0.77 x 10^{-3} mm^2/s for Cr in phantom.

Since the ADC values depend very highly on accurate measurements of the b-value, which in turn require accurate measurements of the gradient strength (Equations 3.2 and 3.3), it is imperative to ensure that the gradient values are correct. Therefore, the gradients must be calibrated prior to the initial measurements, by using the known ADC value of one of the metabolites in phantom, in the case of the work presented here creatine was used with an ADC in phantom of 0.80 x 10^{-3} mm^2/s at 20 °C [119]. Creatine was chosen because of its consistency between reported literature. NAA ranged from 0.6 to 0.9 x 10^{-3} mm^2/s and Cho ranged from 0.9 to 1.3 x 10^{-3} mm^2/s [119], Cr was the only consistent metabolite between studies at 0.8 x 10^{-3} mm^2/s. Calibration of the gradients involved calculating the gradients step size in $\mu T/m$ per DAC value (which is a SMIS specific number which is used in the hardware to input the gradient strength). The maximum DAC value is 32767 and the gradient strength is 20,000 $\mu T/m$; therefore, the value we are looking for is the ratio 20000/32767 which equals G/DAC = 0.6104 $\mu T/(m\ DAC)$. That number can then be adjusted as need be until the ADC calculated for Cr is 0.80 x

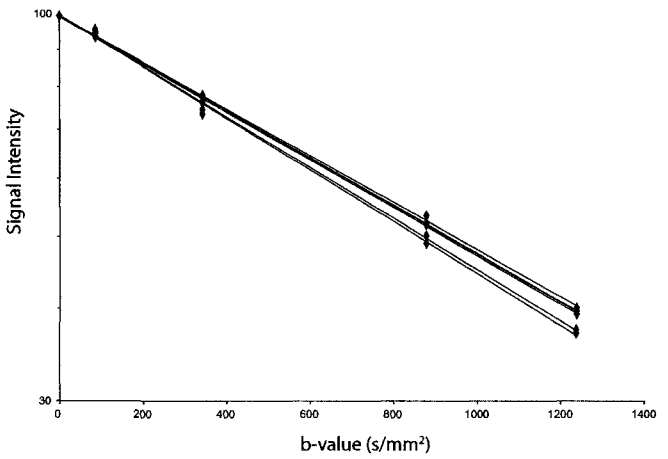

FIGURE 4.9: Diffusion attenuation curves for the creatine metabolite with diffusion sensitizing gradient applied in six different directions after successful calibration. It can clearly be seen that the lines are linear and their slope show little variability as expected from an isotropic phantom.

10^{-3} mm^2/s in all gradient directions. This would be a similar procedure for other MRI systems. It is a way to make sure the gradient number you are inputting to the system is the actual gradient strength used. Confirming the accuracy of the gradient is imperative in DW-MRS, because of the sensitivity of the sequence.

For example, if you were calibrating the X gradient, based on the Cr ADC, and the ADC calculated is 0.86 x 10^{-3} mm^2/s, that is too high, you work backwards from the signal intensity drop and the known timings to calculate G for the DAC value read by the spectrometer. First you need to determine the b-values that would have given us the right ADC value. From there you can use equation 3.3 to solve for the gradient strength, which is assumed to be the actual gradient strength based on our diffusion measurements. If that is performed for each b-value examined, you then plot the actual gradient strengths versus the DAC value and determine the new G/DAC ratio, which is input into the sequence. This number will change depending on the sequence, and should be optimized, or at least checked, anytime a sequence is altered, since the gradients may not be linear (if a different b-value is used), possible different eddy current effects, imperfect gradient profiles, interactions with different parts of the sequence could all affect the calibration of the sequence. Once the gradients have been successfully calibrated, you are ready to start your DW-MRS study, enjoy!

Part II

Experiments

CHAPTER 5

TRACE APPARENT DIFFUSION COEFFICIENT OF METABOLITES IN HUMAN BRAIN

5.1 INTRODUCTION

Magnetic resonance is well established for measuring the diffusion properties of water in the human brain, and it has been proven to be useful in numerous neurological disorders. Diffusion weighted imaging (DWI) of tissue water includes contributions from exchanging intra- and extracellular water, which makes compartment specific interpretation of diffusion characteristics rather complex. The diffusion characteristics of intracellular metabolites can be measured by incorporating diffusion sensitizing gradients with spatial localization in a spectroscopy pulse sequence, i.e. diffusion weighted magnetic resonance spectroscopy (DW-MRS) [98, 99, 101, 119, 122]. The main research focus of DW-MRS thus far has been on animal models of cerebral ischemia [100, 102–107] in which the apparent diffusion coefficients (ADC) of the singlet metabolites reduce significantly in the acute phase of cerebral ischemia, similarly to the ADC reduction of water. These studies indicate that diffusion changes in metabolites may be useful in probing the effect of stroke and other pathologies on the intracellular environment.

To date, there have only been two published studies on the diffusion characteristics of the metabolites N-acetyl aspartate (NAA), creatine and phosphocreatine (tCr), and choline (Cho) in the human brain [28, 29]. Posse et al. [28] discussed problems with measuring the ADC of the metabolites, including low concentration, small ADCs, and macroscopic motion due to involuntary subject movements, respiration, and cerebrospinal fluid related brain pulsations. These motion errors cause a decrease in the signal intensity of the

A version of this chapter was published in:
Ellegood, J., Hanstock, C.C., and Beaulieu, C. Trace ADC of Metabolites in Human Brain. Proc. 12th Meeting of the International Society of Magnetic Resonance in Medicine, Kyoto, Japan (May. 2004).
Ellegood, J., Hanstock, C.C., and Beaulieu, C. Trace ADC of Metabolites in Human Brain using Diffusion-Weighted MRS. Magnetic Resonance in Medicine 2005;53:1025-1032.

metabolite peaks, which in turn results in an apparent increase in the measured ADC. Their study proposed a phase error correction method using the residual water peak as well as cardiac gating for correction of the motion-induced errors. Harada et al. [29] applied these methods and reported that the ADCs of NAA, tCr, and Cho were found to decrease in acute stroke and increase in the peripheral region of a tumor including edema. It was suggested that, since NAA is a neuronal marker, the ADC differences are an indication of neuronal cell viscosity changes as a result of the pathological status of the tissue.

The micro-structural organization of white matter in brain tissue leads to directional-dependence (i.e. anisotropy) of the ADC of water, and presumably of the metabolites as well. However, the Trace/3 ADC provides a rotationally invariant measure of molecular diffusion in tissue [123]. Quantification of the Trace/3 ADC values of these singlet metabolites have been examined in rat brain [118], but they have never been reported in human brain. The two previous human studies examined the ADC of NAA, tCr, and Cho in subcortical white matter of human brain, but the diffusion was only measured in one arbitrary direction. Therefore, the purpose of this study is to quantify the rotationally invariant Trace/3 ADC values of the metabolites NAA, tCr, and Cho in various regions of the healthy human brain. A new phase correction method is proposed for processing the diffusion-weighted spectra.

5.2 Methods

A bird cage head coil (Medical Advances, Milwaukee, WI) was used for MR measurements on a SMIS 3T MRI scanner equipped with a maximum gradient strength of 20 mT/m. The diffusion experiments were performed using a modified single-voxel, diffusion-weighted STEAM (STimulated Echo Acquisition Mode) sequence (Fig. 5.1). The diffusion gradient length (δ) was 20 ms with a diffusion gradient spacing (Δ) of 124.6 ms. The sequence parameters were: 2048 sample points, spectral width 2.5 kHz, acquisition time 800 ms, TE=180 ms, TM=30 ms, TR=3 s, voxel size of 2.5 x 2.5 x 2.5 cm^3 = 15.6 cm^3. Water suppression was achieved using a dual inversion recovery with two hyperbolic secant pulses of 80 ms in duration (inversion times of 1400 ms and 200 ms), followed by water crusher gradients along the X and Y directions of 20 ms duration. The volunteer's head was secured by using a vacuum pillow to minimize macroscopic motion. The diffusion gradient strengths in the X, Y and Z directions were temperature calibrated on the water diffusion decay curves using a known value for the water ADC at 20°C (1.99 x 10^{-3} mm^2/s) [124]. Furthermore, the gradient calibration was fine tuned using the reported

tCr ADC at 20°C because of its consistent value (0.80 x 10^{-3} mm^2/s) [119]. The same four incremental current amplitudes (i.e. DAC values) were used for each gradient direction which yielded the following experimentally determined b-values of 96, 305, 721, and 1305 s/mm^2 for X; 98, 370, 806, and 1479 s/mm^2 for Y; and 89, 471, 1008, and 1768 s/mm^2 for Z. The largest b-values left sufficient metabolite signal in a single average spectrum at the highest diffusion weighting and the 17-24% drop in signal intensity in human brain was adequate to calculate the ADC. To ensure accuracy, the gradient calibration was validated on the metabolites by performing diffusion measurements in 3 orthogonal directions (X, Y, and Z) using an isotropic 100 mL spherical water phantom (see Table 5.1) containing NAA (30 mM), Cr (30 mM), and Cho (10 mM) (Sigma-Aldrich Canada Ltd., Oakville, Ontario).

Metabolite	Apparent Diffusion Coefficient (x 10^{-3} mm^2/s)			
	X	Y	Z	Trace/3
Water	2.07±0.06	2.02±0.05	2.01±0.05	2.03±0.05
NAA	0.66±0.05	0.69±0.04	0.70±0.04	0.68±0.01
tCr	0.79±0.04	0.80±0.05	0.77±0.06	0.79±0.02
Cho	1.00±0.02	0.97±0.05	0.93±0.05	0.97±0.02

TABLE 5.1: Phantom measurements (N = 6, Mean ± SD) of the X, Y, Z, and Trace/3 Apparent Diffusion Coefficients (ADC) in a 100-mL spherical phantom containing water, NAA (30 mM), Cr (30 mM), and Cho (10 mM) at 20°C using the NAA phase correction method. The ADCs in the various directions have little difference in these metabolites, as expected from an isotropic phantom.

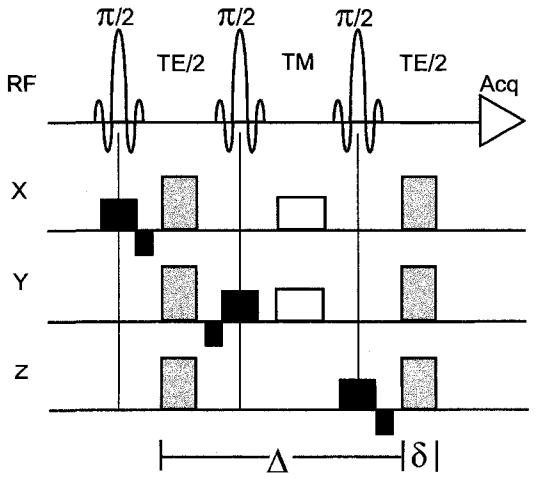

FIGURE 5.1: Diffusion-weighted STEAM sequence. Diffusion gradients (gray), TM spoilers (white), and slice selection and refocusing gradients (black) are shown (gradients not to scale). Water suppression (not shown) consisted of a dual inversion recovery.

Optimization of the first and second order shims resulted in an in-vivo water line width of ~3-5 Hz depending on the region and person. The line width did not change significantly (±0.3Hz) with increasing b-value. We acquired 8 single average spectra for the unsuppressed water peak, and sixty-four single average spectra with water suppression for each of the 4 different b-values and along the 3 orthogonal directions (X, Y, and Z, with respect to the magnet). Four different b-values were acquired to confirm the linearity of the ADC calculation. This acquisition scheme yielded 12 water spectra and 12 summed metabolite spectra for each brain region examined. The total measurement time for the set of 12 summed metabolite spectra was ~43 min at 3 min and 36 secs per spectra. Including axial, coronal, and transverse scout images, as well as the water spectra, a total exam time of ~75 min for each brain region was required. Hence, it was practical to study only one brain region per scanning session.

Processing of the experimental data included eddy current correction using the method outlined in Jehenson et al. [120]. Each individual single average spectrum was then baseline corrected (in case of any offsets between single average spectra), filtered using a 1 Hz linewidth exponential, and phase corrected (zero order on the NAA peak and first order on entire spectrum) before the spectra were summed. The receiver and transmitter phase were not altered throughout the 64 averages. The phase correction was performed to account for linear motion related phase errors that varied between spectra [28]. This method of phase correction on the individual spectra was important since it was observed that averaging of the spectra without phase correction yielded unexpectedly high ADC values due to reduced peak amplitudes at high b-values (i.e. destructive interference). It should be noted that these phase variations between individual spectra were less in the phantom studies than in-vivo for both the zero order (Fig. 5.2) and first order (data not shown) corrections. The small phantom phase variations were likely due to hardware instability or phantom vibration, but most of the in-vivo phase variations were subject-derived. Phase variations in vivo and phantom were ultimately corrected for using the same phase correction method. Note that aside from the results presented in part of Table 5.2, all other results, tables, and figures involve the NAA peak phase correction method. In a separate analysis of the in-vivo data and for comparison to our NAA peak phase correction method, the individual spectra were zero order phase corrected on the water peak in a manner similar to the previously published human DW-MRS studies [28, 29]. The ADCs were calculated from the slope of the ln(peak intensity) versus b-value for both NAA peak and water peak phase corrections methods, and the mean diffusivity was derived subsequently by taking the average ADC obtained from the three orthogonal diffusion directions (denoted by Trace/3 ADC). Relative to the low b-value, the signal

intensity of the NAA peak in the summed spectrum in-vivo dropped by ~17-24% at the high b-value depending on the brain region and diffusion direction (Fig. 5.3).

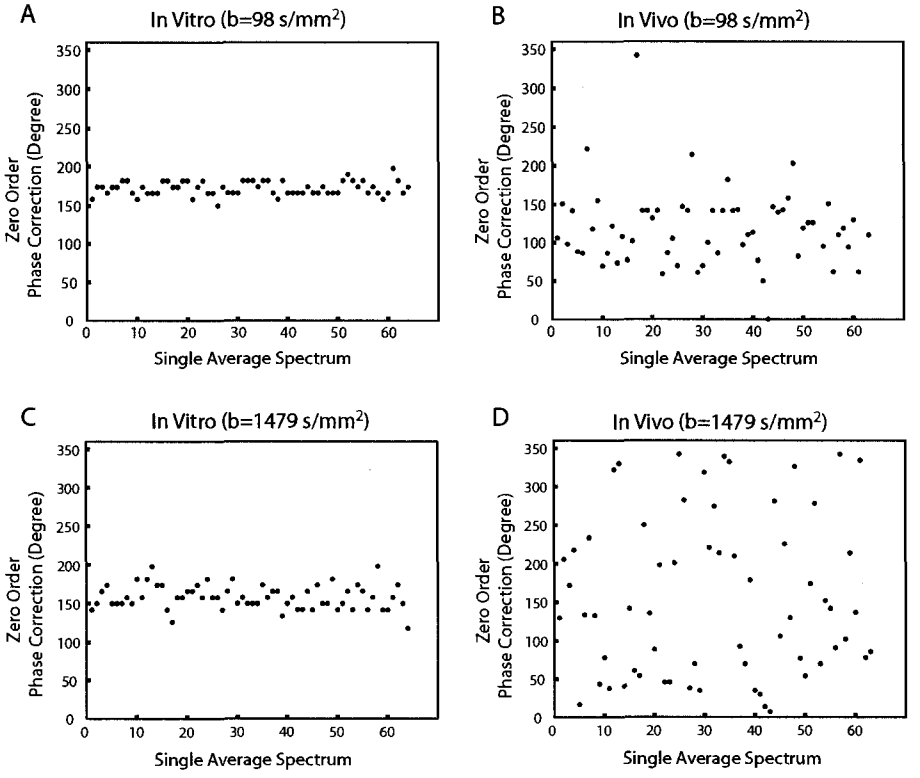

FIGURE 5.2: Phantom (A, C) and in vivo (B, D) zero-order phase correction required for each individual single average spectrum of the NAA peak. Diffusion was measured in the Y direction (anterior-posterior) at the weakest (b = 98 s/mm^2, A, B) and strongest (b = 1479 s/mm^2, C, D) b value. The standard deviation (i.e., variability) of the phase correction required in phantom was found to be 9° for the smallest b value and 16° for the largest b value, whereas in vivo it was 53° for the smallest b value and 104° for the largest b value in this particular case. Note the greater variability for phase correction in vivo relative to phantom, particularly at the higher b value.

NAA, the most prominent peak in the spectrum, was chosen for phase correction in the individual spectra since the SNR of a single average NAA peak for a 15.6 cm^3 voxel at 3T (with our current acquisition parameters) was sufficient for the correction, and NAA was our primary metabolite of interest. A simulation was performed to test the validity of our phase correction program. Sixty-four single average spectra were created with appropriate amplitudes to produce ADCs of 0.14 x 10^{-3} mm^2/s for NAA, 0.17 x 10^{-3} mm^2/s for tCr, and 0.18 x 10^{-3} mm^2/s for Cho. For two distinct b-values (low b=382 s/mm^2 and high b=1517 s/mm^2), random phase errors were implemented similar to the in-vivo observations [in vivo subcortical white matter: zero order - standard deviation

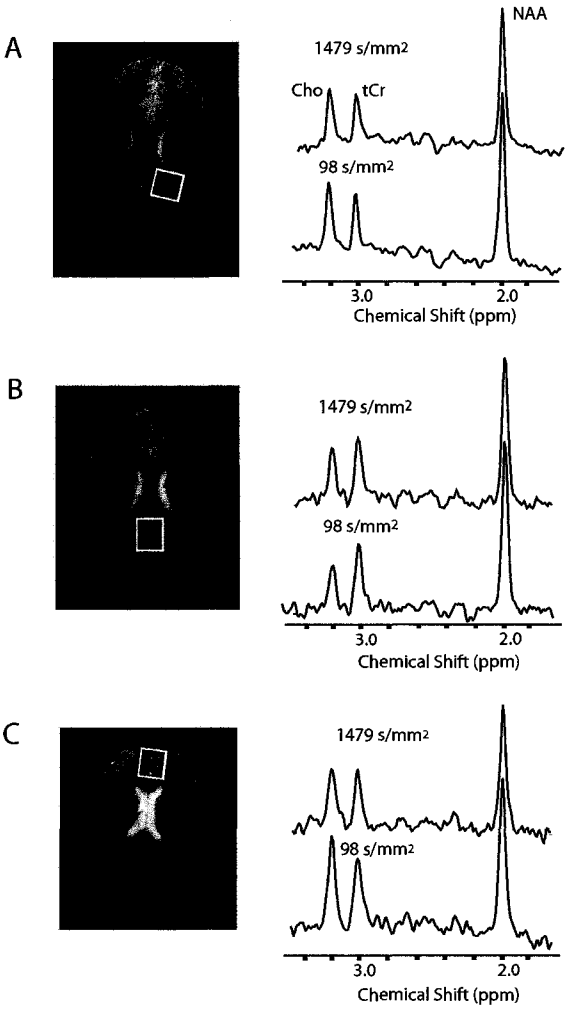

FIGURE 5.3: 3-T spectra at low and high b values with the diffusion gradient applied in the Y (anterior-posterior) direction in (A) subcortical white matter (SWM), (B) occipital gray matter (OGM), and (C) frontal gray matter (FGM). The signal intensity of the NAA peak dropped 17, 20, and 24% at higher b values in the SWM, OGM, and FGM regions, respectively

Region/Metabolite	Trace/3 ADC (x 10^{-3} mm^2/s) Phase Correction Method	
	Water	NAA
Subcortical White Matter (N=6)		
Water	0.78±0.06	—
NAA	0.16±0.03	0.14±0.02
tCr	0.17±0.04	0.19±0.04
Cho	0.21±0.04	0.18±0.06
Occipital Gray Matter (N=4)		
Water	1.05±0.23	—
NAA	0.13±0.01	0.12±0.01
tCr	0.17±0.05	0.16±0.04
Cho	0.14±0.03	0.16±0.02
Frontal Gray Matter (N=4)		
Water	0.99±0.04	—
NAA	0.18±0.03	0.17±0.04
tCr	0.20±0.06	0.18±0.05
Cho	0.19±0.08	0.20±0.07
All Regions (N=14)		
Water	0.91±0.15	—
NAA	0.15±0.03	0.14±0.03
tCr	0.18±0.05	0.17±0.04
Cho	0.18±0.05	0.18±0.05

TABLE 5.2: Trace/3 ADC of Water, NAA, tCr, and Cho in the Subcortical White Matter (SWM), Occipital Gray Matter (OGM), Frontal Gray Matter (FGM), and all regions combined. ADC values were calculated using two phase correction methods: zero-order phase correction on the NAA peak and first-order on the entire spectrum (NAA method) and zero-order phase correction on the water peak (water method).

(SD) of ~56° for low b and ~79° for high b, first order - SD of ~538° for low b and ~584° for high b; simulation parameters: zero order - SD of ~62° for low b and ~77° for high b, first order - SD of ~434° for low b and ~564° for high b]. Then the simulated spectra were run through the program used for the phase correction, the ADCs were calculated, and the differences from the original ADC values were noted. The reproducibility and accuracy of the phasing method was evaluated at three different levels of SNR (6.4, 8.9, 18.0 for b=382 s/mm^2 and 5.6, 7.9, 15.4 for b=1517 s/mm^2). The simulated spectra and processing were run 6 times for each set of conditions to calculated the mean and the variability of the resultant ADC values.

Three different brain regions were examined in healthy volunteers, namely the superior posterior subcortical white matter (SWM) (N=6), occipital gray matter (OGM) (N=4), and gray matter in the frontal cortex (FGM) (N=4) (Fig. 5.3). Statistical analysis of the NAA, tCr, and Cho Trace/3 ADC values used a two tailed paired t-test and $p<0.05$ was considered significant. A single factor ANOVA was used to compare results from dif-

ferent brain regions. Intra-subject variability was measured in the SWM region of three subjects, who were examined on three different occasions.

5.3 Results

Table 5.1 lists the ADCs measured in an isotropic 100 mL spherical water phantom containing NAA, tCr, and Cho. The Trace/3 ADC values in the phantom were 0.68±0.01 x 10^{-3} mm^2/s for NAA, 0.79±0.02 x 10^{-3} mm^2/s for Cr, and 0.97±0.02 x 10^{-3} mm^2/s for Cho which is consistent with values previously reported in the literature ranging from (0.6-0.9) x 10^{-3}, 0.8 x 10^{-3}, and (0.9-1.3) x 10^{-3} mm^2/s for NAA, Cr, and Cho, respectively [119]. Little variation was observed in the X, Y, and Z ADC values, as was expected from an isotropic environment.

The three brain regions examined with DW-MRS are illustrated in Figure 5.3. Example spectra from those regions at low (98 s/mm^2) and high (1479 s/mm^2) b-values are also illustrated in Figure 5.3. The importance of correcting for phase errors using the NAA peak for individual phase correction is shown in Figure 5.4. The reduction in the singlet peak amplitudes as observed in Figure 5.4, for the highest b-value (b=1768 s/mm^2), results in artefactually high ADC values (up to 140% higher, data not shown) if phase correction of individual spectra is not performed.

Trace/3 ADC measurements of water, NAA, tCr, and Cho are displayed in Table 5.2 using either NAA or water peak for phase correction. There is not much difference in the Trace/3 ADC values for the metabolites regardless of the phase correction method chosen. Our subsequent discussions (includes tables and figures) will focus on the diffusion results obtained with our proposed zero-order phase correction on the NAA peak and first order correction on the entire spectrum. The Trace/3 ADC of NAA is consistently lower than tCr and Cho in human brain (p=0.006 for tCr vs. NAA and p=0.005 for Cho vs. NAA). The Trace/3 ADC values ranged from (0.12±0.01 - 0.17±0.04) x 10^{-3} mm^2/s for NAA, (0.16±0.04 - 0.19±0.04) x 10^{-3} mm^2/s for tCr, and (0.16±0.02 - 0.20±0.07) x 10^{-3} mm^2/s for Cho depending on the brain region examined. Reproducibility of the measurements were confirmed by examining the intra-subject variability (Table 5.3) and were found to be consistent with standard deviations ranging from 0.02 to 0.04 x 10^{-3} mm^2/s. The r^2 values of the ln(peak intensity) vs. b value for the NAA peak ranged from 0.70-1.00 with an average value of 0.92±0.08, which confirms the linearity of signal decay. It should be noted that the r^2 values for the tCr and Cho peaks were usually poorer than the NAA values; tCr r^2 values ranged from 0.17-1.00 with an average value of 0.80±0.18, and Cho r^2 values ranged from 0.14-1.00 with an average value of 0.78±0.22.

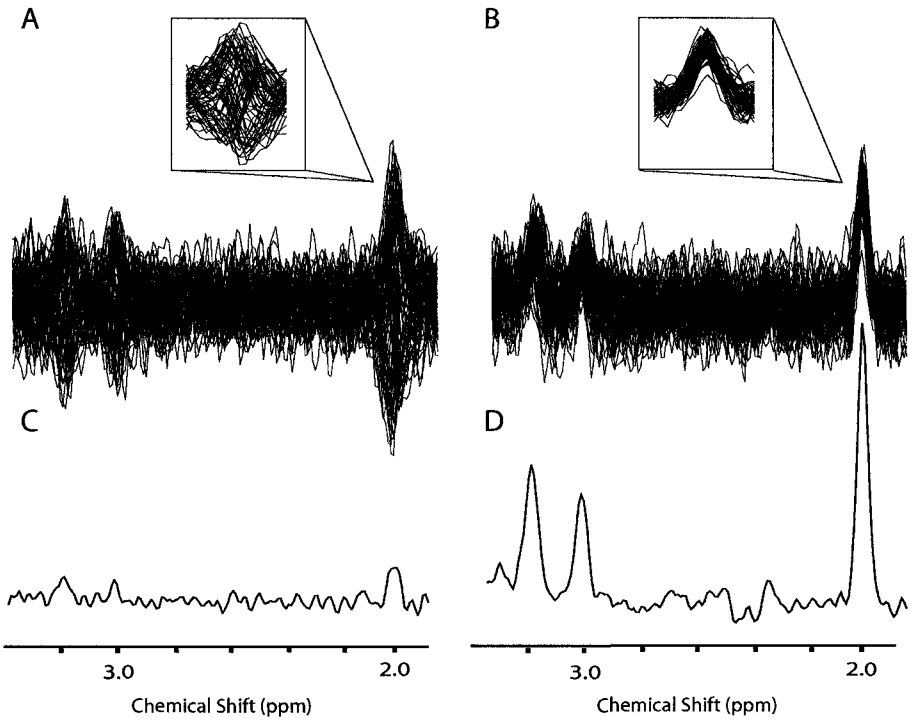

FIGURE 5.4: An overplot of all 64 single average diffusion-weighted (b = 1768 s/mm^2) NAA peaks obtained in the occipital gray matter region (A) before phase correction and (B) after phase correction (zero order on the NAA peak and first order on the entire spectrum). (C) Summation of the unphased spectra displayed in (A) yielded a peak height that was artifactually less than expected. (D) Summation of the phased spectra in (B) emphasizes the importance of phase correction in order to accurately quantify the peak heights used to calculate the apparent diffusion coefficients.

Subcortical White Matter Region	Trace/3 ADC (x 10^{-3} mm^2/s) NAA	tCr	Cho
Intersubject (N=6)	0.14±0.02	0.19±0.04	0.18±0.06
Intrasubject			
Subject 1 (N=3)	0.14±0.03	0.20±0.03	0.13±0.02
Subject 2 (N=3)	0.13±0.02	0.18±0.03	0.18±0.02
Subject 3 (N=3)	0.13±0.02	0.15±0.03	0.13±0.04

TABLE 5.3: An intra- versus intersubject comparison (Mean ± SD) of the Trace/3 Apparent Diffusion Coefficients of NAA, tCr, and Cho in the Subcortical White Matter (SWM) region using the NAA phase correction method

5.4 DISCUSSION

Posse et al. [28] were the first to study quantitatively the diffusion coefficients of NAA, tCr, and Cho in the healthy human brain, which were determined to be 0.18±0.02 x 10^{-3}, 0.15±0.03 x 10^{-3}, and 0.13±0.03 x 10^{-3} mm^2/s, respectively, in the subcortical white matter. However, the diffusion-sensitizing gradients were only applied in one oblique direction (i.e., X, Y, and Z gradients applied simultaneously). Harada et al. [29] also measured the metabolite ADCs of NAA (0.17±0.02 x 10^{-3} mm^2/s), tCr (0.19±0.01 x 10^{-3} mm^2/s), and Cho (0.20±0.02 x 10^{-3} mm^2/s) approximately along the same direction and in the same region. Harada et al. attributed the differences in ADC values between their study and that of Posse et al., to the use of Posse's larger volume of interest (18 cm^3 vs. 8 cm^3) and larger maximal b-value (2200 s/mm^2 vs. 1650 s/mm^2). However, it is also possible that the difference in ADCs resulted from inconsistent single diffusion directions between studies, which may have resulted from different head placements within the scanner. The rotationally invariant Trace/3 ADC, used in our study, eliminates any directional dependence. Our Trace/3 ADC values in the subcortical white matter region (similar to the one region measured by Posse et al. and Harada et al.) were 0.14±0.02 x 10^{-3}, 0.19±0.04 x 10^{-3}, and 0.18±0.06 x 10^{-3} mm^2/s for NAA, tCr, and Cho, respectively (Table 5.2). Although these values are consistent with values reported previously in human brain, the Trace/3 ADC of NAA was somewhat lower than the single-direction ADC values. In our study the Trace/3 ADCs were measured in three different brain regions (15.6 cm^3 volume of interest), and they ranged from (0.12 - 0.17) x 10^{-3} mm^2/s for NAA, (0.16 - 0.19) x 10^{-3} mm^2/s for tCr, and (0.16 - 0.20) x 10^{-3} mm2/s for Cho. The three brain regions were chosen to quantify the diffusion in a predominately white matter region (SWM), and two predominately gray matter regions, one in the occipital lobe (OGM) and the other in the frontal cortex (FGM) (Fig. 5.3). The NAA ADC in the FGM region was found to be slightly

higher than the NAA ADC in the other two regions (p=0.09 for SWM, p=0.04 for OGM), but this difference, could in part, be caused by the lower SNR in the FGM region (Table 5.4).

Previous studies of healthy rat brain [100, 103, 104, 106, 107, 115] have reported single direction ADC values of (0.11 - 0.27) x 10^{-3} mm^2/s for NAA, (0.12 - 0.27) x 10^{-3} mm^2/s for tCr, and (0.09 - 0.28) x 10^{-3} mm^2/s for Cho, and our Trace/3 ADC values in the human brain reflect the lower portion of that range. Trace/3 ADC measurements in the rat brain have been measured to be 0.15±0.01 x 10^{-3} mm^2/s for NAA, 0.15±0.01 x 10^{-3} mm^2/s for tCr, and 0.13±0.01 x 10^{-3} mm^2/s for Cho [118]. In the seven studies mentioned above there appears to be no consistent rank order of the metabolite ADC values in rat brain. Generally, in five of the seven animal studies, Cho has the lowest ADC. In the Posse study [28] the Cho ADC was reported to be lower than the tCr ADC which in turn was lower than the NAA ADC. This was contrary to what was found in the Harada study [29] where the ADCs followed the trend of NAA < tCr $\simeq$ Cho. In our study, when we examine all regions combined, singlet metabolites followed the same trend as the Harada study where NAA was found to be significantly lower that tCr and Cho (Table 5.2). The lower Trace/3 ADC of NAA may not be unexpected given that the phantom diffusion coefficients of the singlet metabolites have the trend NAA < tCr < Cho. However, the tCr and Cho Trace/3 ADC values appear to be almost identical in-vivo, whereas the Trace/3 ADC of Cho is 23% larger than tCr in phantom. It should be noted that the diffusion time (Δ-$\delta/3$) in our sequence was rather long (118 ms), and hence the measurements are in the restricted diffusion regime. Diffusion restriction effects are difficult to avoid in-vivo, because minimal diffusion times (< 10 ms), with sufficient b-values, are hard to achieve with the weaker gradients on human MRI systems.

The two previous studies on humans [28, 29] phase corrected each individual single average spectrum using the water peak as a reference for zero order correction. In order to compare the ADCs resulting from phase correction on the residual water peak, rather than the NAA peak as proposed in our study, the spectra were analyzed by zero-order phase correction of the water peak (Table 5.2). The average ADC of the metabolites for the subcortical white matter region were found to be 0.16±0.03 x 10^{-3} mm^2/s for NAA, 0.17±0.04 x 10^{-3} mm^2/s for tCr, and 0.21±0.06 x 10^{-3} mm^2/s for Cho, which is inconsistent with the much higher ADC values in the previous ungated human study by Harada et al. but it is in good agreement with their gated results [29] and our NAA phase correction method (Table 5.2). A possible explanation for their higher ungated ADC values may be that the poorer spectral SNR at 1.5T affected the quality of the phase correction of the metabolites. If access to a higher field is possible, it may be beneficial to perform the

phase correction on the NAA peak so the single average spectra can be examined for the consistency of the phase correction (Figure 5.4B). Also, at higher b-values there may be insufficient residual water to phase correct on due to water's faster diffusion. In addition, a strong residual water peak may be detrimental since it can distort the baseline and ultimately the quantification of the peak height, particularly in the tCr/Cho region. For these reasons, it may be beneficial to use the NAA peak as the reference for phase correction, especially if NAA is your primary metabolite of interest.

Phase correction on the single-average NAA peak, with SNR of ~8 at low b (382 s/mm^2) in the subcortical white matter, produced reproducible Trace/3 ADC results with very low variability (SD, ~0.02 x 10^{-3} mm^2/s for intra-subject NAA, Table 5.3). To test the accuracy of our phase correction method a simulation was performed in which single average spectra were generated with appropriate phase errors and noise. The average SNR values calculated from our in-vivo data ranged from 6.4 to 8.0 depending on the region (Table 5.4). The simulations demonstrated that the variability of the ADCs and the ADC value tended to increase with lower SNR (Table 5.5). Therefore, our reported values in vivo may be overestimating the ADC values of the metabolites by a small amount, but the lower NAA ADC relative to tCr and Cho is likely correct, because the hierarchy between the metabolites remained intact in the simulations despite the lower SNR (Table 5.5). The experimental Trace/3 ADC values averaged over all three regions were within the errors of the simulated data with the lowest SNR, which supports the accuracy of our phasing method. The simulation also indicates that a single average SNR above 7 for NAA should be targeted to yield reproducible results with our phasing method. The average SNR of the final summed 64 average spectra in the brain was 47±6 (Table 5.4) for the low b-values. Also, the linearity of the experimental diffusion decay curves (average r^2 for NAA = 0.92±0.08) is supportive of this phase correction method. The main drawback of the phase correction method using the NAA peak as a reference is that it requires adequate SNR in a single average spectrum (SNR $\geq$ 7), and therefore, this procedure may not work as well at lower magnetic fields such as 1.5T or at very high b-values with greater attenuation of the NAA peak.

Posse et al. and Harada et al. [28, 29] also used cardiac gating as a means to minimize motion contamination, in addition to the phase correction. Harada et al. [29] calculated ADCs in control subjects with and without cardiac gating. They reported that the ADC of water, NAA, tCr, and Cho all increased by 20-30% without cardiac gating, which was attributed to motion induced by cerebrospinal fluid related brain pulsations. However, our Trace/3 ADC results acquired without cardiac gating were 40-50% lower than the ADC values obtained by Harada et al [29] in the absence of cardiac gating. Our ADC

Region	Mean SNR for single averaged in vivo NAA spectra	
	b=305–471 s/mm^2	b=1305–1768 s/mm^2
FGM (N=4)	6.4±0.5	5.5±0.7
OGM (N=4)	7.2±0.5	6.2±0.5
SWM (N=6)	7.7±1.0	6.0±0.9
All Regions (N=14)	7.2±0.9	6.1±0.8
Region	Mean SNR for summed (64 averages) in vivo NAA spectra	
	b=305–471 s/mm^2	b=1305–1768 s/mm^2
FGM (N=4)	42±2	38±4
OGM (N=4)	48±4	43±4
SWM (N=6)	51±6	44±6
All Regions (N=14)	47±6	42±6

TABLE 5.4: Signal-to-Noise Ratio (SNR) of the in vivo single average and summed spectrum of NAA for each brain region

values obtained without cardiac gating, for both phasing methods, are in the range of those reported in the gated studies. The avoidance of cardiac gating minimizes the examination time, allows a consistent TR that avoids potential T1-related errors, and leads to simpler implementation particularly on high-field research scanners often not equipped for cardiac gating.

Mean SNR for single averaged simulated NAA spectra		ADC (x10^{-3} mm^2/s)		
b=382 s/mm^2	b=1517 s/mm^2	NAA	tCr	Cho
Truth		0.14	0.17	0.18
18	15.4	0.13±0.01	0.17±0.03	0.17±0.01
8.9	7.9	0.14±0.01	0.19±0.03	0.20±0.02
6.4	5.6	0.16±0.04	0.22±0.10	0.20±0.06

TABLE 5.5: ADC values calculated with the proposed NAA phasing routine on single average spectra which were simulated with random phase errors and various SNR

There are, however, some limitations to this study. One such limitation is the large voxel size of 15.6 cm^3 (2.5 cm isotropic) which includes contributions from a variety of tissue microstructures. Therefore, quantification of metabolite diffusion in specific tissue types and brain regions is difficult. Increasing the SNR will allow the voxel size to be decreased without adversely affecting the ADC measurements. Without going to higher fields, which is one obvious solution to the SNR problem, we can modify other acquisition

parameters to yield improved SNR. Our echo time is rather long for a STEAM sequence (180 ms), considering the main advantage of using a STEAM sequence is the ability to use a short echo time [125]. The T2 values for metabolites in the occipital gray and white matter of the human brain at 3T are 247 and 295 ms for NAA, 152 and 156 ms for tCr, and 207 and 187 ms for Cho [30]. In the occipital gray matter, decreasing the TE from 180 ms to say 75 ms, by reducing excessive gradient delays in the TE period, would increase the signal for NAA, tCr, and Cho by 53%, 100%, and 66% respectively. The long TE used in our study was primarily due to the timing required for the diffusion gradients (20 ms), which were symmetrically placed within the rf pulse intervals and due to the long timing delays ($\sim$35 ms) that were left after the diffusion gradients to ensure the decay of most eddy currents. In future studies these timings will be optimized and minimized to take full advantage of the STEAM sequence. Our rationalization for the use of the STEAM sequence was to ultimately measure diffusion of the coupled resonances. Examining the diffusion characteristics of the singlet resonances is a logical first step given that NAA is the most prominent peak in the proton spectra of the brain and the relevance of NAA to brain pathology. For examination of the singlet resonances, it might also be useful to use a diffusion-weighted PRESS (Point REsolved SpectroScopy) sequence as in the study by Harada et al. [29], because the total signal yield would not be halved as it is in STEAM.

Another limitation is the long scan time of $\sim$43 min for the 12 metabolite spectra obtained along either the X, Y, or Z direction with 4 b-values each. This is not a problem for cooperative volunteers; however, for clinical use, time becomes a factor. Since we had data for 64 averages (similar to previous studies, Posse et al. 64 averages, and Harada et al. 94 averages), we examined the ability to reproduce the diffusion results with less averages (48, 32, and 16). Figure 5.5 illustrates the Trace/3 ADC values for NAA, tCr, and Cho versus the number of averages. It shows an increase in the ADCs and the variability of the data as the number of averages is reduced. For accurate quantification of the NAA Trace/3 ADC using the STEAM method described in this study, one only needs 16 averages for a 15.6 cm^3 voxel; therefore it is feasible to decrease the measurement to only $\sim$11 min. However, for the measurement of Cho and tCr Trace/3 ADCs, a minimum of 48 averages are required to accurately quantify the ADCs, reducing the total scan time to $\sim$32 min. In this initial study, we used 4 different b-values in order to ensure linearity of the decay curves. Since the data was consistently linear, particularly for NAA, it would be reasonable to only use two b-values in the future, and therefore cut the scan time in half. The combination of these modifications should allow us to get accurate diffusion data for all three singlet metabolites in under 20 minutes (not including voxel localization, shimming, and acquisition of water spectra). Despite the limitations mentioned above,

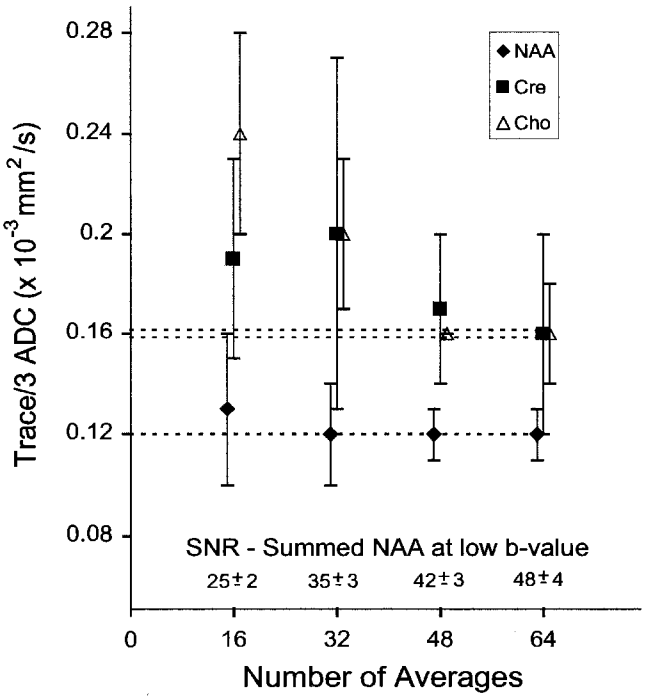

FIGURE 5.5: An increase in the value and variability (SD) of the Trace/3 apparent diffusion coefficient (ADC) of the metabolites can be seen as the number of averages is decreased from the initial 64 spectra data set (dotted lines represent Trace/3 ADC values at 64 averages). With the particular parameters used in this study at 3 T and a voxel volume of 15.6 cm^3, it appears as though 16 averages is the minimum required for NAA, whereas 48 averages are needed for tCr and Cho.

this DW-MRS study using a STEAM sequence with appropriate phasing of the individual NAA spectra, provides the first rotationally invariant Trace/3 ADC values for NAA, tCr, and Cho in three different regions of the human brain.

CHAPTER 6

DIFFUSION TENSOR SPECTROSCOPY (DTS) OF HUMAN BRAIN

6.1 INTRODUCTION

The physical property of diffusion of water molecules has shown great utility in magnetic resonance imaging for studying a multitude of neurological disorders, and in neurodevelopment and aging. Diffusion ordered spectroscopy (DOSY) has demonstrated enormous potential in the fields of chemistry and biochemistry [126]; however, the investigation of metabolite diffusion (molecules other than water) in vivo has lagged behind due to technical challenges such as limited signal-to-noise ratio, poor spatial resolution, pulse sequence availability, significant post-processing, lengthy acquisition times, and limited brain coverage. Despite these challenges, the pursuit of metabolite diffusion in diseased tissue is worthwhile since it may yield insights into changes in the underlying intra-cellular environment with disease [98–101]. In contrast, localizing changes in water diffusion to a specific compartment of the brain has been difficult and controversial. It has long been shown that reductions in water diffusion are the most sensitive indicator of early cerebral ischemia [22], and that despite the theory that this decrease is due to a water shift from extra-cellular to intra-cellular space, purely intra-cellular metabolites also show a reduction of diffusion by a similar magnitude without any compartmental shifts [100, 102–107]. Thus diffusion-weighted spectroscopy can add insight into the biophysical properties of diffusion in tissue, but it remains to be tested whether or not diffusion of intra-cellular metabolites will provide evidence of neuronal/axonal abnormalities in the absence of changes in either water diffusion or other MR properties in a variety of neurological dis-

A version of this chapter was published in:
Ellegood, J., Hanstock, C.C., and Beaulieu, C. Diffusion Tensor Spectroscopy (DTS) of the Human Brain. Proc. 13th Meeting of the International Society of Magnetic Resonance in Medicine, Miami, USA (May 2005).
Ellegood, J., Hanstock, C.C., and Beaulieu, C. Diffusion Tensor Spectroscopy (DTS) of Human Brain. Magnetic Resonance in Medicine 2006; 55: 1-8.

orders beyond ischemia.

Since diffusion is known to be anisotropic in white matter, for either water or metabolites [112, 117, 118], it can only be characterized properly by measuring the full diffusion tensor, with an unavoidable time penalty. The mean diffusivity and the degree of anisotropy provide independent and unique inferences on the micro-structural integrity of the white matter tracts [93]. N-acetyl aspartate (NAA) is located in the intracellular space of neurons and axons, while creatine and phosphocreatine (tCr), and choline (Cho) are located, not only in the neurons and axons, but also in the more presumably isotropic environments within astrocytes, oligodendrocytes, and meningeal cells [60]. It may be hypothesized that tCr and Cho might exhibit different degrees of anisotropy as compared to NAA within various human brain regions, depending on the cellular environment. Furthermore, the three primary singlet metabolites may have unique diffusion changes with neurological injury given their cellular distribution.

Given the challenges outlined above, it may come as no surprise that there have only been four previously published studies reporting apparent diffusion coefficients (ADCs) of metabolites in the human brain. The ADC values of NAA, tCr, and Cho were measured along one diffusion direction in the periventricular white matter in two of these studies [28, 29], ignoring probable anisotropic diffusion effects. In order to eliminate directional bias, the rotationally invariant Trace/3 ADC of those same metabolites was reported in three regions, two primarily gray matter (frontal and occipital) and the other primarily white matter [127]. A recent study that measured diffusion in two directions demonstrated a 2-3 fold greater ADC for NAA diffusion parallel to the axonal direction, relative to perpendicular, of the splenium of the corpus callosum in two healthy volunteers [117]. Although this latter study demonstrated anisotropy of NAA diffusion, the full diffusion tensor, which requires the measurement of a minimum of 6 diffusion directions, and the output summary parameter fractional anisotropy (FA) has not been evaluated for any metabolite in human brain.

The purpose of this study was to measure the diffusion tensor of NAA, tCr, and Cho in the healthy human brain in six distinct regions (four white matter and two cortical gray matter) and to calculate the Fractional Anisotropy (FA), Trace/3 ADC (i.e. mean diffusivity), and eigenvalues (i.e. directional ADCs) of those metabolites.

6.2 Methods

Scans were performed on an SMIS 3T MRI equipped with a maximum gradient strength of 20 mT/m. Initially, gradient-echo images along transverse, sagittal, and coronal plane

were acquired (TE = 22 ms, TR = 500 ms, Slice Thickness = 5 mm, 11 slices per direction), then an in-house single-voxel, diffusion-weighted STEAM sequence [33, 122, 128] was used to measure the diffusion of the metabolites NAA, tCr, and Cho. The diffusion sequence parameters were: δ = 15 ms, Δ = 208.3 ms, TM = 170 ms, TE = 76.6 ms, TR = 3 s, 2048 sample points, spectral width 2.5 kHz, and an FID acquisition time ~800 ms. Water suppression was achieved using a dual inversion recovery with two hyperbolic secant pulses of 80 ms in duration (inversion times of ~1400 ms and ~200 ms), followed by water crusher gradients along the X and Y directions of 20 ms duration. The diffusion gradient strengths in the $\pm$X, $\pm$Y and $\pm$Z directions were calibrated using the reported ADC values at 20°C for tCr (0.80 x 10^{-3} mm^2/s) [119], since its value has been shown to be very consistent. Twelve spectra were acquired (6 spectra at low b, 654 s/mm^2, and 6 spectra at high b, 1890 s/mm^2) for each region in six different directions [(-1,-1,0), (-1,0,-1), (0,-1,-1), (1,-1,0), (1,0,-1),(0,1,-1)], where (Gx, Gy, Gz) signifies the diffusion sensitizing gradient direction. The lower b-value of 654 s/mm^2 was used in order to adequately dephase any unwanted magnetization, and the higher b-value of 1890 s/mm^2 was used in order to cause a 15% drop in signal intensity from low to high b-value based on an approximate metabolite ADC of 0.15 x 10^{-3} mm^2/s [127] while still providing adequate SNR for the phase correction on a single average spectrum. The gradient calibration was validated by performing diffusion measurements in the same six gradient directions using an isotropic 125 mL spherical water phantom (Table 6.1) containing physiological concentrations of NAA (9.0 mM), Cr (6.4 mM), and Cho (1.7 mM) (Sigma-Aldrich Canada Ltd., Oakville, Ontario).

Five healthy volunteers (ages 18 - 35 years) were scanned for each brain region, yielding a total of 30 examinations. Note that the same five volunteers were not used for all six brain regions. The volunteer's head was secured by using a vacuum pillow to minimize macroscopic motion. Spectroscopic voxels were registered to six brain regions (two cortical gray matter and four white matter) as shown in the series of MR images illustrated in Figure 6.1. The cortical spinal tract and corpus callosum were selected because they are large white matter tracts (needed for the typically large spectroscopy voxels) that have different tract orientations, namely inferior-superior and left-right, respectively. The frontal and occipital gray matter regions were selected because they allowed sampling of 60% gray matter [129].

Each brain region required the optimization of the first and second order shims and resulted in an in-vivo water line width of ~3-6 Hz. The line width did not change significantly ($\pm$0.3Hz) with either increasing b-value or different diffusion gradient directions. We acquired eight single average spectra for the unsuppressed water peak, which were

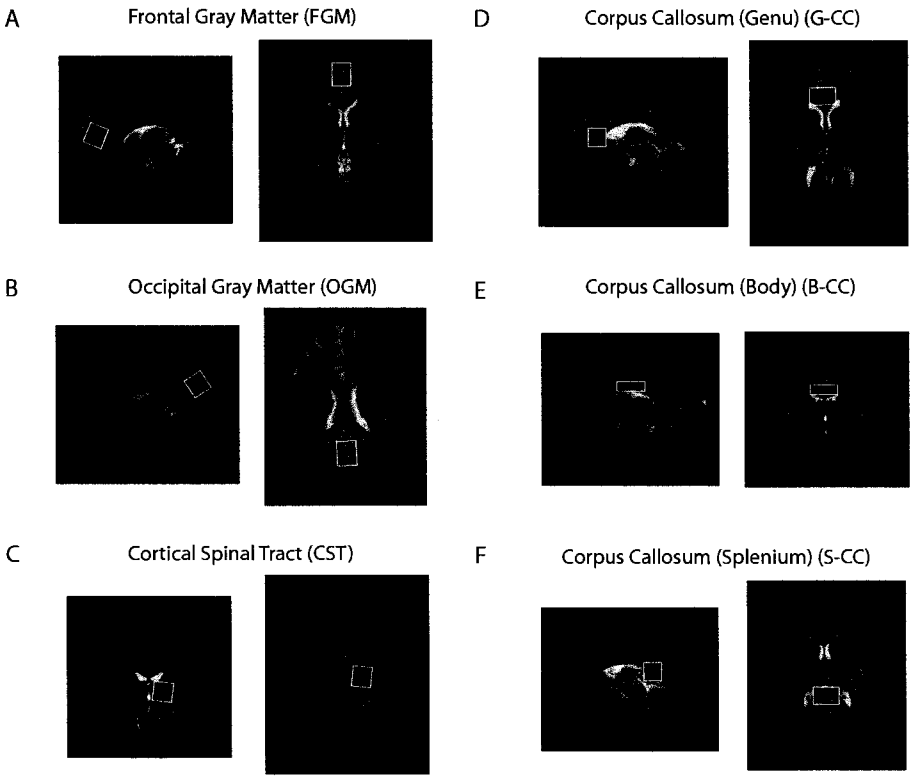

FIGURE 6.1: The 6 brain regions that were examined: (A) a 2.2 x 2.2 x 2.2 = 10.6 cm^3 voxel located in the frontal gray matter (FGM region), (B) a 2.2 x 2.2 x 2.2 = 10.6 cm^3 voxel located in the occipital gray matter (OGM region), (C) a 2.2 x 2.2 x 2.2 = 10.6 cm^3 voxel surrounding the cortical spinal tract (CST region), (D) a 2.0 x 2.0 x 3.0 = 12.0 cm^3 voxel surrounding the genu of the corpus callosum (G-CC region), (E) a 1.0 x 3.2 x 3.2 = 10.2 cm^3 voxel surrounding the body of the corpus callosum (B-CC region), and (F) a 2.0 x 2.0 x 3.0 = 12.0 cm^3 voxel surrounding the splenium of the corpus callosum (S-CC region).

required for eddy current correction [120], and sixty-four single average spectra for the metabolite spectra (with water suppression) for each of the two b-values along each of the six directions. This acquisition scheme yielded 12 summed water spectra and 12 summed metabolite spectra for each brain region examined. The total measurement time for the set of 12 summed metabolite spectra was ~43 min. Including axial, coronal, and transverse scout images, as well as the water spectra, a total exam time of ~75 min for each brain region was required. Hence, it was practical to study only one brain region per scanning session.

DW-MRS requires individual phase correction on single average spectra before summation in order to correct for motion induced phase errors between the individual spectra [28, 127]. Two phase correction methods have been shown to be accurate in determining ADC values from diffusion weighted spectra; one method used a zero order phase correction on the residual water peak before summation (Water phase correction method) [28], and the other used a zero order correction on the NAA peak with a first order correction on the entire spectrum (NAA phase correction method) [127]. It should be noted that before any phase correction was performed a 1 Hz linewidth exponential filter was applied. In this study we used both phase correction methods to generate the spectra. The NAA phase correction method was used for estimation of the NAA peak amplitude, while the water phase correction method was used for tCr and Cho. This was considered appropriate since the signal intensity of the NAA peak was always larger (by $\sim$ 10 %) when using the NAA phase correction method, and the signal intensity of tCr and Cho were often larger (by $\sim$ 7 %) when using the water phase correction method. The greater peak height was taken to indicate a more coherent phase correction, since the linewidth was consistent regardless of the phase correction method. It was determined that, if the NAA phase correction method was used to quantify the tCr or Cho peak, the ADC of tCr and Cho were artefactually increased, and this was likewise true for the NAA ADC when the water phase correction method was used. Peak height was used to measure the metabolite signal intensity, which was felt to be accurate as the metabolite shim varied only slightly ($\pm$ 0.3Hz). The average variability per direction for the zero order phase correction required in-vivo was ~85° for water and ~110° for NAA. The average variability per direction for the first order phase correction required in-vivo in the NAA phase correction method was ~130°. The ADC values were calculated from the slope of the ln(peak intensity) versus b-value. The full diffusion tensor was calculated for each region studied, and the eigenvalues (λ_1, λ_2, and λ_3) were determined by the diagonalization of the tensor, which in turn were used to calculate the Trace/3 ADC and FA [93].

Comparisons of both Trace/3 ADC and FA were made between metabolites within

regions as well as between cortical gray and white matter. Significant differences between metabolites in the same regions were calculated with a student's t-test (two-tailed, paired). All other comparisions were calculated from a student's t-test (two-tailed, unpaired).

6.3 Results

Table 6.1 lists the Trace/3 ADC and FA values measured in an isotropic 125 mL spherical phantom containing an aqueous solution at 21°C with physiological concentrations of NAA (9.0 mM), Cr (6.4 mM), and Cho (1.7 mM), which yielded the signal to noise ratio (SNR, calculated by dividing the signal intensity by the standard deviation of the noise of the real spectrum) values of 92, 64, and 44 respectively, at low b (654 s/mm^2). The Trace/3 ADC values were determined to be 0.65 $\pm$ 0.01 x 10^{-3} mm^2/s for NAA, 0.77 $\pm$ 0.03 x 10^{-3} mm^2/s for Cr, and 0.92 $\pm$ 0.04 x 10^{-3} mm^2/s for Cho, all of which are consistent with previously reported literature ranging from (0.6-0.9) x 10^{-3}, 0.8 x 10^{-3}, and (0.9-1.3) x 10^{-3} mm^2/s for NAA, Cr, and Cho, respectively [119]. The individual eigenvalues showed little variation and any observed differences in the eigenvalues were due to the sorting bias of noisy data. The low FA values of the three metabolites in solution, 0.14 $\pm$ 0.05 for NAA, 0.11 $\pm$ 0.02 for Cr, and 0.08 $\pm$ 0.01 for Cho, were expected for the isotropic environment. The differences between the NAA and Cho FA values in the phantom are significant, and can be explained by the magnitude of their individual ADCs. In an ideal isotropic environment the eigenvalues (λ_1, λ_2, and λ_3) will all be equal. Unfortunately in practice, due to sorting bias of noisy data, that is not the case and there is a spread in the eigenvalues. If all three metabolites have the same spread in their eigenvalues (say $\pm$ 0.09 x 10^{-3} mm^2/s) their FA values will be different. For example, a spread of $\pm$ 0.09 x 10^{-3} mm^2/s for an ADC of 0.65 x 10^{-3} mm^2/s (NAA) is a 14% difference whereas a spread of $\pm$ 0.09 x 10^{-3} mm^2/s for an ADC of 0.92 x 10^{-3} mm^2/s (Cho) is only a 10% change. The FA of NAA could be larger than that of Cho because NAA has a greater percentage variability in its eigenvalues. If we "simulate" eigenvalues for each metabolite where λ_2 is the Trace/3 ADC and λ_1 and λ_3 are $\pm$ 0.09 x 10^{-3} mm^2/s from the Trace/3 ADC, the "simulated" values of FA given this constant spread of eigenvalues are 0.14, 0.12, and 0.10 which is consistent with the actual phantom FA values of 0.14, 0.11, 0.08 for NAA, tCr, and Cho, respectively.

Example in-vivo spectra at low and high b-values are shown in Fig. 6.2. The example spectra in Fig 6.2A are taken from the frontal gray matter region (Fig. 6.1A) at low and high b-values. Signal to Noise Ratios (SNR) of the summed spectrum for the three metabolites in the FGM region at low b (b = 654 s/mm^2) are 25 $\pm$ 4 for NAA, 14 $\pm$ 2 for

Metabolite	Trace/3 ADC (x 10^{-3} mm^2/s)	Fractional Anisotropy
N-Acetyl Aspartate (9.0mM)	0.65±0.01	0.14±0.05
Creatine (6.4mM)	0.77±0.03	0.11±0.02
Choline (1.7mM)	0.92±0.04	0.08±0.01

TABLE 6.1: Phantom measurements (N=6, mean ± SD) of the X, Y, Z, and Trace/3 apparent diffusion coefficients (ADC) in a 125 mL spherical phantom containing water, NAA (30 mM), Cr (30 mM), and Cho (10 mM) at 20 °C using NAA phase correction method. The ADCs in the various directions have little difference in these metabolites, as expected from an isotropic phantom.

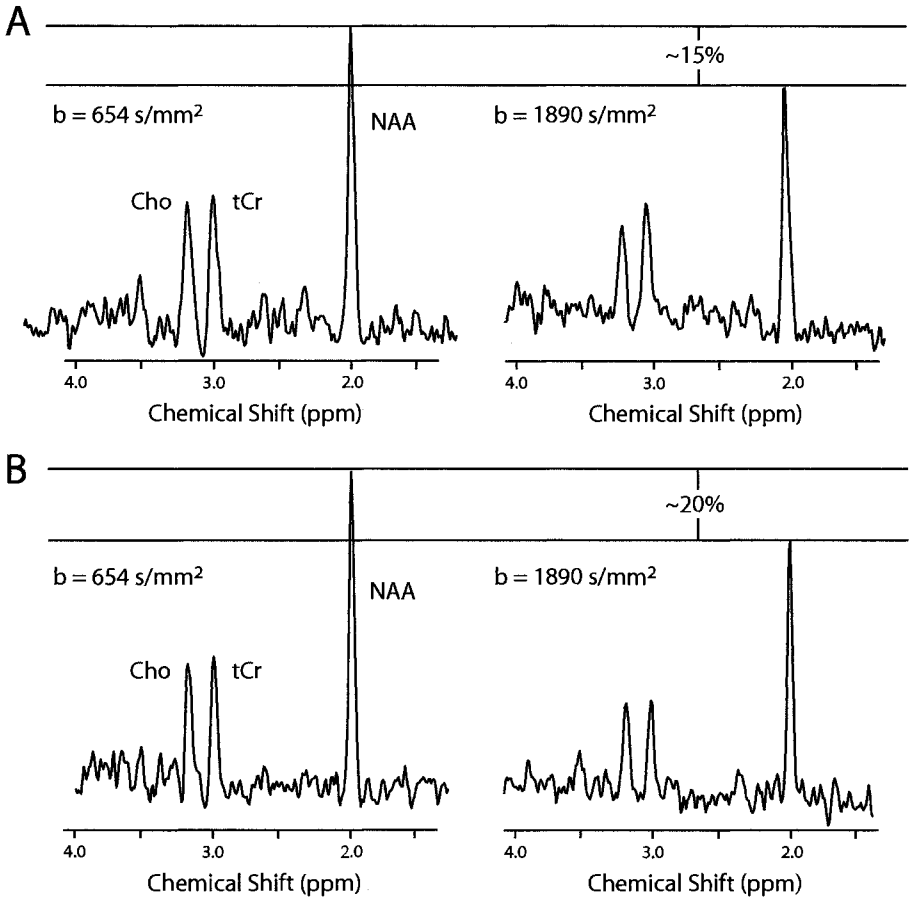

FIGURE 6.2: Example spectra taken at low (654 s/mm^2) and high (1890 s/mm^2) b-values from (A) the frontal gray matter (FGM) region and (B) the body of the corpus callosum (B-CC) region. Both sets of spectra were taken in the (-1,-1,0) gradient direction. The corresponding drop in signal intensity for NAA between low and high b-value for these typical spectra were 15% and 20% for the FGM and B-CC region, respectively.

tCr, and 14 ± 3, for Cho. The example spectra in Fig 6.2B are taken from the body of the corpus callosum (Fig. 6.1D) at low and high b. The SNR values of the summed spectrum

of the CST region at low b are 22 ± 3 for NAA, 10 ± 2 for tCr, and 11 ± 2 for Cho, the G-CC region at low b are 16 ± 2 for NAA, 6 ± 1 for tCr, and 6 ± 1 for Cho, the B-CC region at low b are 25 ± 6 for NAA, 11 ± 4 for tCr, and 11 ± 3 for Cho, the S-CC region at low b are 13 ± 1 for NAA, 5 ± 1 for tCr, and 5 ± 1 for Cho, the FGM region at low b are 27 ± 4 for NAA, 15 ± 2 for tCr, and 15 ± 3 for Cho, and the OGM region at low b are 29 ± 2 for NAA, 15 ± 2 for tCr, and 10 ± 1 for Cho.

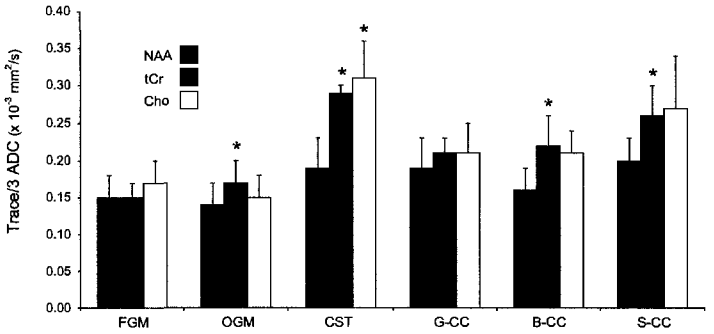

FIGURE 6.3: The Trace/3 ADC values of tCr were found to be larger than that of NAA in 3 of the 4 white matter regions (CST, B-CC, and S-CC) and in 1 of the gray matter structures (OGM). Overall, the Trace/3 ADC values for all these metabolites in white matter were significantly greater than their corresponding values in cortical gray matter (* indicates significant difference between Trace/3 ADC of NAA and either tCr or Cho at $p < 0.05$, paired t test).

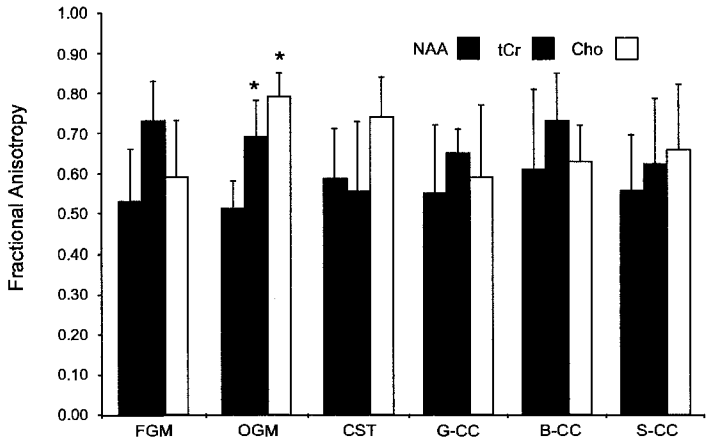

FIGURE 6.4: Fractional Anisotropy values for NAA, tCr, and Cho in the 6 brain regions. Surprisingly, FA values of NAA were found to be consistent (i.e., no significant differences) between all regions regardless of if they were white or gray matter. Although high FA values were expected for the white matter, the high FA values for the metabolites in the FGM and OGM are not in line with the low FA of ~0.2 that is usually observed for water in the cortical gray matter. Five of the 6 regions did not show significant differences of FA for NAA versus either tCr or Cho (* indicates significant difference between FA of NAA and either tCr or Cho at $p < 0.05$, paired t test).

Trace/3 ADC, FA, and eigenvalues of NAA, tCr, and Cho for all six brain regions in the healthy volunteers are displayed in Table 6.2. In three of the four white matter regions and one of the gray matter regions the Trace/3 ADC value for NAA was found to be significantly lower than the Trace/3 ADC for tCr, whereas, the Trace/3 ADC of Cho was only significantly increased when compared to NAA in the CST region (Fig. 6.3). When averages for either all the white matter or all the gray matter structures were examined, the Trace/3 ADC of NAA ($0.18 \pm 0.04 \times 10^{-3}$ mm^2/s) was significantly less than that for both tCr ($0.25 \pm 0.04 \times 10^{-3}$ mm^2/s) and Cho ($0.26 \pm 0.07 \times 10^{-3}$ mm^2/s) in the white matter ($p < 0.001$ for tCr and Cho, paired t-test) whereas no significant differences between metabolites were observed for the mean Trace/3 ADC values in the cortical gray matter (NAA $0.14 \pm 0.03 \times 10^{-3}$ mm^2/s, tCr $0.16 \pm 0.03 \times 10^{-3}$ mm^2/s, and Cho $0.16 \pm 0.03 \times 10^{-3}$ mm^2/s). Also, the mean diffusivity of each metabolite was significantly greater in the white matter than in the gray matter. The parallel diffusion (i.e. λ_1) in five of the six regions (not in the G-CC) was significantly larger for tCr and Cho when compared to NAA, which is the same ADC trend seen for the metabolites in aqueous solution (i.e. phantom). The FA values of NAA ranged from 0.51 to 0.61, and no significant differences were found between regions, even when comparing white (0.57 ± 0.15) and gray matter (0.52 ± 0.10) (Fig. 6.4). The FA values of all three metabolites did not differ in the white matter, but there were some differences noted in the occipital gray matter.

The directional information obtained from the principal eigenvector of NAA was compared to that known from DTI of water in the same regions (Fig. 6.5). In the two gray matter regions (frontal and occipital) there was no consistent direction for NAA diffusion when comparing the five volunteers in either region (Fig. 6.5A and 6.5B). In the cortical spinal tract region, all five volunteers had a blue (superior-inferior) directional preference for NAA, as expected when compared to the water DTI data (Fig. 6.5C). The white matter tracts of the corpus callosum near the midline are oriented left-right and should appear red in the principal eigenvector color maps, as was seen for NAA diffusion for all five volunteers in the body (Fig. 6.5E), three of the five volunteers showed primarily red contributions in the genu (Fig. 6.5D), and four of the five volunteers in the splenium (Fig. 6.5F) of the corpus callosum.

6.4 Discussion

The Trace/3 ADC of NAA was found to be significantly smaller than the Trace/3 ADC of tCr and Cho in the white matter. However, in the gray matter, there were no significant differences between metabolites. Comparing the same metabolites, the Trace/3 ADC val-

Metabolite	Eigenvalues (x 10^{-3} mm^2/s)			Trace/3 ADC	Fractional
	λ_1	λ_2	λ_3	(x 10^{-3} mm^2/s)	Anisotropy
Frontal Gray Matter (N=5)					
NAA	0.23±0.03	0.16±0.05	0.06±0.03	0.15±0.03	0.53±0.13
tCr	0.29±0.04	0.12±0.05	0.03±0.02	0.15±0.02	0.73±0.10
Cho	0.28±0.04	0.18±0.05	0.06±0.05	0.17±0.03	0.59±0.14
Occipital Gray Matter (N=5)					
NAA	0.21±0.04	0.14±0.03	0.06±0.03	0.14±0.03	0.51±0.07
tCr	0.31±0.03	0.15±0.06	0.04±0.02	0.17±0.03	0.69±0.09
Cho	0.33±0.07	0.09±0.02	0.03±0.01	0.15±0.03	0.79±0.06
Cortical Spinal Tract (N=5)					
NAA	0.31±0.10	0.16±0.02	0.07±0.05	0.18±0.05	0.59±0.12
tCr	0.47±0.09	0.27±0.10	0.09±0.07	0.28±0.02	0.56±0.17
Cho	0.59±0.10	0.27±0.13	0.05±0.04	0.30±0.06	0.74±0.10
Corpus Callosum - genu (N=5)					
NAA	0.30±0.09	0.19±0.06	0.07±0.06	0.19±0.04	0.55±0.17
tCr	0.35±0.03	0.25±0.04	0.03±0.06	0.21±0.02	0.65±0.06
Cho	0.35±0.17	0.22±0.04	0.06±0.07	0.21±0.04	0.59±0.18
Corpus Callosum - body (N=5)					
NAA	0.28±0.04	0.13±0.07	0.07±0.04	0.16±0.03	0.61±0.20
tCr	0.42±0.13	0.20±0.07	0.03±0.03	0.22±0.04	0.73±0.12
Cho	0.35±0.06	0.24±0.05	0.04±0.03	0.21±0.03	0.63±0.09
Corpus Callosum - splenium (N=5)					
NAA	0.30±0.04	0.20±0.03	0.08±0.05	0.19±0.03	0.54±0.12
tCr	0.44±0.09	0.24±0.04	0.11±0.08	0.25±0.04	0.63±0.16
Cho	0.48±0.11	0.24±0.13	0.07±0.05	0.26±0.08	0.67±0.15

TABLE 6.2: Eigenvalues, Trace/3 ADC values, and FA (mean ± SD) from all six regions examined in the human brain.

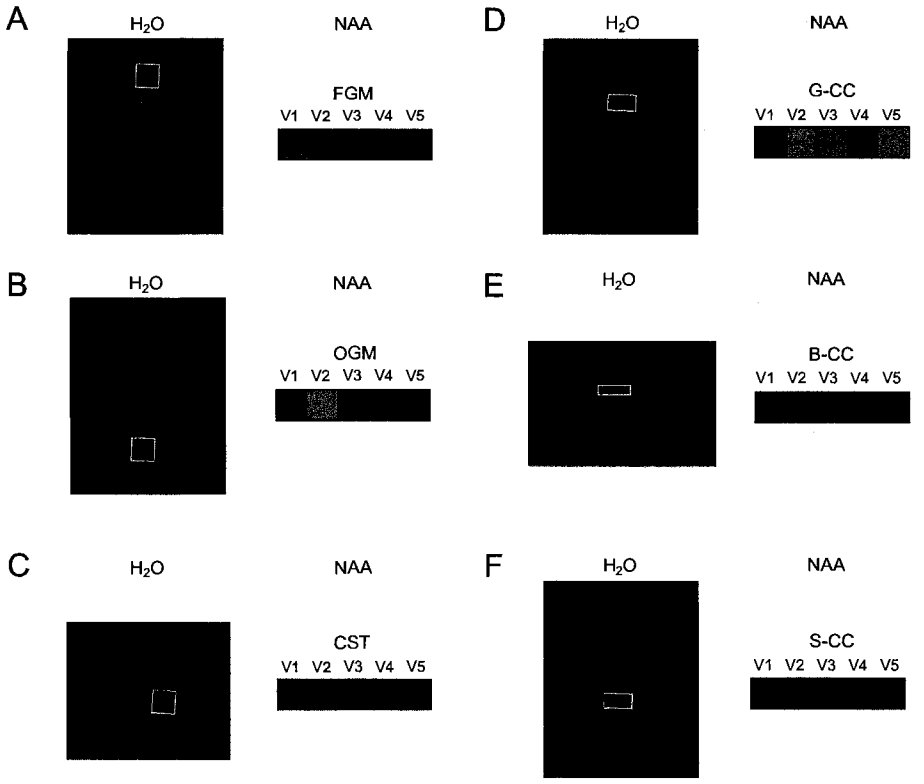

FIGURE 6.5: Diffusion directional information obtained for NAA for a given voxel in 5 volunteers (V_1, V_2, V_3, V_4, and V_5) per region and that of water DTI (images not acquired on 3T in the volunteers in this study): (A) frontal gray matter, (B) occipital gray matter, (C) cortical spinal tract, (D) genu of the corpus callosum, (E) body of the corpus callosum, and (F) splenium of the corpus callosum. The color images follow the standard color scheme (red - left / right, blue - inferior / superior, and green - anterior / posterior). Consistent orientations are not expected for the cortical gray matter (A,B); however, there is good agreement between water and NAA principal eigenvector directions, particularly for the cortical spinal tract (C) and the body of the corpus callosum (E).

ues were larger in the white matter than in the gray matter, as opposed to water Trace/3 ADC, which displays similar values between gray and white matter in the healthy adult brain at typically used b-values of ~1000 s/mm^2. The increased mean diffusivity of the NAA in white matter compared to the gray matter may be a reflection of the reduced barriers to diffusion along the length of the axons as indicated by the significantly greater parallel diffusivity (λ_1, Table 6.2) and no such increase in the perpendicular diffusion [(λ_2 +λ_3)/2]. The increased mean diffusivity in the white matter for tCr and Cho cannot be explained by the same rationale, as the parallel diffusion and the perpendicular diffusion were both significantly increased in the white matter when compared to the gray matter. This may indicate that tCr and Cho are in a less hindered environment compared to NAA in the white matter. The lower mean diffusivity (and λ_1) of NAA in white matter relative to tCr/Cho may just reflect the intrinsically slower diffusion of NAA even in aqueous solution (Table 6.1). Rotationally-invariant Trace/3 ADC values have been reported previously in human brain [127], and two of those regions (FGM and OGM) were reproduced in this study with slightly smaller voxel sizes, 2.2 x 2.2 x 2.2 = 10.6 cm^3 (current) instead of 2.5 x 2.5 x 2.5 = 15.6 cm^3 (previous). The Trace/3 ADC values for NAA in the previous study, which used a different acquisition method (three directions instead of six), were consistent with the Trace/3 ADC values reported in this current study.

Anisotropic diffusion studies of metabolites such as NAA have been performed on the excised bovine optic nerve [112] and the splenium of the corpus callosum in the human brain [117]. Both studies showed faster diffusion of NAA parallel to the axis of the nerve or white matter bundle (~2-3 fold increase). In agreement, we found the parallel diffusion (λ_1) of NAA in the splenium to be 0.30 x 10^{-3} mm^2/s and the perpendicular diffusion [(λ_2 +λ_3) / 2] to be 0.15 x 10^{-3} mm^2/s (Table 6.2), which reflects a 2-fold increase in diffusion parallel versus perpendicular. If we calculate a "pseudo-Trace/3 ADC value" from the previous human study, which measures diffusion only in two directions [117] (i.e. [Parallel ADC + (2 x Perpendicular ADC)]/3), the Trace/3 ADC values would be 0.18 x 10^{-3} mm^2/s and 0.20 x 10^{-3} mm^2/s for their two volunteers. This data is consistent with our NAA Trace/3 ADC value (0.20 $\pm$ 0.03 x 10^{-3} mm^2/s) from the same region (S-CC). However, in order to quantify accurately and robustly the anisotropy in the human brain, without using a subject position dependent method, one really needs to calculate the full diffusion tensor, as done in our current study.

The FA of NAA in the white matter ranged from 0.55 to 0.61 which is less than reported water anisotropy values of the cortical spinal tract and corpus callosum [130]. We conclude that, the partial volume effects in our relatively large spectroscopy voxels could be causing this difference. FA values of tCr and Cho in the white matter ranged from 0.51 to 0.74. We

anticipated lower FA values for tCr and Cho when compared to NAA, since they are not solely located in the axons but rather are also found in astrocytes, oligodendrocytes, and meningeal cells [60]. However, the absence of this observation may reflect the dominant contribution of the axons to the tCr and Cho peak amplitudes. The direction of the principal eigenvector of NAA in the white matter regions corresponded well to what has been shown previously in water DTI studies, namely blue (superior-inferior) for the cortical spinal tract (Fig. 6.5C) and red (left-right) for the corpus callosum (Fig. 6.5D,E,F). The main point of determining the directional information of NAA was to indicate that our DTS was yielding appropriate results.

The FA of the metabolites in cortical gray matter was expected to be similarly low to what has been shown in water; however, high FA values of $\sim$0.5 for NAA, $\sim$0.7 for tCr, and 0.6 - 0.8 for Cho were observed (Table 6.2). A possible explanation of this high FA could be partial volume inclusion of white matter in the relatively large voxel. The gray matter voxels in this study are composed of approximately 60% gray matter [129], and therefore, the 40% of the voxel which is white matter could be inflating the FA. However, the lack of any consistent white matter tract direction and the complex folding in these regions ought to have mitigated this effect. The NAA diffusion in the two gray matter structures showed no consistent directional preference for all five volunteers in either region (Fig. 6.5A and 6.5B). Because of the relatively weak gradient strengths available on our scanner (20 mT/m) and the need for a large b-value (1890 s/mm^2) and short TE (76.6 ms), the diffusion time was rather long (203 ms) which could lead to some restriction effects. However, the one-dimensional root mean square displacement of water (ADC $\sim$ 0.70 x 10^{-3} mm^2/s, diffusion time $\sim$ 45 ms) and metabolites (ADC $\sim$ 0.15 x 10^{-3} mm^2/s, diffusion time $\sim$ 203 ms) are approximately the same ($\sim$8 μm). The diffusion signal attenuation curves of the three main singlet metabolites examined in excised bovine optic nerve have been shown to be sensitive to diffusion times over the range of 65 - 245 ms [112]. Future studies at shorter diffusion times (with access to stronger gradients) should clarify the importance of restriction effects for diffusion of metabolites in the human brain.

Although the diffusion data of the metabolites in white matter appears reasonable, it is difficult to reconcile the high FA of the metabolites in cortical gray matter. The signal to noise ratio (SNR) of $\sim$25 for NAA and $\sim$14 for tCr and Cho in cortical gray matter is rather low, and thus the high FA in the gray matter could, in fact, be artefactual due to the known noise sensitivity of FA as opposed to the more robust Trace/3 ADC. However, the SNR of gray matter is similar to that of white matter which yielded reasonable results. In order to examine the consistency of the Trace/3 ADC and FA values we examined three different attributes, (i) linearity of the diffusion attenuation curves over the range

of b-values used in this study, (ii) intra-subject variability, and (iii) intra-session values of Trace/3 ADC and FA from subsets of the same spectral data set. First, two point fits were used in this diffusion tensor spectroscopy study in order to keep excessive scan time to a minimum; however, two point fits could lead to more variability in the ADC calculation for the six directions which in turn could increase the FA. We tested the linearity of the diffusion curves in the OGM region by acquiring spectra from four different b-values in each of the six directions. The average r^2 value for NAA when three people were examined with a four b-value fit (32 averages per spectrum) was determined to be 0.78 $\pm$ 0.20, which is not unreasonable but does indicate a deviation from linearity in some of the scans. Second, intra-subject variability (3 subjects, each scanned 3 separate occasions) was examined for NAA in the occipital gray matter to look at the consistency of the Trace/3 ADC and FA. The average variability for one person examined on three separate occasions was relatively small for the Trace/3 ADC ($\pm$ 0.02 x 10^{-3} mm^2/s). However, the average variability for one person examined on three separate occasions was quite large for the FA ($\pm$ 0.17 absolute or 17-37% variability). Third, we examined the intra-session variability of the NAA diffusion parameters in the occipital gray matter and the body of the corpus callosum by using a bootstrap method. Thirty-two or 48 of the 64 single average spectra were randomly selected from each of the two b-values in each of the six directions. ADC values were then calculated for NAA from these new thirty-two average spectra in the six different directions. This was repeated 100 times in order to create a pool of 100 ADC values for NAA in any of the six directions for a given volunteer. Trace/3 ADC and FA values were then calculated by taking random ADC values for each of the six directions from the pool of 100 that were previously calculated. This was repeated 100 times. The average and variability of the eigenvalues, Trace/3 ADC, and FA for a given session were then calculated. The variability in the Trace/3 ADC measurement within a single session was extremely low (0.02 x 10^{-3} mm^2/s for a subset of 32 and 0.01 x 10^{-3} mm^2/s for a subset of 48), but it was much larger for FA (mean variability $\pm$ 0.13 for a subset of 32 and $\pm$ 0.10 for a subset of 48). The FA data is certainly more variable than the Trace/3 ADC data, although at this point we are unable to explain or discredit the high FA data for the cortical gray matter, as the FA of NAA was still large compared to what is seen with water in spite of this variability. This will be discussed in more detail, as it was investigated in Chapter 8.

Certain limitations remain and need to be addressed when making DTS measurements, such as the long scan time, large voxel size, and low SNR. Granted that these DTS measurements are challenging the characterization of the diffusion tensor of metabolites in healthy brain is nonetheless still a goal, and a pre-requisite for eventual patient stud-

ies. The accuracy and robustness of DTS depends on balancing the reduction of partial volume effects by acquiring data from smaller voxel sizes, while retaining enough SNR in order to allow zero-order phase correction on the single average NAA and to calculate reliable ADC values. Future studies will require shortening the total scan time, which is ~75 min (DTS portion alone is ~43 min). This might be achieved by the acquisition of only one low b-value with negligible diffusion weighting and 6 high b-values, and would reduce the scan time by 18 minutes with the current 64 averages per b-value. Also, time savings associated with less averages would result from acquiring spectra at a higher field and using a diffusion weighted PRESS sequence instead of STEAM which would double the signal for the singlet metabolites at the same echo time. Other improvements, such as more diffusion encoding directions may be more accurate for calculating the diffusion tensor; however, the scan time penalty may prohibit this protocol improvement. Higher b-values would also be more beneficial in order to get better measures of some of the very low ADC values; however, this would create challenges for both methods of phase correction on the individual single average spectra, because at extremely high b-values the water and the metabolite peaks in the direction of fastest diffusion may have too low an SNR.

6.5 Summary

The diffusion tensor of the three primary singlet metabolites has been measured for gray and white matter in the human brain. The Trace/3 ADC of NAA was found to be significantly lower than tCr and Cho in the white matter; however this trend was not observed in the cortical gray matter where the Trace/3 ADC was consistent between metabolites. The Trace/3 ADC of each metabolite was significantly greater in white matter than in gray matter. FA values for all metabolites were found to be unexpectedly larger than water FA in the cortical gray matter. The FA of all metabolites in the white matter were consistent with reported water FA values. Directional information obtained from the principle eigenvector of NAA in white matter is consistent with known anatomy and with the water DTI information.

CHAPTER 7

ANISOTROPIC DIFFUSION OF METABOLITES IN PERIPHERAL NERVE USING DIFFUSION WEIGHTED MAGNETIC RESONANCE SPECTROSCOPY AT ULTRA-HIGH FIELD

7.1 INTRODUCTION

Magnetic resonance is well established for measuring diffusion properties of water in the human brain and neural tissue. In 1990, the diffusion behavior of water was examined in the cat central nervous system by using diffusion-weighted magnetic resonance imaging with the diffusion sensitization gradients applied in different directions (X, Y, and Z) [22]. Faster diffusion (i.e. greater signal attenuation) was noted parallel (versus perpendicular) to the white matter tracts in cat brain and this was termed anisotropic diffusion. Diffusion anisotropy of water in neural tissue has been examined quite extensively since that date, but particularly after the introduction of diffusion tensor imaging (DTI) in 1994 [23, 24], and more recently this fundamental property of water in white matter has been used to perform 3D tractography of the fibers in the brain [25, 95–97]. DTI of tissue water includes contributions from exchanging intra- and extracellular water, which makes compartment specific interpretation of diffusion characteristics rather complex. It has long been shown that reductions in water diffusion are a sensitive indicator of early cerebral ischemia [22], and despite the theory that this decrease is due to a water shift from extra-cellular to intra-cellular space, purely intra-cellular metabolites also show a reduction of diffusion by

A version of this chapter was published in:
Ellegood, J., McKay, R.T., Hanstock, C.C., and Beaulieu, C. Diffusion Weighted Magnetic Resonance Spectroscopy of Peripheral Nerve at 18.8T. Proc. 14th Meeting of the International Society of Magnetic Resonance in Medicine, Seattle, USA (May 2006).
Ellegood, J., McKay, R.T., Hanstock, C.C., and Beaulieu, C. Anisotropic Diffusion of Metabolites in Peripheral Nerve using Diffusion Weighted Magnetic Resonance Spectroscopy at Ultra-High Field. Journal of Magnetic Resonance 2007; 184: 20-28.

a similar magnitude without any compartmental shifts [100, 102–107]. These metabolite diffusion studies are usually interested in either single direction diffusion or rotationally-invariant mean diffusivity.

To date, there have only been two published human studies that have studied anisotropic diffusion of intracellular metabolites in tissue [117, 131]. One study measured the ADC of NAA parallel and perpendicular to the corpus callosum in the normal human brain at 1.5T and found the ADC parallel to be ~2-3 times greater than the ADC perpendicular [117]; however they examined only two human volunteers and measured only one metabolite, NAA. More recently the full diffusion tensor of gray and white matter in the normal human brain at 3T was examined [131] and indicated that the fractional anisotropy of tCr (0.66 ± 0.13) and Cho (0.67 ± 0.14) was significantly higher than NAA (0.56 ± 0.13, tCr p=0.001 and Cho p=0.001, paired t-test), which may seem counterintuitive since tCr and Cho are not solely located in the axons (presumably highly anisotropic) as is NAA but rather are also found in environments expected to be more isotropic such as astrocytes and oligodendrocytes [59].

Accurate in vivo DW-MRS measurements are quite challenging due to subject movement, shimming issues, low SNR, and large voxel sizes that include a variety of distinct neural structures. A model system, such as an excised sciatic nerve, eliminates all of those factors. In such a preparation, the nerve is aligned and fixed in position which yeilds a better shim, much more time available to average, and permits observation of a single well defined structure (a bundle of axons). Also, the size of the nerve allows the use of a spectrometer with a magnetic field strength much higher than used in vivo. The anisotropy of the intracellular metabolites N-acetyl aspartate (NAA), creatine and phosphocreatine (tCr), and choline (Cho) have been measured previously in the excised bovine optic nerve at 11.7 T [112]. The ADC values were measured parallel and perpendicular to the long axis of the optic nerve using extremely high b-values (100,000 - 300,000 s/mm^2), and the diffusion decay curves were fit to a bi-exponential. The diffusion attenuation curves varied with diffusion gradient direction for NAA, tCr, and Cho; however the focus of that study was on q-space analysis at extremely high b-value, and therefore differences in diffusion with direction at lower b-values were not examined. The purpose of this chapter was to examine the anisotropic diffusion of the three main metabolites (NAA, tCr, and Cho), as well as any other measurable metabolites, in the excised frog sciatic nerve, with the ultimate goal to relate this information to the anisotropic nature of the metabolite diffusion in the white matter of the human brain.

7.2 Methods

7.2.1 Nerve Sample Preparation

All sciatic nerve samples were taken from adult Xenopus laevis, the African clawed frog, which had been housed in an aquatic environment at room temperature. In total, nine nerve samples from five frogs were used in this study. Following euthanasia in MS-222 (3-aminobenzoic acid ethyl ester), ~3 cm segments of nerve were removed and placed in an oxygenated physiological buffer (112 mM NaCl, 3.0 mM KCl, 1.6 mM $MgSO_4$, 3.0 mM $CaCl_2$, 5.0 mM glucose, 3.0 mM HEPES). The perineurial sheath surrounding the nerve was removed from all nerve samples. The nerve samples were immersed in Fluorinert (FC-77, Sigma-Aldrich Canada Ltd. Oakville, Ontario, Canada) and were aligned along the z-axis of the magnet by tying thread to one end and pulling the nerve (and Flourinert) into a small capillary tube (1 mm inner diameter) after which both ends were sealed with parafilm. The capillary tube was then oriented within a Wilmad 535P - 5mm NMR tube along the z-axis and was surrounded by 99% D2O (required for the lock signal, Fig. 7.1). All nerve samples were placed in the NMR between 45 min and 3 hours of extraction.

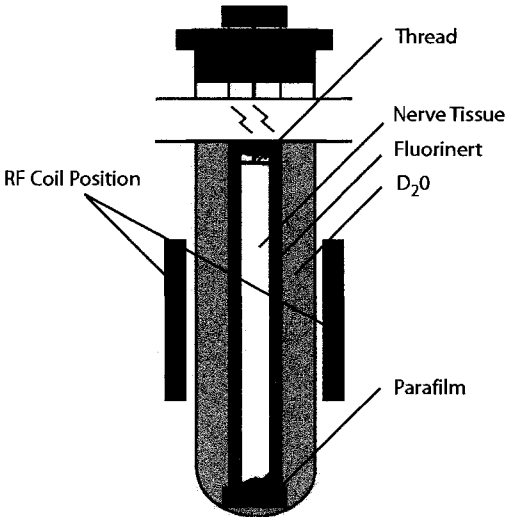

Figure 7.1: Diagram of the setup for the 5 mm NMR tube. The excised sciatic nerve of the frog was immersed in a fluorinated compound to prevent dehydration and placed in a 1 mm inner diameter capillary tube, which was aligned parallel to the Z-axis of the magnet. The capillary tube was surrounded by 99% D_2O, which was required for the lock signal.

Thanks to Isidro Bonilla for performing the nerve extractions

7.2.2 NMR Experiments

An 800 MHz (18.8 T) Varian Inova NMR spectrometer running VNMRJ 1.1D equipped with a XYZ-gradient HCN 5mm probe with a maximum gradient strength of ~30 G/cm along the X and Y axes and ~60 G/cm along the Z-axis, was used for all diffusion experiments. A diffusion-weighted spin-echo pulse sequence with 5.0 ms diffusion gradient pulses (δ) and a diffusion gradient separation (Δ) of 20.0 ms yielded a diffusion time (Δ-$\delta/3$) of 18.3 ms. Sequence parameters were as follows: TE = 30 ms, TR = 3 s, SW=12000 Hz, number of complex points = 24002. Water suppression was achieved using a water selective 90 degree shaped Gaussian pulse prior to the hard 90 in the spin-echo pulse sequence. The gradient strengths of the X, Y, and Z gradients were calibrated based on a Cr diffusion coefficient of 0.80 x 10^{-3} mm^2/s at 20 °C [101] using a 600μL phantom containing NAA (3 mM), Cr (3 mM), and Cho (1 mM). Seven separate calibrated b-values were measured for each direction (227, 539, 903, 1107, 1444, 1710, and 1970 s/mm^2 for the X-direction, 235, 530, 796, 1063, 1382, 1626, and 1871 s/mm^2 for the Y-direction, and 245, 689, 1046, 1305, 1662, 1949, and 2322 s/mm^2 for the Z-direction). A temperature of 20 °C was used for both phantom and nerve experiments.

A 1 Hz exponential filter was used during spectral processing. The shimmed linewidth at half height for the NAA peak was 5 $\pm$ 3 Hz. The apparent diffusion coefficients were calculated by measuring the slope of ln(signal intensity) versus b-value. The signal intensity was calculated using a home built Matlab program, and was a measure of the amplitude of the maximum value of the peak relative to a fitted baseline through the peak. The fitted baseline consisted of a straight line fit through points adjacent to both sides of the designated peak. The phantom study on NAA, Cr, and Cho was repeated three times to ensure the accuracy of the b-value calibration for each gradient direction. ADC values were measured in the X, Y, and Z directions from separate samples (N=1) of phosphocreatine (PCr), taurine (Tau), glutamate, and glutamine that were not included in the original calibration. Diffusion experiments in the phantoms acquired 16 averages. The diffusion coefficients of NAA, Cr, and Cho in the X, Y, and Z direction as well as the mean diffusivity, i.e. Trace/3 ADC, were consistent with previously reported phantom diffusion coefficients [101], and the low FA values of 0.01 - 0.08 for all metabolites showed the expected isotropy (Table 7.1).

Nerve experiments were performed using the same b-values used in the calibration study (listed previously). The number of averaged transients used in the nerve experiments ranged from 64 to 512, with more averages being used to examine peaks of lower SNR. The total scan time for the 64 average experiments was ~ 90 min. Since the excised

nerve axis was aligned with the laboratory frame, the apparent diffusion coefficient (ADC) measured along the Z axis corresponds to the largest eigenvalue (i.e. parallel diffusion) whereas the ADC values along the two orthogonal axes correspond to the two smaller eigenvalues (i.e. perpendicular diffusion) of the diffusion tensor. The mean diffusivity (Trace/3 ADC) and the fractional anisotropy (FA) were calculated from these eigenvalues. It has been shown previously that ~18 metabolites are visible in the rat brain at 9.4 T with a TE of 2 ms [132]; however, due to problems such as J-modulation and T2 relaxation over the relatively long spin-echo time of 30 ms, only five metabolites were quantified in the frog sciatic nerve, namely NAA (2.01 ppm), tCr (3.03 ppm), Cho (3.21 ppm), Tau (3.25 ppm), and Glx (3.75 ppm, i.e. cannot distinguish glutamine and glutamate in this case). The assignment of metabolite peaks was based on previous literature [132] as well as individual metabolite spectra measured in aqueous phantom (Figures 2.26 and 7.2). Glx was only visible in 3 and Tau in 4 nerve samples, respectively, likely due to a better shim, thicker nerve, and higher SNR in those cases. The Tau peak was hard to distinguish in the Z-direction at b-values larger than 1700 s/mm^2; therefore, Tau had only 5 b-values used for ADC calculation in the Z-direction. Glx was not sensitive to this effect due to a smaller drop in amplitude for the Glx peak along Z with increasing b-values compared to the Tau peak.

In this paper, Cr and PCr were averaged together, by measuring the combined methyl peak at 3.03 ppm where there was no defined separation, to yield a measurement of tCr assuming that the diffusion coefficients of these two metabolites are similar in nerve. Note in fact that in an aqueous phantom, the diffusion of Cr and PCr are not the same, and neither are glutamate and glutamine (Table 7.1). Three of the nerve samples had sufficient spectral resolution that allowed the separation of the Cr and PCr peaks located at 3.91 ppm and 3.93 ppm, respectively, which are the resonances originating from the methylene protons of Cr/PCr. Examination of this data revealed PCr had a consistently higher ADC in the Y direction when compared to the X direction and Cr had a consistently higher ADC in the X direction when compared to the Y. There is no reason to expect consistent differences between the perpendicular X and Y directions (not observed for other metabolites). Examination of the low diffusion-weighted (b~200 s/mm^2) spectra for X, Y, and Z ADC measurements showed a reduction in the amplitude of the PCr peak located at 3.93 ppm over time and an increase in the intensity of the Cr peak located at 3.91 ppm. Thus the ADC measurements for Cr and PCr individually are corrupted due to changing concentrations of these two metabolites (lack of oxidative phosphorylation [133]) during the measurement. Figure 7.3 shows the change of PCr into Cr over time, in which the Z direction was measured first from low to high b-value, followed by the

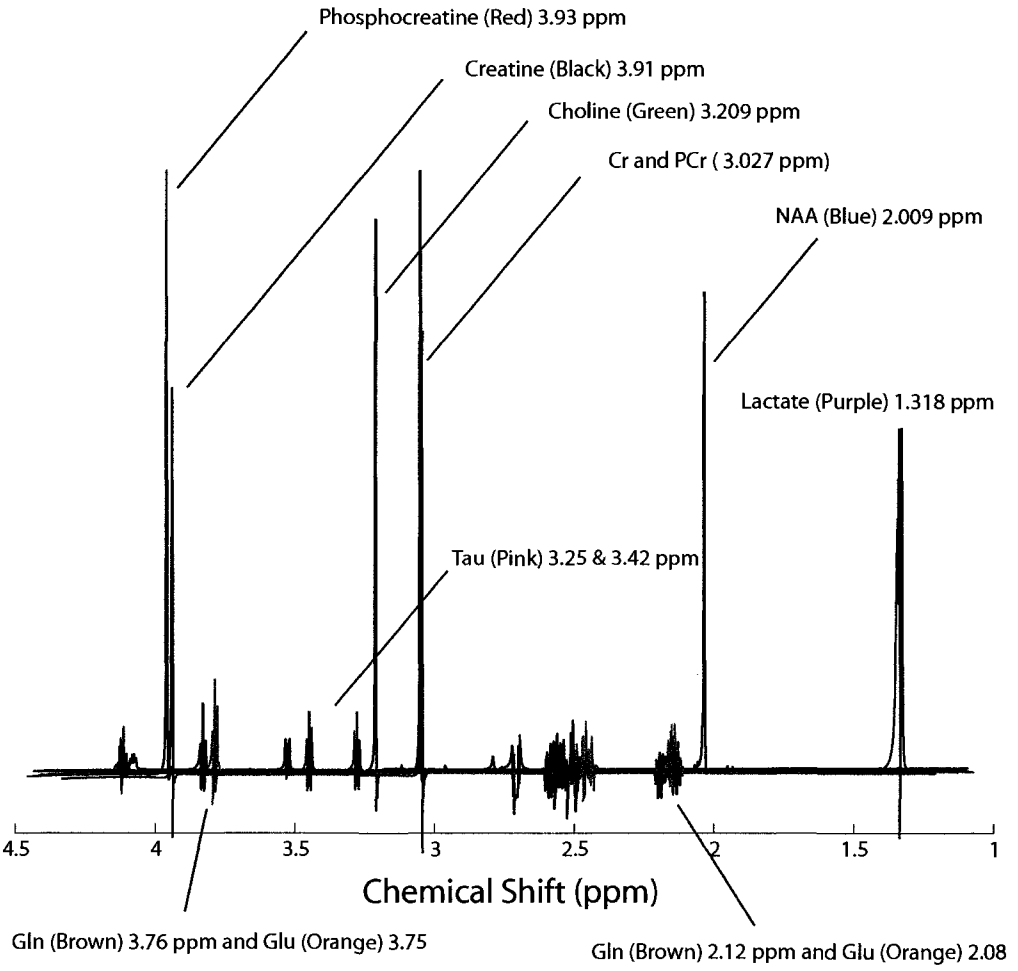

FIGURE 7.2: Over-plotted Phantom spectrum, of NAA, Creatine and Phosphocreatine, Choline, Glutamate, Glutamine, Taurine, and Lactate acquired individually in aqueous phantom. This was used to help assign the peaks in our nerve spectra. The spectra shown here were acquire with the exact same sequence parameters as the nerve spectra.

Y direction low to high b-value, and then the X direction high to low b value. It can clearly be seen in Figure 7.3 that at the same approximate b-value the signal intensity of the PCr and Cr peaks are different at different time points (blue circle), and furthermore at the same approximate high b-value (red circle) two spectra taken in succession show no significant change in the intensity of the PCr and Cr peak.

The diffusion measurements of the total creatine peak, including both PCr and Cr, were deemed reasonable given the consistency of the total creatine area over the entire experiment. Each individual nerve was scanned at b=0 s/mm^2 at both the beginning and the end of the scan session. Changes in the metabolite peak area at these two time points, are expressed as mean $\pm$ SD percent values as follows: NAA = 0.6 $\pm$ 4.0 %, tCr = 0.0 $\pm$

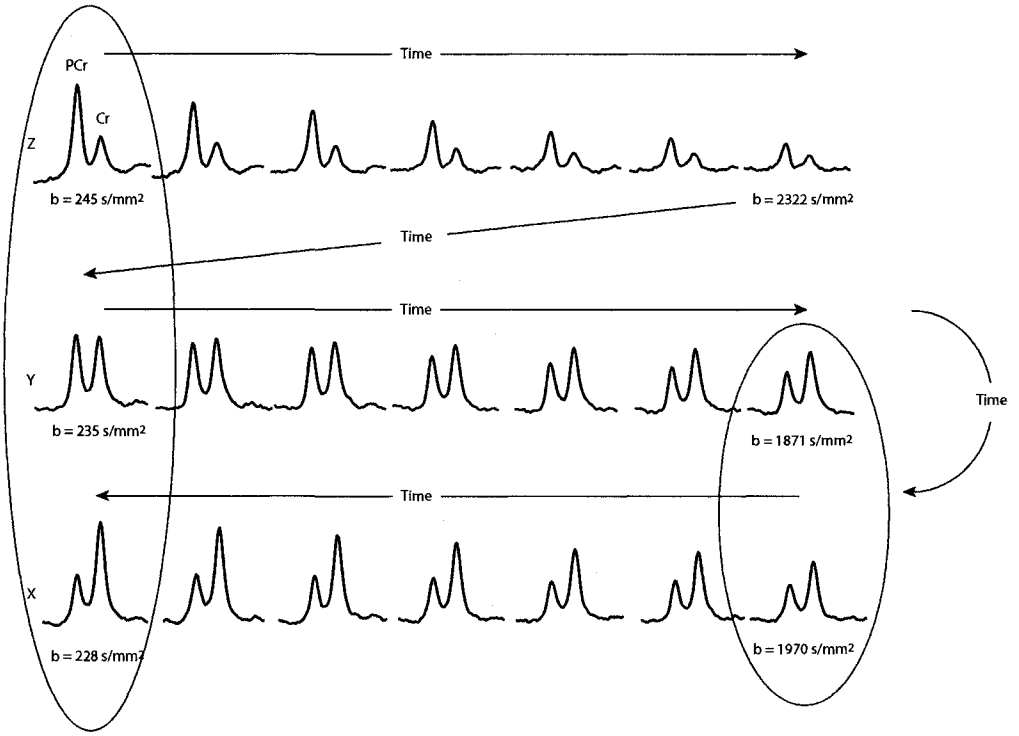

FIGURE 7.3: Changes in Creatine and Phosphocreatine over time in dying nerve tissue. Shows the change of PCr into Cr over time, in which the Z direction was measured first from low to high b-value, followed by the Y direction low to high b-value, and then the X direction high to low b value.At the same approximate b-value the signal intensity of the PCr and Cr peak are different at different time points (blue circle), and furthermore at the same approximate high b-value (red circle) two spectra taken in succession show no significant change in the intensity of the PCr and Cr peak.

3.4 %, Cho = 1.8 ± 7.0 %, Tau = -1.6 ± 5.7 %, and Glx = 2.6 ± 2.8 %; therefore, there are no significant differences of peak area before and after for any metabolite (paired t-test).

7.3 RESULTS

Table 7.1 lists the ADC values in the X, Y, and Z directions of NAA, Cr, PCr, Cho, Tau, Glu, and Gln each measured in a 600 μL isotropic phantom. NAA, Cr and Cho were combined in a single phantom used for calibration of the gradients and their Trace/3 ADC values in the phantom were determined to be 0.65 ± 0.05 x 10^{-3} mm^2/s, 0.82 ± 0.01 x 10^{-3} mm^2/s, and 0.97 ± 0.01 x 10^{-3} mm^2/s for NAA, Cr, and Cho, respectively, which is consistent with previous literature values [101]. The low FA values of 0.03 to 0.08 indicate isotropic diffusion, although the observed small differences between X, Y, and Z ADC values in the phantom are due to noise.

Metabolite	Apparent Diffusion Coefficient (x 10^{-3} mm^2/s)				Fractional
	X	Y	Z	Trace/3	Anisotropy
N-Acetyl Aspartate (N=3)	0.64±0.08	0.66±0.10	0.65±0.02	0.65± .05	0.08±0.02
Creatine (N=3)	0.80±0.02	0.84±0.05	0.80±0.05	0.82±0.01	0.06±0.01
Phosphocreatine (N=1)	0.51	0.51	0.57	0.53	0.07
Choline (N=3)	0.94±0.02	0.98±0.02	0.98±0.02	0.97±0.01	0.03±0.01
Taurine (N=1)	1.00	1.05	0.98	1.01	0.03
Glutamate (N=1)	0.68	0.7	0.68	0.68	0.01
Glutamine (N=1)	0.79	0.85	0.74	0.79	0.07

TABLE 7.1: Diffusion measurements of N-acetyl aspartate (NAA, 3 mM), creatine (Cr, 3 mM) and choline (Cho, 1 mM) combined in a 600 μL aqueous solution (N = 3), and phosphocreatine, taurine, glutamate, and glutamine (all 25 mM) in separate 600 μL aqueous solutions (N = 1).

Example ^1H nerve spectra are shown in Figure 7.4, with diffusion gradients either perpendicular (Y direction) or parallel (Z direction) to the long axis of the nerve at low (235 and 245 s/mm^2) and high (1871 and 1949 s/mm^2 for Y and Z, respectively) b-values at 18.8 T. Note that contrary to human brain spectra, tCr has a higher concentration when compared to NAA in the frog sciatic nerve. Spectral acquisitions yielded average signal to noise ratios for the 64 average spectra of 48 ± 23, 57 ± 29, 22 ± 10, 11 ± 2, and 11 for the NAA, tCr, Cho, Tau, and Glx peaks, respectively at the lowest b-value spectra in the X direction in the nerves. Glx was only observed in one of the 64 average spectra, hence the lack of a standard deviation (it was found in two other spectra with more averages). The peaks of NAA, Cr, and Cho can clearly be seen, as well as the corresponding linear decay with increasing b value. Figure 7.5 displays the diffusion decay curves for the phantom (7.5A) and the five metabolites, NAA (B), tCr (C), Cho (D), Tau (E), and Glx (F) in the nerve along the X, Y and Z directions. Note the greater signal attenuation at higher b-value in the Z direction in Figures 7.5B, C, D, and E indicating faster diffusion along the length of the nerve samples. Faster Z-diffusion is not evident in the Glx decay curves (Fig. 7.5F).

The Trace/3 ADC and FA values of NAA, tCr, Cho, Tau, and Glx measured in the frog sciatic nerve are listed in Table 7.2. The Trace/3 ADC values ranged from 0.19 - 0.26 x 10^{-3} mm^2/s (0.22 ± 0.02 x 10^{-3} mm^2/s, mean ± SD) for NAA, 0.23 - 0.33 x 10^{-3} mm^2/s (0.28 ± 0.03 x 10^{-3} mm^2/s) for tCr, 0.13 - 0.20 x 10^{-3} mm^2/s (0.16 ± 0.02 x 10^{-3} mm^2/s) for Cho, 0.21 - 0.29 x 10^{-3} mm^2/s (0.25 ± 0.03 x 10^{-3} mm^2/s) for Tau, and 0.13 - 0.19 x 10^{-3} mm^2/s (0.17 ± 0.03 x 10^{-3} mm^2/s) for Glx. The FA values ranged from 0.26 - 0.57 (0.41 ± 0.09, mean ± SD) for NAA, 0.44 - 0.67 (0.59 ± 0.07) for tCr, 0.44 - 0.76 (0.61 ± 0.11) for Cho, 0.52 - 0.73 (0.60 ± 0.10) for Tau, and 0.15 - 0.26 (0.20 ± 0.06) for Glx.

The r^2 values for the signal attenuation curves of the nine nerve samples ranged from

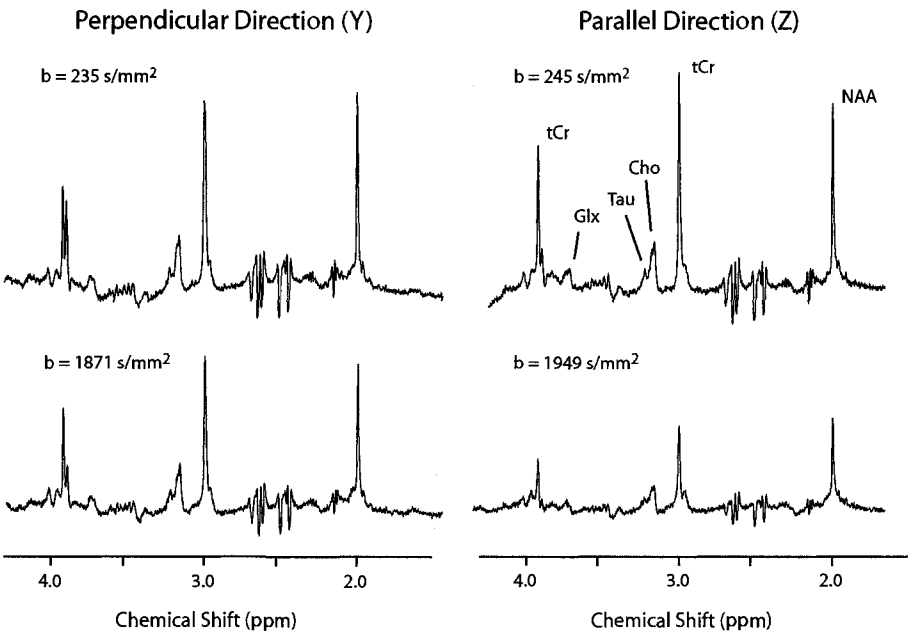

FIGURE 7.4: Example spectra (TE = 30 ms) from low (235 and 245 s/mm^2) and high b-values (1871 and 1949 s/mm^2) in the perpendicular (Y) and parallel (Z) directions in excised frog sciatic nerve. It can clearly be seen that the signal intensity in the parallel diffusion (Z) direction decays faster than the signal intensity in the perpendicular diffusion (Y) direction. Contrary to what is seen in human brain spectra, where NAA is the largest peak, in the peripheral nerve tCr is the largest peak in the spectrum. Also, note that differences in tCr appearance at ~3.9 ppm at low b-value between Z (measured earlier) and Y (measured later) is caused by changes in the concentration of PCr (left peak decreasing) and Cr (right peak increasing) after excision of the nerve (see Section 7.2.2).

0.90 - 1.00 (0.98 ± 0.03, mean ± SD) for NAA, 0.73 - 1.00 (0.96 ± 0.06) for tCr, and 0.50 - 1.00 (0.84 ± 0.16) for Cho. The lower average r^2 value for Cho probably is due to the lower SNR of Cho compared to the other two metabolites. With the even lower SNR data of the coupled peaks (Tau and Glx), the r^2 values ranged from 0.45 - 0.93 (0.76 ± 0.16) for Tau and 0.65 - 0.97 (0.88 ± 0.09) for Glx.

7.4 DISCUSSION

Previous water diffusion measurements in the excised frog sciatic nerve have reported a Trace/3 ADC value of 0.76 x 10^{-3} mm^2/s for water [134], which is ~ 3.5 times larger than the Trace/3 ADC value of (0.22 ± 0.02 x 10^{-3} mm^2/s) for NAA reported in the current study. The Trace/3 ADC of NAA in excised frog sciatic nerve is consistent with the NAA Trace/3 ADC value found in the corpus callosum of the two previous human studies 0.20 ± 0.02 x 10^{-3} mm^2/s [131] and 0.18 or 0.20 x 10^{-3} mm^2/s (pseudo Trace/3

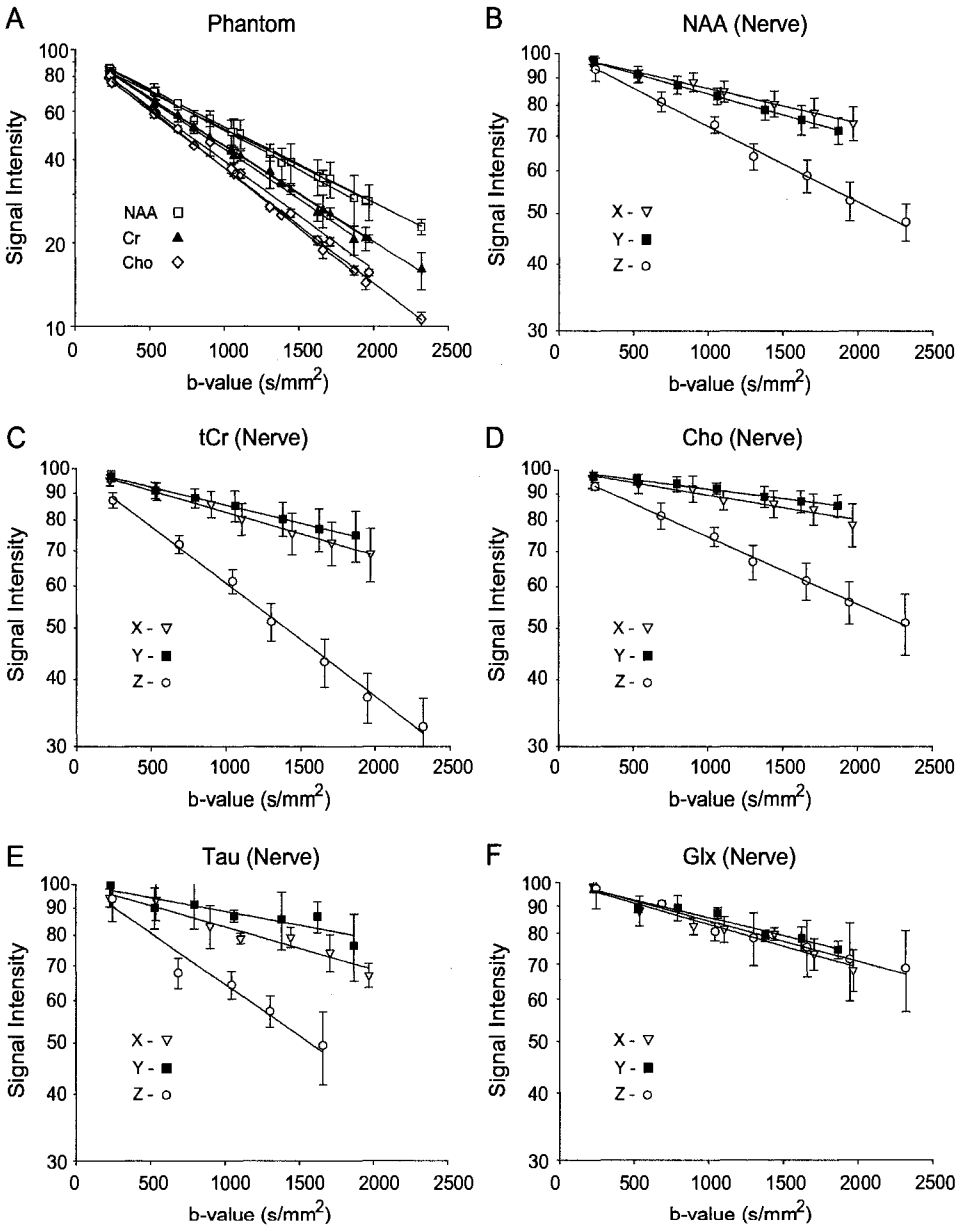

FIGURE 7.5: Decay curve for (A) an aqueous solution (N = 3) of NAA, Cr, and Cho which demonstrated isotropic diffusion (X, Y, and Z curves all shown) and (B) NAA (N = 9), (C) tCr (N = 9), (D) Cho (N = 9), (E) Tau (N = 4), and (F) Glx (N = 3) in peripheral nerve in the perpendicular (X, Y) and parallel (Z) directions. In the parallel Z-direction, the faster diffusion can clearly be seen in the nerve for all metabolites except Glx. The tCr parallel diffusion is the fastest, and the Cho perpendicular diffusion is the slowest. Tau also demonstrates considerable anisotropy whereas Glx appears isotropic. The error bars reflect the standard deviation of the signal intensity over all nerve samples at each b-value.

Metabolite	Apparent Diffusion Coefficient (x 10^{-3} mm^2/s)				Fractional
	X	Y	Z	Trace/3	Anisotropy
N-Acetyl Aspartate (N=9)	0.15±0.04	0.18±0.03	0.33±0.04	0.22±0.02	0.41±0.09
Total Creatine (N=9)	0.19±0.06	0.16±0.06	0.49±0.05	0.28±0.03	0.59±0.07
Choline (N=9)	0.11±0.04	0.08±0.02	0.29±0.05	0.16±0.02	0.61±0.11
Taurine (N=4)	0.19±0.02	0.12±0.06	0.44±0.03	0.25±0.03	0.60±0.10
Glutamate/Glutamine (N=3)	0.19±0.04	0.15±0.02	0.17±0.07	0.17±0.03	0.20±0.06

TABLE 7.2: ADC values perpendicular (X and Y) and parallel (Z) to the long axis of the frog sciatic nerve as well as derived diffusion parameters, Trace/3 ADC and fractional anisotropy.

ADC) [117]. However, one should be aware that these ADC measurements were taken at different temperatures, with the in-vitro frog nerve being measured at room temperature (20 °C) while the in-vivo human brain was measured at physiological temperature (37 °C). The lower temperature of 20 °C used in this study would cause the ADC of the metabolites examined to be lower than they would be at physiological temperature of the human brain. Also, the ADC values of the metabolites in in-vitro frog nerve could theoretically be less than in-vivo prior to excision given the known reductions (~30%) in metabolite ADC after stroke in rodent models [100, 102–107]. Furthermore, studies in rat trigeminal nerve have shown an ~20% decrease in pseudo Trace/3 ADC of water post mortem [135], so a similar decrease might be expected for metabolites in excised nerve. However, an in-vivo measurement of in-vivo frog sciatic nerve with the vertical bore 800 MHz spectrometer is not possible. Given both factors of lower temperature and ischemic effects, yet similar Trace/3 ADC values in in-vitro frog sciatic nerve and human brain white matter, the metabolites in frog sciatic nerve are likely more mobile than in human corpus callosum (assuming same temperature). This is presumably due to the frog sciatic nerve consisting of larger axons (typically 4-10 μm, some 15-20 μm) [134, 134] that are also less densely packed than the smaller axons of the corpus callosum (1-3 μm) [136].

With regard to the singlet metabolites, the Cho Trace/3 ADC in this study tends to be the smallest ($p<0.001$ versus tCr and $p<0.001$ versus NAA) followed by NAA ($p<0.01$ versus tCr) and then the tCr ADC is the highest. This is contrary to what was seen in our previous human brain paper, where the Trace/3 ADC trend was NAA < tCr $\simeq$ Cho [127]. However, a recent survey of different studies of metabolite diffusion has suggested that the actual value of the mean diffusivity of Cho may be affected by the echo time of the acquisition, with shorter echo times yielding lower ADC values [137]. The mean diffusivity of Cho in the nerve is reduced to the largest extent relative to its diffusion in a phantom of bulk water (84% reduction for Cho versus 66% for NAA). The Tau Trace/3 ADC (0.25 ± 0.03 x 10^{-3} mm^2/s) is consistent with the other Trace/3 ADC values in nerve. Two previous studies have reported single direction ADC values for Tau and Glu

in rat brain in-vivo [107, 115]. The ADC values for Tau were 0.103 $\pm$ 0.003 x 10^{-3} mm^2/s [115] and 0.198 $\pm$ 0.059 x 10^{-3} mm^2/s [107] at 37 °C. These values are smaller than those reported from the frog sciatic nerve at 20 °C; however they were only measured in one direction and in a region containing a variety of different structures. The ADC values for Glu from those studies were 0.112 $\pm$ 0.002 x 10^{-3} mm^2/s [115] and 0.147 $\pm$ 0.021 x 10^{-3} mm^2/s [107], the first being smaller and the second falling within the range of our value in nerve 0.17 $\pm$ 0.03 x 10^{-3} mm^2/s. A recent study on primate brain has reported single direction ADC values for Glu of 0.21 x 10^{-3} mm^2/s [138], which is larger than what has been shown previously in the rat brain, but is consistent with what has been shown in this study for Glx. Similar to the NAA discussion above, absolute ADC comparisons between studies are complicated by measurements at different temperatures as well as the in-vivo versus in-vitro issue.

The parallel diffusion, in our current study, is significantly greater for four of the five metabolites measured when compared with perpendicular diffusion, with p-values ranging from 1.6 x 10^{-5} to 7.0 x 10^{-7}, Glx being the exception showing no significant directional preference. The average parallel diffusion of NAA was 0.33 $\pm$ 0.04 x 10^{-3} mm^2/s and the average perpendicular diffusion (average of X and Y combined) of NAA was 0.17 $\pm$ 0.03 x 10^{-3} mm^2/s, which yielded a parallel over perpendicular ratio of 2.0 $\pm$ 0.3. The other parallel over perpendicular diffusion ratios were determined to be 2.9 $\pm$ 0.4 for tCr, 3.2 $\pm$ 1.0, for Cho, and 3.0 $\pm$ 0.7 for Tau. The interesting finding was the low anisotropy of Glx indicated by a parallel over perpendicular ratio of 1.0 $\pm$ 0.4. Two human studies have also reported similar parallel over perpendicular diffusion ratios of NAA in the white matter of the human brain. One study measured the ADC value of NAA in the corpus callosum of the human brain of two healthy volunteers, and found that the ADC value measured parallel to the fibers in the corpus callosum (0.33 and 0.30 x 10^{-3} mm^2/s) was ~2-3 times greater than the ADC value measured perpendicular (0.10 and 0.15 x 10^{-3} mm^2/s) [117]; the other study measured eigenvalues for four different large white matter structures in the human brain and found parallel over perpendicular ADC ratios of 2.1 to 2.8 for NAA, 2.5 to 3.7 for tCr, and 2.5 to 3.7 for Cho [131], which are consistent with the singlet metabolite ADC ratios measured in the peripheral nerve.

The FA values in the frog sciatic nerve were ordered Glx $\ll$ NAA < tCr $\sim$ Cho $\sim$ Tau and ranged from 0.20 to 0.62, which are lower than FA values of water previously reported in the frog sciatic nerve of 0.73 (extrapolated assuming λ_1 =parallel ADC and λ_2 =λ_3 =perpendicular ADC) [134]. A previous study that calculated FA values in 4 different white matter regions in the human brain found that the FA of NAA was significantly less than tCr and Cho in the white matter [131]. The primary cells in the peripheral nerve

are Schwann cells and the axons of the dorsal root ganglion neurons. In cell cultures of these cell lines it was shown that NAA was only found within the neurons, where as Cr and Cho were found in both the neurons and Schwann cells [59]. In spite of the previous human study, it was expected that NAA, localized in the axonal compartment of the peripheral nerve, would have a larger FA than tCr and Cho because of the localization of tCr and Cho in Schwann cells, likely isotropic, in addition to axons. However, the FA value of NAA (0.41 $\pm$ 0.09) in peripheral nerve was found to be significantly less than tCr (0.59 $\pm$ 0.07) and Cho (0.61 $\pm$ 0.11) (p = 0.0002 and p=0.02, respectively).

In the previous human study it was thought that the higher FA of tCr and Cho might be a result of the lower SNR in the human brain of tCr and Cho when compared to NAA; however that is not the case in the peripheral nerve where tCr has the highest SNR among the metabolites. The higher tCr FA arises from tCr having a much larger parallel ADC (Z) than NAA (0.49 $\pm$ 0.05 x 10^{-3} mm^2/s versus 0.33 $\pm$ 0.04 x 10^{-3} mm^2/s), which could be an extension of the faster diffusion of tCr in unrestricted bulk water and the difference in molecular weight (175.1 g/mol for NAA, and 149.2 g/mol for Cr). The perpendicular diffusion (X and Y) of NAA and tCr are very similar (0.17 $\pm$ 0.03 x 10^{-3} mm^2/s for NAA and 0.18 $\pm$ 0.06 x 10^{-3} mm^2/s for tCr) and show no significant differences, which may indicate a similar restriction in the perpendicular direction. Cho also has a larger FA than NAA in the frog sciatic nerve. This difference arises from the much smaller perpendicular ADC values (X and Y) of Cho (0.10 $\pm$ 0.04 x 10^{-3} mm^2/s) versus that of NAA (0.17 $\pm$ 0.03 x 10^{-3} mm^2/s), which is opposite from what is seen with tCr, while Cho and NAA have similar parallel diffusivities (Table 7.2). Choline diffuses faster in bulk water than both NAA and Cr; however, the similar parallel diffusion of Cho to NAA, and the much lower perpendicular diffusion, would seem to indicate that Cho diffusion is further hindered in the nerve, perhaps because of the close association of Cho with membrane. Previous work which measured the diffusion of metabolites parallel and perpendicular to white matter tracts in the human corpus callosum and cortical spinal tract show also that tCr in the white matter has a larger parallel diffusion when compared to NAA but the human study did not show a smaller perpendicular diffusion for Cho when compared to NAA [131]. The Tau FA value (0.60 $\pm$ 0.10) was consistent with the FA values of tCr and Cho having a similar parallel (0.44 $\pm$ 0.03 x 10^{-3} mm^2/s) and perpendicular (0.15 $\pm$ 0.05 x 10^{-3} mm^2/s) ADC value as tCr. Glx on the other hand had a much smaller FA value, 0.20 $\pm$ 0.06, which indicated that it is in an isotropic environment when compared with the other metabolites.

The measurement of the Trace/3 ADC and FA of the lower SNR metabolites Tau and Glx are certainly open to discussion as the measurement of these metabolites proved to

be challenging. Although Tau tended to follow trends in FA and Trace/3 ADC that were similar to what is seen with the main singlet metabolites (NAA, tCr, and Cho), Glx did not. The low FA value of Glx in the peripheral nerve, 0.20 $\pm$ 0.06, was unexpected but interesting, and thus questions arise about the accuracy of the measurement. The ADC was calculated by measuring the slope of ln(signal intensity) versus b-value, and while this is entirely valid and reproducible for the strong singlet resonances, perhaps it may be more accurate to measure the slope of the ln(signal area of peak) versus b-value for a broad multiplet. The area under the Glx peak was measured for each b-value of the three nerve samples where Glx was detected. The diffusion parameters resulting from the two methods (area versus peak height) were not statistically different; however more testing, with a greater number of samples, in a different environment (brain), and possibly even with a sequence optimized for the detection of glutamate and/or glutamine needs to be examined to confirm this result. This may be difficult given the challenges associated with measuring ADC from the coupled resonance peaks. If the observation of a reduced FA holds up to future scrutiny, a possible explanation for Glx having a low FA could be that the majority of Glx is located within the Schwann cells as well as perhaps some in the synaptic vesicles (isotropic environment) within the axons. Since the Schwann cells have been shown in immunohistochemical studies of the peripheral nerve to contain the majority of glutamine and glutamine related synthetase [70], it is possible that most of the Glx peak we are measuring derives from glutamine located mainly in the Schwann cells.

When interpreting the data in this study one must keep in mind some of the limitations. This frog nerve study was an in vitro preparation and thus was performed at a lower temperature than previous diffusion studies of neurological tissue in vivo. It should also be noted that even if there is no change in the concentration of the metabolites before and after the measurements (as reported in the methods), there may be a gradual deterioration of the barriers between compartments over time after excision of the nerve. However, the linearity of the decay curves over time, and similar ADC values (no significant differences, paired t-test) measured at different times (30 min to 3 hr apart) for both X and Y directions suggest that such effects were not apparent in our measurements. Previous animal and human studies have shown reductions in metabolite ADCs in ischemic brain [29, 100, 102–107]. Since we are working with excised tissue (i.e. ischemic) in this work, ADC values in our study may be lower than the actual ADC values in vivo. Differences between the frog sciatic nerve (model system) and intact human brain white matter do exist, such as axonal size, axonal density, and cells responsible for myelination (Schwann cells in the peripheral nervous system versus oligodendrocytes in the central nervous system). However, our results indicate that the anisotropic diffusion of metabolites is acting

in a similar fashion for both frog and human nervous tissue.

7.5 Conclusions

The Trace/3 ADC and FA of NAA, tCr, Cho, Tau, and Glx were measured at 18.8T in a model system of human brain white matter, the excised frog sciatic nerve. Mean diffusivity was lowest for Cho and Glx, whereas it was quite similar for NAA, tCr, and Tau. The degree of anisotropy of tCr and Cho was higher than for NAA in frog sciatic nerve, in agreement with previous human brain white matter findings. Although preliminary, the FA of Glx was much smaller than the other four metabolites, indicating near isotropic diffusion. The differences in FA amongst the metabolites likely reflect their unique microenvironments and could be beneficial as an indicator of compartment specific changes with disease.

7.6 Addendum to Published Paper

It has been shown in the human brain that approximately 18 chemicals are visible at extremely low echo time [46]. It was expected that, since a magnetic field strength of 18.8T was used in this study, examination of a wide range of metabolites would be possible. However, in reality only 5 metabolites were examined (counting Glu and Gln as one). In the course of the study all expected chemicals, based on the previous research [46], were examined in solution.

7.6.1 Methods

The methods used to examine the phantom chemicals were completely analogous to the methods in section 7.2.2.

7.6.2 Results

Table 7.3 lists the ADC values measured in the X, Y, and Z directions, the Trace/3 ADC, and FA of a 600μL sample of $\sim$25 mmol/L of 19 different chemicals in solution. FA values calculate from this data ranged from 0.01 - 0.08 showing the expected low anisotropy. Also listed in the table are the molecular weight of each of the molecules. As mentioned in section 3.2, diffusion is dependent on the molecular weight of the molecule, as well as other factors.

Metabolite	ADC ($x10^{-3}$ mm^2/s) X	Y	Z	Trace/3	Fractional Anisotropy	Molecular Weight (g/mol)
Glutathione	0.39	0.56	0.51	**0.49**	0.17	307.30
Phosphocreatine	0.51	0.51	0.57	**0.53**	0.07	255.10
Glycerophosphocholine	0.59	0.59	0.52	**0.57**	0.07	440.50
NAAG	0.53	0.57	0.62	**0.57**	0.08	304.30
Phosphorylcholine	0.63	0.64	0.65	**0.64**	0.02	257.70
NAA	0.62	0.66	0.69	**0.66**	0.06	175.10
Scyllo-Inositol	0.64	0.69	0.67	**0.67**	0.04	180.20
Glutamate	0.68	0.70	0.68	**0.68**	0.01	147.13
Phosphoethanolamine	0.66	0.70	0.72	**0.70**	0.04	141.10
Glucose	0.67	0.66	0.78	**0.70**	0.10	180.20
Myo-Inositol	0.73	0.74	0.75	**0.74**	0.01	180.20
Glutamine	0.79	0.85	0.74	**0.79**	0.07	146.10
Creatine	0.83	0.74	0.85	**0.81**	0.07	149.15
Lactate	0.80	0.86	0.79	**0.81**	0.05	96.01
Alanine	0.85	0.87	0.90	**0.87**	0.03	89.09
Aspartate	0.88	0.91	0.92	**0.91**	0.02	155.10
GABA	0.90	0.93	0.92	**0.92**	0.02	103.10
Choline	1.00	0.97	0.99	**0.98**	0.02	139.60
Taurine	1.00	1.05	0.98	**1.01**	0.03	125.10

TABLE 7.3: ADC values measured at 18.8T along the X, Y, and Z directions as well as the Trace/3 ADC for 19 different chemicals in aqueous solution (~25 mmol/L)

Figure 7.6 shows a plot of the ADC value vs. molecular weight for the 19 different chemicals in solution. A strong correlation is seen with a decrease in the ADC corresponding with an increase in the molecular weight.

The spectra of the 19 chemicals can be seen in Figures 7.7, 7.8, and 7.9. The chemical shift range for the majority of peaks is $\sim$ 2-4 ppm range, which is where the majority of the information available for in-vivo human brain spectroscopy is located. Notable exceptions are the Glu, Lac, and Ala peaks in Figure 7.9.

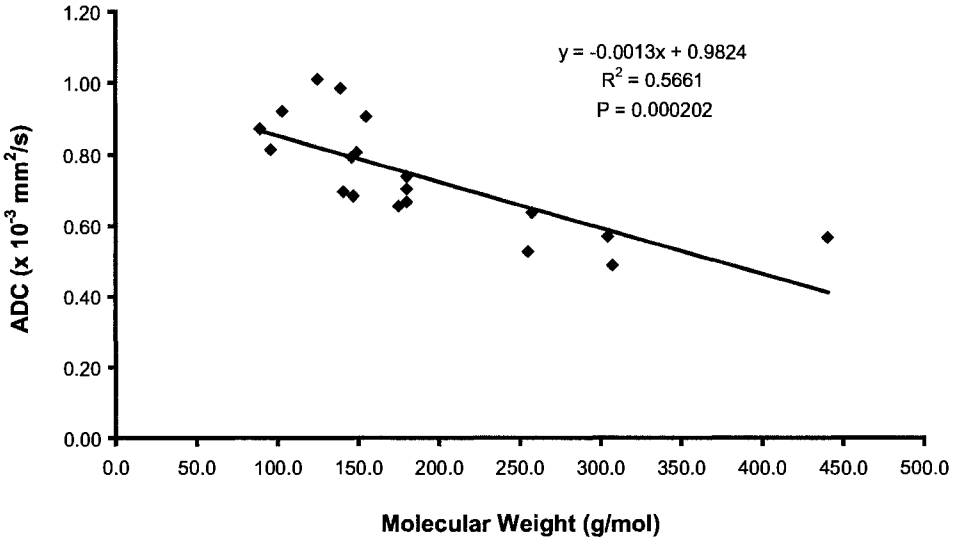

FIGURE 7.6: Graph of the Apparent Diffusion Coefficient (ADC) vs. the molecular weight for 19 different chemicals in aqueous solution. A clear correlation of ADC and Molecular weight can be seen.

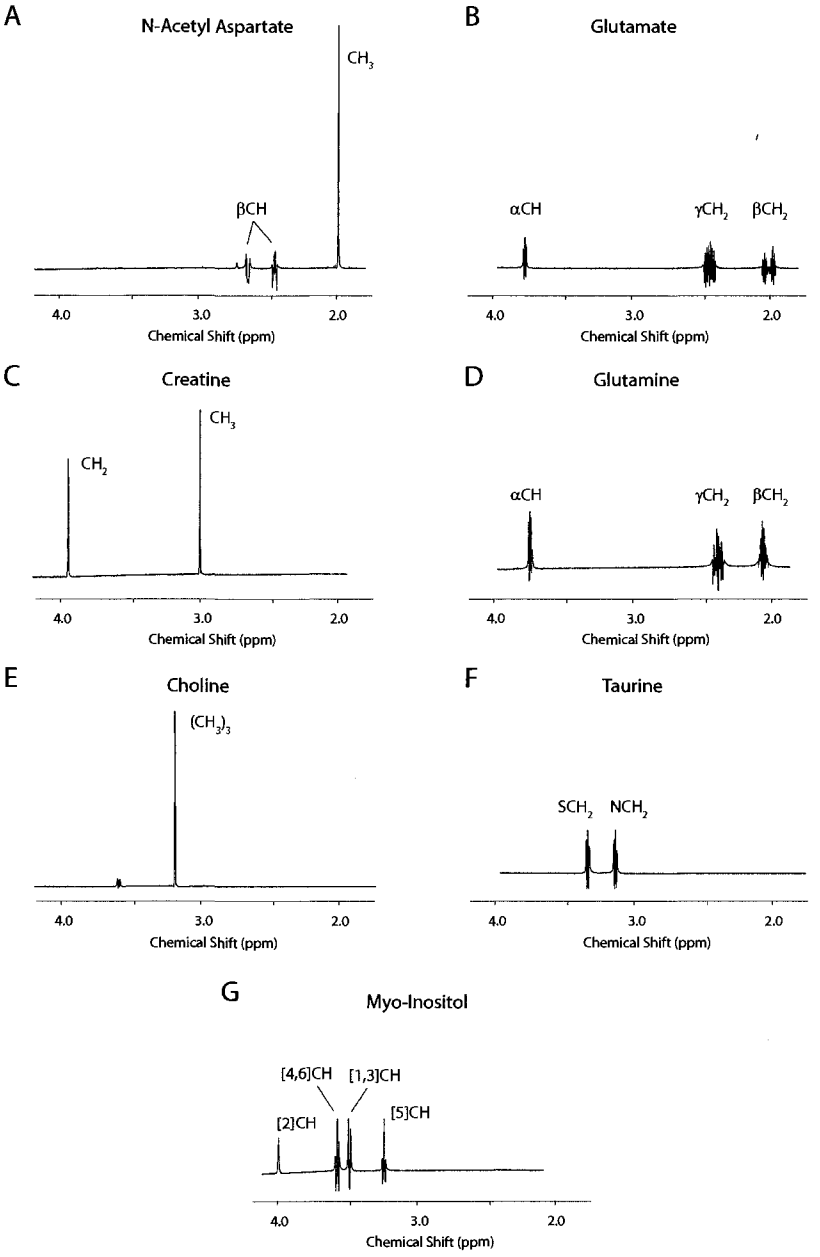

FIGURE 7.7: Metabolite Spectra for NAA (A), Glu (B), Cr (C), Gln (D), Cho (E), Tau (F), and mI (G). Spectra were acquired from in-vitro aqueous samples (~25 mmol/L) at 18.8T. Spectra are not to scale.

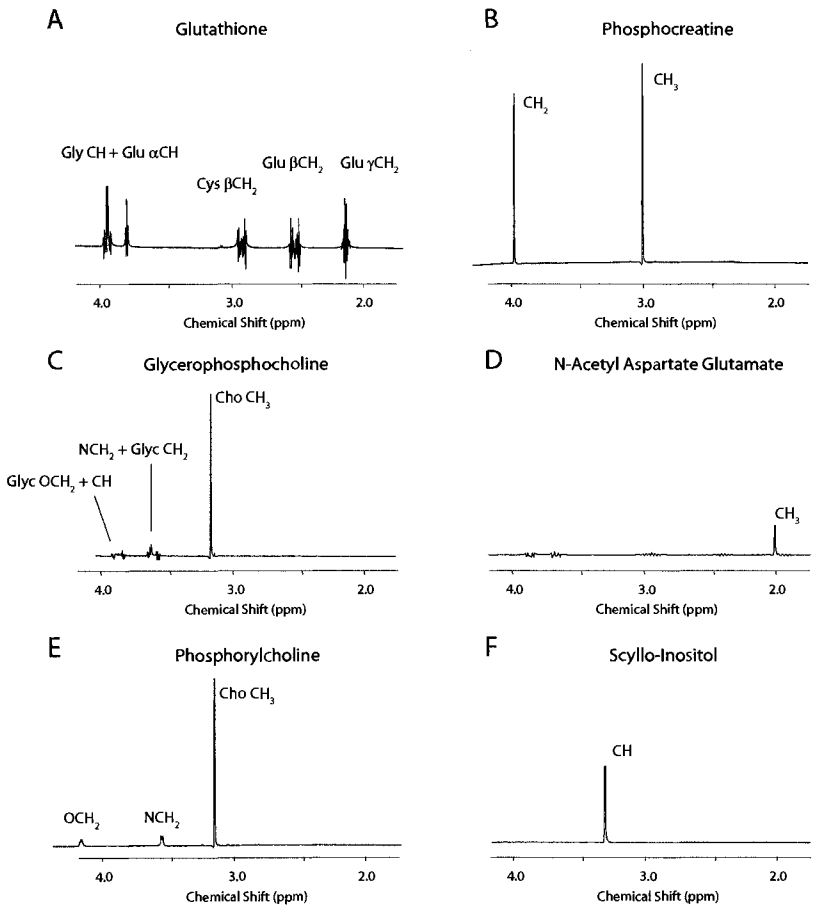

FIGURE 7.8: Metabolite Spectra for Glutathione (A), Phosphocreatine (B), Glycerophosphocholine (C), N-Acetyl Aspartate Glutamate (D), Phosphorylcholine (E), and Scyllo-Inositol (F). Spectra were acquired from in-vitro aqueous samples (~25 mmol/L) at 18.8T. Spectra are not to scale.

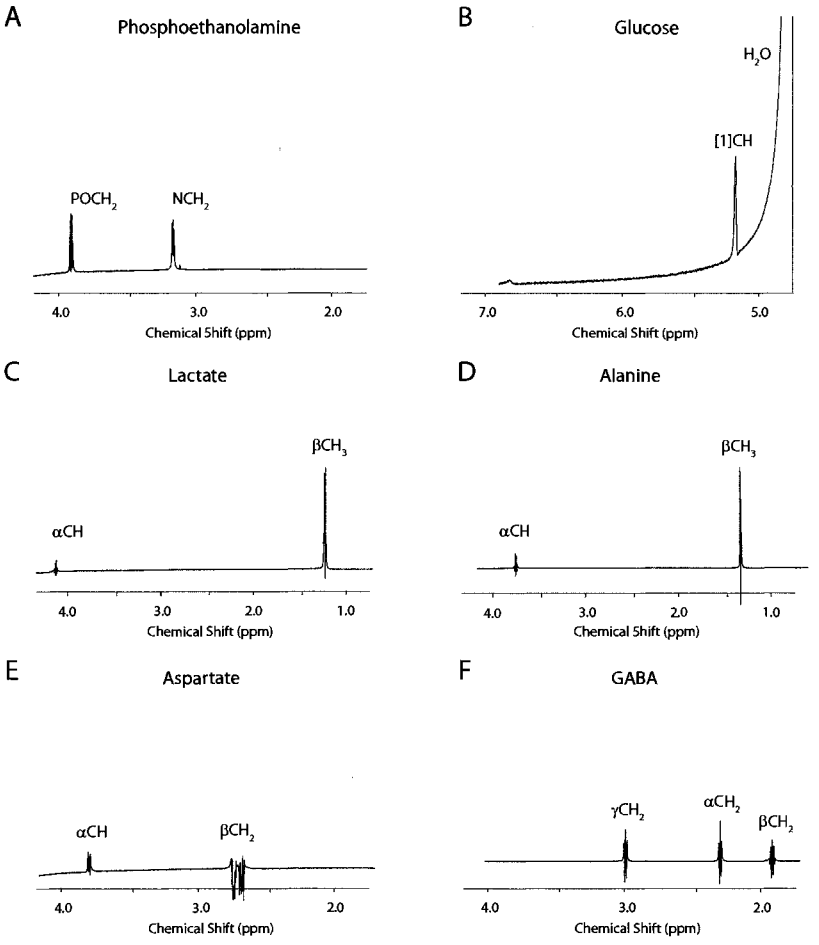

FIGURE 7.9: Metabolite Spectra for Phosphoethanolamine (A), Glucose (B), Lactate (C), Alanine (D), Aspartate (E), and GABA (F). Spectra were acquired from in-vitro aqueous samples (~25 mmol/L) at 18.8T. Spectra are not to scale.

Chapter 8

Diffusion Tensor Spectroscopy of Myo-Inositol: Implications for the Measurement of FA

8.1 Introduction

Diffusion measurements of water in human brain, using magnetic resonance imaging, have been examined extensively to date, and shown promise in studying a multitude of neurological disorders. Since, the initial discovery of water diffusion effects in the diagnostic imaging of acute stroke [22] and the inherent nature of anisotropy in diffusion weighted MRI [139], diffusion weighted imaging has become a staple in both the clinic and the lab. The invention of Diffusion Tensor Imaging (DTI) has only furthered the study of diffusion and diffusion anisotropy in human brain [23, 23], which has branched out to include 3D tractography of the fibers in human brain [95, 96]. Although DTI of water has been shown to be quite useful, tissue water is known to include contributions from exchanging intra- and extracellular water, which makes compartment specific interpretations rather complex, and therefore examining a single compartment might provide a more accurate assessment of the underlying cellular environment. Purely intracellular metabolites such as N-acetyl aspartate (NAA) and myo-inositol (mI), may be useful in differentiating between different structures in brain. mI is known to be located primarily in the glial cells such as astrocytes [66], whereas NAA is thought to be located primarily in the neurons and axons [59].

Recently, Diffusion Tensor Spectroscopy (DTS) of the metabolites NAA, creatine and phosphocreatine (tCr), and choline (Cho) has been performed in human brain in six different regions (Chapter 6). In order to further that examination and investigate mI in vivo at 3T, the sequence timings must be calculated for optimal mI signal [140]. In the previous

DTS study those optimal timings were not met, and therefore mI was not, and has not been, examined in human brain. The diffusion of NAA and mI should be quite different, with the astrocytes and glial cells having no specific order (i.e. isotropic), and the axons being highly ordered (i.e anisotropic), see Section 2.9. Hopefully the investigation of mI will help answer some questions brought up by the previous DTS study. The high fractional anisotropy (FA) of ~0.5 to 0.8 for NAA, tCr, and Cho in the two gray matter regions in that study was unsettling and is not consistent with what has been shown in water DTI studies, with approximate FA values of ~0.2 in cortical gray matter. There was a variety of suggestions as to why this was the case, such as the region being only 60% gray matter, but the high FA in the gray matter had no consistent directional orientation between volunteers as would be expected if the large FA was from the white matter in the voxel.

It has been shown recently [141] that the optimal conditions for two point measurements of the Apparent Diffusion Coefficient (ADC) may not have been met in the previous DTS study, and that perhaps a higher b-value is required. The original studies which perform DW-MRS on human brain used b-values of 2200 [28] and 1650 s/mm^2 [29], which is why a b-value of ~2000 s/mm^2 was originally chosen for the work presented in this thesis. Based on the measurement of 1-octanol, it has been suggested that a 40% to 80% drop in signal intensity is required [141] for accurate two point diffusion measurements of ADC values (i.e. the slope of the signal intensity drop versus b-value Figure 3.6). Therefore, any previous DTS studies using b-values in the human brain of approximately ~2000 s/mm^2 would not be optimal for measurements of the metabolite ADC, since for ADC values of ~0.15 x 10^{-3} mm^2/s (similar ADC to metabolites in-vivo) that would only mean a ~25% drop in signal intensity from a b=0 signal intensity, and in the previous studies initial b-values of ~600 s/mm^2 were used (Chapter 6 and [131]), which would result in an even smaller drop in signal intensity between successive b-values. Furthermore, the variability in a single direction ADC used for a DTS measurement tends to be rather large, ±0.10 x 10^{-3} mm^2/s. While this variability is not a problem for the measurement of the water ADC in tissue (~0.70 x 10^{-3} mm^2/s) where the ADC would vary by ~14%, for the measurement of the metabolite ADC in tissue (~0.15 x 10^{-3} mm^2/s) the ADC would vary by ~66%, which may be the direct cause for the high FA in gray matter reported in our study. This argument assumes that the variability in the measure is consistent at the smaller ADC values. Different ADC variabilities and their effect on fractional anisotropy (FA) values are shown in Table 8.1; this highlights the requirement for decreasing the variability in the measurement of in-vivo metabolites.

The purpose of this study was to use DTS to measure the diffusion characteristics of

ADC Variability	ADC (x 10^{-3} mm^2/s) λ_3	λ_2	λ_1	Trace/3	Fractional Anisotropy
Water ~0.70 x 10^{-3} mm^2/s					
±0.10	0.60	0.70	0.80	0.70	0.14
±0.09	0.61	0.70	0.79	0.70	0.13
±0.08	0.62	0.70	0.78	0.70	0.11
±0.07	0.63	0.70	0.77	0.70	0.10
±0.06	0.64	0.70	0.76	0.70	0.09
±0.05	0.65	0.70	0.75	0.70	0.07
Metabolite ~0.15 x 10^{-3} mm^2/s					
±0.10	0.05	0.15	0.25	0.15	0.59
±0.09	0.06	0.15	0.24	0.15	0.54
±0.08	0.07	0.15	0.23	0.15	0.49
±0.07	0.08	0.15	0.22	0.15	0.44
±0.06	0.09	0.15	0.21	0.15	0.38
±0.05	0.10	0.15	0.20	0.15	0.32

TABLE 8.1: Trace/3 ADC and FA calculations for different ADC variabilities in the eigenvalues. Notice the changes in FA at the same ADC variability based solely on the magnitude of the intrinsic diffusion coefficient. This highlights the requirement for decreasing the variability in the measurement of in-vivo metabolites.

mI in the human brain. Because mI is thought to be more isotropic due to its location in glial cells which are not ordered like axons (Figure 2.17 and Section 2.9), a high FA value for mI in human brain gray matter, using a similar b-values as used in the previous DTS study, would again indicate the unreliability of that method for calculating FA. DTS measurements at a higher b-value, ~5000 s/mm^2, in gray and white matter regions were performed to compare with this initial work. Using a b-value of ~5000 s/mm^2 should cut down on some possible errors associated with the ADC measurements, since this will yield a signal intensity drop of around ~50%. Furthermore to gain further insight on the sensitivity of FA to low diffusion coeffients, a variety of isotropic alcohols will be examined with diffusion coefficients ranging from ~0.12 to 0.50 x 10^{-3} mm^2/s, with specific attention paid to 1-octanol, which has a similar intrinsic ADC, 0.142 x 10^{-3} mm^2/s, as metabolites in human brain. The ultimate goal of this project is to determine if DTS measurements in human brain are feasible, and if so what needs to be done to ensure the accuracy of those measurements.

8.2 METHODS

All experiments were performed on a SMIS 3T MRI equipped with a maximum gradient strength of 20 mT/m. Initially gradient echo images along transverse, sagittal, and coro-

nal planes were acquired (TE = 22 ms, TR = 500 ms, slice thickness = 5 mm, 11 slices per direction). An in-house single voxel, diffusion weighted PRESS sequence, which was optimized for the detection of mI, based on previous non diffusion spectroscopy simulations and experiments [140], with a TE_1 of 36 ms, and a TE_2 of 160 ms (Figure 8.1), was used to measure the diffusion of NAA, tCr, Cho, and mI. Water suppression was achieved using a dual inversion recovery with two hyperbolic secant pulses of 80 ms in duration, with inversion times of ~1400 ms and ~200 ms, followed by water crusher gradients along the X and Y directions for 20 ms. The diffusion gradient strengths were calibrated using the reported ADC value of Cr at 20 °C of 0.80 x 10^{-3} mm^2/s [119], since its value has been shown to be consistent.

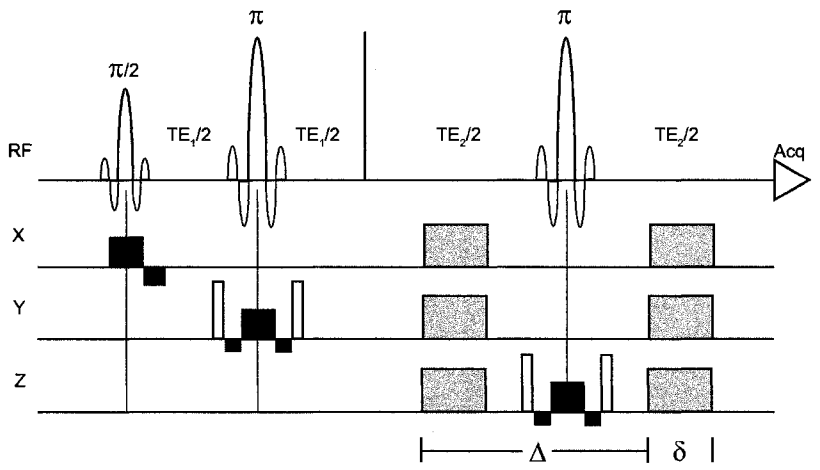

FIGURE 8.1: Diffusion-weighted PRESS sequence. Diffusion gradients (gray), spoilers (white), and slice selection and refocusing gradients (black) are shown (gradients not to scale). Water suppression (not shown) consisted of a dual inversion recovery.

8.2.1 PHANTOM WORK

The first step, in the intial phantom study, was to confirm the gradient calibration by examining a 125 mL spherical water phantom containing concentrations of NAA (9.0mM), Cr (6.4mM), Cho (1.7mM), and mI (6.8 mM) (Figure 8.2). All chemicals in this study were purchased from Sigma-Aldrich Canada Ltd., Oakville, Ontario.

The diffusion was measured in 6 different gradient directions: [(1,1,0), (1,0,1), (0,1,1), (-1,1,0), (-1,0,1), and (0,1,-1)], where (Gx, Gy, Gz) signifies the diffusion sensitizing gradient direction. The diffusion parameters were as follows: δ = 18 ms, Δ = 80 ms, which yielded a maximum b-value of 1238 s/mm^2. In total 4 b-values were used to ensure the accuracy of the calibration. Peak height was used to measure the metabolite signal intensity from the

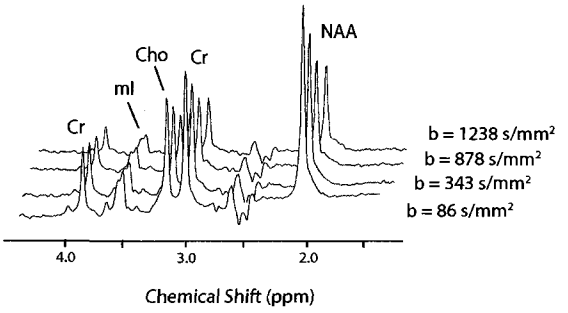

FIGURE 8.2: Example Spectra from a 125 mL spherical aqueous phantom consisting of NAA, Cr, Cho and mI at increasing b-values.

single direction spectra. The Trace/3 ADC (Mean Diffusivity) and Fractional Anisotropy (FA) values were calculated in this initial phantom work to determine the accuracy of the calibration, Table 8.2. The FA values are relatively low, ranging from 0.09 to 0.18, which indicate isotropy as expected. The Trace/3 ADC values of NAA, Cr, and Cho are consistent with previous literature [119], and the mI Trace/3 ADC is a little bit smaller than our previous one measurement at 800 MHz in section 7.6.2 of 0.74 x 10^{-3} mm^2/s at 20 °C.

Phantom (N=8)	Trace/3 ADC (x10^{-3} mm^2/s)	Fractional Anisotropy
NAA	0.64±0.03	0.18±0.03
Cr	0.82±0.04	0.12±0.04
Cho	0.95±0.04	0.09±0.03
mI	0.69±0.04	0.18±0.04

TABLE 8.2: Mean Diffusivity (MD) and Fractional Anisotropy (FA) values for NAA, Cr, Cho, and mI in phantom at room temperature. The reasonable FA values indicate isotropy as expected.

8.2.2 In-Vivo Work

In-vivo DTS spectra were obtained from two regions in the human brain of 5 volunteers (ages 22-36 years). Both regions were investigated using a 2.7 x 2.7 x 2.7 cm^3 voxel located in either the occipital gray matter (OGM, Figure 8.3A), or the subcortical white matter (SWM, Figure 8.3B). ADCs were calculated in six different directions, consistent with the phantom study above. In the OGM region two experiments were performed, one which had b-values of 502 and 1815 s/mm^2 (δ = 22 ms and Δ = 80 ms), these b-values were chosen to be consistent with our previous DTS study (Chapter 6), and another with b-values of 347 and 5018 s/mm^2 (δ = 36 ms and Δ = 87 ms). The sequence used for the high

b-value study was validated on the alcohols and will be discussed in detail in the section 8.2.3. The same five volunteers were used for each of these studies in the OGM region. Example spectra from the OGM region of the human brain, both the low b-value and high b-value study, can be seen in Figure 8.4. Example spectra from the SWM region, for two different directions ((1,1,0) direction with an NAA ADC of 0.23 x 10^{-3} mm^2/s and (0,1,-1) direction with an NAA ADC of 0.15 x 10^{-3} mm^2/s), can bee seen in Figure 8.5.

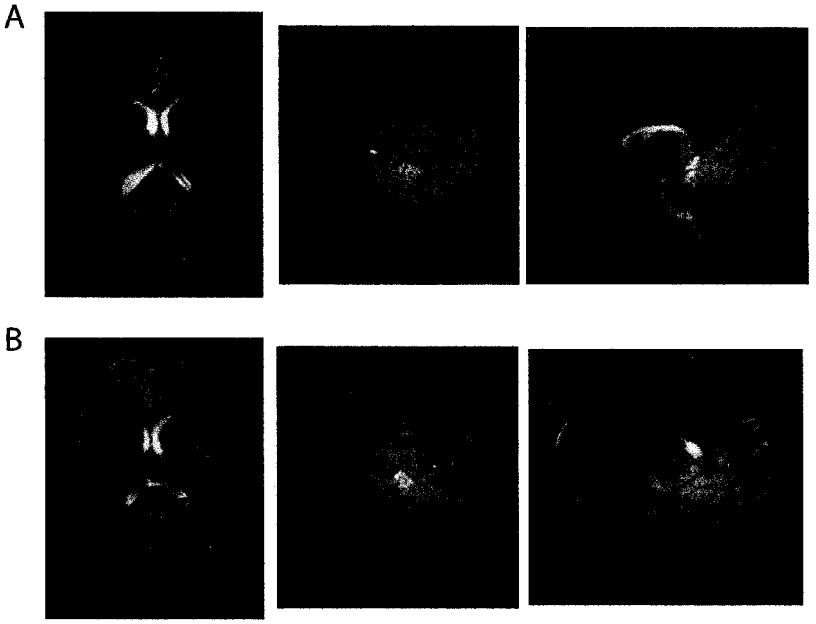

FIGURE 8.3: Transverse, Coronal, and Sagittal images indicating the localization of the voxel in the Occipital Gray Matter (OGM, A) or the Subcortical White Matter (SWM, B).

Each brain region required the optimization of the first and second order shims and resulted in an in-vivo water line width of ~5-7 Hz. We acquired eight single average spectra for the unsuppressed water peak, which were required for eddy current correction [120], and sixty-four single average spectra for the metabolite spectra (with water suppression) for each of the two b-values along each of the six directions. This acquisition scheme yielded 12 summed water spectra and 12 summed metabolite spectra for each brain region examined. The total measurement time for the set of 12 summed metabolite spectra was ~43 min. Including axial, coronal, and transverse scout images, as well as the water spectra, a total exam time of ~75 min for each brain region was required. Hence, it was practical to study only one brain region per scanning session.

DW-MRS requires individual phase correction on single average spectra before summation in order to correct for motion induced phase errors between the individual spectra [28, 127]. Two phase correction methods have been shown to be accurate in determining

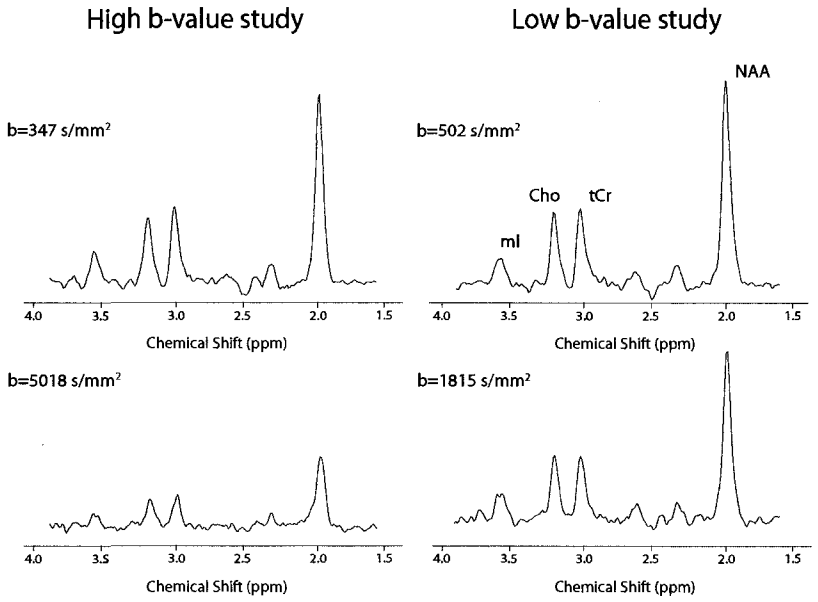

FIGURE 8.4: Example Spectra from the (1,1,0) direction in the OGM region in human brain. Spectra from both the high and low b-value studies are shown.

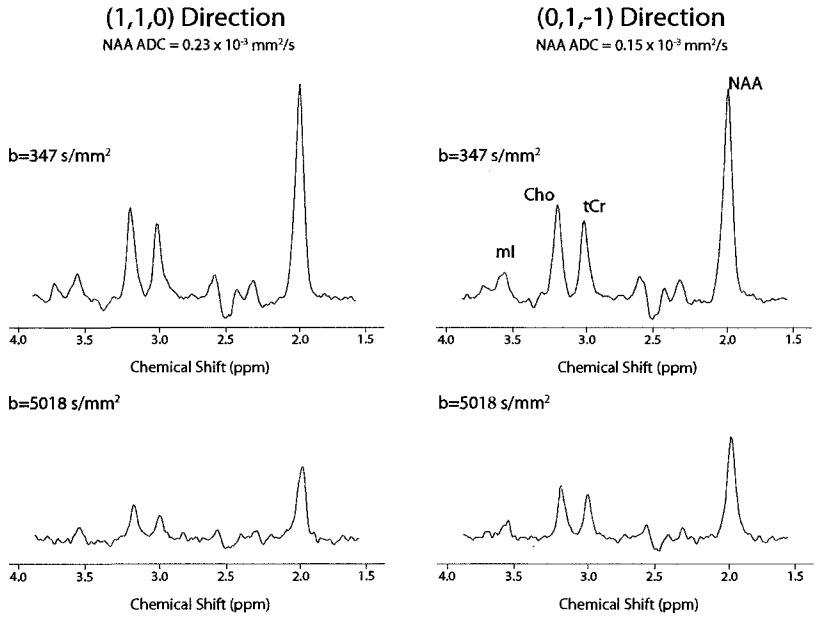

FIGURE 8.5: Example Spectra from the (1,1,0) direction and (0,1,-1) direction in the SWM region in human brain. ADC values differed with diffusion gradient direction.

ADC values from diffusion weighted spectra; one method used a zero order phase correction on the residual water peak before summation (Water phase correction method) [28], and the other used a zero order correction on the NAA peak (NAA phase correction method) [127]. It should be noted that before any phase correction was performed a 1 Hz linewidth exponential filter was applied. While it has been shown that NAA phase correction should be performed for quantification of the NAA signal intensity, and water phase correction should be performed for quantification of tCr and Cho [131], it was not practical in this study to used the NAA phase correction method. The extremely high b-value (5018 s/mm^2) cut signal intensity of NAA in half, which made phase correction on the NAA peak unreliable at extremely high b. Figure 8.6 shows the 64 single average and summed spectra for NAA at 5018 s/mm^2 with both NAA phase correction and Water phase correction. The signal intensity of the NAA is lower when the NAA phase correction method is used, which is contrary to what was shown in section 4.3.1.1. Therefore, water phase correction was performed for all spectra in order to keep consistent, in spite of the fact that NAA phase correction worked fine for b = 1815 s/mm^2.

Figure 8.7 shows the 64 single average spectra at the two maximum b-values, 1815 and 5018 s/mm^2. The water phase correction method seems to be working well in both cases, albeit better when the SNR is higher at 1815 s/mm^2. Peak height was used to measure all signal intensities in this study.

8.2.3 Alcohol Work

1-octanol was used to test the high b-value diffusion sequence because of its similar diffusion coefficient with the metabolites in the human brain. Using NAA, Cr, Cho, and mI was no longer accurate for the assessment of the high b-value study, since their rapid diffusion coefficients of 0.64, 0.82, 0.95 and 0.69 x 10^{-3} mm^2/s respectively correspond to a signal intensity at a b-value of 5018 s/mm^2 of 4.0, 1.6, 0.9, and 3.1 %, which is too small. 1-octanol, one the other hand, has a known diffusion coefficient of 0.142 x 10^{-3} mm^2/s [141], and in this study was measured using the same DTS method as in the in-vivo study above. A two-point estimation was used, with b-values of 502 and 1815 s/mm^2 for a low b-value study (δ=22 ms, Δ=80 ms) and 348 and 5018 mm^2/s for a high b-value study (δ=36 ms, Δ=87 ms), which amounted to signal intensity drops of 16% and 48%, respectively, at the greater b value relative to the smaller one. The first and second order shims were optimized and resulted in alcohol line width of $\sim$3 Hz on the largest peak in the spectra. 32 averages were acquired at each of the corresponding b-values for six diffusion directions. The measurements were repeated 5 times on different days. The Trace/3 ADC and FA were calculated from the six individual ADC values. The voxel size used in the 1-octanol

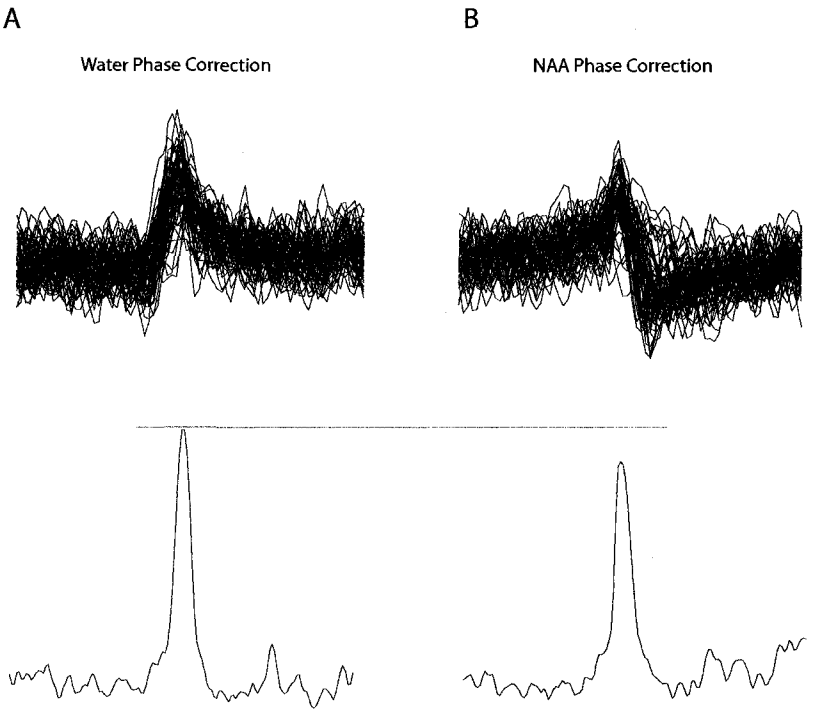

FIGURE 8.6: Sixty-four single average and summed spectra of NAA using either the water phase correction method (A) or the NAA phase correction method (B) on data from the OGM region with a b-value of 5018 s/mm^2. The signal intensity of the NAA peak is less when the NAA phase correction method is used, which is different when compared to the data in section 4.3.1.1 and therefore NAA phase correction was deemed unreliable for high b-value acquisitions.

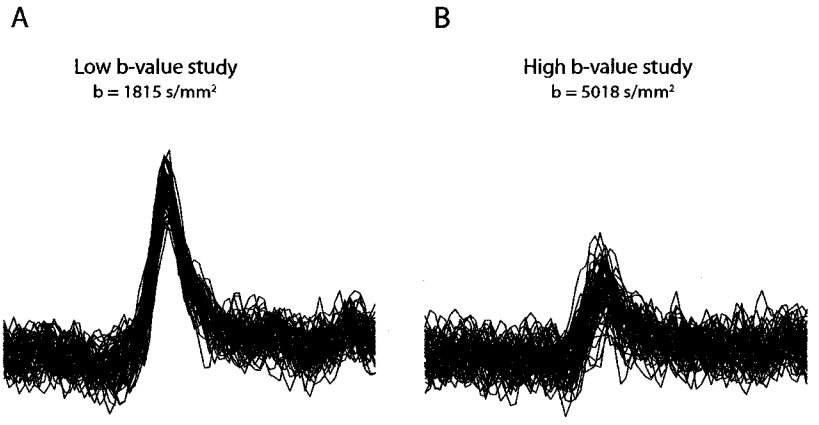

FIGURE 8.7: Sixty-four water phase corrected single average spectra of NAA for the OGM region at the two max b-values used, 1815 s/mm^2 and 5018 s/mm^2.

study was kept small (5 mm x 5 mm x 5 mm = 125 mm^3) in order to try and keep the signal to noise (SNR) reasonable in comparison to the in-vivo work; however the phantom SNR was still quite a bit larger than in-vivo (1-octanol SNR = ~375, in vivo NAA SNR in OGM = ~75 at b=502 s/mm^2). Example spectra of 1-octanol can be found in Fig. 8.8 at the 4 different b-values used in this study, A) b=347 s/mm^2, B) 508 s/mm^2, C) 5018 s/mm^2, and D) 1815 s/mm^2.

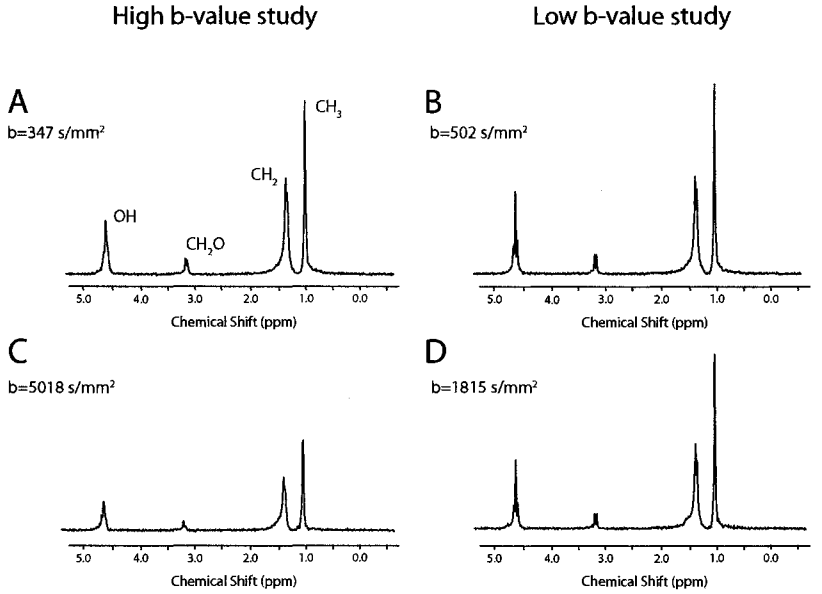

FIGURE 8.8: Example Spectra from 1-Octanol at the 4 different b-values used in this study, A) b=347 s/mm^2, B) 508 s/mm^2, C) 5018 s/mm^2, and D) 1815 s/mm^2. For 1-octanol (ADC = 0.142 x 10^{-3} mm^2/s) a signal intensity drop of 17% in the low b-value study (B,D), and a signal intensity drop of 47% in the high b-value study (A,C) was observed for the CH_3 peak in the spectra shown.

In order to determine the accuracy of FA measurements with decreasing ADC a variety of alcohols were used with a range of ADC values, 1-propanol (~0.5 x 10^{-3} mm^2/s), 1-butanol (~0.4 x 10^{-3} mm^2/s), 1-pentanol (~0.3 x 10^{-3} mm^2/s), 1-hexanol (~0.25 x 10^{-3} mm^2/s), 1-octanol (~0.14 x 10^{-3} mm^2/s), and 1-nonanol (~0.12 x 10^{-3} mm^2/s). Example spectra from the 6 different alcohols can be seen in Figure 8.9. Trace/3 ADC and FA values were calculated for both the low b-value and high b-value studies for the 6 different alcohols.

Unlike the in-vivo work phase correction was not performed for the Alcohol peaks. Aside from the fact that very little phase change was observed, magnitude spectra (as opposed to real spectra in the in-vivo case) were used for quantification. This was done in order to simplify the measurement of the peak intensity, since many of the alcohols are

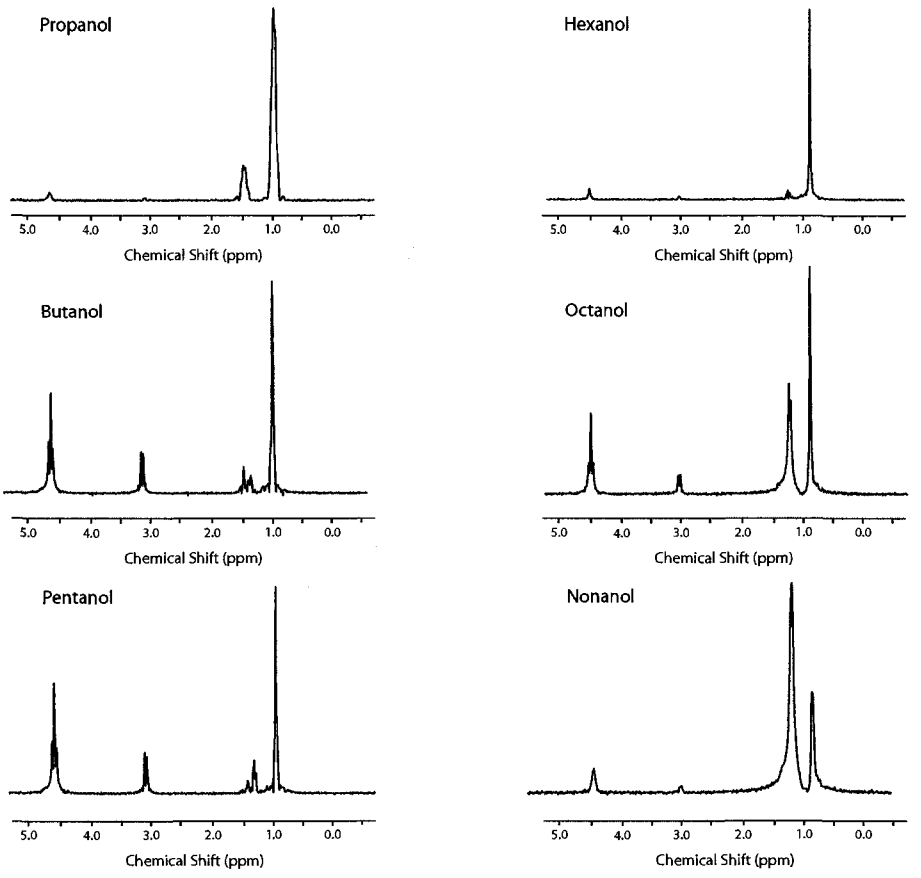

FIGURE 8.9: Example Spectra from 1-propanol, 1-butanol, 1-pentanol, 1-hexanol, 1-octanol, and 1-nonanol.

multiplets which makes peak height measurement more complex. In magnitude spectra the noise in the spectrum is all positive and therefore affects the peak height measurement considerably at lower SNR, however in the Alcohol work the SNR was quite large so this difference was considered negligible. While measuring the area of the multiplets may have been more accurate, peak height was used since the SNR was good and the signal intensities in the in-vivo work were measured using peak height.

8.3 Results

8.3.1 In-Vivo Work

Table 8.3 lists the Eigenvalues, Trace/3 ADC, and FA for the OGM region in the human brain, for both the low and high b-value studies. The FA of all 4 of the metabolites is significantly increased when the low b-value (1815 s/mm^2) is used as compared to when the high b-value (5018 s/mm^2) is used. This seems to indicate that the values reported in the low b-value work tend to be artificially inflated due to an inaccurate assessment of the single direction ADCs, which in turn leads to a greater spread in the eigenvalues (0.10 to 0.35 x 10^{-3} mm^2/s in the low b-value study compared to 0.14 to 0.23 x 10^{-3} mm^2/s in the high b-value study) thus increasing the FA. The Trace/3 ADC was significantly increased for NAA and Cho in the low b-value study, which was unexpected, as it was thought that Trace/3 ADC would be generally robust in comparison to the FA values.

	Occipital Gray Matter Region				
	ADC (x 10^{-3} mm^2/s)				Fractional
Metabolite	λ_1	λ_2	λ_3	Trace/3	Anisotropy
Low b-value study (N=5)					
NAA	0.35±0.07*	0.22±0.05	0.10±0.06	0.22±0.05*	0.53±0.14*
tCr	0.38±0.07*	0.22±0.08	0.07±0.02	0.22±0.05	0.60±0.10*
Cho	0.35±0.08*	0.22±0.05	0.09±0.07	0.22±0.05*	0.54±0.13*
mI	0.35±0.11*	0.22±0.07	0.05±0.04*	0.21±0.06	0.63±0.10*
High b-value study (N=5)					
NAA	0.23±0.03	0.18±0.03	0.14±0.03	0.18±0.02	0.25±0.10
tCr	0.24±0.03	0.19±0.02	0.13±0.03	0.19±0.02	0.30±0.07
Cho	0.21±0.03	0.17±0.02	0.12±0.03	0.17±0.03	0.28±0.06
mI	0.18±0.03	0.15±0.03	0.11±0.03	0.15±0.03	0.25±0.08

Table 8.3: Eigenvalues, Trace/3 ADC, and Fractional Anisotropy (FA) for the occipital gray matter region for both the low and high b-value studies. A much larger FA value is reported in the low b-value study when compared with the high b-value work. * indicates significance ($p<0.05$, Paired T-Test) when compared with the high b-value study.

Table 8.4 lists the Eigenvalues, Trace/3 ADC, and FA for the SWM and the OGM region

in the human brain, using the high b-value study. Trace/3 ADCs of the four metabolites do not differ between the white and gray matter regions, in agreement with the similar water Trace/3 ADCs between gray and white matter in adult human brain (Chapter 6). This table shows a significant increase in the FA of all 4 metabolites in the white matter region when compared with the gray matter region. This significant difference was not seen previously between the gray and white matter regions (Chapter 6 and [131]). It would seem to indicate that the high FA in gray matter for that previous study may in fact have been inflated, again due to the incorrect or more variable measurement of the single direction ADCs by not having a high enough b-value. It should also be noted that the mI FA value was also increased in the white matter, which was unexpected since mI was thought to be mainly located in isotropic structures. The mI data presented in the SWM could be erroneous due to the lower SNR for mI (6.7±1.0) when compared to NAA (43.0±6.3), tCr (17.5±2.7), and Cho (18.5±4.1). Furthermore, we are going to repeat the acquisition in the SWM region for the low b-value study in order to see if significant differences are seen in that case relative to the high b value study shown in Table 8.4.

	ADC (x 10^{-3} mm^2/s)				Fractional
Metabolite	λ_1	λ_2	λ_3	Trace/3	Anisotropy
Subcortical White Matter Region (N=5)					
NAA	0.33±0.08*	0.19±0.03	0.12±0.02	0.21±0.02	0.47±0.13*
tCr	0.32±0.07*	0.19±0.02	0.09±0.02	0.20±0.02	0.51±0.13*
Cho	0.26±0.06	0.15±0.05	0.08±0.01	0.16±0.02	0.51±0.14*
mI	0.25±0.06	0.14±0.02	0.06±0.02*	0.15±0.02	0.54±0.12*
Occipital Gray Matter Region (N=5)					
NAA	0.23±0.03	0.18±0.03	0.14±0.03	0.18±0.02	0.25±0.10
tCr	0.24±0.03	0.19±0.02	0.13±0.03	0.19±0.02	0.30±0.07
Cho	0.21±0.03	0.17±0.02	0.12±0.03	0.17±0.03	0.28±0.06
mI	0.18±0.03	0.15±0.03	0.11±0.03	0.15±0.03	0.25±0.08

TABLE 8.4: Eigenvalues, Trace/3 ADC, and Fractional Anisotropy (FA) for the SWM and OGM regions in human brain acquired using the high maximum b value of 5018 s/mm^2. A much larger FA value is reported in the white matter region for all four metabolites. * indicates significance ($p<0.05$, T-Test) when compared with the occipital gray matter region.

8.3.2 ALCOHOL WORK

Table 8.5 lists the Trace/3 ADC and FA of 1-octanol, for all 4 peaks in the spectrum, for both the low b-value and high b-value studies. Significant increases are seen in the FA for all 4 of the octanol peaks in the low b-value study, which seem to indicate that the higher b-value study is more accurately measuring the ADC of isotropic octanol. Ideally the reported FA for octanol would be zero, and while an FA of ~0.3 is still high

in comparison to the phantom data in Table 8.2, it is certainly more accurate than that reported in Table 8.5 for the low b-value study. Some of the reason behind this higher FA for octanol may be explained by Table 8.1, as the variability is increased at lower ADC values the FA increases. Also of note is the significantly higher Trace/3 ADC for Peak 1 in the octanol spectrum in the low b-value study, similar to what is seen in-vivo with NAA and Cho.

1-Octanol (N=5)	SNR	Low b-value study Trace/3 ADC (x 10^{-3} mm^2/s)	Low b-value study Fractional Anisotropy	High b-value study Trace/3 ADC (x 10^{-3} mm^2/s)	High b-value study Fractional Anisotropy
CH_3 Peak	~375	0.20±0.03*	0.56±0.06*	0.16±0.01	0.31±0.10
CH_2 Peak	~190	0.14±0.01	0.56±0.06*	0.14±0.00	0.33±0.02
CH_2O Peak	~30	0.19±0.03	0.60±0.17*	0.17±0.02	0.40±0.09
OH Peak	~140	0.19±0.03	0.57±0.08*	0.17±0.01	0.46±0.02

TABLE 8.5: Trace/3 ADC and Fractional Anisotropy (FA) values for a 500 mL 1-octanol phantom for both the low and high b-value studies. A much larger FA value is reported in the low b-value study when compared with the high b-value work. It should be noted that the FA values for 1-octanol are still in comparison to typical phantom FA values (less than 0.2) in phantoms with more rapidly diffusing molecules. * indicates significance ($p<0.05$, T-Test) when compared with the high b-value study.

Table 8.6 gives the Trace/3 ADC and FA values for 1-propanol, 1-butanol, 1-pentanol, 1-hexanol, 1-octanol, and 1-nonanol.

Alcohol (N=5)	SNR b=508 s/mm^2 (Mean±SD)	Trace/3 ADC (x 10^{-3} mm^2/s) Low b-value	Trace/3 ADC (x 10^{-3} mm^2/s) High b-value	Fractional Anisotropy Low b-value	Fractional Anisotropy High b-value
Propanol	232±75	0.54±0.03	0.54±0.01	0.21±0.13	0.18±0.03
Butanol	268±61	0.41±0.04	0.40±0.01	0.32±0.07*	0.19±0.03
Pentanol	231±33	0.30±0.01	0.29±0.01	0.37±0.10*	0.15±0.07
Hexanol	214±51	0.27±0.03*	0.23±0.01	0.48±0.15*	0.20±0.06
Octanol	375±34	0.20±0.03*	0.16±0.01	0.56±0.06*	0.31±0.10
Nonanol	230±61	0.16±0.03	0.13±0.02	0.63±0.16	0.46±0.13

TABLE 8.6: Trace/3 ADC and Fractional Anisotropy (FA) values (Mean ± Standard Deviation) for a different alcohol phantoms for both the low and high b-value studies. * indicates significance ($p<0.05$, T-Test) when compared with the high b-value study.

Peaks for the alcohol phantoms were chosen on the basis of similar intensity. SNR values of the peaks used for the alcohols at b = 508 s/mm^2 are listed in Table 8.6. Two trends can be seen in Table 8.6: (i) as the Trace/3 ADC decreases, the FA increases up to a point in which an isotropic medium registers as anisotropic, and (ii) the low b-value study shows an increase in its FA at higher diffusion coefficients than the high b-value study. In fact significant differences of FA between the low and high b-value studies are seen at ADCs as high as ~0.40 x 10^{-3} mm^2/s (Butanol, Figure 8.10). Recall that all these

phantoms are pure liquids and should yield isotropic diffusion (i.e. low FA values near zero).

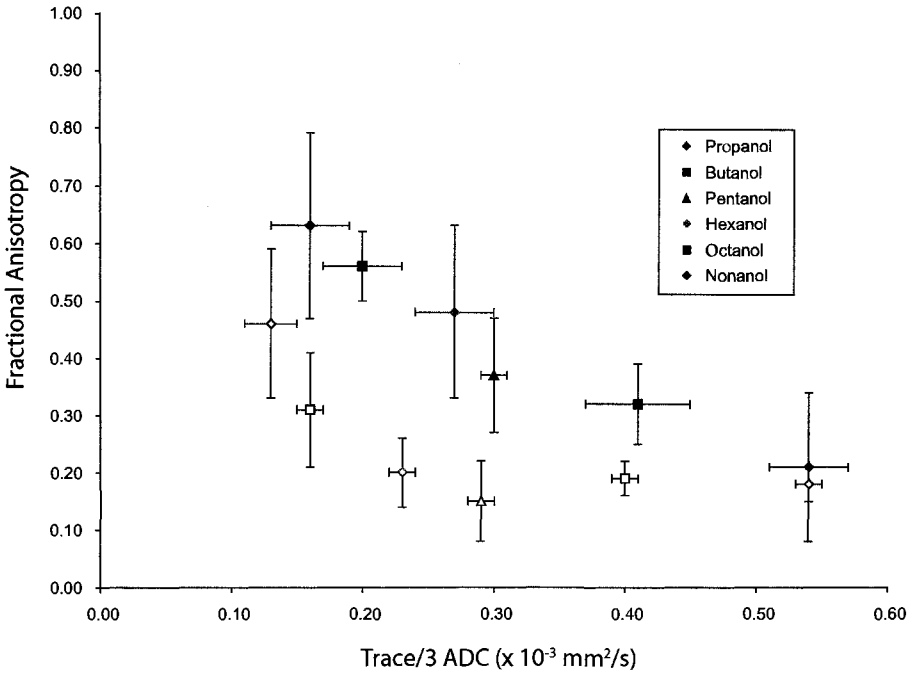

FIGURE 8.10: Fractional Anisotropy versus Trace/3 ADC obtained from the low (filled symbols) and high b value (open symbols) studies in 6 different alcohols that should exhibit isotropic diffusion.

8.4 DISCUSSION

8.4.1 IN-VIVO WORK

The diffusion data from mI is quite interesting. As was mentioned previously the Trace/3 ADC of mI was significantly smaller in SWM and OGM region when compared to NAA. It was hypothesized that this may be due to the restriction of the mI in a small isotropic compartment (i.e. astrocytes) when compared to NAA. However, judging by the FA data in the SWM of mI it is questionable whether mI is actually in an isotropic compartment in the white matter. The high FA of 0.54±0.12 for mI is even larger than the FA of NAA (0.47±0.13) in the SWM, although not significant. Recalling the alcohol data, the question is, however, whether or not this FA value for mI is artificially inflated due to it's low SNR (at b=347 s/mm^2 SNR of mI in SWM is 6.7±1.0 and OGM is 11.5±1.9) and small ADC ($\sim$0.15 x 10^{-3} mm^2/s). If we compared the FA values for Peak 1 (0.31±0.10) and Peak 3 (0.40±0.09) of 1-octanol there is an increase in the FA just based solely on the SNR of

the peak (Peak 1 SNR $\sim$ 375, Peak 3 SNR $\sim$ 30), which could account for some of the difference in FA, since the SNR of mI is much lower than that of NAA (Figure 8.4). In order to answer the question of whether or not mI is isotropic in comparison to NAA, it must be measured in a more controlled environment with a higher SNR, such as a central nerve, since no mI is found in frog peripheral nerve (Chapter 7 and [142]). The FA data from mI, as currently reported here, is entirely suspect due to the low SNR and low ADC, which may account for the high FA; however mI may in fact be localized in a different compartment than NAA as suspected since the Trace/3 ADC is significantly smaller than NAA as well as the reported λ_1 eigenvalue. If we were to measure ADC values from an even higher b-value perhaps we would start to see a difference in the mI FA when compared to NAA FA in the SWM region, however we would need to increase the SNR of mI in the region, so perhaps a new region that may have a higher mI content should be investigated.

Increasing the signal intensity drop in order to improve the accuracy of the single direction ADC calculations was expected to only increase the accuracy of the FA measurement in vivo. However, it also seems to have an effect on the Trace/3 ADC. In 2 of the 4 metabolites, NAA and Cho, significant increases were seen when the max b was 1815 s/mm^2, which would seem to indicate that those values were artificially inflated, and therefore perhaps the Trace/3 ADC values reported in the high b-value study are more accurate. Previous DTS Trace/3 ADC results from NAA, tCr, and Cho in the OGM region of human brain were determined to be 0.14$\pm$0.03, 0.17$\pm$0.03, and 0.15$\pm$0.03 x 10^{-3} mm^2/s respectively [131]. Aside from NAA, these are consistent with our values reported here in the high b-value study of 0.18$\pm$0.02, 0.19$\pm$0.02, and 0.17$\pm$0.03 x 10^{-3} mm^2/s for NAA, tCr, and Cho respectively, but lower than those reported in the low b-value study of 0.22$\pm$0.05, 0.22$\pm$0.05, and 0.22$\pm$0.05 x 10^{-3} mm^2/s for NAA, tCr, and Cho respectively. Since, the previous DTS study on human brain also used a low b-value of 1890 s/mm^2 for the maximum b-value [131], it was unexpected to get larger Trace/3 ADCs in our low b-value study. A possible explanation for the larger ADCs reported here in our low b-value study is the voxel size was larger 19.7 cm^3 vs. 10.6 cm^3, as well as the different sequence (PRESS instead of STEAM) used with a shorter diffusion time 80 ms vs. 208.3 ms. The NAA Trace/3 ADC reported here is larger than reported in the previous DTS study, perhaps this is due to the different phase correction methods used between the two studies, in the current study water phase correction has been used for quantification of NAA, and in the previous DTS study the single average phase correction was performed on NAA, this alone could inflate the ADC of NAA (Section 4.3.1.1). Regardless, the Trace/3 ADC values reported here from the high b-value study are for the most part consistent with

previously reported literature values.

Between the SWM and OGM regions the Trace/3 ADC values were not significantly different, which is consistent with a previous study which measured the Trace/3 ADC of the metabolites NAA, tCr, and Cho in the same two regions [127]: 0.16, 0.17, and 0.21 x 10^{-3} mm^2/s in the SWM region, and 0.13, 0.17, 0.14 x 10^{-3} mm^2/s in the OGM region. In the SWM region in this current study, the Trace/3 ADC of Cho and mI were significantly smaller than NAA and tCr. While the mI ADC has never been calculated in vivo prior to this work, the Cho ADC has been reported in previous papers as having a smaller ADC [28]. This may in part be because of the close association of Cho to the membranes, and the fact that it's highly restricted in the brain or nervous tissue [142]. In the OGM region a similar trend was seen, however in this case only mI was found to have a smaller Trace/3 ADC when compared to NAA and tCr. mI is thought to be located primarily in the glial cells which are thought to be an isotropic structure, perhaps this smaller Trace/3 ADC of mI is also due to a larger restriction, albeit an isotropic one, in the brain, where as metabolites such as NAA get to travel along the white matter tracts, mI may be restricted within the glial cell. The λ_1 eigenvalue seems to indicate that this may in fact be true, since the λ_1 of mI is significantly smaller than the λ_1 for NAA in both regions (p=0.02 in SWM and p=0.03 in OGM).

The really interesting part of this study is found in Table 8.3, where the FA of the metabolites show significant differences between the two methods (i.e. high and low b-value study) in the same region of the brain measured from the same five volunteers. That table clearly indicates the need for a $\sim$50% drop in signal intensity in order for accurate quantification of the single direction ADC values in gray matter, and helps answer some of the troubling questions posed by our previous DTS study (Chapter 6 and [131]). Namely, the high FA values reported in the occipital and frontal gray matter regions (0.51, 0.69, 0.79 for NAA, tCr, and Cho in the OGM region respectively, and 0.53, 0.73, 0.59 for NAA, tCr, and Cho in the frontal gray matter region respectively), which are likely incorrect and too high (i.e. metabolite diffusion is not anisotropic in the cortical gray matter when high b values were used in the DTS acquisition in this chapter as expected). Our reported FA values for the low b-value PRESS DTS study, in the same OGM region (albeit with a larger voxel) are consistent, 0.53, 0.60, 0.54 for NAA, tCr, and Cho, respectively, with our earlier publication using STEAM DTS. It is clear therefore, when we look at the FA values using a high max b-value (0.25, 0.30, and 0.28 for NAA, tCr, and Cho, respectively), that these values reported currently (low b-value study) and the previously reported data [131] in gray matter are artificially inflated. The inflation seems to come about from the significant increase in the λ_1 value in the low b-value study for all 4 metabolites, Table 8.3.

The FA values measured in the SWM region for all 4 metabolites are significantly higher then those reported in the OGM region, which is to be expected. Also, the directional preference for the SWM region should be a combination of left-right (coming off of the corpus callosum) and anterior-posterior (from the corpus callosum to the occipital cortex), as can be seen from Figure 8.11. Figure 8.11 shows a water DTI colormap of human brain, where the colors signify the directional preference of the water molecule, red = left-right, green = anterior-posterior, blue = superior-inferior. Our metabolite voxel, therefore should have combinations of red and green, which is what was found (Figure 8.11). Each of the five volunteers had large contributions of the colors red and green, which is consistent with the fiber tracts in that area of the brain, although the DTI color map shows a primarily green color, the fiber tract is crossing the voxel diagonally and therefore there would have a reasonable contribution from the red direction as well.

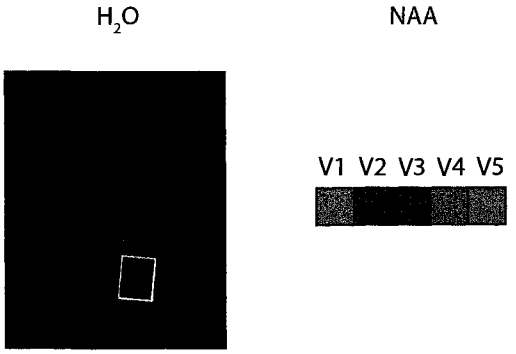

FIGURE 8.11: A DTI colormap indicating the directional preference of the water molecule. The voxel used for the SWM region is also displayed on the colormap. The voxel color corresponding to the directional preference of NAA in the five volunteers (V1-5) is shown.

Although it was not significant the FA of tCr and Cho did have higher mean values when compared to the FA of NAA, which is consistent with our previous DTS results (with low maximum b value) in both the human brain [131], and nervous tissue [142].

8.4.2 ALCOHOL WORK

The diffusion measurements on the various alcohols, certainly highlights the need for accurate experimentation before blindly applying DTS to human brain and possibly making poor assumptions. Figure 8.10 highlights a marked difference between measuring the diffusion of small ADCs with low b-values and high b-values. Even at an ADC of $\sim$0.4 x 10^{-3} mm^2/s in an isotropic phantom we see significant differences between the two methods, with the low b-value study FA of 0.32$\pm$0.07 and the high b-value study FA of 0.19$\pm$0.03. The high b-value study hovers around FA values of 0.15 to 0.20 up until the

Trace/3 ADC value decreases below ~0.23 x 10^{-3} mm^2/s, where as when a low maximum b-value is used the FA never falls bellow 0.20 for the alcohols measured here. It should be noted that the FA values for NAA (Trace/3 ADC = 0.64 x 10^{-3} mm^2/s), Cr (Trace/3 ADC = 0.82 x 10^{-3} mm^2/s), Cho (Trace/3 ADC = 0.95 x 10^{-3} mm^2/s), and mI (Trace/3 ADC = 0.69 x 10^{-3} mm^2/s) in aqueous isotropic phantom for the low b-value (1238 s/mm^2) used in the calibration were never above 0.20 (Table 8.2). Futhermore the FA values for 1-octanol and 1-nonanol were also higher than the other alcohols in the high b-value study (0.31 and 0.46 respectively), which seems to indicate that the DTS method, even when using a high b-value, may still be too variable at the lower ADC metabolites, and therefore the lower ADC values, due to the variability of the method, may in fact require an even higher b-value for accurate measurement of their diffusion parameters. The Trace/3 ADC also looks to be affected by the maximum b-value used. In the low b-value study the Trace/3 ADC of 1-hexanol and 1-octanol were significantly overestimated, and the other alcohols followed the trend of a higher Trace/3 ADC in the low b-value study, although not significant (Figure 8.10).

What does this mean for DTS in human brain? Is it still feasible? In the opinion of this author yes, but certain methods need to be taken into account when measuring ADC values in vivo. At least a ~50% signal drop is required for accurate DW-MRS measurements. If a lower b-value is used the FA may be artificially increased. However, in white matter, where the difference in the ADC between directions may outweigh the variability in the method, these measurements may in fact be accurate. However, this still needs to be examined in-vivo. The same regions used in the previous DTS study should be examined (Chapter 6 and [131]), when mI is not the focus of the study and adequate SNR can be achieved in those regions. Keep in mind that even when using a high b-value such as 5000 s/mm^2, you still may be overestimating the FA of metabolites with small diffusion coefficients and may be required to go to an even higher b-value. Careful calibration must also be performed, the best FA (i.e. lowest) in isotropic solutions of the metabolites must be achieved prior to examination of them in-vivo, because if you start poorly it's only going to get worse in-vivo. In this study the FA of 1-octanol (similar ADC to metabolites in human brain) had an FA of approximately 0.31, and a solution of 1-octanol is clearly isotropic; in the OGM region we found similar FA values for the 4 metabolites (0.25, 0.30, 0.28, and 0.25 for NAA, tCr, Cho, and mI respectively). Even though these FA values in the OGM region may seem high in comparison to the Water FA in gray matter of the human brain (~0.2), they are just as isotropic as a 500 mL solution of 1-octanol. Also the Trace/3 ADC, despite the significant differences between the two methods, is still quite robust and seems to be consistent between methods. Therefore, Trace/3 ADC is certainly a valuable

measure in human brain. More confidence in the DTS measurement can always be had by going to a higher field such as 4.7 T where better resolution and signal can be had, plus stronger gradients if available can be used in order to shorten the TE considerably, but TE, for at least the measurement of mI, may be dependent on the timings required for the optimization of the signal at 4.7 T.

8.5 Addendum

Future experiments are in progress to perform DTS in the human brain in 4 of the regions used in the previous DTS study (Chapter 6) using the exact STEAM sequence from that study but with a higher b value of 5000 s/mm^2. The body of the corpus callosum, the cortical spinal tract, the frontal gray matter, and the occipital gray matter will be examined, all in a effort to confirm or disprove the FA values reported in Chapter 6. A slightly longer TE may be used in these experiments in order to incorporate the larger diffusion gradients required, which may require slightly larger voxels to achieve adequate SNR, however this difference will be negligible in the comparison. Furthermore, as mentioned above the SWM region will be re-examined with the low b-value mI-optimized PRESS study in an effort to disprove or prove the accuracy of the DTS measurement of white matter at a lower maximum b-value. Perhaps we could examine a few more regions using the PRESS DTS mI sequence in an effort to get a higher concentration of mI to determine if it is anisotropic or isotropic in the white matter dominant regions in human brain.

Chapter 9

Single Shot Diffusion Trace Spectroscopy

9.1 Introduction

Diffusion Weighted Magnetic Resonance Spectroscopy (DW-MRS) has proven to be useful in the examination of the intracellular environment under normal and pathological conditions (see introductions of Chapters 5, 6, 8, and [28, 29]. The main problem with clinical experimentation is the long scan time required for making the diffusion measurements, with Trace/3 ADC (a measure of the mean diffusivity) and Diffusion Tensor Spectroscopy (DTS) measurements being shown previously, to take ~75 minutes (Chapters 5 and 6). One way to combat this long scan time is to only examine the diffusion in one direction [29]; however, since the diffusion is known to be variable depending on the direction measured, for both water [22] and the metabolites (Chapter 6), measuring Apparent Diffusion Coefficients (ADCs) in only one direction is not ideal. In order to have a rotationally invariant measure of the diffusion of metabolites in a specific region, one must calculate the Trace/3 ADC, which is the average of the Trace of the Diffusion Tensor (Equation 3.4). The Trace/3 ADC of metabolites has been calculated previously in this thesis (Chapter 5). However, with that measurement, sixty-four averages were measured, with four b-values in each of three directions, which led to a total scan time of approximately 75 minutes. Seventy five minutes is too long, but this total scan time can be shortened; two b-values can be used per direction as well as less averages. These improvements may reduce the total scan time down to <45 minutes, where it may become reasonable to examine certain pathologies. However, in some neurological disorders it may be beneficial to scan more that one region in one session, which would not be possible with the current protocol.

In 1995, it was shown that the water Trace/3 ADC could be measured in a single shot in chicken gizzards [143]. A family of diffusion imaging pulse sequences were designed

to measure the Trace/3 ADC without needing to acquire X, Y, and Z measurements separately in that paper and they will be discussed in this section. Therefore, instead of requiring four measurements (non diffusion spectrum and 3 diffusion spectra at high b), only two measurements would be needed (non diffusion spectrum and one high b value spectrum), effectively reducing the scan time in half. This could make the diffusion measurements feasible in a clinical population and still yield the desired rotationally invariant Trace/3 ADC. Figure 9.1 shows the gradient schemes examined in that study.

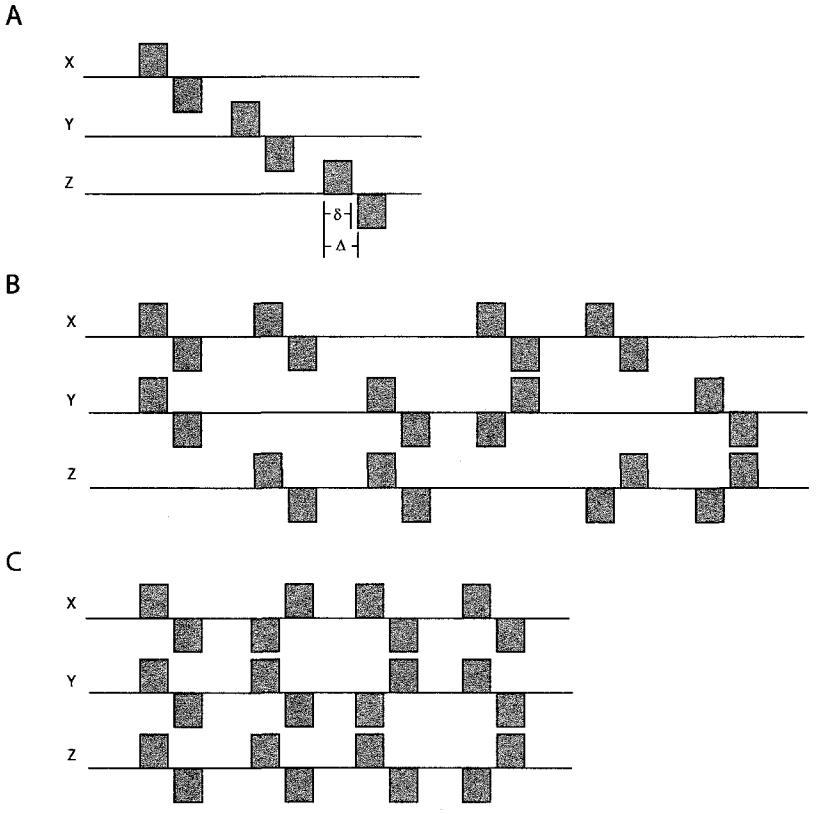

FIGURE 9.1: Different bipolar gradient schemes that can used for calculation of the Trace/3 ADC in a Single-Shot as opposed to 3 different orthogonal diffusion measurements.

Figure 9.1A unfortunately is not very efficient with respect to the gradient power. In principle this situation can be improved by applying the gradients simultaneously, however this involves the off-diagonal elements in the diffusion tensor which we are trying to avoid. Figure 9.1B and C do not suffer from this problem. In the bipolar gradient combinations in those figures the diagonal and off-diagonal elements of the diffusion tensor are involved; however, because of the ordering and phase of certain bipolar gradients (+/- or -/+), the off diagonal elements cancel by the end of the sequence. When square bipolar gradients are applied simultaneously and of equal polarity (i.e. both +/-) in the X and Y

axis, the diffusion sensitization is therefore proportional to:

$$D_{xx}G_x^2 + D_{yy}G_y^2 + \left(D_{xy} + D_{yx}\right) G_xG_y \tag{9.1}$$

If however the same two bipolar gradients are applied with the opposite polarity (i.e. one +/- and the other -/+) then the diffusion sensitization will be proportional to:

$$D_{xx}G_x^2 + D_{yy}G_y^2 - \left(D_{xy} + D_{yx}\right) G_xG_y \tag{9.2}$$

Therefore, consecutive applications of these two bipolar gradient sets will cancel the off-diagonal elements of the diffusion tensor and the diagonal terms will add. Similar results can be determined with three simultaneous bipolar gradient pairs.

Another sequence mentioned in that study incorporated longer diffusion times, as opposed to the short diffusion times (i.e. small Δ) of bipolar gradient pulses. A longer Δ is beneficial as a higher b-value can be obtained, since b-value is directly proportional to Δ. Figure 9.2 displays that gradient scheme incorporated into a spin echo pulse sequence.

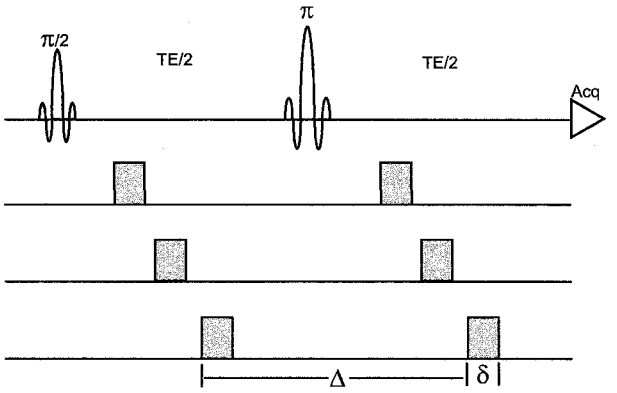

FIGURE 9.2: A spin echo pulse sequence with diffusion gradients used as an attempt to measure the Trace/3 ADC in a single shot with longer diffusion times than presented for the gradient schemes in Figure 9.1

The gradient scheme presented in Figure 9.2, even though the gradients are not applied simultaneously, does not measure the diagonal elements of the diffusion tensor alone, and has some contributions from the off-diagonal elements as well. If we examine the X and Y gradient pairs in Figure 9.2, then from the time when the first Y gradient is on until the time when the second X gradient is off, the diffusion sensitization will again be proportional to Equation 9.1, which is not ideal. Nonetheless it may be a reasonable approximation.

Measuring the diffusion in a single shot has been applied to MR imaging of water on a clinical human scanner [144], which incorporated the gradient scheme in Figure 9.1C,

modified for use in a spin echo imaging sequence. In 2001, this method was first applied to spectroscopy, where the Trace/3 ADC was measured for three metabolites, N-acetyl aspartate (NAA), creatine and phosphocreatine (tCr), and choline (Cho) in rat muscle and brain [118]. The sequence used in that study can be seen in Figure 9.3.

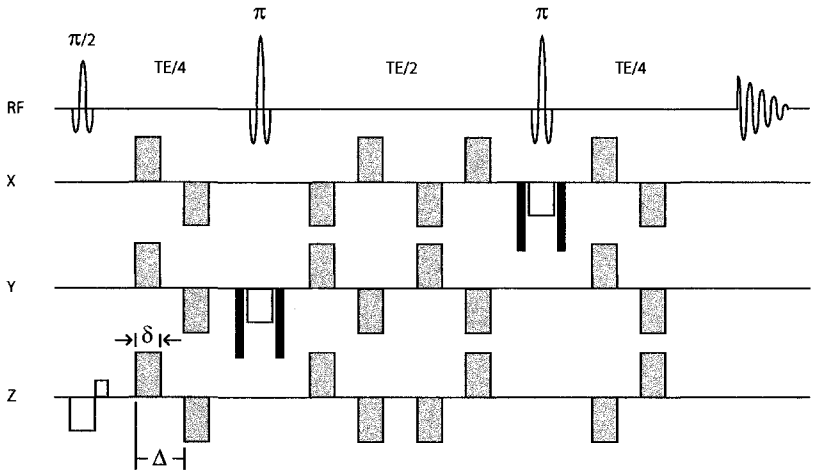

FIGURE 9.3: A single shot diffusion trace spectroscopy sequence used to determine the Trace/3 ADC in a single measurement. Note that the water suppression pulses are not shown.

It is the sequence in Figure 9.3 that the first half of this chapter will focus on, and this sequence has been termed the SS-PRESS sequence (i.e. SS for single shot). The original goal of this study was to test and validate the SS-PRESS sequence for use in the human brain of healthy volunteers, with the ultimate goal of applying this sequence to different neurological disorders.

9.2 SS-PRESS SEQUENCE

9.2.1 PHANTOM WORK

All scans were performed on an SMIS 3T MRI equipped with a maximum gradient strength of 20 mT/m. Initially, gradient-echo images along transverse, sagittal, and coronal plane were acquired (TE = 22 ms, TR = 500 ms, Slice Thickness = 5 mm, 11 slices per direction).

Two separate sequences were used to calculate metabolite ADCs. One Sequence consisted of a regular diffusion-weighted PRESS sequence (DW-PRESS Sequence, Fig. 9.4), with the diffusion gradients orientated in the X, Y, or Z direction; the other sequence consisted of a complex gradient pattern aimed at calculating the trace of the diffusion tensor

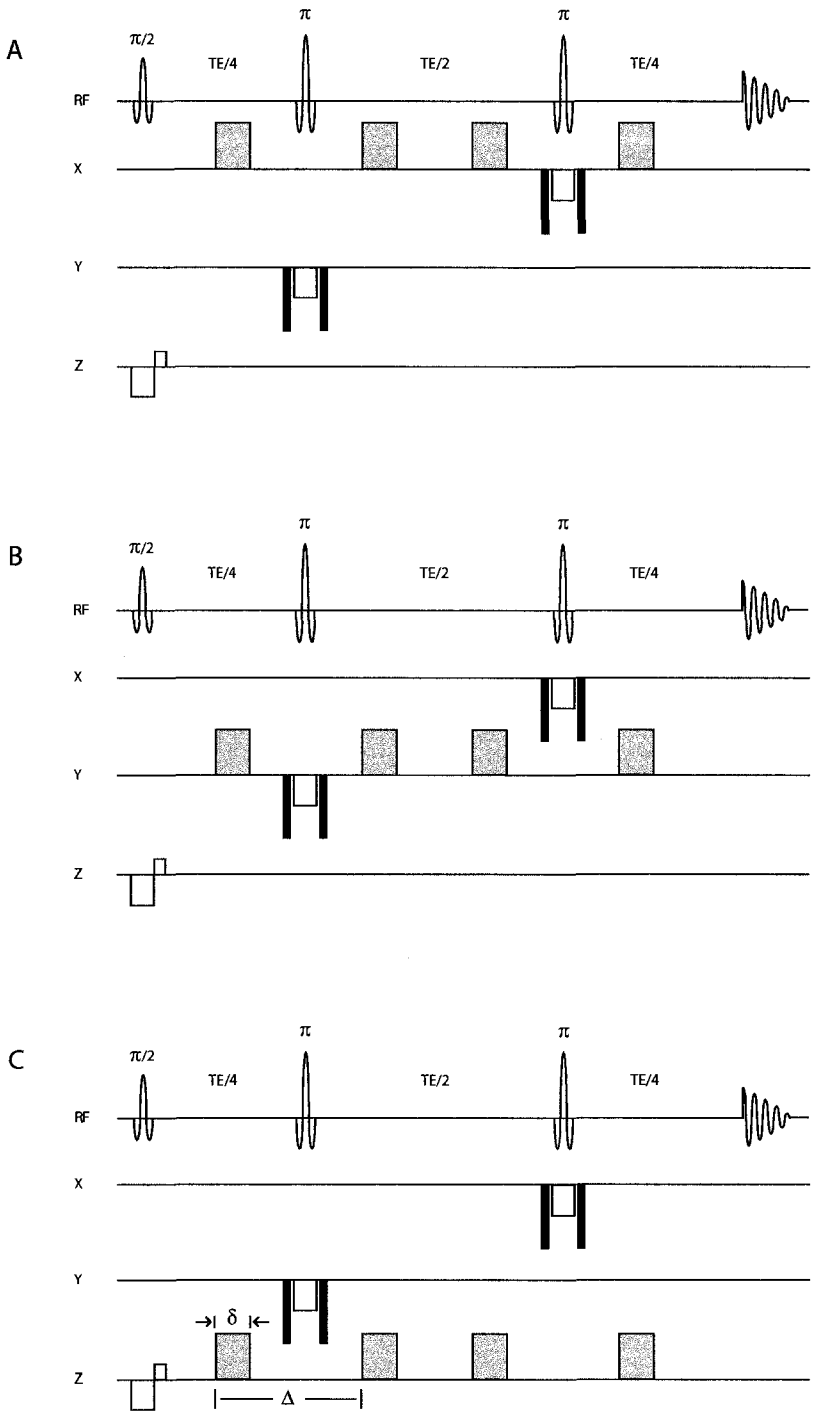

FIGURE 9.4: DW-PRESS sequences used for the measure of diffusion in the A) X, B) Y, and C) Z Direction. These three diffusion measurements are the standard way of calculating the Trace/3 ADC.

in a single-shot (SS-PRESS, Fig. 9.3). The parameters used in the DW-PRESS sequence were: δ = 20 ms, Δ = 65.7 ms, TE = 238 ms, TR = 3 s. The parameters used in the Single-Shot Diffusion Trace Sequence were: δ = 20 ms, Δ = 25 ms, TE = 260 ms, TR = 3 s. In both sequences water suppression was achieved using a dual inversion recovery with two hyperbolic secant pulses of 80 ms in duration (inversion times of 1400 ms and 200 ms), followed by water crusher gradients along the X and Y directions of 20 ms duration. The SS-PRESS sequence has a relatively short Δ when compared to the other sequences used in the previous chapters, which tends to decrease the b-value; however, the b-value in the SS-PRESS sequence is not just calculated from one bipolar gradient pair. It is a combination of 12 sets of bipolar gradients, which allows this short Δ while not sacrificing the b-value.

9.2.1.1 Isotropic Phantom

An isotropic 125 mL spherical water phantom containing NAA (30 mM), Cr (30 mM), and Cho (10 mM) (Sigma-Aldrich Canada Ltd., Oakville, Ontario) was used to confirm the accuracy of the pulse sequences. The DW-PRESS sequence was calibrated on the known ADC value for Cr at 20°C (0.80 x 10^{-3} mm^2/s [119]) and was used to measure the ADC values of NAA, tCr, and Cho in three orthogonal directions (X, Y, and Z). Those calibration values were then used for the SS-PRESS sequence as well. Eight b-values were used per direction ranging from 84 to 1351 s/mm^2. ADCs for the three directions were then calculated by measuring the slope of the ln(signal intensity) versus b-value. The Trace/3 ADC was then calculated by averaging the ADC values from each of the three directions. The Single-Shot Diffusion Trace Sequence was also used in the same isotropic environment. Again, eight b-values were used for this measurement, and they ranged from 123 to 1969 s/mm^2, and then the Trace/3 ADC was calculated for the Single-Shot method.

9.2.1.2 Anisotropic Phantom

Two anisotropic phantoms were created using the vascular bundles from celery stalks, which has been done previously and water diffusion has shown to be anisotropic [145–147]. Creating the phantoms involved shaving away some of the outer layers of celery in order to pull the vascular bundles out from within the celery stalks. Normally, the bundles would then be cut into pieces ~5 cm long and after being aligned with each other were placed within a beaker packed reasonably tight. The bundles were kept wet in order to get a strong water signal. A 1.5 cm x 2.5 cm x 2.5 cm = 9.4 cm^3 voxel was placed in the center of the bundles. Six measurements were performed on each of the two phantoms

Metabolite	Directional ADC (x 10^{-3} mm^2/s) X	Y	Z	Average of Directional ADCs (x 10^{-3} mm^2/s)	Single Shot Trace ADC (x 10^{-3} mm^2/s)
Isotropic Phantom (N=6)					
NAA	0.65±0.02	0.67±0.02	0.65±0.03	0.65±0.01	0.64±0.02
Cr	0.83±0.04	0.83±0.05	0.79±0.04	0.83±0.03	0.84±0.02
Cho	0.96±0.04	0.97±0.06	0.94±0.04	0.96±0.03	0.98±0.03
Anisotropic Phantom 1 (Water Only)					
6 - Trials					
Mean±SD	1.20±0.09	1.23±0.08	2.25±0.05	1.56±0.07	1.56±0.08
Anisotropic Phantom 2 (Water Only)					
6 - Trials					
Mean±SD	1.16±0.12	1.11±0.08	2.01±0.06	1.43±0.08	1.54±0.05

TABLE 9.1: Diffusion measurements of NAA, Cr, and Cho combined in a 125 mL aqueous solution (N = 6), and measurement of water in an anisotropic phantom made using celery vascular bundles aligned along the z-axis of the magnet.

and a different voxel was picked for each measurement in order to get some variability. Metabolites were not included in this study given the relatively poor shim and low signal from the water ADC (metabolites would have been worse). It was felt that in order to test whether or not the SS-PRESS sequence was measuring correct Trace/3 ADC values, water was certainly adequate. Again, the DW-PRESS sequence was used to measure the ADC values of water in three orthogonal directions (X, Y, and Z). Eight b-values were used per direction ranging from 84 to 1351 s/mm^2. ADCs for the three directions were then calculated by measuring the slope of the ln(signal intensity) versus b-value. The Trace/3 ADC was then calculated by averaging the ADC values from each of the three directions. The Single-Shot Diffusion Trace Sequence was also used in the same voxel. Again, eight b-values were used for this measurement, and they ranged from 123 to 1969 s/mm^2, and then the Trace/3 ADC was calculated for the Single-Shot method.

For the anisotropic phantoms the vascular budles of the celery were aligned parallel to the z-axis of the magnet; therefore a higher ADC should be seen in the Z-direction, and from Table 9.1 we can clearly see that the sequence is working as intended. The Trace/3 ADC determined by SS-PRESS and DW-PRESS (X,Y,Z) were within error of each other and thus the SS-PRESS sequence appears to be working correctly in the phantom.

9.2.2 In Vivo Work

In the previous DW-MRS studies (Chapters 5 and 6) the transition from phantom work to in-vivo was relatively seamless. The only problems that ever came about were often signal to noise issues, or with the original DW-MRS work the single average phase correction.

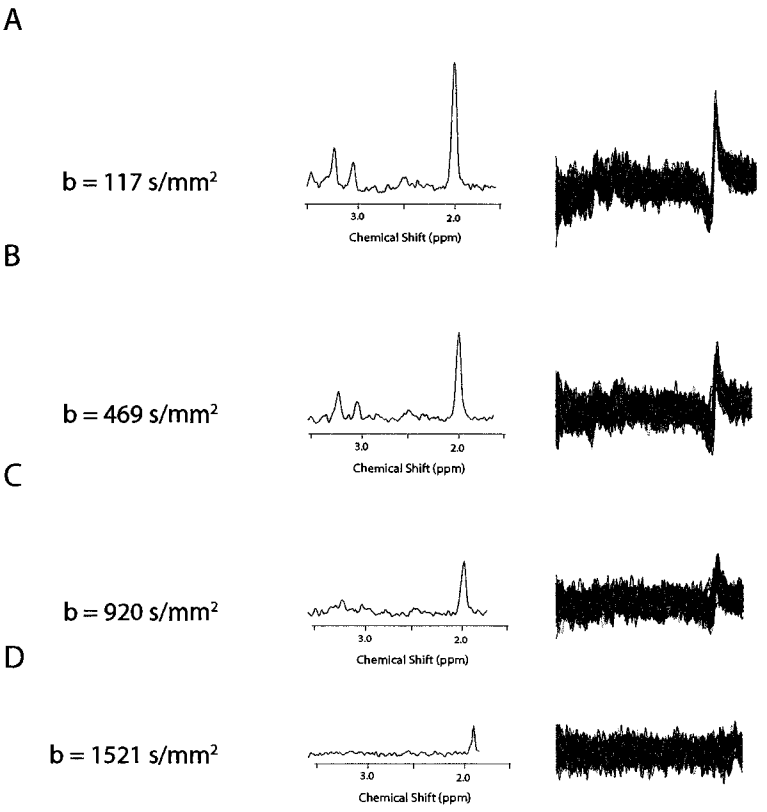

FIGURE 9.5: Example Spectra taken from the human brain at 3 T from low to high b-value using the SS-PRESS method. The spectra on the left are the summed 64 average spectra taken from the OGM region, while the spectra on the right are an overplot of the 64 single averages to indicate that the phase correction program is working as expected. The peak signal intensities are dropping off far faster than they should be.

Figure 9.5A-D are examples of spectra taken from the occipital gray matter region in the human brain at 3T from low (A) to high (D) b-value. Now aside from the spectrum in Fig. 9.5D having an extremely low signal to noise ratio, there is a bigger problem. The signal intensities are dropping off faster than expected with b value, and hence, the ADC value calculated for NAA for the given set of spectra in Fig. 9.5 is 1.03 x 10^{-3} mm^2/s, which is ~7 times bigger than the approximate value of the ADC of NAA in-vivo (0.15 x 10^{-3} mm^2/s). In fact the number calculated is actually larger than the intrinsic diffusion coefficient of NAA in aqueous phantom, which is 0.65 x 10^{-3} mm^2/s at 20 °C. Since the

sequence works extremely well in phantom, the question then becomes what is different between a phantom and the human brain that would affect the diffusion measurement in such a drastic measure. The short answer is motion. The fact that 4 sets of bipolar gradients are on simultaneously in all 3 axes may be over sensitizing the sequence to the smallest amount of motion.

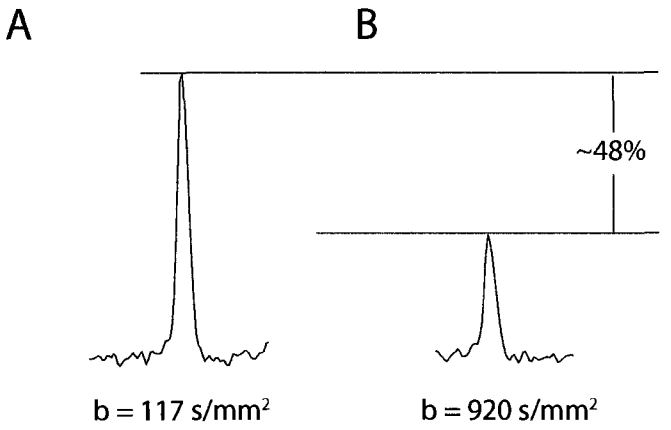

FIGURE 9.6: Summed spectra taken from the occipital gray matter in the human brain at a b-value of 117 (A) and 920 (B) s/mm^2.

Over the b-value range from 117 to 920 s/mm^2 an approximately 11% drop in signal intensity would be expected if NAA had an ADC of 0.15 x 10^{-3} mm^2/s. However, as you can clearly see from Fig. 9.6 that is not the case. Furthermore, if this is clearly a motion issue you would expect the signal intensity to be changing all over the place during each single average acquisition, and surely during one of those 64 single averages the signal must be comparable to an 11% drop as expected. Therefore, if we examine the 64 single average overplotted spectra in Figure 9.5 a little closer, we should find varying degrees of signal intensity between single averages. However, this is not the case, with each of the spectra individually being consistently smaller (Figure 9.7). Again, if this was solely a movement issue, then the individual spectra should be varying in height more than they are, and the fact that they are consistently lower than they should be in even a single average is troubling.

The phantom used in this study was a 125 mL spherical phantom and the placement of a 2.5 cm x 2.5 cm x 2.5 cm = 15.6 cm^3 voxel filled up the majority of the phantom. A 4 L milk jug phantom was made in order to approximate the typical size of the head, and the results were similar in between the two phantoms. Using the exact same sequence, on the exact same day, a small phantom was examined followed by the larger phantom followed by a human volunteer. The two phantom studies yielded similar values for Cr

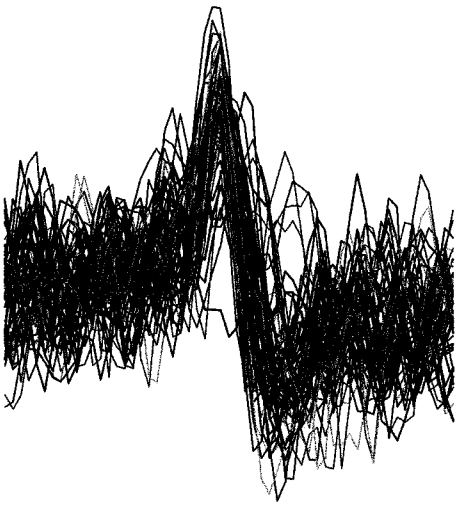

FIGURE 9.7: Overplot of 64 single average spectra of NAA, after phase correction, measured in the occipital gray matter at a b-value of 920 s/mm^2.

and Cho (NAA was not included in the large phantom because of its high cost and the large quantity required), the Cr ADC was determined to be 0.77 x 10^{-3} mm^2/s in the small phantom and 0.77 x 10^{-3} mm^2/s in the large phantom, Cho was similar with a ADCs of 0.87 x 10^{-3} mm^2/s and 0.89 x 10^{-3} mm^2/s for the small and large phantom respectively. The volunteer examined right after had an ADC value for NAA of 0.77 x 10^{-3} mm^2/s, which is again way too large, and again larger than the intrinsic ADC for NAA in aqueous phantom.

Five volunteers were examined in the occipital gray matter region in total, using the DW-PRESS and SS-PRESS sequences shown in Figures 9.4 and 9.3, respectively. The ADC values of NAA ranged from 0.23 to 1.03 x 10^{-3} mm^2/s, with an average value of (Mean $\pm$ SD) 0.55$\pm$0.33, and therefore, not only do we have consistently high values, we also have quite a large variability. Therefore, we decided to try other possible gradient schemes in order to measure the Trace/3 ADC in a single shot. Because our previous research used the STEAM sequence with great success (Chapters 5 and 6), we decided to try these new gradient schemes with the STEAM sequence as opposed to PRESS.

9.3 STEAM SEQUENCES

9.3.1 THE SEQUENCES

The impression after the first attempt was that the sequence and/or the gradient scheme used in that SS-PRESS sequence may have been causing the problems in-vivo (phantoms

studies gave correct diffusion parameters), since we had never used a sequence with that many gradient waveforms prior to the work presented here. In the original single-shot trace imaging paper they used a variety of different gradient schemes as show in Figure 9.1 [143]. We used 3 new modified STEAM sequences based on the schemes outlined in the original single-shot trace imaging paper [143]. The first sequence was the same sequence as in Fig. 9.3, modified for use with the STEAM sequence (Figure 9.8), which included reversing the polarity of the second and fourth set of bipolar gradients. This sequence was termed the single-shot STEAM sequence (SS-STEAM).

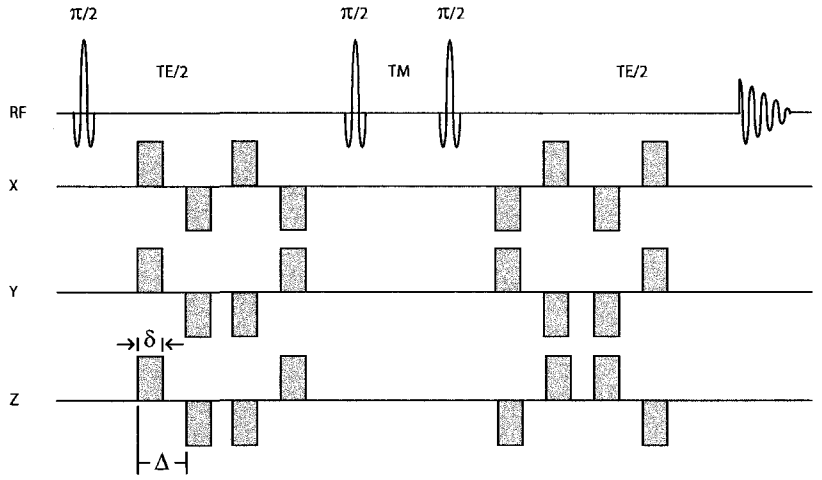

FIGURE 9.8: A single-shot diffusion trace spectroscopy sequence using the STEAM sequence, slice selection and crusher gradients not shown, termed single shot STEAM sequence (SS-STEAM). Water suppression pulses are not shown.

The second scheme using the STEAM sequence was 3 sets of bipolar gradients on at separate times one on each axis, before and after the mixing time (Figure 9.9) similar to what is shown in Figure 9.1A. This sequence was termed the bipolar STEAM sequence (BP-STEAM).

The third sequence that was used was noted in the Mori paper to not yield the actual Trace/3 ADC, because of it's inclusion of some of the off-diagonal elements. While theoretically it may not yield exactly the Trace/3 ADC as with the others, experimentally it was felt that it may yield a reasonable Trace/3 ADC result, since the errors in diffusion spectroscopy are relatively large, making the difference most likely negligible (Figure 9.10). It was also thought that since this sequence has far fewer gradient pulses, namely 6, whereas the SS-PRESS scheme has 24 gradients, it may be less sensitive to motion. Furthermore, this sequence was the most similar to previous sequences used by this lab in calculating diffusion coefficients, which was thought to be a benefit. This sequence was

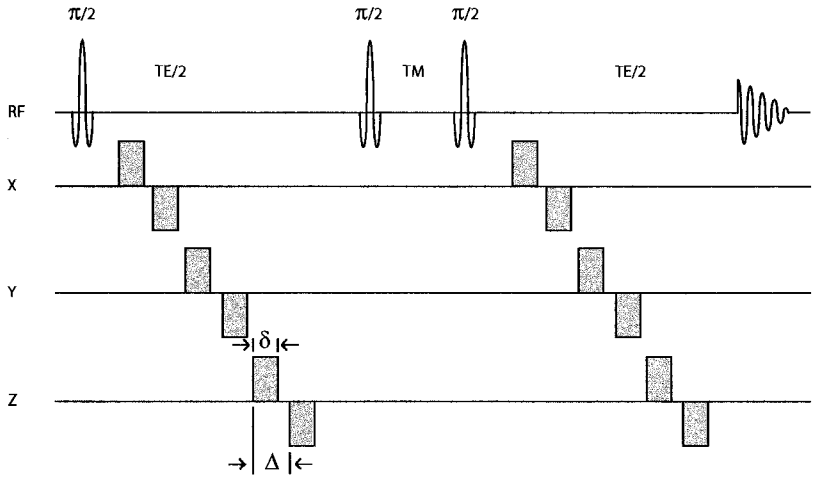

FIGURE 9.9: A single-shot diffusion trace spectroscopy sequence using the STEAM sequence, slice selection and crusher gradients not shown, termed bipolar STEAM sequence (BP-STEAM). Water suppression pulses are not shown.

termed the long diffusion time STEAM sequence (LDT-STEAM).

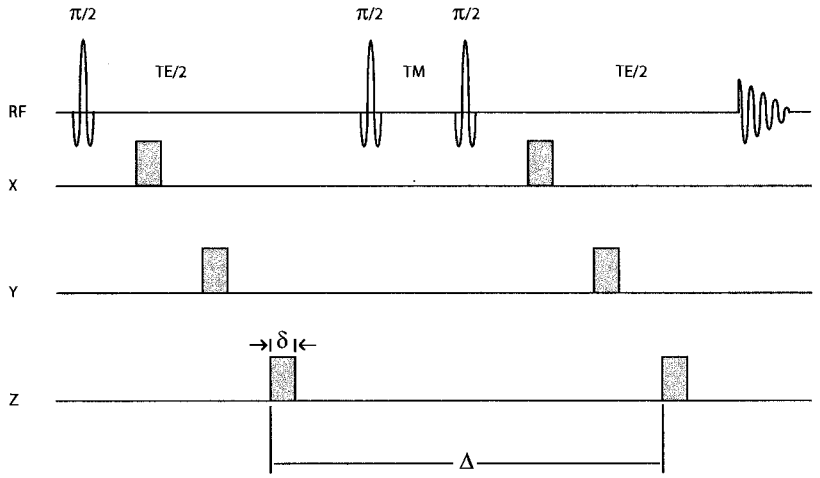

FIGURE 9.10: A single-shot diffusion trace spectroscopy sequence using the STEAM sequence, slice selection and crusher gradients not shown, termed long diffusion time STEAM sequence (LDT-STEAM). Water suppression pulses are not shown.

9.3.2 RESULTS AND DISCUSSION

9.3.2.1 ISOTROPIC PHANTOM

All three STEAM diffusion spectroscopy sequences were calibrated and tested on a 125 mL spherical phantom containing a combination of NAA, Cr, and Cho. First we measured all three directions (X, Y, and Z) with a regular diffusion weighted STEAM sequence (Figure

5.1). and then proceeded to measure the same isotropic phantom using the three single-shot sequences. The results can be found in Table 9.2.

Metabolite	Directional ADC (x 10^{-3} mm^2/s) X	Y	Z	Average of Directional ADCs (x 10^{-3} mm^2/s)
Isotropic Phantom (N=8)				
NAA	0.59±0.03	0.70±0.06	0.62±0.07	0.63±0.02
Cr	0.79±0.04	0.80±0.07	0.80±0.06	0.80±0.04
Cho	1.03±0.05	0.94±0.07	0.94±0.06	0.97±0.03

Metabolite	SS-STEAM Trace/3 ADC (x 10^{-3} mm^2/s)	BP-STEAM Trace/3 ADC (x 10^{-3} mm^2/s)	LDT-STEAM Trace/3 ADC (x 10^{-3} mm^2/s)
Isotropic Phantom (N=8)			
NAA	0.61±0.07	0.64±0.03	0.60±0.02
Cr	0.82±0.04	0.82±0.04	0.77±0.06
Cho	0.97±0.09	0.97±0.09	0.91±0.06

TABLE 9.2: Diffusion measurements of NAA, Cr, and Cho combined in a 125 mL aqueous solution (N = 8) using 3 different single shot trace diffusion spectroscopy STEAM sequences. SS-STEAM = Fig. 9.8, BP-STEAM = Fig. 9.9, LDT-STEAM = Fig. 9.10

Once again from Table 9.2 the sequences are calibrated and working correctly in an isotropic phantom. Prior to making and testing the anisotropic phantom, the sequences were tested on human volunteers to determine if the Trace/3 ADC values calculated were within the range of the expected ADC values. Since with the sequence in Figure 9.3, if the ADC calculated is wrong it will not be a minimal difference, as the NAA ADC was ~7 times larger when using the original PRESS sequence in vivo; therefore doing this will provide a quick measure of the accuracy of the sequences and help to decide where to progress from there. Using SS-STEAM sequence (TE = 192.6 ms, TM = 30ms, δ=15 ms, Δ=30ms, TR=3s, max b-value = 1742 s/mm^2, 64 averages, 4 mins per b-value x 3 b-values = ~12 min for metabolite spectral acquisition), we examined and measured the Trace/3 ADC of NAA in the OGM of two people. The ADC of NAA was determined to be 0.28 and 0.32 x 10^{-3} mm^2/s, which is not as bad as previous measurements, but still almost double what had been previously reported in brain. When we examined the BP-STEAM sequence, because of the extra time used for basically 6 gradients to ramp up and down in each section of the echo time, the SNR of the sequence was not high enough to perform the measurement. For a diffusion gradient length of δ=20 ms, and a bipolar separation of 10 ms (i.e. Δ=30 ms) at a gradient strength of 19 mT/m this would yield a b-value

of 240 s/mm^2 for one gradient pair, multiply that by the six bipolar gradient pairs in the BP-STEAM sequence for a total b-value of 1445 s/mm^2, which isn't very large. If we calculate the minimum echo time for just the gradients in order to get to that b-value, with no separation between RF pulses and gradient pairs, for the completion of this sequence with the gradient parameters mentioned here it is (one gradient pair is 50 ms long, 20 ms + 10 ms + 20 ms) 300 ms minimum, which is too long an TE for in-vivo study. The LDT-STEAM sequence (TE = 244.6 ms, TM = 180 ms, δ=30 ms, Δ= 45 ms, TR=3s, max b-value=2439 s/mm^2, 64 averages, 4 mins per b-value x 3 b-values = $\sim$12 min for metabolite spectral acquisition) on the other hand seemed to work in vivo with NAA ADC values of 0.11, 0.13, and 0.16 x 10^{-3} mm^2/s in three normal volunteers, which indicated to us that this new sequence may be working, and thus it was investigated further. However, the SNR was still quite low in this measurement and while the NAA ADC values were calculated in this initial measurement they were not examined again in-vivo. The TE of 244.6 ms causes the low SNR ($\sim$2-4, at max b-value 2439 s/mm^2). Improvements and optimization need to be made on this sequence to increase the SNR which will allow for quantification of the metabolites.

9.3.2.2 Anisotropic Phantom

In order to test the accuracy of the sequence in general for measuring the ADC in a single shot the ADC of water was examined in an anisotropic phantom. Using the LDT-STEAM sequence we examined the diffusion of water in an anisotropic celery phantom. In Table 9.3 we can see that the sequence is clearly working for water in anisotropic phantom. Although the Trace/3 ADC and the XYZ Average are slightly off in anisotropic phantom #1, they are consistent in the second anisotropic phantom. The differences in the ADC values are highlighted when the alignment of the vascular bundles switches from the z-axis in phantom #1 to the x-axis in phantom #2.

Again the sequence examined was determined to be working, for the most part, in both isotropic and anisotropic phantom (for water). While there are still SNR issues with the use of this sequence in-vivo for the metabolties, we wanted to examine the ability of the current incarnation of LDT-STEAM to measure the Trace/3 ADC of water in human brain.

Table 9.4 lists measurements of the Water ADC using the LDT-STEAM sequence (TE = 244.6 ms, TM = 180 ms, δ=30 ms, Δ= 45 ms, TR=3s, max b-value=2439 s/mm^2) from 7 different volunteers in the body of the corpus callosum, the same region used in Chapter 6. Two diffusion spectroscopy sequences were compared: X, Y, and Z directional ADC measurements in the human brain using the regular diffusion weighted STEAM sequence

Metabolite	Directional ADC (x 10^{-3} mm^2/s) X	Y	Z	Average of Directional ADCs (x 10^{-3} mm^2/s)	Single Shot Trace ADC (x 10^{-3} mm^2/s)
Anisotropic Phantom #1 (Water Only - Aligned Along Z-Direction)					
4 - Trials					
Mean	1.24±0.01	0.86±0.02	1.66±0.04	1.25±0.02	1.39±0.01
Anisotropic Phantom #2 (Water Only - Aligned Along X-Direction)					
4 - Trials					
Mean	2.27±0.02	0.90±0.01	1.00±0.01	1.39±0.01	1.41±0.02

TABLE 9.3: Diffusion measurements using LDT-STEAM of water in an anisotropic phantom of celery vascular bundles aligned along the z- or x-axis of the gradients.

and the single-shot Trace/3 ADC method using the LDT-STEAM sequence. The average ADC and the Single Shot Trace ADC were not consistent throughout the 7 volunteers and in fact were significantly different ($p<0.05$, Paired T-Test). When three measurements are made for the average ADC value, perhaps that variability in the ADC measurement is averaged out over the three measurements, whereas when one measurement is made for the single-shot method that variability is not averaged away, and possibly could be causing this error. If this is solely a noise issue then one would expect the Trace/3 ADC to either be higher or lower than the XYZ average not consistently lower as seen here. Perhaps using this LDT-STEAM sequence may not be the best choice as stated in the original single-shot paper since it still has contributions from the off-diagonal elements. However, further testing of the metabolite resonances at high field need to be examined.

Volunteer	Directional ADC (x 10^{-3} mm^2/s) X	Y	Z	Average of Directional ADCs (x 10^{-3} mm^2/s)	Single Shot Trace ADC (x 10^{-3} mm^2/s)
1	1.48	0.68	0.94	1.03	0.72
2	1.21	0.76	0.69	0.89	0.67
3	1.08	0.75	0.69	0.84	0.64
4	1.03	0.41	0.78	0.74	0.69
5	1.55	0.64	1.00	1.06	1.00
6	1.49	0.76	1.08	1.11	1.09
7	1.70	0.40	1.22	1.11	0.78
Average	1.36±0.25	0.63±0.16	0.91±0.20	0.97±0.15	0.80±0.18

TABLE 9.4: Diffusion measurements of water in the X, Y, Z direction, and the single shot LDT-STEAM, from the body of the corpus callosum in human volunteers. The XYZ average and Trace/3 ADC calculated from the LDT-STEAM sequence are also reported.

All the sequences presented here need to be tested at higher field and higher gradient strengths, the LDT-STEAM sequence in particular in order to quantify the metabolites.

The gradient strength on the magnet used in this study was only 20 mT/m, and therefore in order to increase the b-value to a reasonable number it required a long diffusion gradient which increased the TE of an already long sequence and decreased the SNR. Due to the squared relationship of the gradient strength with b-value (Equation 3.3), if the gradient strength could be doubled then the diffusion gradient length can be decreased by a factor of 4, which will in turn decrease the echo time and increase the available SNR by minimizing T_2 losses. Another possibility for increasing the SNR may be to use the same gradient scheme in the LDT-STEAM sequence, however incorporate it into a PRESS sequence not unlike the one used in Chapter 8, with a short TE_1 and a long TE_2 where the gradients are located. Using a PRESS sequence, rather than STEAM, will also double the SNR available from the singlet metabolites, NAA, tCr, and Cho.

9.4 Summary

Overall, measuring the Trace/3 ADC in a single-shot is extremely important in order to save time and make diffusion spectroscopy more amenable to clinical patient studies. However, it is difficult to measure in-vivo based on the experiments performed in this current study. A similar method as used in Chapter 5 (measuring the Trace/3 ADC with a 3 direction measurement), may be beneficial when examining certain pathologies. Certain changes in the length of the sequence, however, may be required, such as decreasing the overall acquisition time (currently 75 min). For a sequence with a TR of approximately 3 s, and 64 averages per b-value, one should be able to acquire all spectral data in a period of $\sim$20 min with only two b-values per direction. Including the shimming and localization sequences it should be possible to scan a patient in under 45 min. However, for an acute stroke or something similar when Time = Brain, this scan time may still be too long.

While the overall goal of this project was not achieved in-vivo, there are changes that can be made to possibly improve on it in the future. It needs to be investigated further what exactly is causing this extreme motion sensitivity in the original SS-PRESS sequence. Recall that the sequences developed in this Chapter work well on both isotropic and anisotropic phantoms. The PRESS sequence has been shown to be useful in the investigation of the diffusion of metabolites ([29], Chapter 8); therefore what is causing the errors in-vivo when the complex gradient pattern is added and how can it be overcome?

Part III

Conclusions and Future Directions

CHAPTER 10

CONCLUDING REMARKS

DW-MRS has been examined quite extensively in this thesis, starting with the original Trace/3 ADC measurement of the three metabolites NAA, tCr, and Cho in three different regions in the human brain, moving on to the measurement of the full diffusion tensor of the human brain in six different regions, and following that original DTS work with the investigation of metabolite diffusion in the frog sciatic nerve, as well as mI in healthy human brain. Finally, a measurement of the Trace/3 ADC in a single-shot in-vivo was attempted in human brain. The work here is preliminary and required in order to establish baseline metabolite diffusion parameters. Future work in this area should be quite beneficial to the study of many neurological disorders. This section give a brief summary of the individual experiments as well as describes some of the limitations associated with the research presented here and an outlook on the future directions of measurements of the Trace/3 ADC and the full diffusion tensor of metabolites in-vivo.

10.1 SUMMARY

10.1.1 TRACE ADC IN HUMAN BRAIN

This was our first attempt at measuring the diffusion of metabolites in human brain. The rotationally invariant Trace/3 ADC of the metabolites NAA, tCr, and Cho were calculated in three specific regions in the healthy human brain. This study improved upon the previous two published studies by incorporating a new phase correction method, as well as measuring a rotationally invariant diffusion coefficient. We found that the Trace/3 ADC value for NAA was significantly less than tCr and Cho. The work presented in this chapter was published in one of the leading scientific journals in the field of MRI [127], and serves a baseline for future studies.

10.1.2 DTS of Human Brain

This study built upon our previous Trace/3 ADC work by examining the diffusion in six non-collinear directions in an effort to calculate the entire diffusion tensor. We measured the diffusion in six separate and distinct regions, two gray matter and four white matter. From the diffusion tensor we were able to calculate the eigenvalues, Trace/3 ADC, and FA values for those six regions. The directional information obtained from NAA is consistent, as expected, with the directional information obtained with water (i.e. NAA diffuses preferentially along the fiber tracts in white matter). The Trace/3 ADC value of NAA was found to be significantly less than tCr and Cho in 3 of the 4 white matter structures, however this same effect was not seen in the gray matter. The validity of some of the FA measurements came into question. The FA of tCr and Cho was larger than the FA of NAA, which was unexpected since NAA was thought to be in a more anisotropic environment, and the FA of all three metabolites in gray matter was quite high and indicated anisotropy which was also unexpected due to the known isotropic nature of the gray matter. We investigated these FA measurements further in the next two studies.

10.1.3 DW-MRS of Frog Sciatic Nerve

The high FA values reported for tCr and Cho in the human brain DTS study was quite unsettling. NAA was thought to be located in highly anisotropic structures (i.e. axons), whereas tCr and Cho, although also located in the axons, are also thought to be located in more isotropic structures such as oligodendrocytes and astrocytes (see Section 2.9). A simple model system, such as the excised frog sciatic nerve used in this study, eliminates some of the motion errors associated with the in-vivo work. Again, we found higher FA values for tCr and Cho when compared to NAA. Also, the increased field strength used in this study (18.8 T as opposed to 3 T) allowed the measurement of the diffusion characteristics of Tau and Glx as well. The FA values reported for Glx were $\sim$0.20 which indicated isotropy. However, the Glx peak was only found in 3 of the 9 nerves examined, and therefore, more experiments are needed to confirm this finding. The differences in the FA values between the metabolites examined in this study do seem to indicate that they are residing in different compartments within the nerve, which may also be true in human brain.

10.1.4 DTS of Myo-Inositol: Implications for the Measurement of FA

The high FA values reported for the metabolites in the gray matter regions in the previous human brain DTS study were questionable. It was thought that the variability of the ADC measurements may be too high to measure the FA accurately. A recent study showed that the accuracy of a two point ADC measurement can be increased by a greater signal intensity drop between the two points (i.e. using a much higher b-value). We decided to test this theory on the accuracy of the FA measurement in isotropic alcohols and human brain. FA values calculated when using a low maximum b-value (1815 s/mm^2), similar to the previous DTS work, were significantly increased when compared to FA values using a high maximum b-value (5018 s/mm^2). A variety of different regions, white and gray matter, need to be investigated to further confirm the accuracy of this new method.

10.1.5 Single-Shot Diffusion Trace Spectroscopy

A variety of different sequences are tested for the measurement of the Trace/3 ADC in a single shot. The sequences used seem to work well in phantom; however, the transition to in-vivo study is quite challenging, as the sequences seem to be quite sensitive to motion. More work needs to be done to examine what is causing the perceived motion sensitivity. Measuring the Trace/3 ADC in a single-shot, however, is extremely important, because it will save time and make diffusion spectroscopy more amenable to clinical patient studies. A similar method as used in Chapter 5 (measuring the Trace/3 ADC with a 3 direction measurement), may work if the motion sensitivity issue cannot be solved, but certain changes in the length of the sequence (i.e. number of b-values used) may be required.

10.2 Limitations

10.2.1 Trace ADC in Human Brain

This was our first attempt at measuring the diffusion of metabolites in human brain, and thus it was overly cautious in some aspects. The voxel size used in the study was rather large (2.5 x 2.5 x 2.5 = 15.6 cm^3), and was located in the corona radiata and centrum semiovale. Smaller voxel sizes similar to the DTS study of around 11 cm^3 have been shown to be adequate. A white matter region, such as the corpus callosum, would have made it easier to see anisotropic diffusion changes. The echo time was also quite large for this sequence. A TE of 180ms was not required, as diffusion spectroscopy STEAM sequences were performed later with an echo time of 76.6 ms in the DTS study; however double

gradients were used in the DTS allowing a shorter echo time, but a smaller echo time in the Trace/3 ADC study should still be possible. Originally the echo time of that sequence was left long to combat some of the eddy current effects, and later when the eddy correction method, which is used throughout this thesis, was applied it was never shortened. The scan time used for this measurement was also quite long. Four b-values were used for the study and as was discovered later, again in the DTS study, you can achieve similar ADC values with only two b-values. Using less b-values would have allowed for a quicker scan time, which may have helped achieve some clinical experimentation. Using less averages may have also allowed us to shorten the scan time, however as it was seen in this study that does affect the overall measurement of the Trace/3 ADC if we use too few (Figure 5.5). As we found out later in Chapter 8, the b-value used in this study may not have been optimal, perhaps a higher b-value yielding an approximate signal intensity drop of $\sim$50% may have been beneficial and given a more accurate Trace/3 ADC measurement.

Overall, our first attempt at DW-MRS was a success and was published in one of the leading scientific journals in the field of MRI [127].

10.2.2 DTS of Human Brain

Originally one of the main limitations of the DTS study was thought to be the low SNR, because the SNR was thought to be causing the higher FA of the metabolites in in-vivo gray matter. As it turns out the higher FA of the metabolites in the gray matter is caused by the b-value not providing enough of a signal intensity drop in-vivo, as was discovered later in Chapter 8. A new study, currently in progress that will be published outside of this thesis, will be examining the FA measurements made in four of the regions that were examined in this DTS work with a higher b-value. This is an attempt to determine if the FA measured with lower maximum b values from in-vivo white matter are real or similarly inflated as the gray matter in Chapter 8.

It would be beneficial in the future to replicate this work at 4.7 T, because of the added benefit of more SNR and better spectral resolution. The 4.7 T magnet in our lab also has higher gradient strengths (35 mT/m versus 20 mT/m), which will allow for a shortening of the TE. To get a b-value of $\sim$5000 s/mm^2 at a Δ of 80 ms and assuming the gradients are on in two directions, it would require a δ of 36 ms for the 3 T (20mT/m) and 20 ms for the 4.7 T (35 mT/m), which will save 32 ms from your TE. Keep in mind that the b-value is proportional to the gradient strength squared. The move to a higher field with more gradient strength may even allow for the examination of different metabolites not explored in this thesis.

STEAM was chosen originally because it was used in the first diffusion spectroscopy

study on human brain [28]. A comparison between the PRESS and STEAM sequences for use in DTS experimentation may have been interesting, as STEAM was used for the majority of the research presented here. The signal acquired from the PRESS sequence should have, at least for the singlet resonances of NAA, tCr, and Cho, double the SNR, which may allow smaller voxels to be used; however, this is a trade off because with the PRESS sequence normally the echo time is longer. Therefore, it would have been interesting to do a cost-benefit analysis of the PRESS and STEAM sequences to determine which is the best for DTS or Trace/3 ADC measurements in-vivo.

Overall, this paper was the first published paper on Diffusion Tensor Spectroscopy in the human brain [131], and while the FA measurements in gray matter may be suspect it certainly paved the way for the investigation of DTS in brain.

10.2.3 DW-MRS of Frog Sciatic Nerve

This paper while very interesting for a comparison between the human DTS study, could have been so much more. Unfortunately the timing of the project was not perfect. The 18.8 T magnet, which was used in this study, was in the process of implementing a new "cold head" probe. This "cold-head" only had a single axis gradient on it. The tri-axis gradient probe, which we were working with, therefore, was only able to be used for a period of one week! In that limited time, we (with the help of Ryan McKay at NANUC) were able to examine the diffusion of 10 nerve samples; however, only to a small b-value. Previous work has shown that the diffusion attenuation curves of the metabolite NAA in excised bovine nerve are not mono-exponential at extremely high b-values (up to 300,000 s/mm^2) [112, 113]. It would have been interesting to examine this effect on the 18.8 T. Also examining the effect of different diffusion times at constant echo time , as well as different echo times at constant diffusion time on the metabolite diffusion; this may have yielded more information about the metabolite diffusion in nerve.

It was also disappointing to not get a chance to build on this study further. It would have been interesting to examine more than just the frog sciatic nerve. The diffusion parameters in this study, may have been better explained by examining a myelinated central nerve, a myelinated peripheral nerve, and a non-myelinated nerve, similar to what has been done previously on water diffusion with nerves of the Garfish [92]. However, due to time constraints and working on other projects this idea never came to fruition.

Overall, the project did quite a lot to validate the work presented in the DTS study, and even answered some questions about the metabolite diffusion in human brain white matter.

10.2.4 DTS of Myo-Inositol: Implications for the Measurement of FA

The main limitation of this study is the lack of a comparable measure for the white matter regions used in the original DTS study, since we chose a region in the sub-cortical white matter that was thought to have a decent shim and signal compared to our attempts at a region in the corpus callosum. The same regions used in the previous DTS study need to be repeated at a b-value which causes a 50% drop in signal intensity, perhaps with a different sequence not optimized for mI. Furthermore, the question arose in Chapter 8, is a 50% drop for metabolites in the human brain enough, or do we have to go even higher? How high of a b-value is high enough?

1-nonanol has an intrinsic diffusion coefficient of $\sim 0.12 \times 10^{-3}$ mm^2/s, which is a lower ADC than those measured for the metabolites in this study. An experiment in which the b-value is continuously increased up to perhaps a ~70% drop in signal intensity should be examined, which would require a b-value of 11,000 s/mm^2. However at 3T, with a gradient strength of 20 mT/m this may not be feasible as a 55 ms diffusion gradient pulse would be required (Δ = 87 ms). Furthermore, the specific effect of noise coupled with a low ADC should be examined; one of the small peaks of 1-octanol or 1-nonanol can be examined at reduced SNR (i.e. by decreasing the averages) to perhaps show a difference in the FA with decreasing SNR despite being at a high b-value, in an effort to explain the high FA of mI in white matter.

Overall, this project was a needed investigation of the intricacies of the DTS measurements and should provide some very valuable advice and caution to the MR community interested in diffusion spectroscopy measurements of human brain. However, further testing needs to be done to determine the best way and minimum acquisition requirements to perform DTS in-vivo.

10.2.5 Single-Shot Diffusion Trace Spectroscopy

The biggest limitation of this study is that we never got the sequence working in a living human being. The sequence itself works perfectly on isotropic and anisotropic phantoms. However, when applied to the human brain the Trace/3 ADC obtained was erroneously high using the exact same single shot pulse program and parameters. Tests need to still be performed to determine what exactly is causing this error in the in-vivo measurements. The error is likely due to an interaction between the numerous diffusion gradients and patient-induced motion, but it is not clear at this stage how to overcome this. Using the existing single-shot PRESS sequence one could test different diffusion times, echo times, or diffusion gradient lengths in order to see if there is any correlation with the erroneous

Trace/3 ADC measurements.

In the opinion of this author the best gradient scheme to use is the long diffusion time scheme, which was used for the majority of the last half of Chapter 9. This sequence is in Figure 9.10. However, the SNR required for accurate single average phase correction was not optimal, and therefore using the same gradient scheme with either a PRESS sequence (STEAM was used in this study) or going to a higher field may be required.

Overall, it's disappointing that this project never got off the ground. It would have been interesting to examine different neurological disorders with this sequence.

10.3 Future Directions

At the time of this writing DW-MRS is still quite a wide open field, only three groups in the world are currently publishing in this topic area. There are certainly improvements that can be made to the research presented here and ideas were given throughout the thesis hinting at new projects that can be examined.

10.3.1 Single Shot Diffusion Trace Spectroscopy

Although it was mentioned before, testing single-shot diffusion trace spectroscopy at a higher field needs to be done. The greater signal to noise as well as stronger, perhaps more stable, gradients are only going to benefit the diffusion measurements. However, if for some reason problems still persist with the single shot Trace/3 ADC sequence in vivo, measuring the Trace/3 ADC in three directions should be feasible in clinical scan times. The acquisition of the metabolite spectra alone, with two b-values in each of three directions, would only take $\sim$24 min, if we include shimming, scout images, and water spectra it should be possible to scan in < 45 min.

A variety of MRS studies have shown changes in metabolite concentration in different neurological disorders. Furthermore, there may be cases in which the concentration may not change but another MR visible characteristic like T1, T2, or the focus of this thesis diffusion, could change with pathology. Water diffusion in acute stroke is a perfect example where acutely there are no visible changes on T1, T2 or proton density, but there are marked 40% changes in the diffusion coefficient of water in the ischemic tissue. It would be interesting to measure the Trace/3 ADC of metabolites in some of the specific neurological disorders mentioned below.

10.3.1.1 Acute Cerebral Ischemia

A variety of papers have examined the diffusion of metabolites in animal models of cerebral ischemia [100, 102–107]. The apparent diffusion coefficients (ADC) of the singlet metabolites reduce significantly in the acute phase of cerebral ischemia, similarly to the ADC reduction of water. This is interesting as the metabolites are only in one compartment and presumably don't undergo compartmental shifts like water does during ischemia. This has only been shown once in the human brain [29], and in that study only one diffusion direction was measured. The full Trace/3 ADC needs to be measured in the human brain during acute cerebral ischemia in order to confirm this ADC reduction for all the metabolites mentioned here. Differences in the diffusion of the metabolites in the region of ischemia may provide new information about salvageable and unsalvageable tissue, as well as possibly providing more information about the underlying cause of these diffusion changes seen with water and metabolites.

10.3.1.2 Cancer

Metabolic changes are commonly associated with different cancers, and Cho changes in MRS are commonly found in cancer studies [8, 65]. It has been shown previously in the human brain that the diffusion of the metabolites NAA, tCr, and Cho have increased in a cerebral glioma in human brain [29]. However, again this measurement was only performed in a single direction. The examination of the Trace/3 ADC in different types of cancer may lead to important advances in the diagnosis and/or determination of the type of cancer, assuming of course that there are differences in the metabolite diffusion between cancers. Water diffusion has been shown to be different in various types of cancer [148], and also in distinguishing absesses from tumors [149]. It has been shown that MRS is quite useful in distinguishing types and grades of tumors [150], thus it would be interesting to examine these different types and/or grades of tumors using DW-MRS, to see if their classification can be improved further.

10.3.1.3 Parkinson's Disease

Recently DTI changes in Parkinson's disease have been shown to be useful in the monitoring of the progression of the disease [151]. It would be interesting to examine the Trace/3 ADC as well as use DTS on the afferent projections of the substantia nigra located in the striatum, in order to quantify any changes in the NAA and other metabolites (the substantia nigra is too small a structure for single voxel spectroscopy). NAA changes have been seen in Parkinson's disease [4], and therefore perhaps diffusion changes of NAA may provide more accurate information about the progression of the disease. It has been

shown using DTI that patients with Parkinson's disease significantly decrease FA along a line from the substantia nigra to the lower part of the putamen/caudate complex [152]. It is not known if the water FA change is caused by neuronal loss, gliosis, or demyelination; therefore, it would be interesting to examine the metabolite diffusion for any possible insight into the rationale behind these changes.

10.3.2 The Future of DW-MRS in Brain

The work presented in this thesis has opened the door for future studies of diffusion spectroscopy of metabolites in human brain. While DW-MRS is quite challenging in the human brain, due to limited signal-to-noise ratio, poor spatial resolution, pulse sequence availability, significant post-processing, lengthy acquisition times, and limited brain coverage, we showed that diffusion measurements of mean diffusivity and fractional anisotropy of metabolites in human brain were possible. Also, certain feasibility issues were raised as well as guidelines that will help further this research in other labs. The hope for DW-MRS in human brain is that, despite all these challenges, it will provide more information about the structure and/or function of different neurological disorders.

BIBLIOGRAPHY

[1] P.C. Lauterbur. Image Formation by Induced Local Interactions: Examples Employing Nuclear Magnetic Resonance. *Nature*, 242:190–191, 1973.

[2] C. A. Davie, G. K. Wenning, G. J. Barker, A. Brennan, N. Quinn, and D. H. Miller. MRS to differentiate multiple system atrophy from idiopathic Parkinson's disease. *Lancet*, 342(8872):681–682, Sep 1993.

[3] B. A. Holshouser, M. Komu, H. E. Möller, J. Zijlmans, H. Kolem, D. B. Hinshaw, P. Sonninen, P. Vermathen, A. Heerschap, and H. Masur. Localized proton NMR spectroscopy in the striatum of patients with idiopathic Parkinson's disease: a multicenter pilot study. *Magn Reson Med*, 33(5):589–594, May 1995.

[4] F. Federico, I. L. Simone, V. Lucivero, G. Iliceto, M. De Mari, P. Giannini, D. M. Mezzapesa, A. Tarantino, and P. Lamberti. Proton magnetic resonance spectroscopy in Parkinson's disease and atypical parkinsonian disorders. *Mov Disord*, 12(6):903–909, Nov 1997.

[5] C. A. Davie, C. P. Hawkins, G. J. Barker, A. Brennan, P. S. Tofts, D. H. Miller, and W. I. McDonald. Serial proton magnetic resonance spectroscopy in acute multiple sclerosis lesions. *Brain*, 117 (Pt 1):49–58, Feb 1994.

[6] P. M. Matthews, E. Pioro, S. Narayanan, N. De Stefano, L. Fu, G. Francis, J. Antel, C. Wolfson, and D. L. Arnold. Assessment of lesion pathology in multiple sclerosis using quantitative MRI morphometry and magnetic resonance spectroscopy. *Brain*, 119 (Pt 3):715–722, Jun 1996.

[7] C. C. Ford, R. H. Griffey, N. A. Matwiyoff, and G. A. Rosenberg. Multivoxel 1H-MRS of stroke. *Neurology*, 42(7):1408–1412, Jul 1992.

[8] S. S. Gill, D. G. Thomas, N. Van Bruggen, D. G. Gadian, C. J. Peden, J. D. Bell, I. J. Cox, D. K. Menon, R. A. Iles, and D. J. Bryant. Proton MR spectroscopy of

intracranial tumours: in vivo and in vitro studies. *J Comput Assist Tomogr*, 14(4):497–504, 1990.

[9] B. Chance, D. P. Younkin, R. Kelley, W. J. Bank, H. D. Berkowitz, Z. Argov, E. Donlon, B. Boden, K. McCully, and N. M. Buist. Magnetic resonance spectroscopy of normal and diseased muscles. *Am J Med Genet*, 25(4):659–679, Dec 1986.

[10] R. D. Oberhaensli, G. J. Galloway, D. Hilton-Jones, P. J. Bore, P. Styles, B. Rajagopalan, D. J. Taylor, and G. K. Radda. The study of human organs by phosphorus-31 topical magnetic resonance spectroscopy. *Br J Radiol*, 60(712):367–373, Apr 1987.

[11] R. H. Griffey. Carbon-13 magnetic resonance spectroscopy. Problems and promise. *Invest Radiol*, 24(12):1017–1019, Dec 1989.

[12] M. C. Malet-Martino and R. Martino. Magnetic resonance spectroscopy: a powerful tool for drug metabolism studies. *Biochimie*, 74(9-10):785–800, 1992.

[13] H. Y. Carr and E. M. Purcell. Effects of Diffusion on Free Precession in Nuclear Magnetic Resonance Experiments. *Phys. Rev.*, 94(3):630–638, May 1954.

[14] M. E. Moseley, Y. Cohen, J. Mintorovitch, L. Chileuitt, H. Shimizu, J. Kucharczyk, M. F. Wendland, and P. R. Weinstein. Early detection of regional cerebral ischemia in cats: comparison of diffusion- and T2-weighted MRI and spectroscopy. *Magn Reson Med*, 14(2):330–46, 1990.

[15] M. E. Moseley, J. Kucharczyk, J. Mintorovitch, Y. Cohen, J. Kurhanewicz, N. Derugin, H. Asgari, and D. Norman. Diffusion-weighted MR imaging of acute stroke: correlation with T2-weighted and magnetic susceptibility-enhanced MR imaging in cats. *AJNR Am J Neuroradiol*, 11(3):423–9, 1990.

[16] J. S. Tsuruda, W. M. Chew, M. E. Moseley, and D. Norman. Diffusion-weighted MR imaging of the brain: value of differentiating between extraaxial cysts and epidermoid tumors. *AJNR Am J Neuroradiol*, 11(5):925–31; discussion 932–4, 1990.

[17] J. V. Hajnal, M. Doran, A. S. Hall, A. G. Collins, A. Oatridge, J. M. Pennock, I. R. Young, and G. M. Bydder. MR imaging of anisotropically restricted diffusion of water in the nervous system: technical, anatomic, and pathologic considerations. *J Comput Assist Tomogr*, 15(1):1–18, 1991.

[18] M. Adachi, T. Hosoya, T. Haku, K. Yamaguchi, and T. Kawanami. Evaluation of the substantia nigra in patients with Parkinsonian syndrome accomplished using

multishot diffusion-weighted MR imaging. *AJNR Am J Neuroradiol*, 20(8):1500–1506, Sep 1999.

[19] H. B. Larsson, C. Thomsen, J. Frederiksen, M. Stubgaard, and O. Henriksen. In vivo magnetic resonance diffusion measurement in the brain of patients with multiple sclerosis. *Magn Reson Imaging*, 10(1):7–12, 1992.

[20] J. Pelletier, M. Habib, O. Lyon-Caen, G. Salamon, M. Poncet, and R. Khalil. Functional and magnetic resonance imaging correlates of callosal involvement in multiple sclerosis. *Arch Neurol*, 50(10):1077–1082, Oct 1993.

[21] P. Christiansen, P. Gideon, C. Thomsen, M. Stubgaard, O. Henriksen, and H. B. Larsson. Increased water self-diffusion in chronic plaques and in apparently normal white matter in patients with multiple sclerosis. *Acta Neurol Scand*, 87(3):195–9, 1993.

[22] M. E. Moseley, Y. Cohen, J. Kucharczyk, J. Mintorovitch, H. S. Asgari, M. F. Wendland, J. Tsuruda, and D. Norman. Diffusion-weighted MR imaging of anisotropic water diffusion in cat central nervous system. *Radiology*, 176(2):439–45, 1990.

[23] P. J. Basser, J. Mattiello, and D. LeBihan. MR diffusion tensor spectroscopy and imaging. *Biophys J*, 66(1):259–67, 1994.

[24] P. J. Basser, J. Mattiello, and D. LeBihan. Estimation of the effective self-diffusion tensor from the NMR spin echo. *J Magn Reson B*, 103(3):247–54, 1994.

[25] P. J. Basser, S. Pajevic, C. Pierpaoli, J. Duda, and A. Aldroubi. In vivo fiber tractography using DT-MRI data. *Magn Reson Med*, 44(4):625–32, 2000.

[26] C. Pierpaoli, A. Barnett, S. Pajevic, R. Chen, L. R. Penix, A. Virta, and P. Basser. Water diffusion changes in Wallerian degeneration and their dependence on white matter architecture. *Neuroimage*, 13(6 Pt 1):1174–1185, Jun 2001.

[27] Christian Beaulieu, Christopher Plewes, Lori Anne Paulson, Dawne Roy, Lindsay Snook, Luis Concha, and Linda Phillips. Imaging brain connectivity in children with diverse reading ability. *Neuroimage*, 25(4):1266–1271, May 2005.

[28] S. Posse, C. A. Cuenod, and D. Le Bihan. Human brain: proton diffusion MR spectroscopy. *Radiology*, 188(3):719–25, 1993.

[29] M. Harada, M. Uno, F. Hong, S. Hisaoka, H. Nishitani, and T. Matsuda. Diffusion-weighted in vivo localized proton MR spectroscopy of human cerebral ischemia and tumor. *NMR Biomed*, 15(1):69–74, 2002.

[30] V. Mlynarik, S. Gruber, and E. Moser. Proton T (1) and T (2) relaxation times of human brain metabolites at 3 Tesla. *NMR Biomed*, 14(5):325–31, 2001.

[31] J. P. Wansapura, S. K. Holland, R. S. Dunn, and W. S. Ball. NMR relaxation times in the human brain at 3.0 tesla. *J Magn Reson Imaging*, 9(4):531–538, Apr 1999.

[32] P. A. Bottomley. Spatial localization in NMR spectroscopy in vivo. *Ann N Y Acad Sci*, 508:333–348, 1987.

[33] J. Frahm, H. Bruhn, M. L. Gyngell, K. D. Merboldt, W. Hanicke, and R. Sauter. Localized high-resolution proton NMR spectroscopy using stimulated echoes: initial applications to human brain in vivo. *Magn Reson Med*, 9(1):79–93, 1989.

[34] Frederic H. Martini. *Fundamentals of Anatomy and Physiology, 7th Edition*. Pearson Education Inc., 2006.

[35] Charles P. Slichter. *Principles of Magnetic Resonanc, Third Enlarged and Updated Edition*. Springer-Verlag, 1996.

[36] R. E. Hurd, D. Gurr, and N. Sailasuta. Proton spectroscopy without water suppression: the oversampled J-resolved experiment. *Magn Reson Med*, 40(3):343–347, Sep 1998.

[37] J. W. van Der Veen, D. R. Weinberger, G. Tedeschi, J. A. Frank, and J. H. Duyn. Proton MR spectroscopic imaging without water suppression. *Radiology*, 217(1):296–300, Oct 2000.

[38] H. Serrai, L. Senhadji, D. B. Clayton, C. Zuo, and R. E. Lenkinski. Water modeled signal removal and data quantification in localized MR spectroscopy using a time-scale postacquistion method. *J Magn Reson*, 149(1):45–51, Mar 2001.

[39] D. B. Clayton, M. A. Elliott, J. S. Leigh, and R. E. Lenkinski. 1H spectroscopy without solvent suppression: characterization of signal modulations at short echo times. *J Magn Reson*, 153(2):203–209, Dec 2001.

[40] Zhengchao Dong, Wolfgang Dreher, and Dieter Leibfritz. Experimental method to eliminate frequency modulation sidebands in localized in vivo 1H MR spectra acquired without water suppression. *Magn Reson Med*, 51(3):602–606, Mar 2004.

[41] Wolfgang Dreher and Dieter Leibfritz. New method for the simultaneous detection of metabolites and water in localized in vivo 1H nuclear magnetic resonance spectroscopy. *Magn Reson Med*, 54(1):190–195, Jul 2005.

[42] J. F. Shen and J. K. Saunders. Double inversion recovery improves water suppression in vivo. *Magn Reson Med*, 29(4):540–542, Apr 1993.

[43] A. Hasse, J. Frahm, W. Hanicke, and D. Matthaei. 1H NMR chemical shift selective (CHESS) imaging. *Phys Med Biol*, 30:341–344, 1985.

[44] Eric P. Widmaier, Hershal Raff, and Kevin T. Strang. *Vander's Human Physiology: The Mechanisms of Body Function, Tenth Edition*. McGraw Hill Companies Inc., 2006.

[45] R. Kreis, T. Ernst, and B. D. Ross. Development of the human brain: in vivo quantification of metabolite and water content with proton magnetic resonance spectroscopy. *Magn Reson Med*, 30(4):424–437, Oct 1993.

[46] J. Pfeuffer, I. Tkac, S. W. Provencher, and R. Gruetter. Toward an in vivo neurochemical profile: quantification of 18 metabolites in short-echo-time (1)H NMR spectra of the rat brain. *J Magn Reson*, 141(1):104–20, 1999.

[47] R. B. Thompson and P. S. Allen. Sources of variability in the response of coupled spins to the PRESS sequence and their potential impact on metabolite quantification. *Magn Reson Med*, 41(6):1162–1169, Jun 1999.

[48] R. B. Thompson and P. S. Allen. Response of metabolites with coupled spins to the STEAM sequence. *Magn Reson Med*, 45(6):955–965, Jun 2001.

[49] H. H. Tallan, S. Moore, and W. H. Stein. N-Acetyl-L-aspartic acid in brain. *J Biol Chem*, 219(1):257–64, 1956.

[50] D. L. Birken and W. H. Oldendorf. N-acetyl-L-aspartic acid: a literature review of a compound prominent in 1H-NMR spectroscopic studies of brain. *Neurosci Biobehav Rev*, 13(1):23–31, 1989.

[51] M. L. Simmons, C. G. Frondoza, and J. T. Coyle. Immunocytochemical localization of N-acetyl-aspartate with monoclonal antibodies. *Neuroscience*, 45(1):37–45, 1991.

[52] A. R. Guimaraes, P. Schwartz, M. R. Prakash, C. A. Carr, U. V. Berger, B. G. Jenkins, J. T. Coyle, and R. G. González. Quantitative in vivo 1H nuclear magnetic resonance spectroscopic imaging of neuronal loss in rat brain. *Neuroscience*, 69(4):1095–1101, Dec 1995.

[53] K. K. Bhakoo and D. Pearce. In vitro expression of N-acetyl aspartate by oligodendrocytes: implications for proton magnetic resonance spectroscopy signal in vivo. *J Neurochem*, 74(1):254–62, 2000.

[54] J. Urenjak, S. R. Williams, D. G. Gadian, and M. Noble. Specific expression of N-acetylaspartate in neurons, oligodendrocyte-type-2 astrocyte progenitors, and immature oligodendrocytes in vitro. *J Neurochem*, 59(1):55–61, 1992.

[55] E. Martin, A. Capone, J. Schneider, J. Hennig, and T. Thiel. Absence of N-acetylaspartate in the human brain: impact on neurospectroscopy? *Ann Neurol*, 49(4):518–521, Apr 2001.

[56] H. C. Charles, F. Lazeyras, K. R. Krishnan, O. B. Boyko, L. J. Patterson, P. M. Doraiswamy, and W. M. McDonald. Proton spectroscopy of human brain: effects of age and sex. *Prog Neuropsychopharmacol Biol Psychiatry*, 18(6):995–1004, Oct 1994.

[57] R. Heun, S. Schlegel, M. Graf-Morgenstern, J. Tintera, J. Gawehn, and P. Stoeter. Proton magnetic resonance spectroscopy in dementia of Alzheimer type. *Int J Geriatr Psychiatry*, 12(3):349–358, Mar 1997.

[58] M. L. Lai, Y. I. Hsu, S. Ma, and C. Y. Yu. Magnetic resonance spectroscopic findings in patients with subcortical ischemic stroke. *Zhonghua Yi Xue Za Zhi (Taipei)*, 56(1):31–35, Jul 1995.

[59] K. K. Bhakoo, I. T. Williams, S. R. Williams, D. G. Gadian, and M. D. Noble. Proton nuclear magnetic resonance spectroscopy of primary cells derived from nervous tissue. *J Neurochem*, 66(3):1254–63, 1996.

[60] J. Urenjak, S. R. Williams, D. G. Gadian, and M. Noble. Proton nuclear magnetic resonance spectroscopy unambiguously identifies different neural cell types. *J Neurosci*, 13(3):981–9, 1993.

[61] K. K. McCully, H. Kakihira, K. Vandenborne, and J. Kent-Braun. Noninvasive measurements of activity-induced changes in muscle metabolism. *J Biomech*, 24 Suppl 1:153–161, 1991.

[62] C.K. Matthews, K.E. van Holde, and K.G. Ahern. *Biochemistry, Third Edition*. Addison Wesley Longman, 2000.

[63] A. Connelly, G. D. Jackson, J. S. Duncan, M. D. King, and D. G. Gadian. Magnetic resonance spectroscopy in temporal lobe epilepsy. *Neurology*, 44(8):1411–1417, Aug 1994.

[64] S. H. Zeisel, K. A. Da Costa, P. D. Franklin, E. A. Alexander, J. T. Lamont, N. F. Sheard, and A. Beiser. Choline, an essential nutrient for humans. *Faseb J*, 5(7):2093–8, 1991.

[65] C. Remy, M. Von Kienlin, S. Lotito, A. Francois, A. L. Benabid, and M. Decorps. In vivo 1H NMR spectroscopy of an intracerebral glioma in the rat. *Magn Reson Med*, 9(3):395–401, Mar 1989.

[66] A. Brand, C. Richter-Landsberg, and D. Leibfritz. Multinuclear NMR studies on the energy metabolism of glial and neuronal cells. *Dev Neurosci*, 15(3-5):289–298, 1993.

[67] A. M. Landtblom, L. Sjöqvist, B. Söderfeldt, H. Nyland, and K. A. Thuomas. Proton MR spectroscopy and MR imaging in acute and chronic multiple sclerosis–ringlike appearances in acute plaques. *Acta Radiol*, 37(3 Pt 1):278–287, May 1996.

[68] E. P. Pioro. MR spectroscopy in amyotrophic lateral sclerosis/motor neuron disease. *J Neurol Sci*, 152 Suppl 1:S49–S53, Oct 1997.

[69] E. P. Pioro, A. W. Majors, H. Mitsumoto, D. R. Nelson, and T. C. Ng. 1H-MRS evidence of neurodegeneration and excess glutamate + glutamine in ALS medulla. *Neurology*, 53(1):71–79, Jul 1999.

[70] K. E. Miller, B. A. Richards, and R. M. Kriebel. Glutamine-, glutamine synthetase-, glutamate dehydrogenase- and pyruvate carboxylase-immunoreactivities in the rat dorsal root ganglion and peripheral nerve. *Brain Res*, 945(2):202–11, 2002.

[71] Y. Kinoshita and A. Yokota. Absolute concentrations of metabolites in human brain tumors using in vitro proton magnetic resonance spectroscopy. *NMR Biomed*, 10(1):2–12, Jan 1997.

[72] Roger M Bourne, Peter Stanwell, Jonathan R Stretch, Richard A Scolyer, John F Thompson, Carolyn E Mountford, and Cynthia L Lean. In vivo and ex vivo proton MR spectroscopy of primary and secondary melanoma. *Eur J Radiol*, 53(3):506–513, Mar 2005.

[73] Zhiyong Tong, Toshiaki Yamaki, Kuniaki Harada, and Kiyohiro Houkin. In vivo quantification of the metabolites in normal brain and brain tumors by proton MR spectroscopy using water as an internal standard. *Magn Reson Imaging*, 22(5):735–742, Jun 2004.

[74] Jan Albrecht and Arne Schousboe. Taurine interaction with neurotransmitter receptors in the CNS: an update. *Neurochem Res*, 30(12):1615–1621, Dec 2005.

[75] Laura A. Brandao. *MR Spectroscopy of the Brain*. Lippincott Williams and Wilkins, 2004.

[76] P. B. Toft, P. Christiansen, O. Pryds, H. C. Lou, and O. Henriksen. T1, T2, and concentrations of brain metabolites in neonates and adolescents estimated with H-1 MR spectroscopy. *J Magn Reson Imaging*, 4(1):1–5, 1994.

[77] P. Christiansen, A. Schlosser, and O. Henriksen. Reduced N-acetylaspartate content in the frontal part of the brain in patients with probable Alzheimer's disease. *Magn Reson Imaging*, 13(3):457–462, 1995.

[78] Frank Träber, Wolfgang Block, Rolf Lamerichs, Jürgen Gieseke, and Hans H Schild. 1h metabolite relaxation times at 3.0 tesla: Measurements of t1 and t2 values in normal brain and determination of regional differences in transverse relaxation. *J Magn Reson Imaging*, 19(5):537–545, May 2004.

[79] D. Leibfritz and W. Dreher. Magnetization transfer MRS. *NMR Biomed*, 14(2):65–76, Apr 2001.

[80] K. Kantarci, C. R. Jack, Y. C. Xu, N. G. Campeau, P. C. O'Brien, G. E. Smith, R. J. Ivnik, B. F. Boeve, E. Kokmen, E. G. Tangalos, and R. C. Petersen. Regional metabolic patterns in mild cognitive impairment and Alzheimer's disease: A 1H MRS study. *Neurology*, 55(2):210–217, Jul 2000.

[81] T. M. Rudkin and D. L. Arnold. Proton magnetic resonance spectroscopy for the diagnosis and management of cerebral disorders. *Arch Neurol*, 56(8):919–926, Aug 1999.

[82] C. M. Ellis, G. Lemmens, S. C. Williams, A. Simmons, J. Dawson, P. N. Leigh, and K. R. Chaudhuri. Changes in putamen N-acetylaspartate and choline ratios in untreated and levodopa-treated Parkinson's disease: a proton magnetic resonance spectroscopy study. *Neurology*, 49(2):438–444, Aug 1997.

[83] T. Q. Hoang, S. Bluml, D. J. Dubowitz, R. Moats, O. Kopyov, D. Jacques, and B. D. Ross. Quantitative proton-decoupled 31P MRS and 1H MRS in the evaluation of Huntington's and Parkinson's diseases. *Neurology*, 50(4):1033–1040, Apr 1998.

[84] P. B. Barker, J. H. Gillard, P. C. van Zijl, B. J. Soher, D. F. Hanley, A. M. Agildere, S. M. Oppenheimer, and R. N. Bryan. Acute stroke: evaluation with serial proton MR spectroscopic imaging. *Radiology*, 192(3):723–732, Sep 1994.

[85] J. van der Grond, R. Balm, L. J. Kappelle, B. C. Eikelboom, and W. P. Mali. Cerebral metabolism of patients with stenosis or occlusion of the internal carotid artery. A 1H-MR spectroscopic imaging study. *Stroke*, 26(5):822–828, May 1995.

[86] E. Achten. Aspects of proton MR spectroscopy in the seizure patient. *Neuroimaging Clin N Am*, 8(4):849–862, Nov 1998.

[87] D. L. Arnold, N. De Stefano, S. Narayanan, and P. M. Matthews. Proton MR spectroscopy in multiple sclerosis. *Neuroimaging Clin N Am*, 10(4):789–98 ,ix–x, Nov 2000.

[88] P. A. Narayana, T. J. Doyle, D. Lai, and J. S. Wolinsky. Serial proton magnetic resonance spectroscopic imaging, contrast-enhanced magnetic resonance imaging, and quantitative lesion volumetry in multiple sclerosis. *Ann Neurol*, 43(1):56–71, Jan 1998.

[89] P. M. Matthews, G. Francis, J. Antel, and D. L. Arnold. Proton magnetic resonance spectroscopy for metabolic characterization of plaques in multiple sclerosis. *Neurology*, 41(8):1251–1256, Aug 1991.

[90] E. L. Hahn. Spin Echoes. *Phys. Rev.*, 80(4):580–594, Nov 1950.

[91] E.O. Stejskal and J.E. Tanner. Spin Diffusion Measurements : Spin Echoes in the Presence of a Time-Dependent Field Gradient. *The Journal of Chemical Physics*, 42(1):288–292, 1965.

[92] C. Beaulieu and P. S. Allen. Determinants of anisotropic water diffusion in nerves. *Magn Reson Med*, 31(4):394–400, 1994.

[93] P. J. Basser and C. Pierpaoli. Microstructural and physiological features of tissues elucidated by quantitative-diffusion-tensor MRI. *J Magn Reson B*, 111(3):209–19, 1996.

[94] S. Pajevic and C. Pierpaoli. Color schemes to represent the orientation of anisotropic tissues from diffusion tensor data: application to white matter fiber tract mapping in the human brain. *Magn Reson Med*, 42(3):526–40, 1999.

[95] T. E. Conturo, N. F. Lori, T. S. Cull, E. Akbudak, A. Z. Snyder, J. S. Shimony, R. C. McKinstry, H. Burton, and M. E. Raichle. Tracking neuronal fiber pathways in the living human brain. *Proc Natl Acad Sci U S A*, 96(18):10422–7, 1999.

[96] D. K. Jones, A. Simmons, S. C. Williams, and M. A. Horsfield. Non-invasive assessment of axonal fiber connectivity in the human brain via diffusion tensor MRI. *Magn Reson Med*, 42(1):37–41, 1999.

[97] R. Xue, P. C. van Zijl, B. J. Crain, M. Solaiyappan, and S. Mori. In vivo three-dimensional reconstruction of rat brain axonal projections by diffusion tensor imaging. *Magn Reson Med*, 42(6):1123–7, 1999.

[98] C. T. Moonen, P. C. van Zijl, D. Le Bihan, and D. DesPres. In vivo NMR diffusion spectroscopy: 31P application to phosphorus metabolites in muscle. *Magn Reson Med*, 13(3):467–77, 1990.

[99] C. H. Sotak. Multiple quantum NMR spectroscopy methods for measuring the apparent self-diffusion coefficient of in vivo lactic acid. *NMR Biomed*, 4(2):70–2, 1991.

[100] K. D. Merboldt, D. Horstermann, W. Hanicke, H. Bruhn, and J. Frahm. Molecular self-diffusion of intracellular metabolites in rat brain in vivo investigated by localized proton NMR diffusion spectroscopy. *Magn Reson Med*, 29(1):125–9, 1993.

[101] K. Nicolay, K. P. Braun, R. A. Graaf, R. M. Dijkhuizen, and M. J. Kruiskamp. Diffusion NMR spectroscopy. *NMR Biomed*, 14(2):94–111, 2001.

[102] A. van der Toorn, H. B. Verheul, J. W. Berkelbach van der Sprenkel, C. A. Tulleken, and K. Nicolay. Changes in metabolites and tissue water status after focal ischemia in cat brain assessed with localized proton MR spectroscopy. *Magn Reson Med*, 32(6):685–91, 1994.

[103] M. Wick, Y. Nagatomo, F. Prielmeier, and J. Frahm. Alteration of intracellular metabolite diffusion in rat brain in vivo during ischemia and reperfusion. *Stroke*, 26(10):1930–3; discussion 1934, 1995.

[104] A. van der Toorn, R. M. Dijkhuizen, C. A. Tulleken, and K. Nicolay. Diffusion of metabolites in normal and ischemic rat brain measured by localized 1H MRS. *Magn Reson Med*, 36(6):914–22, 1996.

[105] R. M. Dijkhuizen, R. A. de Graaf, K. A. Tulleken, and K. Nicolay. Changes in the diffusion of water and intracellular metabolites after excitotoxic injury and global ischemia in neonatal rat brain. *J Cereb Blood Flow Metab*, 19(3):341–9, 1999.

[106] O. Abe, T. Okubo, N. Hayashi, N. Saito, N. Iriguchi, I. Shirouzu, Y. Kojima, T. Masumoto, K. Ohtomo, and Y. Sasaki. Temporal changes of the apparent diffusion coefficients of water and metabolites in rats with hemispheric infarction: experimental study of transhemispheric diaschisis in the contralateral hemisphere at 7 tesla. *J Cereb Blood Flow Metab*, 20(4):726–35, 2000.

[107] W. Dreher, E. Busch, and D. Leibfritz. Changes in apparent diffusion coefficients of metabolites in rat brain after middle cerebral artery occlusion measured by proton magnetic resonance spectroscopy. *Magn Reson Med*, 45(3):383–9, 2001.

[108] P. van Gelderen, D. DesPres, P. C. van Zijl, and C. T. Moonen. Evaluation of restricted diffusion in cylinders. Phosphocreatine in rabbit leg muscle. *J Magn Reson B*, 103(3):255–260, Mar 1994.

[109] R. A. de Graaf, A. van Kranenburg, and K. Nicolay. In vivo (31)P-NMR diffusion spectroscopy of ATP and phosphocreatine in rat skeletal muscle. *Biophys J*, 78(4):1657–64, 2000.

[110] Y. Assaf and Y. Cohen. In vivo and in vitro bi-exponential diffusion of N-acetyl aspartate (NAA) in rat brain: a potential structural probe? *NMR Biomed*, 11(2):67–74, 1998.

[111] Y. Assaf and Y. Cohen. Non-mono-exponential attenuation of water and N-acetyl aspartate signals due to diffusion in brain tissue. *J Magn Reson*, 131(1):69–85, 1998.

[112] Y. Assaf and Y. Cohen. Structural information in neuronal tissue as revealed by q-space diffusion NMR spectroscopy of metabolites in bovine optic nerve. *NMR Biomed*, 12(6):335–44, 1999.

[113] Y. Assaf and Y. Cohen. Assignment of the water slow-diffusing component in the central nervous system using q-space diffusion MRS: implications for fiber tract imaging. *Magn Reson Med*, 43(2):191–9, 2000.

[114] T. Nakada, I. L. Kwee, and H. Igarashi. Brain maturation and high-energy phosphate diffusivity: alteration in cytosolic microenvironment and effective viscosity. *Brain Res Dev Brain Res*, 80(1-2):121–126, Jul 1994.

[115] J. Pfeuffer, I. Tkac, and R. Gruetter. Extracellular-intracellular distribution of glucose and lactate in the rat brain assessed noninvasively by diffusion-weighted 1H nuclear magnetic resonance spectroscopy in vivo. *J Cereb Blood Flow Metab*, 20(4):736–46, 2000.

[116] J. M. Hakumaki, H. Poptani, A. M. Puumalainen, S. Loimas, L. A. Paljarvi, S. Yla-Herttuala, and R. A. Kauppinen. Quantitative 1H nuclear magnetic resonance diffusion spectroscopy of BT4C rat glioma during thymidine kinase-mediated gene therapy in vivo: identification of apoptotic response. *Cancer Res*, 58(17):3791–9, 1998.

[117] C. D. Kroenke, J. J. Ackerman, and D. A. Yablonskiy. On the nature of the NAA diffusion attenuated MR signal in the central nervous system. *Magn Reson Med*, 52(5):1052–9, 2004.

[118] R. A. de Graaf, K. P. Braun, and K. Nicolay. Single-shot diffusion trace (1)H NMR spectroscopy. *Magn Reson Med*, 45(5):741–8, 2001.

[119] K. Nicolay, A. van der Toorn, and R. M. Dijkhuizen. In vivo diffusion spectroscopy. An overview. *NMR Biomed*, 8(7-8):365–74, 1995.

[120] P Jehenson, M Westphal, and N Schuff. Analytical Method for the Compensation of Eddy-Current Effects Induced by Pulsed Magnetic Field Gradients in NMR Systems. *Journal of Magnetic Resonance*, 90:264–278, 1990.

[121] S. W. Provencher. Estimation of metabolite concentrations from localized in vivo proton NMR spectra. *Magn Reson Med*, 30(6):672–679, Dec 1993.

[122] J.E. Tanner. Use of the Stimulated Echo in NMR Diffusion Studies. *The Journal of Chemical Physics*, 52(5):2523–2526, 1970.

[123] P. J. Basser. Inferring microstructural features and the physiological state of tissues from diffusion-weighted images. *NMR Biomed*, 8(7-8):333–44, 1995.

[124] R. Mills. Self-Diffusion in Normal and Heavy Water in the Range 1-45 degrees. *Journal of Physical Chemistry*, 77(5):685–688, 1973.

[125] C. T. Moonen, M. von Kienlin, P. C. van Zijl, J. Cohen, J. Gillen, P. Daly, and G. Wolf. Comparison of single-shot localization methods (STEAM and PRESS) for in vivo proton NMR spectroscopy. *NMR Biomed*, 2(5-6):201–8, 1989.

[126] C. S. Johnson. Diffusion ordered nuclear magnetic resonance spectroscopy: principles and applications. *Prog Nuc Mag Res Spec.*, 34:203–256, 1999.

[127] J. Ellegood, C. C. Hanstock, and C. Beaulieu. Trace apparent diffusion coefficients of metabolites in human brain using diffusion weighted magnetic resonance spectroscopy. *Magn Reson Med*, 53(5):1025–32, 2005.

[128] K. D. Merboldt, W. Hanicke, and J. Frahm. Self-Diffusion NMR Imaging Using Stimulated Echoes. *J. Magn. Reson.*, 64:479–486, 1985.

[129] N. J. Coupland, C. J. Ogilvie, K. M. Hegadoren, P. Seres, C. C. Hanstock, and P. S. Allen. Decreased prefrontal Myo-inositol in major depressive disorder. *Biol Psychiatry*, 57(12):1526–34, 2005.

[130] C. Pierpaoli, P. Jezzard, P. J. Basser, A. Barnett, and G. Di Chiro. Diffusion tensor MR imaging of the human brain. *Radiology*, 201(3):637–48, 1996.

[131] J. Ellegood, C. C. Hanstock, and C. Beaulieu. Diffusion tensor spectroscopy (DTS) of human brain. *Magn Reson Med*, 55(1):1–8, 2006.

[132] J. Pfeuffer, S. W. Provencher, and R. Gruetter. Water diffusion in rat brain in vivo as detected at very large b values is multicompartmental. *Magma*, 8(2):98–108, 1999.

[133] O. A. Petroff, T. Ogino, and J. R. Alger. High-resolution proton magnetic resonance spectroscopy of rabbit brain: regional metabolite levels and postmortem changes. *J Neurochem*, 51(1):163–71, 1988.

[134] C. Beaulieu and P. S. Allen. An in vitro evaluation of the effects of local magnetic-susceptibility-induced gradients on anisotropic water diffusion in nerve. *Magn Reson Med*, 36(1):39–44, 1996.

[135] M. D. Does and J. C. Gore. Compartmental study of diffusion and relaxation measured in vivo in normal and ischemic rat brain and trigeminal nerve. *Magn Reson Med*, 43(6):837–44, 2000.

[136] F. Aboitiz, A. B. Scheibel, R. S. Fisher, and E. Zaidel. Fiber composition of the human corpus callosum. *Brain Res*, 598(1-2):143–53, 1992.

[137] Julien Valette, Martine Guillermier, Laurent Besret, Philippe Hantraye, Gilles Bloch, and Vincent Lebon. Isoflurane strongly affects the diffusion of intracellular metabolites, as shown by 1H nuclear magnetic resonance spectroscopy of the monkey brain. *J Cereb Blood Flow Metab*, 27(3):588–596, Mar 2007.

[138] J. Valette, M. Guillermier, L. Besret, F. Boumezbeur, P. Hantraye, and V. Lebon. Optimized diffusion-weighted spectroscopy for measuring brain glutamate apparent diffusion coefficient on a whole-body MR system. *NMR Biomed*, 18(8):527–33, 2005.

[139] M. E. Moseley, J. Kucharczyk, H. S. Asgari, and D. Norman. Anisotropy in diffusion-weighted MRI. *Magn Reson Med*, 19(2):321–6, 1991.

[140] Hyeonjin Kim. *The Optimized Detection of Myo-Inositol and Other Metabolites with Strongly-Coupled Spin Systems in In-Vivo Magnetic Resonance Spectroscopy*. PhD thesis, University of Alberta, 2004.

[141] J. Bedet, D. Canet, S Leclerc, P. Mutzenhardt, D. Stemmelen, and G. Trausch. Opimal conditions for two-point estimation of self-diffusion coefficients through rf gradient NMR experiments. *Chemical Physics Letters*, 408:237–240, 2005.

[142] J. Ellegood, R.T. McKay, C.C. Hanstock, and C. Beaulieu. Anisotropic diffusion of metabolites in peripheral nerve using diffusion weighted magnetic resonance spectroscopy at ultra-high field. *J Magn Reson*, 184(1):20–28, Jan 2007.

[143] S. Mori and P. C. van Zijl. Diffusion weighting by the trace of the diffusion tensor within a single scan. *Magn Reson Med*, 33(1):41–52, 1995.

[144] T. Chun, A. M. Ulu, and P. C. van Zijl. Single-shot diffusion-weighted trace imaging on a clinical scanner. *Magn Reson Med*, 40(4):622–628, Oct 1998.

[145] M. E. Moseley, M. F. Wendland, and J. Kucharczyk. Magnetic resonance imaging of diffusion and perfusion. *Top Magn Reson Imaging*, 3(3):50–67, Jun 1991.

[146] C. H. Sotak and L. Li. MR imaging of anisotropic and restricted diffusion by simultaneous use of spin and stimulated echoes. *Magn Reson Med*, 26(1):174–83, 1992.

[147] C. Beaulieu. The basis of anisotropic water diffusion in the nervous system - a technical review. *NMR Biomed*, 15(7-8):435–55, 2002.

[148] S. H. Park, K. H. Chang, I. C. Song, Y. J. Kim, S. H. Kim, and M. H. Han. Diffusion-weighted MRI in cystic or necrotic intracranial lesions. *Neuroradiology*, 42(10):716–721, Oct 2000.

[149] K. Noguchi, N. Watanabe, T. Nagayoshi, T. Kanazawa, S. Toyoshima, M. Shimizu, and H. Seto. Role of diffusion-weighted echo-planar MRI in distinguishing between brain brain abscess and tumour: a preliminary report. *Neuroradiology*, 41(3):171–174, Mar 1999.

[150] Franklyn A Howe and Kirstie S Opstad. 1H MR spectroscopy of brain tumours and masses. *NMR Biomed*, 16(3):123–131, May 2003.

[151] C. Nilsson, K. Markenroth Bloch, S. Brockstedt, J. Lätt, H. Widner, and E-M. Larsson. Tracking the neurodegeneration of parkinsonian disorders–a pilot study. *Neuroradiology*, 49(2):111–119, Feb 2007.

[152] K. Yoshikawa, Y. Nakata, K. Yamada, and M. Nakagawa. Early pathological changes in the parkinsonian brain demonstrated by diffusion tensor MRI. *J Neurol Neurosurg Psychiatry*, 75(3):481–484, Mar 2004.